Yukon Geological Survey

BULLETIN 16

Bedrock geology of NTS 95C/5 (Pool Creek) and NTS 95D/8 map sheets, southeast Yukon

by
Lee C. Pigage

With contributions from G. Gehrels, R. MacNaughton, A.D. McCracken, J.K. Mortensen, B. Norford, G. Nowlan, M.J. Orchard, L. Pyle, I.R. Smith, J. Utting and M. Villeneuve

2009



Published under the authority of the Minister of Energy, Mines and Resources, Government of Yukon
http://www.emr.gov.yk.ca
Printed in Whitehorse, Yukon, 2009.

© Minister of Energy, Mines and Resources, Government of Yukon

ISBN 978-1-55362-446-2

This, and other Yukon Geological Survey publications, may be obtained from:

Geoscience Information and Sales
Yukon Geological Survey
102-300 Main Street
Box 2703 (K-102)
Whitehorse, Yukon, Canada Y1A 2C6
phone (867) 667-3201, fax (867) 667-3198, e-mail geosales@gov.yk.ca
Visit the Yukon Geological Survey website at www.geology.gov.yk.ca

In referring to this publication, please use the following citation:
Pigage, L.C., 2009. Bedrock geology of NTS 95C/5 (Pool Creek) and NTS 95D/8 map sheets, southeast Yukon. Yukon Geological Survey, Bulletin 16, 150 p.

This document is available in colour on the Yukon Geological Survey website.
Production by K-L Services, Whitehorse, Yukon.

Unless otherwise specified, all photos by Lee Pigage.

Cover photo: View looking north of Pool Creek flowing south into east-flowing Beaver River, UTM 358 130E/6 696 710N, Zone 10 (NTS 95C/5). Formations dip moderately to the right. Lowermost unit forming light cliffs on left is Dunedin Formation. Besa River Formation overlies Dunedin Formation in centre of photo. Ridge on east side of photo is capped by resistent Mattson Formation.

Preface

This study is an outgrowth of the 1998 – 2002 Central Foreland NATMAP Project which was delivered jointly by the Geological Survey of Canada, Yukon Geological Survey and British Columbia Geological Survey. The project included targeted 1:50,000 bedrock mapping in the Liard Basin and adjacent foothills to resolve stratigraphic and structural questions and assess the area's mineral and hydrocarbon potential. Lee Pigage was the primary Yukon contributor, mapping the Pool Creek map sheet (95C/05) in 2000 and 2001. Following the NATMAP project he mapped sheet 95D/08 between 2003 and 2005. These maps were released recently (Geoscience Map 2008-1 and 2008-2, respectively), and this bulletin provides detailed descriptions of the upgraded geologic framework and the new results of mapping.

Rocks in the study area span the Proterozoic to Eocene and record the formation and subsequent tectonic reworking of this part of the Selwyn basin. Previously unnamed Proterozoic sedimentary units have been tentatively correlated with Proterozoic strata of ancestral North America, and a new Cambrian-Ordovician stratigraphic unit (Crow Formation) is defined. New U-Pb ages generated as part of this study show that syenitic plutons in the Pool Creek area, while in close spatial proximity, are separated by ca. 600 m.y. Revised stratigraphic and radiometric age constraints provide an improved understanding of the setting for skarn, SEDEX and vein-related showings in the area, and reveal potential for a number of previously undocumented mineral deposit types, including Mississippi Valley- and Irish-type Pb-Zn, and intrusion-associated REE and U.

The Yukon Geological Survey's participation in field work was jointly funded by the Department of Indian Affairs and Northern Development and the Yukon Government Department of Economic Development through the Yukon Geology Program.

Carolyn Relf
Director
Yukon Geological Survey
Energy, Mines and Resources
Yukon Government

Abstract

The Pool Creek map sheet (NTS 95C/5) and map sheet NTS 95D/8 in southeast Yukon contain eight successions of sedimentary rocks ranging from Proterozoic to Paleocene in age with a total thickness of 5000 to 15 000 m. Early to middle Paleozoic strata are best preserved, with younger strata being only locally preserved. Proterozoic strata have been tentatively correlated with Pinguicula Group, Mackenzie Mountains Supergroup and Windermere Supergroup. The newly defined Cambrian-Ordovician Crow Formation documents shallow water to subaerial siliciclastic sedimentary rocks related to a local paleogeographic high. Silurian-Devonian strata contain the transition from the MacDonald carbonate platform northward to the Selwyn marine basin. Units older than Jurassic are part of a regional west- to southwest-facing marine passive margin of ancestral North America. The poor preservation of sedimentary successions younger than Jurassic is linked to Cordilleran deformation caused by accretion of exotic terranes to the western margin of North America.

Intrusive igneous activity in the Neoproterozoic and Eocene occurred in close proximity in the map area, with the Proterozoic Pool Creek syenite and an Eocene biotite syenite being separated geographically by less than 1 km. Extrusive volcanic rocks are dated stratigraphically or with isotopic age dating as Proterozoic, Cambrian-Ordovician, Paleocene and Eocene. Stratigraphic constraints on extrusive activity are locally poorly known. Proterozoic and Paleozoic volcanic rocks are basalts; Paleocene and Eocene volcanic rocks include both rhyolite and basalt.

The map area contains structural features related to two deformation events, one pre-late Cambrian and the other post-Triassic and pre-late Paleocene. Evidence for the early deformation event is restricted to southeast-trending open folds in Proterozoic sedimentary rocks in the north-central part of the Pool Creek map sheet. Deformation features related to the second, post-Triassic, deformation event in the map area consist dominantly of reverse faults and associated open to tight folds. Faults and folds trend north to northeast. The western part of the area is a dominantly homoclinal succession dipping west, and the eastern part of the area is a dominantly homoclinal succession dipping east. Structural styles for the post-Triassic deformation can be related to the different lithofacies present in the map area, with folding being more prevalent in shale units and faulting being more prevalent in thick carbonate units.

Previous mineral exploration has not resulted in the discovery of major mineral deposits in the area. Mineral deposit models appropriate for the area include barite vein deposits, SEDEX zinc-lead deposits, Mississippi Valley-type zinc-lead deposits, Irish-type zinc-lead deposits, and intrusion-related uranium and REE deposits. Thermal maturation indices confirm the sedimentary rocks are overmature for hydrocarbon generation. Clastic units have epitaxial quartz overgrowths on quartz clasts, reducing porosity and permeability. The closest hydrocarbon fields are gas fields hosted in Manetoe facies dolomite approximately 95 km to the east; Manetoe facies was not recognized at surface in the map area.

CONTENTS

Preface i

Abstract iii

Introduction 1
- Location and physiography 2
- Access 3
- Glacial history 3
- Previous work 4
- Regional geology 4

Stratigraphy 5
- Introduction 5
- Succession 1 (Proterozoic) 8
  - Proterozoic sandstone (Unit Ps) 8
  - Proterozoic volcaniclastic laminated argillite (Unit Pa) 11
  - Toobally Formation (PT) 19
- Succession 2 (Cambrian-Ordovician) 24
  - Crow Formation (new) (ЄOC) 24
  - Rabbitkettle Formation (ЄOR) 33
- Succession 3 (Ordovician-Silurian) 35
  - Sunblood Formation (OSu) 35
  - Ordovician-Silurian sandstone, siltstone and conglomerate (OSs) 37
- Succession 4 (Silurian-Devonian) 39
  - Nonda Formation (SN) 39
  - Road River Group (SDRR-a and SDRR-b) 40
  - Muncho-McConnell and Stone formations undivided (SDMMS) 43
  - Dunedin Formation (DD-l and DD-d) 44
- Succession 5 (Devonian-Lower Carboniferous) 46
  - Besa River Formation (DCBR) 46
  - Mattson Formation (CM, CM-a, CM-b) 48
- Succession 6 (Permian) 51
  - Fantasque Formation (PF) 51
- Succession 7 (Triassic) 53
  - Grayling and Toad formations undivided (ŦGT) 53
- Succession 8 (Paleocene) 54
  - Paleocene sediments (Ꝑssc) and Paleocene basalt (Ꝑb) 54

Igneous rocks 58
- Introduction 58
- Neoproterozoic Pool Creek nepheline syenite (PPCsy) 58
- Eocene biotite syenite (Ebsy) 60
- Eocene(?) igneous breccia (Eib) 60

Structural geology 62
- Introduction 62
- Pre-late Cambrian deformation D_1 62
- Post-Triassic/pre-late Paleocene deformation D_2 63
- Beaver River Structure 68
- Liard line 68
- Early Paleozoic normal faulting 69

Stratigraphic and tectonic discussion 70
- Succession 1 71

Succession 2 71
Succession 3 71
Succession 4 72
Succession 5 72
Succession 6 72
Succession 7 72
Succession 8 72
Economic geology 73
Mineral potential 73
Hydrocarbon potential 74
Overall summary 75
Acknowledgements 76
Selected references 77
Appendix I. Detrital zircon geochronology 85
Introduction 85
Arizona Laserchron Center 85
Pacific Centre for Isotopic and Geochemical Research 86
Analytical results 86
Appendix II. Igneous geochronology 133
Introduction 133
Methodology 133
Appendix III. Whole rock geochemistry 135
Appendix IV. Fossil identification 143
Appendix V. Rock-Eval analyses 148
Analytical conditions and instrumentation 148

Pages 1-84, Figures

Figure 1. Location map for NTS 95C/5 and NTS 95D/8 in southeast Yukon, p. 1

Figure 2. Ordovician-Silurian paleogeography of northern Canadian Cordillera, p. 2

Figure 3. Schematic cross-section of stratigraphic successions present in map area, p. 5

Figure 4. Chronostratigraphy for Proterozoic and early Paleozoic formations in Figure 3, p. 6

Figure 5. Chronostratigraphy for late Paleozoic, Mesozoic and Cenozoic formations in Figure 3, p. 7

Figure 6. Planar laminated beds in grey siltstone of Unit **Ps**, p. 8

Figure 7. Soft sediment deformation folds in grey siltstone of Unit **Ps**, p. 8

Figure 8. Thin section photo of unknown metamorphic mineral in hornfelsed siltstone of Unit **Ps**, p. 9

Figure 9. Rare siltstone interbed within massive white sandstone of Unit **Ps**, p. 9

Figure 10. Thin section photo of massive quartz sandstone of Unit **Ps**, p. 9

Figure 11. Interbedded siltstone-argillite and sandstone in Unit **Pa**, p. 11

Figure 12. Soft sediment folding and faulting within Unit **Pa**, p. 11

Figure 13. Large, subangular limestone clast within Unit **Pa**, p. 11

Figure 14. Contact between maroon siltstone and underlying green siltstone within Unit **Pa**, p. 12

Figure 15. Dolomitic sandstone interval within Unit **Pa**, p. 12

Figure 16. Cut slab of intraformational breccia within Unit **Pa**, p. 12

Figure 17. Maroon basalt conglomerate member (Unit **Pa-bc**) within Unit **Pa**, p. 13

Figure 18. Closeup of subangular basalt clasts in Unit **Pa-bc**, p. 13

Figure 19. Harker diagram of major oxides vs SiO_2 for different lithologies in Unit **Pa**, p. 14

Figure 20. Bivariate plots of elements and element ratios vs LOI (loss on ignition), Unit **Pa**, p. 15

Figure 21. Compositional diagrams for Unit **Pa** analyses in Table III-1, p. 16

Figure 22. Tectonic discriminant diagrams for Unit **Pa** analyses in Table III-1, p. 17

Figure 23. Polymictic conglomerates to pebbly mudstones, Toobally Formation, p. 19

Figure 24. Randomly oriented carbonate rock clasts in polymictic conglomerate, Toobally Formation, p. 19

Figure 25. Thin section photo of polymictic conglomerate, Toobally Formation, p. 19

Figure 26. Rare primary sedimentary layering in Toobally Formation, p. 20

Figure 27. Rare basalt clast in matrix-supported conglomerate of Toobally Formation, p. 20

Figure 28. Compositional diagrams for analyses in Table III-2, dykes and clast in Toobally Formation, p. 21

Figure 29. Tectonic discriminant diagrams for analyses in Table III-2, dykes and clast in Toobally Formation, p. 22

Figure 30. Large laminated dolostone clast within Toobally Formation, p. 23

Figure 31. Closeup view of laminated dolostone clast within Toobally Formation, p. 23

Figure 32. Interpreted stratigraphic and structural relations between Toobally Formation and Crow Formation, p. 23

Figure 33. Crow Formation sandstone with scattered monocrystalline quartz pebbles, p. 25

Figure 34. Trough cross-beds in quartz sandstones of Crow Formation, p. 25

Figure 35. Ripple marks on bedding plane, subarkosic sandstone, Crow Formation, p. 26

Figure 36. Desiccation cracks on bedding plane in fine-grained sandstone, Crow Formation, p. 26

Figure 37. Pebbly conglomerate interval within Crow Formation, p. 26

Figure 38. Thin section photo of sandstone, Crow Formation, p. 26

Figure 39. Clast-supported conglomerate, Crow Formation, p. 26

Figure 40. Maroon silty argillite, Crow Formation, p. 27

Figure 41. Interbedded massive sandstone and maroon siltstone, Crow Formation, p. 27

Figure 42. Bedded limestone, Crow Formation, p. 27

Figure 43. Trace fossils on bedding plane, bedded limestone, Crow Formation, p. 27

Figure 44. Closeup of laminae in limestone, Crow Formation, p. 28

Figure 45. Thin section photo of botryoidal dolomite crystals in brown dolostone, Crow Formation, p. 28

Figure 46. Closeup of lapilli tuff, volcanic horizon 2, Crow Formation, p. 28

Figure 47. Pillow in volcanic horizon 1, Crow Formation, p. 29

Figure 48. Thin section photo of volcanic horizon 2, Crow Formation, p. 29

Figure 49. Thin section photo of chlorite and Fe-oxide pseudomorphing olivine(?),volcanic horizon 2, Crow Formation, p. 29

Figure 50. Compositional diagrams for analyses in Table III-3, Crow Formation volcanic horizons 1-4, p. 30

Figure 51. Tectonic discriminant diagrams for analyses in Table III-3, Crow Formation volcanic horizons 1-4, p. 31

Figure 52. Rose diagram of paleocurrent directions from cross-bedding measurements, Crow Formation, p. 32

Figure 53. Stream outcrop of shale to silty shale of the Rabbitkettle Formation, p. 33

Figure 54. Truncated sandstone beds in siltstone of Rabbitkettle Formation, p. 33

Figure 55. Closeup view of limestone clasts in sandstone matrix, Rabbitkettle Formation, p. 34

Figure 56. Closeup view of limestone nodules coalescing to form beds in siltstone, Rabbitkettle Formation, p. 34

Figure 57. Large cliffs of tan-weathering dolostone, Sunblood Formation, p. 35

Figure 58. Fossil burrowing pattern on surface perpendicular to bedding, Sunblood Formation, p. 35

Figure 59. Fossiliferous, recessive limestone, Sunblood Formation, p. 36

Figure 60. Parallel laminated limestone, Sunblood Formation, p. 36

Figure 61. Thin section photos of Sunblood Formation, p. 36

Figure 62. Thin-bedded, fine-grained dolostone with black chert nodules, Sunblood Formation, p. 36

Figure 63. Basaltic sill in Sunblood Formation, p. 37

Figure 64. Thick-bedded quartzose sandstone with interbeds of recessive-weathering dolomitic siltstone and recessive dark grey silty shale, Unit **OSs**, p. 37

Figure 65. Thin section photo of arkosic sandstone, Unit **OSs**, p. 38

Figure 66. Tan-weathering, recessive, bioturbated dolomitic siltstone, Unit OSs, p. 38
Figure 67. Thin-bedded dolostone with irregular, black chert, Nonda Formation, p. 39
Figure 68. Irregular chert nodule pattern on bedding plane of thin-bedded dolostone, Nonda Formation, p. 39
Figure 69. Interbedded massive dolostone and bioclastic dolostone, Nonda Formation, p. 40
Figure 70. Planar laminated, dolomitic, dark grey to black siltstone, Road River Group – facies A, p. 41
Figure 71. Dark grey, bedded limestone, Road River Group – facies A, p. 41
Figure 72. Bedded chert interval within Road River Group – facies A, p. 41
Figure 73. Interbedded resistant sandstone and recessive shale, Road River Group – facies A, p. 42
Figure 74. Slumped outcrop of siliceous silty shale, Road River Group – facies B, p. 42
Figure 75. Outcrop of thick-bedded dolostone, undivided Muncho-McConnell-Stone formations, p. 43
Figure 76. Closeup view of argillaceous, micritic limestone, Dunedin Formation, p. 44
Figure 77. Resistant uppermost limestone interval in Dunedin Formation, p. 45
Figure 78. Cliff outcrop of dark grey dolostones, Dunedin Formation, p. 45
Figure 79. Closeup of black chert lens within dark grey dolostone, Dunedin Formation, p. 45
Figure 80. Closeup of fossiliferous grainstone in dark grey dolostone, Dunedin Formation, p. 46
Figure 81. Carbonaceous shales of the Besa River Formation, p. 46
Figure 82. Large limestone concretion in siliceous shales of the Besa River Formation, p. 47
Figure 83. Bedded chert in Besa River Formation, p. 48
Figure 84. Dark grey limestone bed in Besa River Formation, p. 48
Figure 85. Helicopter view of interbedded sandstone and carbonaceous shale, member CM-a, Mattson Formation, p. 48
Figure 86. Closeup view of massive sandstone, CM-a, Mattson Formation, p. 49
Figure 87. Thin section photo of CM-a, Mattson Formation, p. 49
Figure 88. Liesegang ring weathering pattern along fractures, CM-a, Mattson Formation, p. 49
Figure 89. Thick-bedded, tan- to orange-weathering sandstone, CM-b, Mattson Formation, p. 50
Figure 90. Thin section photo of sandstone, undivided Mattson Formation, p. 50
Figure 91. Vertical beds of quartz sandstone, undivided Mattson Formation, p. 51
Figure 92. Dark brown-weathering, siliceous shales, Fantasque Formation, p. 51
Figure 93. Thinly bedded, dark grey limestone, Fantasque Formation, p. 52
Figure 94. Poorly exposed subcrop of undivided Triassic Grayling and Toad formations, p. 54
Figure 95. Ridge of Paleocene subaerial sediments (Pssc) capped by basalt flow (Pb), p. 55
Figure 96. Closeup view of baked conglomerate immediately beneath the basalt flow, Unit Pssc, p. 55
Figure 97. View looking south of brown basalt flow, Unit Pb, p. 56
Figure 98. Thin section photo of Unit Pb, p. 56
Figure 99. Compositional diagrams for Paleocene basalt (Pb), p. 57
Figure 100. Closeup view of typical outcrop of unfoliated nepheline syenite, Pool Creek syenite, p. 58
Figure 101. Vertical, fine-grained intrusive dykes in Pool Creek nepheline syenite, p. 58
Figure 102. Banded gneissic dykes in Pool Creek nepheline syenite and Unit Ps, p. 59
Figure 103. Pool Creek syenite intrusive into hornfelsed pelites of Unit Ps, p. 59
Figure 104. Thin section photo of sericitized nepheline and K-feldspar, Pool Creek syenite, p. 59
Figure 105. Stream cliff outcrops of Eocene biotite syenite, p. 60
Figure 106. Thin section photo of Eocene biotite syenite, p. 60
Figure 107. Thin section photo of Eocene igneous breccia, p. 61
Figure 108. Rounded to subangular quartz sandstone and basalt clasts, igneous breccia, p. 61
Figure 109. Equal area stereonet plots of poles to bedding in Units Ps and Pa, p. 62
Figure 110. Structural domains A,B,C for map area, p. 64
Figure 111. Small-scale kink/box folds with east vergence in Road River Group silty shales, p. 65
Figure 112. Equal area stereonet plots of structural elements in domain A, deformation D_2, p. 66
Figure 113. Equal area stereonet plots of structural elements in domain B, deformation D_2, p. 66
Figure 114. Equal area stereonet plots of structural elements in domain C, deformation D_2, p. 67
Figure 115. Isopach map of Tippecanoe sequence strata (Ordovician-Silurian) showing Liard depression and approximate position of Liard line and Fort Norman line, p. 68
Figure 116. Large outcrop of ferricrete, p. 73

Pages 1-84, Tables

Table 1a. Cross-bedding in Crow Formation, rotated to horizontal bedding, p. 32
Table 1b. Ripple crest in Crow Formation, rotated to horizontal bedding, p. 32
Table 2. Depositional environments and transgression/regression, p. 70

Appendices Figures

Figure I-1 Location map for detrital zircon samples, 95C/5 and 95D/8, p. 87
Figure I-2. Detrital zircon concordia and probability density, sample 04LP027, Unit Ps, p. 87
Figure I-3. Detrital zircon concordia and probability density, sample 05LP024-1, Unit Ps, p. 88
Figure I-4. Detrital zircon concordia and probability density, sample 05LP024-2, Unit Ps, p. 88
Figure I-5. Composite detrital zircon probability density, Unit Ps, p. 89
Figure I-6. Tectonic framework for Precambrian of North America, p. 89
Figure I-7. Detrital zircon concordia and probability density, sample 05LP025, Unit Pa, p. 90

Figure I-8. Detrital zircon concordia and probability density, sample 05LP026, Unit Pa, p. 90

Figure I-9. Composite detrital zircon probability density, Unit Pa, p. 91

Figure I-10. Detrital zircon concordia and probability density, sample 03LP010, Toobally Formation, p. 92

Figure I-11. Detrital zircon concordia and probability density, sample 02LP120, Crow Formation, p. 92

Figure I-12. Detrital zircon concordia and probability density, sample 02LP121, Crow Formation, p. 93

Figure I-13. Detrital zircon Concordia and probability density sample 04LP028, Crow Formation, p. 93

Figure I-14. Detrital zircon concordia and probability density, sample 05LP003, Crow Formation, p. 94

Figure I-15. Detrital zircon concordia and probability density, sample 05LP011, Crow Formation, p. 94

Figure I-16. Detrital zircon concordia and probability density, sample 05LP034, Crow Formation, p. 95

Figure I-17. Detrital zircon concordia and probability density, sample 05LP069, Crow Formation, p. 95

Figure II-1. Ar/Ar Age plot for sample 00TLA009, Unit Pa-bc, no date, p. 134

Figure II-2. Ar/Ar Age plot for sample 01LP016, Unit Pb, p. 134

Figure III-1. Location map for whole rock geochemistry samples, 95C/5 and 95D/8, p. 135

Figure III-2. Location map for 36-element ICP-MS geochemistry samples, 95C/5 and 95D/8, p. 135

Figure V-1. Location map for Rock-Eval 6 samples, 95C/5 and 95D/8, p. 148

Appendices tables

Table I-1. Detrital zircon samples locations, p. 86

Table I-2a. Detrital Zircon U-Pb geochronologic analyses, sample 04LP027 in Unit Ps, p. 96

Table I-2b. Detrital Zircon U-Pb geochronologic analyses, sample 05LP024-1 in Unit Ps, p. 99

Table I-2c. Detrital zircon U-Pb geochronologic analyses, sample 05LP024-2 in Unit Ps, p. 102

Table I-3a. Detrital Zircon U-Pb geochronologic analyses, sample 05LP025 in Unit Pa, p. 105

Table I-3b. Detrital Zircon U-Pb geochronologic analyses, sample 05LP026 in Unit Pa, p. 108

Table I-4. Detrital Zircon U-Pb geochronologic analyses, sample 03LP010 in Toobally Formation, p. 111

Table I-5a. Detrital Zircon U-Pb geochronologic analyses, sample 02LP120 in Crow Formation, p. 114

Table I-5b. Detrital Zircon U-Pb geochronologic analyses, sample 02LP121 in Crow Formation, p. 117

Table I-5c. Detrital Zircon U-Pb geochronologic analyses, sample 04LP028 in Crow Formation, p. 120

Table I-5d. Detrital Zircon U-Pb geochronologic analyses, sample 05LP003-1 in Crow Formation, p. 123

Table I-5e. Detrital Zircon U-Pb geochronologic analyses, sample 05LP011-1 in Crow Formation, p. 126

Table I-5f. Detrital Zircon U-Pb geochronologic analyses, sample 05LP034-1 in Crow Formation, p. 129

Table I-5g. Detrital Zircon U-Pb geochronologic analyses, sample 05LP069-1 in Crow Formation, p. 131

Table II-1. Ar-Ar data for Paleocene basalt, sample 01LP016, p. 134

Table III-1. Lithogeochemistry of dykes and volcaniclastic rocks within Pa, p. 136

Table III-2. Lithogeochemistry of dykes and clast within Toobally Formation, p. 137

Table III-3. Lithogeochemistry of dykes and volcanic rocks within Crow Formation, p. 138

Table III-4. Lithogeochemistry of various samples, p. 140

Table III-5. Lithogeochemistry of Pool Creek syenite and dykes, Eocene biotite syenite and Eocene igneous breccia, p. 140

Table III-6. ICP analyses – Ting suite, igneous breccia and altered dykes in Toobally Formation, p. 142

Table IV-1. Fossil data for stratigraphic units – Units Ps and Pa, p. 143

Table IV-2. Fossil data for stratigraphic units – Toobally Formation, p. 143

Table IV-3. Fossil data for stratigraphic units – Crow Formation, p. 143

Table IV-4.Fossil data for stratigraphic units – Sunblood Formation, p. 144

Table IV-5. Fossil data for stratigraphic units – Unit OSs, p. 144

Table IV-6. Fossil data for stratigraphic units – Road River Group, p. 145

Table IV-7. Fossil data for stratigraphic units – Nonda Formation, p. 145

Table IV-8. Fossil data for stratigraphic units – undivided Muncho-McConnell-Stone formations, p. 146

Table IV-9. Fossil data for stratigraphic units – Dunedin Formation, p. 146

Table IV-10. Fossil data for stratigraphic units – Besa River Formation, p. 147

Table IV-11. Fossil data for stratigraphic units – Mattson Formation, p. 147

Table IV-12. Fossil data for stratigraphic units – Fantasque Formation, p. 147

Table IV-13. Fossil data for stratigraphic units – Grayling-Toad formations, p. 147

Table V-1. Measured parameters for Rock-Eval 6 analysis, p. 149

Table V-2. Calculated parameters from Rock-Eval 6 analysis, p. 149

Table V-3. Rock-Eval 6 analyses for samples from 95C/5 and 95D/8, p. 150

Plates *(in pocket)*

Plate 1. Geology map of Pool Creek NTS 95C/5, Geoscience Map 2008-1

Plate 2. Geology map of NTS 95D/8, Geoscience Map 2008-2

INTRODUCTION

NTS 95C/5 (Pool Creek) and NTS 95D/8 map areas (Fig. 1) are located in southeast Yukon, midway between Watson Lake, Yukon and Fort Liard, Northwest Territories. This area (Fig. 2) contains the transition between lower Paleozoic shallow-water carbonate rocks of MacDonald platform and fine-grained, deep water, siliciclastic sedimentary rocks of Selwyn basin (Cecile *et al.*, 1997). These lower Paleozoic facies belts were deposited in the Cordilleran miogeocline, a depositional prism of sedimentary rocks of Precambrian to Middle Jurassic age along the relatively stable western continental margin of ancestral North America (Abbott *et al.*, 1986).

Regional framework geological maps for these areas by the Geological Survey of Canada are based on fieldwork completed in the 1950s and 1960s (Douglas, 1976; Gabrielse and Blusson, 1969). Existing MINFILE localities (Deklerk, 2008) are sparse. These map sheets were selected for more detailed geological studies by the

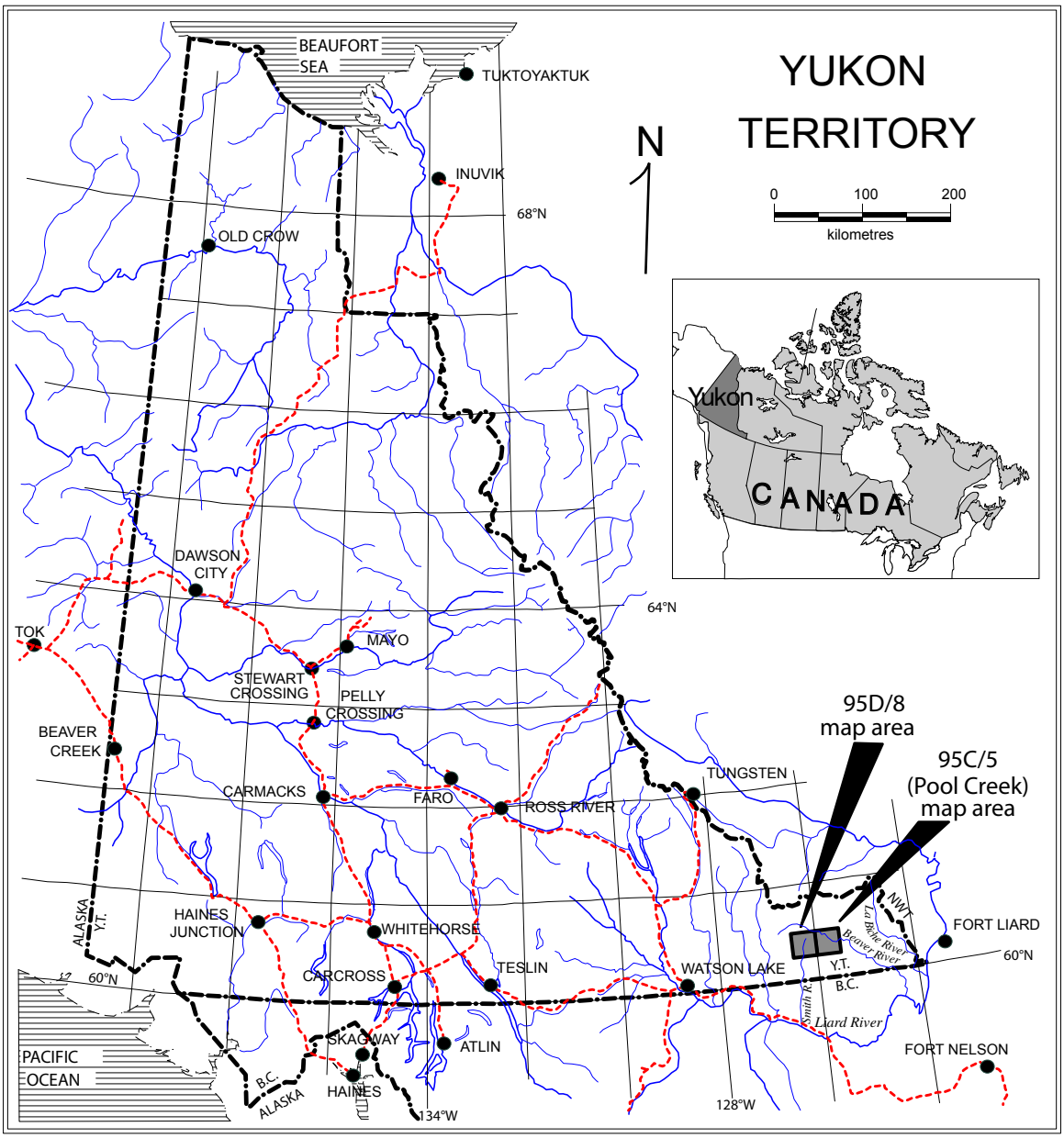


Figure 1. *Yukon geographic location map for NTS map sheets 95C/5 and 95D/8.*

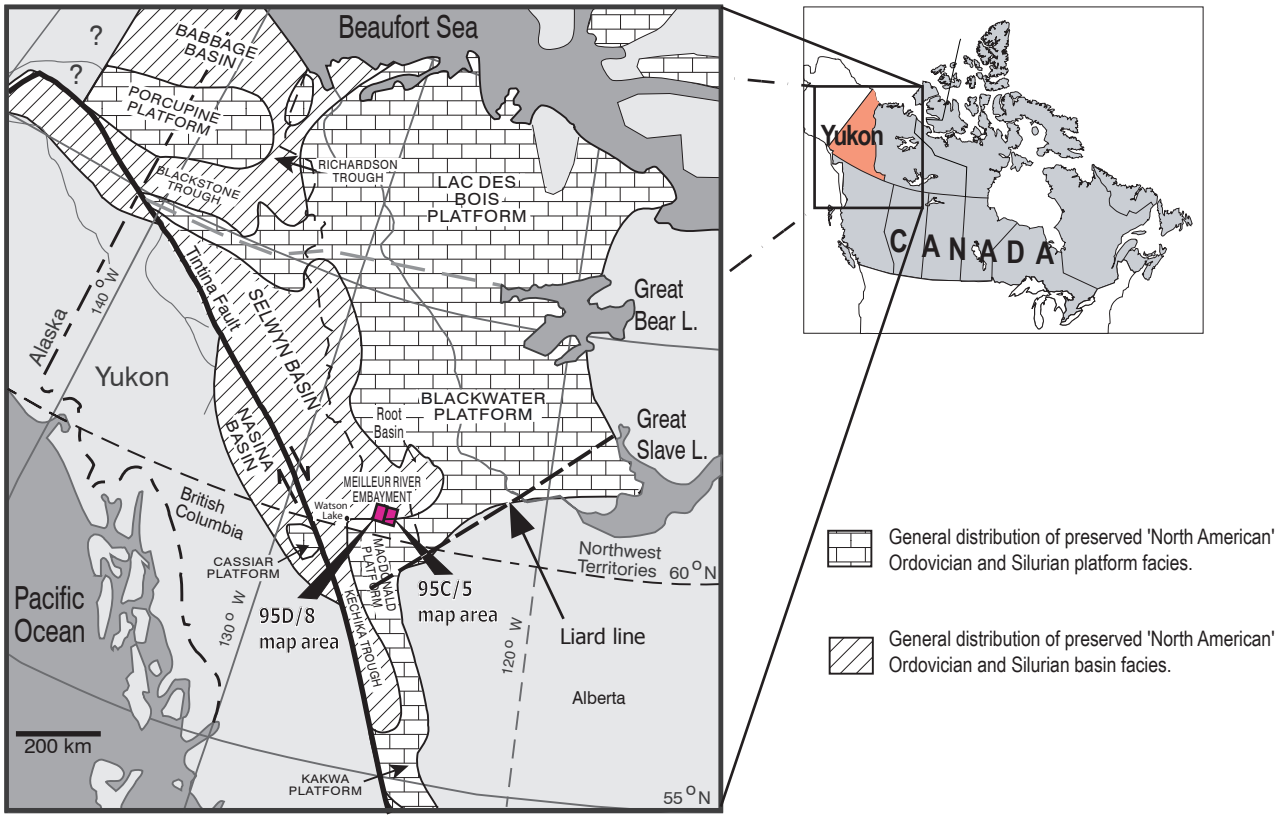


Figure 2. *Yukon location map for NTS map sheets 95C/5 and 95D/8. General distribution of Ordovician-Silurian carbonate platform and basinal shale facies for Canadian Cordillera are indicated. Modified from Cecile et al. (1997).*

Yukon Geological Survey based on their geologic location in proximity to oil and gas exploration potential, mineral exploration potential and locally extensive outcrop.

This report details the results of 1:50 000-scale geological mapping completed in the years 2000 through 2005. Bedrock 1:50 000-scale geological mapping in the Pool Creek map sheet (NTS 95C/5; latitude 60°15'N-60°30'N, longitude 125°30'W-126°00'W) was completed by the Yukon Geology Program as part of the Central Foreland NATMAP Project for a total of 11 weeks during the seasons of 2000 (3 weeks), 2001 (7 weeks) and 2002 (1 week). The Central Foreland NATMAP Project was a multidisciplinary collaborative mapping project to update geological bedrock and surficial mapping of northeastern British Columbia, southeastern Yukon Territory and southwestern Northwest Territories. The intent of the study was to determine the influence of pre-existing ancient crustal structures on the development of Mesozoic and Tertiary deformation structures.

Subsequent to completion of fieldwork with the Central Foreland NATMAP Project, the Yukon Geological Survey continued with bedrock geological 1:50 000-scale mapping in map sheet NTS 95D/8 (latitude 60°15'N-60°30'N, longitude 126°00'W-126°30'W) to further explore structural and stratigraphic studies during field seasons 2003 (1.5 weeks), 2004 (2.5 weeks) and 2005 (3 weeks).

Emphasis during mapping was on stratigraphy and structure. Isotopic age dating, fossil studies, palynology and Rock-Eval studies of collected samples are an integral part of the study and enhance observational information from the field mapping. Map coordinates in this report are based on NAD83 Universal Transverse Mercator, Zone 9 (NTS 95D/8) and Zone 10 (NTS 95C/5) projection. Plates 1 and 2 present bedrock geology for NTS 95C/5 and 95D/8 at 1:50 000 scale, respectively.

LOCATION AND PHYSIOGRAPHY

Pool Creek map sheet is located 135 km west-northwest of Fort Liard, Northwest Territories and 165 km east-northeast of Watson Lake, Yukon Territory. NTS 95D/8 map sheet is located 150 km northeast of Watson Lake. Both map sheets are located within the Hyland Highland physiographic region (Mathews, 1986). Topography in both map sheets consists of low rounded hills with incised stream drainages. Elevations range from

1500 feet (460 m) to 4600 feet (1400 m) ASL. The area is heavily forested with a single north-trending ridge in the Pool Creek map sheet extending above tree line for 8 km. Beaver River flows from northwest to southeast through the area into the Liard River and then into the Mackenzie River which drains northward to the Beaufort Sea. Bedrock exposure is 10% or less, with most outcrops occurring as exposures along streams and rivers. Map sheet NTS 95D/8 contains scattered large lakes which drain either southward into the Smith River or northward into the Beaver River. The string of lakes extending north in the central part of NTS 95D/8 is collectively termed Toobally Lakes. The largest of these extends for about 14 km and is called Toobally Lake in this report.

ACCESS

One former winter access trail for seismic work completed north of the map area (NTS map sheet 95C/12) in the 1970s occurs in the southeast part of the Pool Creek map sheet. This trail is now overgrown, although locally it is amenable to ATV traffic. A trail indicated on maps as extending north from the Smith River and east of the Toobally Lakes is completely overgrown and cannot even be readily discerned from the air.

For this project, access was by helicopter from Fort Liard (map sheet 95C/5) and Watson Lake (map sheet 95D/8). A fixed wing aircraft on floats was used to access camps established adjacent to the larger lakes in map sheet 95D/8. Fieldwork was completed primarily by foot traverses and foot and boat traverses from base camps. Spot checks and short foot traverses were completed in other areas where helicopter landing was feasible.

Beaver River is too shallow for boats with standard propeller outboard motors. An inflatable boat with a jet outboard motor was used for transport during the 2001 and 2005 field seasons. Discharge volumes of Beaver River are highly variable as river level rises rapidly in response to rain storms. Camps on gravel and sand bars along Beaver River must constantly be monitored as bars disappear and emerge during the field season.

GLACIAL HISTORY

Much of central and southern Yukon has had a complex Pleistocene glacial history with up to ten documented glacial advances of Cordilleran ice sheets (Bostock, 1966; Duk-Rodkin *et al.*, 2004). Widespread till (generally <2 m thick), glacial striae, and glacially streamlined landforms (drumlins and flutes) within 95C/5 and 95D/8 map sheets document the prominent east to northeast advance of Cordilleran ice during the most recent McConnell Glaciation (=Late Wisconsinan; Smith, 2000). No evidence of earlier ice advances was found in the area. McConnell Glaciation attained its maximum extent around 23 000 ^{14}C BP (Duk-Rodkin *et al.*, 1996). Subsequent retreat of the Cordilleran ice was rapid, with much of it disappearing by approximately 13 000 ^{14}C BP (Jackson *et al.*, 1991).

Northeastern and southeastern Yukon were also, in part, inundated by Laurentide (continental) ice flowing westward from the Keewatin Sector during the Late Wisconsinan. Reconstruction of Late Wisconsinan glacial history in the La Biche River (NTS 95C) map area indicates that Laurentide ice was first to advance into the region, extending a lobe of ice westward (Smith, 2002). A granite cobble, considered to have been derived from the Canadian Shield, was collected by Smith (pers. comm., 2003) from a modern Beaver River bar deposit in the Pool Creek area (NTS 95C/5). Although deposition of this granite cobble possibly resulted from ice-rafting in a large proglacial lake impounded between the westward advancing Laurentide and eastward advancing Cordilleran ice, its presence in the Pool Creek area may document westward penetration of Laurentide ice into the Pool Creek area. More definitive geomorphic, stratigraphic, sedimentological and chronological evidence collected from areas immediately east and south of the Pool Creek map area clearly establish a more extensive westward penetration of Laurentide ice than previously documented (Smith, 2000).

Cordilleran ice, advancing eastward, coalesced with the Laurentide ice somewhere east of the Pool Creek area, resulting in a buttressing and considerable thickening of the two ice masses (Smith, pers. comm., 2003). This coalescence and thickening is well reflected in the abundant glacially streamlined landforms (drumlins and flutings) in western La Biche River map area (NTS 95C) which show a rotation of Cordilleran ice flow from eastward, to northeast, followed by a final deglacial northern flow (reflecting topographic control of ice along major valleys). The deflection of Cordilleran ice northwards across the regional hydrological divide and several mountain ranges indicates that an ice-free corridor between Cordilleran and Laurentide ice masses did not exist in this area.

Discontinuous glaciofluvial and glaciolacustrine gravel, sand and silt in the La Biche River map area document diverse proximal depositional environments related to advancing and retreating glacial ice from both Laurentide and Cordilleran glacial masses (Smith, 2000; Smith, pers. comm., 2003). The deeply incised canyon in the Pool Creek map, through which Beaver River presently flows, may be the product of Late Wisconsinan glacial diversion

and incision. Prior to the last glaciation, it is suggested that the Pool Creek area represented a hydrological divide, in which one river flowed west into the Toobally Lakes and Smith River basin and a second proto-Beaver River flowed east more or less along its modern course.

PREVIOUS WORK

The Geological Survey of Canada completed 1:253 440-scale geological bedrock mapping in La Biche River map area in 1957 as part of Operation Mackenzie (Douglas and Norris, 1959). The geology of the area was further updated based on subsequent fieldwork and compilations completed in adjacent map areas (Douglas, 1976). Framework geological bedrock mapping in Coal River map area was completed at 1:253 440-scale by the Geological Survey, largely during 1967 (Gabrielse and Blusson, 1969).

Preliminary versions of the bedrock geology for the map area were published as Yukon Geological Survey Open Files (Allen and Pigage, 2000; Pigage and Allen, 2001; Pigage 2004b). Similarly, results of the field work for 95C/5 were incorporated into a compilation bedrock geology open file map for the southwest quarter of 95C (Fallas *et al.*, 2004).

Mineral exploration between 1973 and 1986 identified U-Th-REE prospects in the contact metamorphic aureole of the Pool Creek syenite, sedimentary exhalative (SEDEX) targets in lower Paleozoic shales and carbonate rocks, and barite veins in Devonian carbonate rocks (Deklerk, 2008) in the Pool Creek map area. Recent mineral exploration on NTS map sheet 95C/5 during 2004-2005 has resulted in some exciting assays for nickel (True North Gems press release, 2006). No active mineral claims exist in NTS map sheet 95D/8; the single MINFILE occurrence (Gusty, 095D 002; Deklerk 2008) was discovered by Gabrielse and Blusson during regional mapping (1969). Hydrocarbon exploration activities have been largely east and north of the map area.

REGIONAL GEOLOGY

The map area contains eight successions of sedimentary rocks ranging from Proterozoic to Paleocene in age. Each succession consists of one or more formations with related lithologic facies and depositional environments. The informal term "succession" is used instead of "sequence" because of the precise surfaces and definitions associated with sequence stratigraphy (Catuneanu, 2003). The combined thickness for the sedimentary strata ranges from 5000 to 15 000 m.

In many cases, these successions are separated by unconformities, often marking significant hiatuses. Internally, the successions also locally contain unconformities. Unconformities have been identified underlying succession 2 (Cambrian-Ordovician), succession 6 (Permian), succession 7 (Triassic) and succession 8 (Paleocene). An inferred unconformity also separates succession 3 from succession 4.

Lower to middle Paleozoic strata are best preserved, with younger strata being only locally preserved. Units older than Jurassic are part of a regional west- to southwest-facing marine passive margin of ancestral North America. Sedimentary successions younger than Jurassic are depositionally linked to Cordilleran deformation caused by accretion of exotic terranes to the western margin of North America (Coney *et al.*, 1980).

Intrusive igneous activity in the Neoproterozoic and Eocene occurred in close proximity in the map area: the Proterozoic Pool Creek syenite and an Eocene biotite syenite are less than 1 km apart (Pigage and Mortensen, 2004). Extrusive volcanic rocks are dated stratigraphically or by isotopic age dating as Proterozoic, Cambrian to Ordovician, Paleocene and Eocene. Stratigraphic constraints on extrusive activity are locally poorly known. Proterozoic and Paleozoic volcanic rocks are basalts, and Paleocene and Eocene volcanic rocks include both rhyolite and basalt.

The map area contains structural features related to two deformation events, one pre-late Cambrian and the other post-Triassic. Evidence for the early deformation event is restricted to southeast-trending open folds in Proterozoic sedimentary rocks in the north-central part of the Pool Creek map area. Deformation features related to the second post-Triassic deformation event in the map area consist dominantly of reverse faults and associated open to tight folds. Faults and folds trend north to northeast. Structural styles for these features can be related to the different lithofacies present in the map area (Pigage, 2003).

STRATIGRAPHY

INTRODUCTION

Figure 3 is a schematic cross-section illustrating the regional distribution of the sedimentary successions. The formations and successions are illustrated in chronostratigraphic columns in Figures 4 and 5. These latter figures also indicate the local fossil control available for the different formations.

Succession 1 consists of Proterozoic siliciclastic sedimentary rocks and is exposed in the immediate hanging wall of the Beaver River thrust and the immediate hanging wall of the Toobally fault. Succession 2 (Cambrian-Ordovician) consists of shallow marine shelf to subaerial strata dominated by coarse, locally subarkosic sandstones and maroon siltstones and shales with lesser carbonate and mafic volcanic rocks. Succession 3 (Ordovician-Silurian) delineates shallow platformal carbonate and siliciclastic sediment deposition. The lateral transition from carbonate platformal sedimentary rocks of MacDonald platform to fine clastic, basinal sedimentary rocks of Selwyn basin is documented for the map area in succession 4 (Silurian-Devonian). Succession 5 marks a further major transgression and subsequent regression of seas during Devonian and early Carboniferous time. Deposition of shales, siltstones and fine sandstone during the Permian and Triassic denotes successions 6 and 7, respectively. Succession 8 is only locally preserved and documents terrestrial stream deposition during the Paleocene.

Preliminary descriptions and discussion of these stratigraphic successions were presented in Pigage (2006). More detailed discussions and descriptions of formations making up these successions are presented in the following sections.

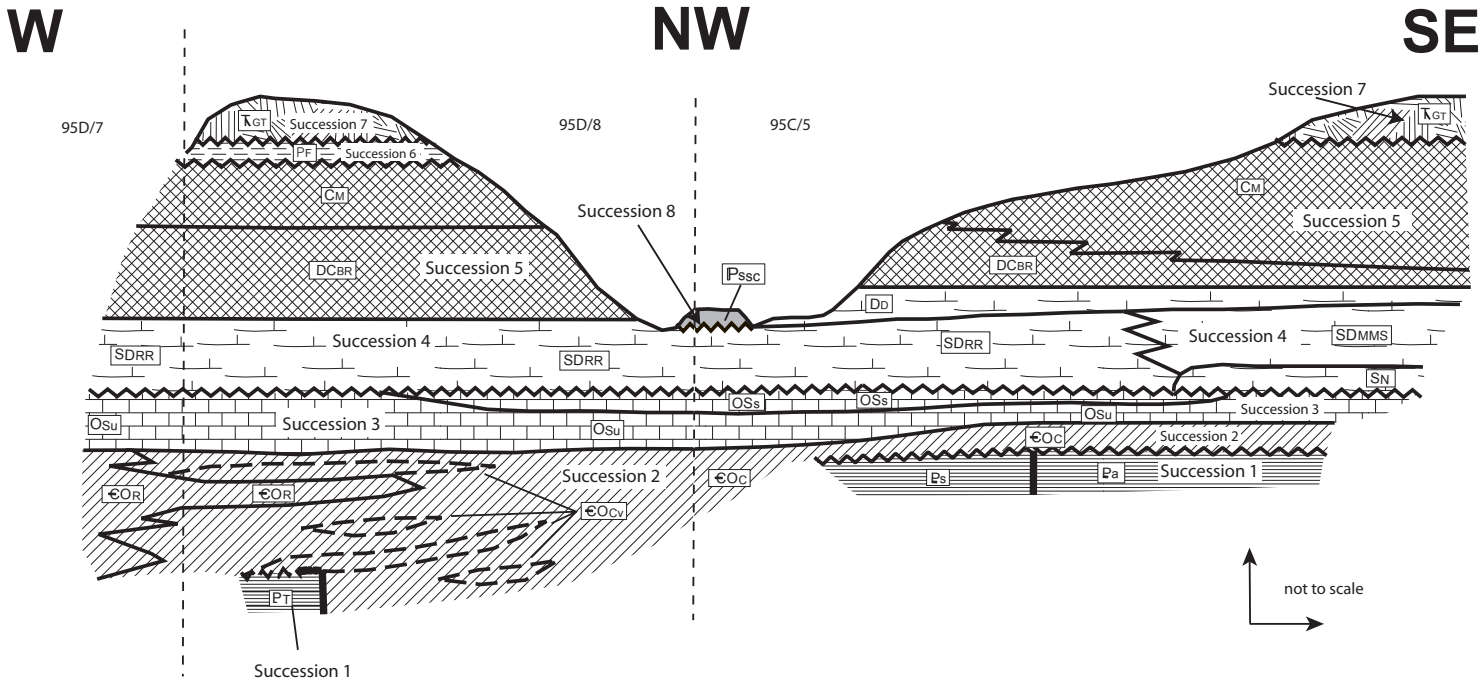
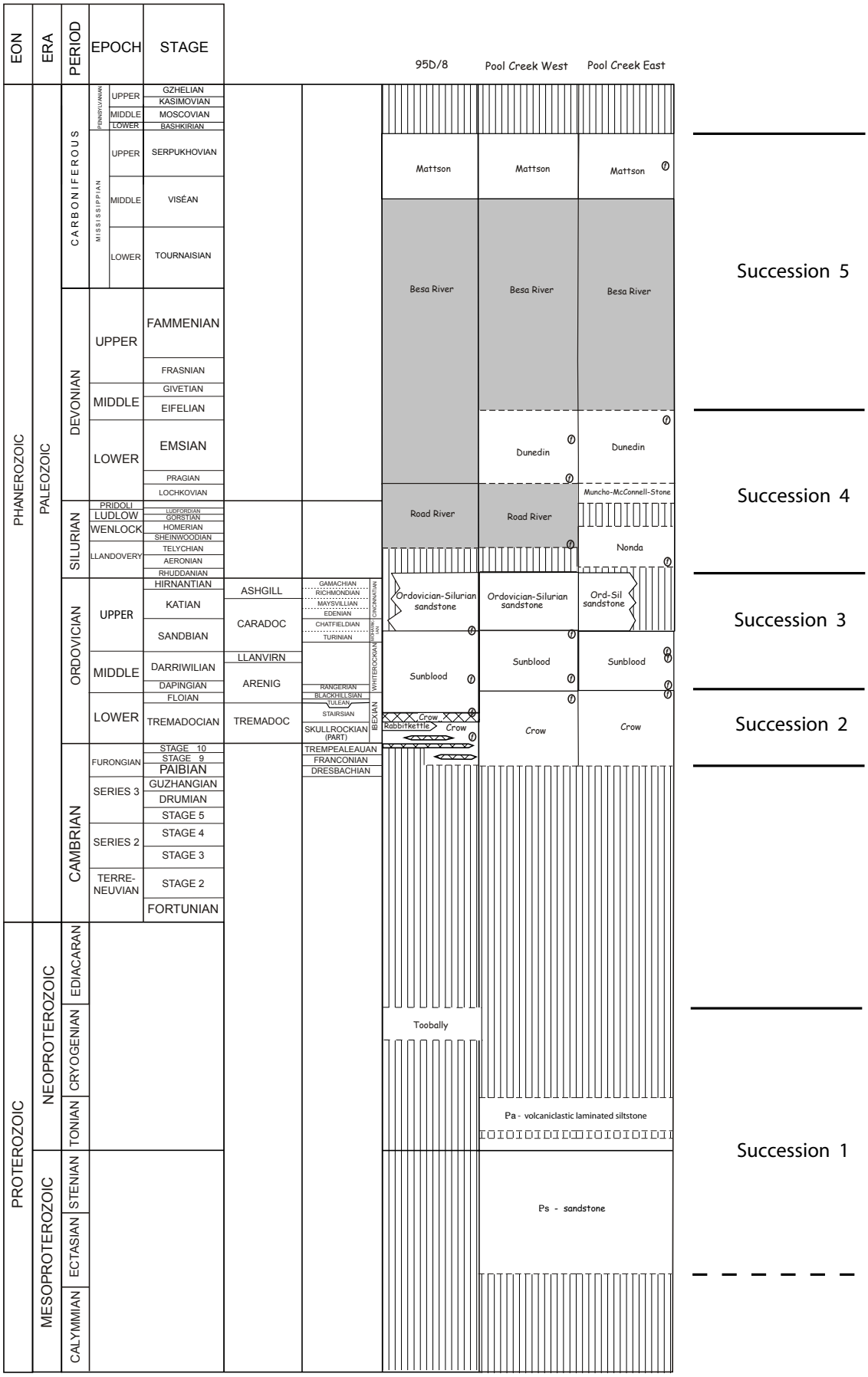


Figure 3. *Schematic cross-section for stratigraphy in 95C/5 and 95D/8. Not to scale. Left part of section oriented east-west; right part oriented northwest-southeast. Modified from Fallas et al. (2004) and Pigage (2006). Unconformity indicated by zigzag line.*

Figure 4.
Chronostratigraphic column for Proterozoic, lower and middle Paleozoic formations in Figure 3. Dashed contact line indicates age range is uncertain. Fossil control from Appendix IV indicated by letter 'f' enclosed by circle. Time scale from Gradstein et al. (2004).



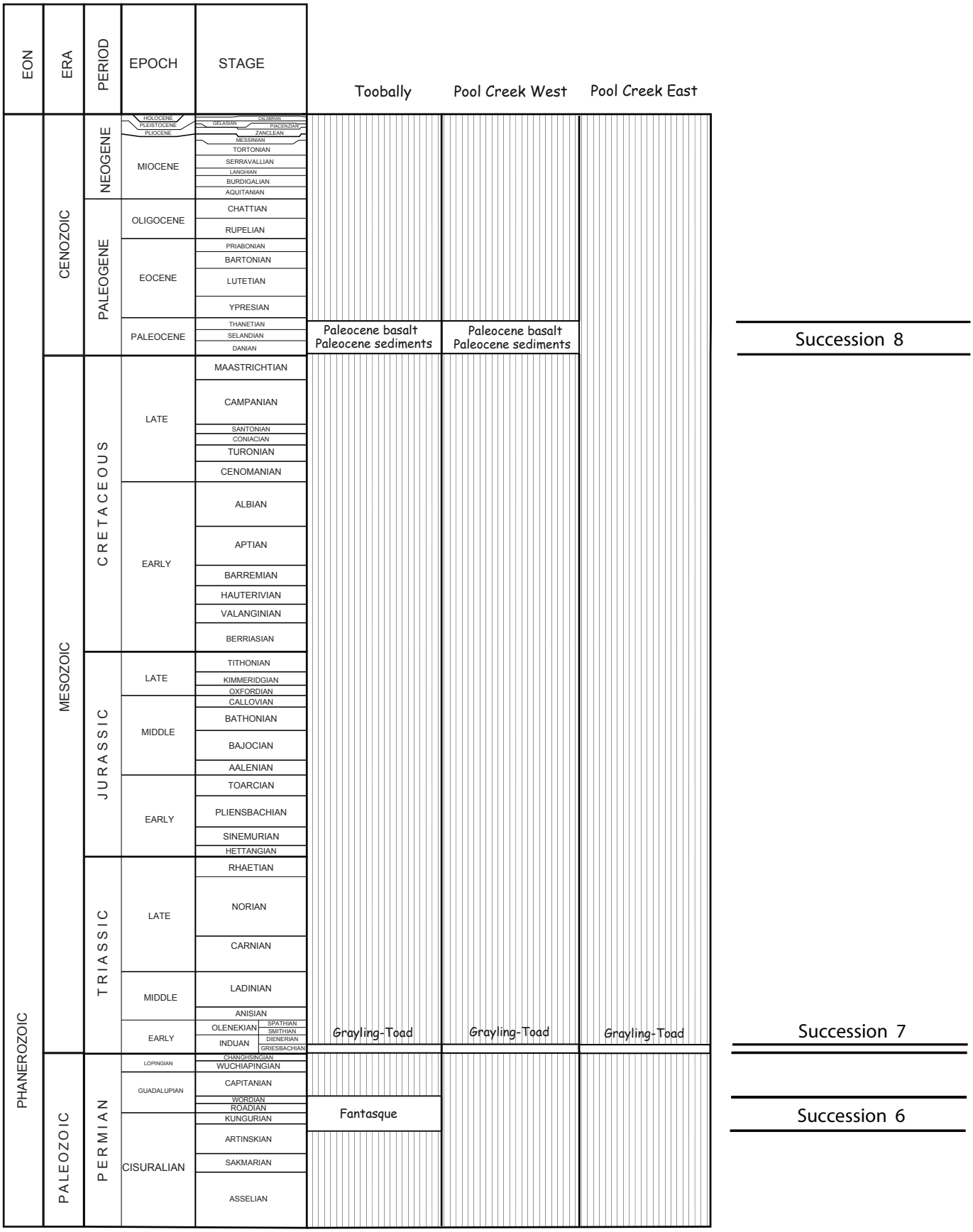


Figure 5. *Chronostratigraphic column for upper Paleozoic, Mesozoic and Cenozoic formations in Figure 3. Fossil control from Appendix IV indicated by letter 'f' enclosed by circle. Time scale from Gradstein et al. (2004).*

SUCCESSION 1 (PROTEROZOIC)

The oldest sedimentary succession is exposed in the core of the anticline in the west-central part of the Pool Creek map sheet and immediately west of the large Toobally Lake in the central part of map sheet NTS 95D/8. The succession in the Pool Creek map sheet is structurally floored by the west-verging Beaver River thrust (see Plate 1). It consists of siliciclastic sedimentary rocks which have been intruded by the Pool Creek nepheline syenite. This succession has been divided into two map units, a black to white quartz sandstone interbedded with siltstone and calc-silicate rock (Unit Ps), and a greenish, laminated volcaniclastic argillite and siltstone (Unit Pa). These two units are separated by an inferred fault, and stratigraphic relations between them are therefore unknown. Unit Ps is considered older than unit Pa because unit Ps is intruded by the Pool Creek syenite (650 Ma), suggesting it was located at a deeper crustal level when intruded in Neoproterozoic time. Outcrop patterns and bedding orientations for both of these units delineate open, east-southeast-trending folds which are not present in overlying strata.

In map sheet NTS 95D/8, succession 1 consists of the Toobally Formation (Pigage and MacNaughton, 2004), a massive to locally indistinctly bedded, orange-weathering, polymictic, matrix-supported conglomerate to pebbly mudstone. It is structurally floored by the east-verging Toobally fault (see Plate 2).

Proterozoic sandstone (Unit Ps)

Introduction

The Proterozoic sandstone/siltstone Unit Ps is best exposed on the ridge top immediately south of the Pool Creek nepheline syenite (UTM 344 500E/6 696 700N, zone 10). All lithologies are hornfelsed and are consequently very hard and resistant to weathering. Locally, the unit is gossanous with abundant orange-brown surface staining. Contacts between different lithologies are typically gradational with interbedding of rock types. The lower contact of this unit is not exposed and has been interpreted as structural (Beaver River thrust). The upper contact is eroded. The exposed thickness of the unit is approximately 335 m. The map pattern suggests that it may have a maximum exposed thickness of 450 m. A minimum inferred thickness of 400 m is reasonable.

Composition

Unit Ps consists of grey, laminated siltstone to sandstone interbedded with black, laminated phyllitic siltstone, massive, pale grey sandstone, cream to white, thin-bedded calc-silicate rock, and very minor white, clast-supported conglomerate with clasts consisting predominantly of quartz sandstone.

The predominant lithology in this unit is a thinly laminated, noncalcareous, fine-grained, argillaceous quartz siltstone. Laminae are spaced 2-10 mm and are wavy to planar parallel (Fig. 6). Beds typically range from 10 to 30 cm in thickness. The unit is largely medium to light grey, although intervals up to 35 m thick are dark grey to black. Weathered surfaces are commonly stained orange to rust brown with extensive, irregular dark brown pyrolusite coatings. No fossils are visible, and samples collected for microfossils are barren (Table IV-1, Appendix IV). Locally, beds show internal folding caused by sedimentary slumping (Fig. 7). More argillaceous intervals contain abundant ovoid contact metamorphic mineral aggregates up to 0.2 mm across (Fig. 8). Siltstone

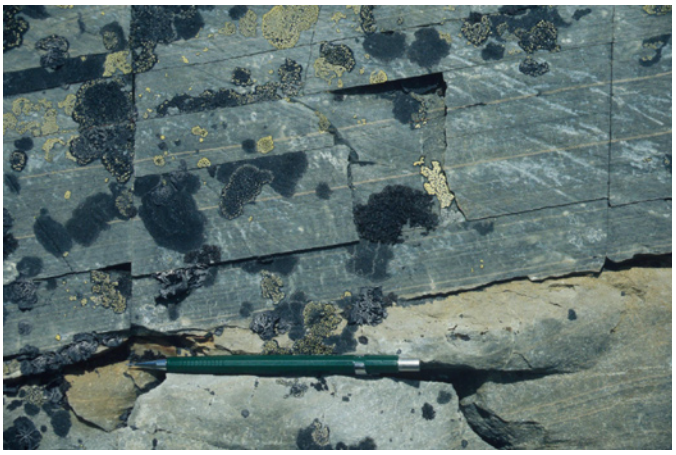


Figure 6. *Finely parallel-laminated quartz siltstone of Unit* ***Ps****, field station 00LP027. Pencil in centre of photo is 14 cm long.*

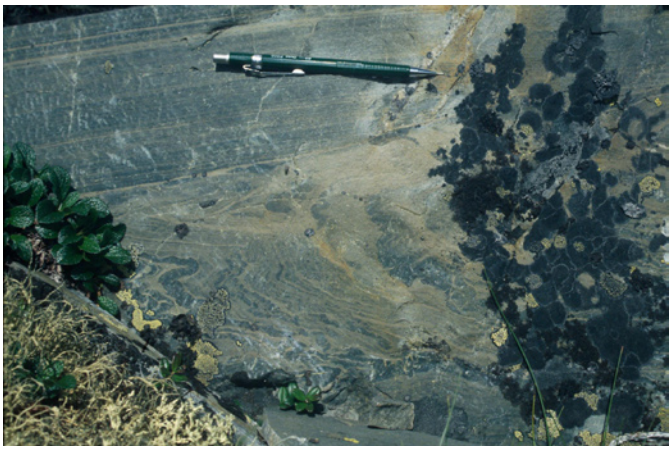


Figure 7. *Soft sediment deformation folds in finely laminated quartz siltstone of Unit* ***Ps****, field station 00LP027. Pencil in centre of photo is 14 cm long.*

intervals interbedded with shale are typically graded (Fig. 8).

A 0.5 m-thick, clast-supported conglomerate occurs on the ridge immediately south of the Pool Creek syenite. The conglomerate consists of white sandstone clasts up to 10 cm across in a white quartz sand matrix.

A massive, white, noncalcareous, medium-grained, quartz sandstone forms a 35 m-thick distinctive marker horizon in the lower part of the unit. Rarely, bedding is delineated by thin, discontinuous siltstone lenses within the massive sandstone (Fig. 9). Both upper and lower contacts are gradational with 10 cm-thick white quartz sandstone beds intercalated with overlying and underlying dark grey to black laminated siltstones. Clasts within the quartz sandstone range from 0.2 to 0.6 mm across and consist of monocrystalline quartz which locally displays epitaxial quartz overgrowths (Fig. 10). The clasts have slight undulatory extinction and intergrown, recrystallized margins.

A thinly banded, strongly hornfelsed calc-silicate rock is exposed immediately south of the Pool Creek syenite. Beds within the calc-silicate rock are 2 to 10 cm thick. Light grey-weathering marble intervals weather recessively, and cream to pale green calc-silicate interbeds weather as resistant ridges. Within calc-silicate intervals, K-feldspar-rich bands alternate with calc-silicate-rich bands (tremolite).

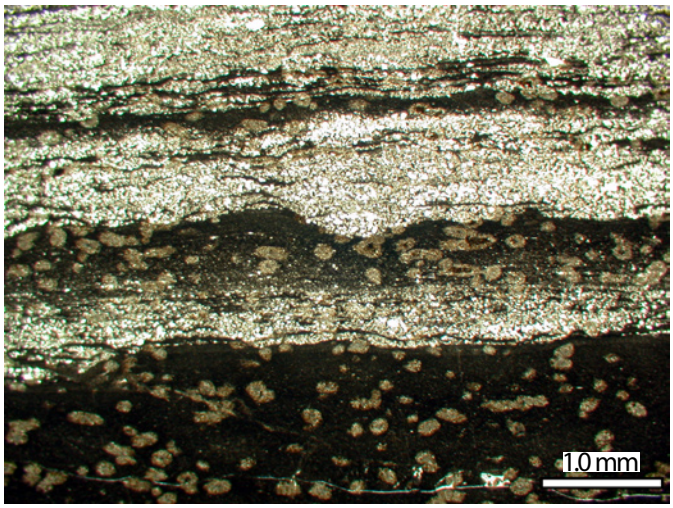


Figure 8. *Thin section photo of dark grey argillaceous, hornfelsed siltstone of Unit* **Ps**, *field station 00LP029. Ovoid, unknown metamorphic mineral is preferentially developed in more pelitic intervals. Note graded bedding visible in centre of photo, plane light. Scale bar is 1.0 mm.*



Figure 9. *Rare siltstone interbed within massive quartz sandstone of Unit* **Ps**, *field station 00LP031. Scale card visible in right centre; divisions are in centimetres.*

Depositional environment, age and correlation

The fine planar laminae within the dominant siltstones indicate a quiet depositional environment below wave-base. Deposition is interpreted as near offshore because of the thick accumulation of sand-sized material. The occurrence of soft sediment deformation features indicates local transport and deposition on a slight slope.

Douglas (1976) assigned this unit to the Besa River and Mattson formations. More recently, Allen *et al.* (2001) mapped this formation as units 1, 2 and part of unit 3, and tentatively considered it to be Precambrian. This unit is intruded by the 650 Ma Pool Creek nepheline syenite and syenitic dykes (Pigage and Mortensen, 2004) and must therefore be older than these intrusions. Tables I-2a through I-2c in Appendix I contain a detailed listing of U-Pb isotopic dates for detrital zircon grains from three

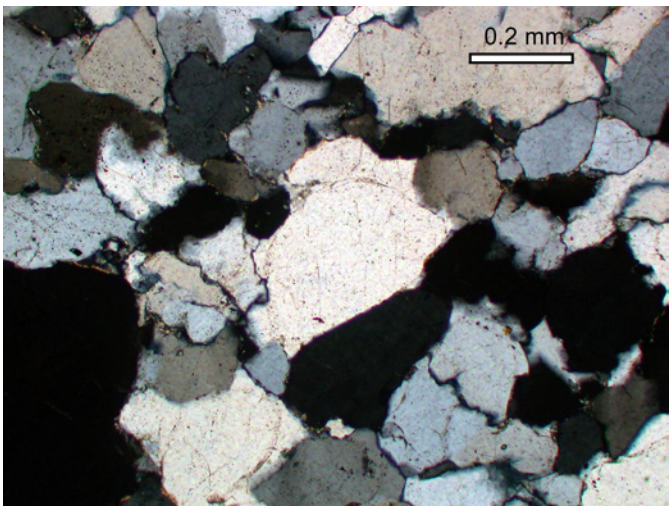


Figure 10. *Thin section photo of massive quartz sandstone of Unit* **Ps**, *field station 04LP027. Epitaxial quartz overgrowths locally on margins of clasts. Quartz clasts display interlocking textures with metamorphic recrystallization and development of subgrains, crossed nicols. Scale bar is 0.2 mm.*

quartz sandstone samples within Unit Ps. The minimum detrital zircon age from the samples is 1723 ± 42 Ma. A maximum stratigraphic age for the unit is therefore approximately 1700 Ma.

Exposed Proterozoic sedimentary rocks in the Canadian Cordillera have been divided into three sequences A, B and C (Young *et al.*, 1979). Sequence C (0.78 to 0.57 Ga) is the youngest and correlates with the Windermere Supergroup (Aitken and McMechan, 1991). Sequence B (1.2 Ga to 0.78 Ga) correlates with the Mackenzie Mountains Supergroup and is exposed in northern Yukon. Sequence A (1.7 to 1.2 Ga) consists of the Purcell (Belt) Supergroup of southern British Columbia, the Wernecke Supergroup and the Pinguicula Group in northern Yukon, and the Muskwa Assemblage of northeastern British Columbia. Given the above isotopic age constraints, Unit Ps is a possible correlative with any of sequences A, B or C.

Geographically, the closest possible correlative is the Hyland Group (Gordey and Anderson, 1993) located 95 km to the west (Gabrielse and Blusson, 1969). Hyland Group strata, however, represents the uppermost part of the Windermere Supergroup (Walker, 1926; Eisbacher, 1981) and is therefore younger than this unit. In northeastern British Columbia (immediately northeast of the Northern Rocky Mountain Trench), Ferri *et al.* (1999) have mapped Neoproterozoic carbonate rocks and quartzite (Unit Pcq) underlying the Gataga volcanics (689 ± 4.6 Ma) which they tentatively correlated with the lower Windermere Supergroup; their Unit Pcq may be correlative with this unit.

A detrital zircon study of a suite of samples from Mackenzie Mountains Supergroup (sequence B) in northern Yukon resulted in numerous dates in the 1000 to 1300 Ma range (Rainbird *et al.*, 1997). Because these ages are absent from the Unit Ps detrital zircons, Unit Ps is not considered to be correlative with Mackenzie Mountains Supergroup (sequence B).

In northeastern British Columbia, sequence A is represented by a 6 km-thick section of carbonate rock, shale and siltstone with lesser sandstone of the Muskwa assemblage. The base of the Muskwa assemblage is not exposed, and it is unconformably overlain by Windermere Supergroup strata (Aitken and McMechan, 1991). Fallas *et al.* (2004) considered Unit Ps as possibly being correlative with the Muskwa assemblage. A detrital zircon study of four sandstone units from the Muskwa assemblage resulted in an age range of ca. 3075-1766 Ma with a concentration of ages near 1850 Ma and a notable lack of ages in the interval 1920-2000 Ma (Ross *et al.*, 2001). In contrast, the Ps samples have a significant number of detrital zircon ages in the interval 1950-2000 Ma (see Appendix I). Because of this age distribution, Unit Ps is not considered correlative with the Muskwa assemblage.

In northern Yukon, sequence A consists of three unconformity-bounded successions, the oldest Wernecke Supergroup, the Slab volcanics and the youngest Pinguicula Group (Thorkelson, 2000; Thorkelson *et al.*, 2005). Deposition of Wernecke Supergroup sediments preceded emplacement of the Wernecke breccias (Thorkelson *et al.*, 2001b) at 1600 Ma. Deposition of the lowermost Unit A of the Pinguicula Group preceded volcanism (Hart River volcanics) and intrusion of the Hart River sills at about 1380 Ma (Abbott, 1997; Thorkelson *et al.*, 2005). Isotopic age dates for 10 detrital zircon analyses from the basal Pinguicula Group have clusters at 1841-1984 Ma and 2497-2719 Ma (Thorkelson *et al.*, 2005), similar to the bimodal pattern of detrital zircons from Unit Ps; detrital zircon ages of the lowermost Pinguicula Group are therefore permissive with Pinguicula Group being correlative with Unit Ps.

Summary

In summary, Unit Ps is Proterozoic (greater than 650 Ma old and younger than 1700 Ma old), consists of predominantly siliciclastic lithologies, and is correlated regionally with either lowermost sequence C strata in northeastern British Columbia (Windermere Supergroup) or uppermost sequence A strata in northern Yukon (Pinguicula Group). Because Unit Ps is considered to be older than Unit Pa, Pinguicula Group is the preferred correlative strata for Unit Ps. Limited detrital zircon studies of Proterozoic units in Yukon and northern British Columbia precludes more specific regional correlation with strata from north Yukon or northeastern British Columbia. Additional detrital zircon research may further restrict the age of deposition of Unit Ps and more tightly constrain detrital zircon patterns for possible correlative strata.

Proterozoic volcaniclastic laminated argillite (Unit Pa)

Introduction

Extensive outcrops of Unit Pa occur on the ridge centred at UTM 346 000E/6 695 000N, zone 10. Rob MacNaughton measured a 372 m-thick stratigraphic section through part of this unit (Allen *et al.*, 2001). The following descriptions are based partly on this measured section. The exposed extent of this formation suggests an approximate thickness of at least 500 m. The lower and upper contacts are not exposed. Unit Pa is interpreted to be in fault-contact with Unit Ps. The Cambrian-Ordovician Crow Formation (see below) unconformably overlies this unit. As with Unit Ps, macroscopic east-southeast-trending open folds in Unit Pa are not present in the overlying stratigraphic units.

Minerals recognized in thin section include quartz, chlorite, epidote and sericite with local amphibole and calcite. Quartz grains are typically monocrystalline. In some samples, incipient hornfels biotite is disseminated through the more argillaceous intervals. Although syenite dykes were not noted in this unit, the metamorphic minerals are considered to be in response to intrusion of the Pool Creek nepheline syenite.

Composition

The predominant lithology consists of greyish green, banded, argillaceous siltstone and argillite with thin, cream-coloured, locally calcareous or dolomitic, very fine-grained, argillaceous sandstone interbeds. Lesser lithologies up to 3 m thick include bedded limestone, very fine-grained to fine-grained pale green sandstone, intraformational breccia to conglomerate, and volcaniclastic conglomerate to breccia.

The argillaceous siltstone and argillite is typically bedded on a 1 to 5 cm scale, with sandstone forming 5-50% of the interval (Fig. 11). Both lithologies are commonly internally laminated; current ripple cross-lamination occurs sporadically. Marginal contacts between the siltstone-argillite and sandstone range from sharp to normally graded. Soft sediment deformation features are common and include loading, convolute bedding, intraformational truncation surfaces, and isoclinal slump folds for intervals ranging up to several metres thick (Fig. 12). Locally, this banded unit may contain dispersed, large (up to 40 cm across), subround to angular grey limestone clasts confined to an approximate stratigraphic horizon (Fig. 13); bedding wraps around these large clasts.

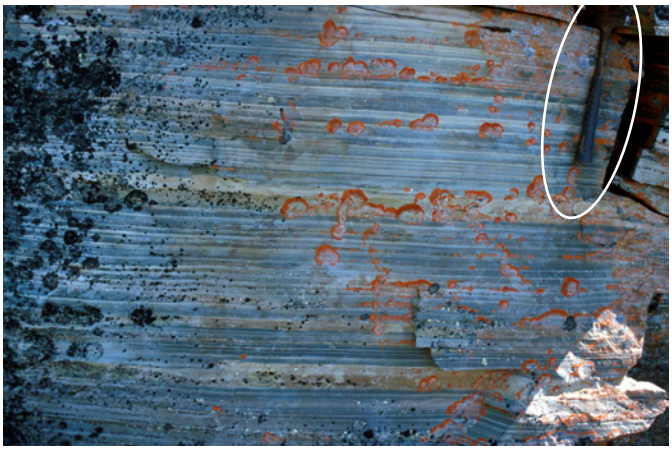


Figure 11. *Typical interlaminated siltstone and sandstone forming the predominant lithology of Unit* ***Pa****, field station 01LP001. Hammer (circled) for scale in upper right of photo.*

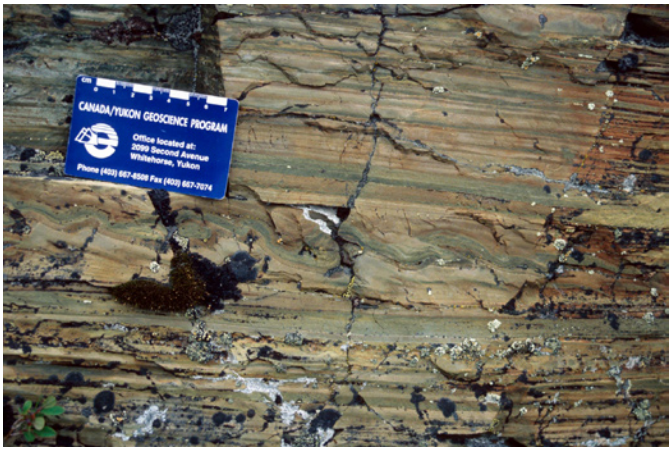


Figure 12. *Soft sediment deformation in Unit* ***Pa****, field station 00LP008. Photo by T. Allen. Major scale divisions in centimetres.*



Figure 13. *Limestone clast (30 x 40 cm) within soft sediment deformed zone of greenish grey laminated siltstone unit* ***Pa****, field station 00TLA019. Photo by T. Allen.*

In several outcrops on the south-facing slope of the above-mentioned ridge, the interbedded argillaceous siltstone and sandstone have intervals up to 5 m thick where the background colour is maroon instead of green. The maroon variant has sharp marginal contacts with the more typical green-coloured type (Fig. 14).

Fine to medium coarse-grained, slightly dolomitic, green- to orange- to tan-weathering, thin- to medium-bedded sandstone forms intervals ranging from 10 cm to 2 m in thickness locally (Fig. 15). Beds typically range from 1 to 15 cm in thickness and are sometimes normally graded. Internally, the sandstone is generally planar laminated. Lesser interbeds of argillaceous siltstone occur within these sandy intervals. Within the measured stratigraphic section, sandstone intervals constitute slightly less than 15% of the entire interval.



Figure 14. *Contact between greenish grey and maroon (on top) banded siltstone in Unit* **Pa**. *(Maroon siltstone unit is approximately 5 m thick and calcareous), field station 00LP008. Photo by T. Allen. Contact occurs approximately at hammer head.*

Breccia and conglomerate intervals ranging from centimetres to metres in thickness are dispersed throughout the formation. Clasts within these intervals are characterized by subround to angular shapes and granule to cobble sizes (Fig. 16). These coarser clastics may be either matrix-supported or clast-supported, with a muddy silt to sand matrix. In some beds, clasts are intraformational, consisting mainly of randomly oriented argillaceous siltstone. In others, the clasts are dominantly allochthonous, consisting largely of limestone or green to maroon basalt. Some breccia beds were observed to pass laterally into slumped horizons or into successions of argillaceous siltstone cut by intraformational truncation surfaces. Conglomerate to breccia intervals constitute less than 5% of the measured stratigraphic section.

One distinctive, greyish red, clast- to matrix-supported, poorly sorted, polymictic, basaltic cobble conglomerate forms a laterally discontinuous member (Unit **Pa-bc**) with



Figure 15. *Orange-weathering, slightly dolomitic sandstone interval within Unit* **Pa**, *field station 05LP025. Detrital zircon sample 05LP025 was collected from this outcrop.*

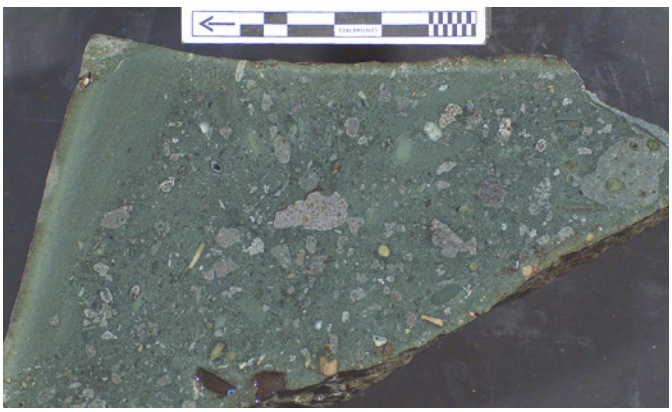


Figure 16. *Cut slab of volcaniclastic breccia sample from Unit* **Pa**. *Photo by Bryan Rutley. Large scale division is 1 cm.*

a strike length of approximately 600 m and a thickness ranging up to 20 m. This member is well exposed near UTM 345 500E/6 694 600N, zone 10. Clasts are subround to subangular, ranging from granules to cobbles. The matrix is predominantly greyish red, very fine-grained, poorly sorted sandstone. Clasts are predominantly basalt (75%) with lesser pale grey to white vein quartz (5%), carbonate rock (5%), sandstone and other unidentified material (15%) (Fig. 17). Basalt clasts typically contain scattered plagioclase microphenocrysts in a groundmass of felted plagioclase microlites and very fine-grained, dark reddish brown material (Fig. 18) Locally, the clasts are amygdaloidal with chlorite, carbonate minerals and quartz infilling subround to irregular vesicles. Argillaceous siltstone immediately beneath the lower contact of this conglomerate contains numerous soft sediment deformation folds.



Figure 17. *Maroon basalt conglomerate member (**Pa-bc**) within Unit **Pa**. Note large sandstone clast near top of outcrop, field station 00TLA009. Photo by T. Allen.*



Figure 18. *Closeup of subangular basalt clasts in Unit **Pa-bc**. Subangular white vein quartz clast in lower right corner of photograph. Field station MWB01-01-07. Photo by Rob MacNaughton.*

Depositional environment

The general fine grain size and lack of high-energy primary sedimentary structures indicate the depositional environment for Unit **Pa** was in quiet water. Similarly, the absence of wave-produced structures is consistent with deposition below wave-base. During periods of sandstone deposition, the supply of sandy sediment was obviously greater. The prevalence of slumping suggests deposition on a slope setting rather than a platform setting (Dalrymple and Narbonne, 1996). The slope setting is also indicated by the massive, unsorted character of the interbedded breccias and conglomerates. The basalt conglomerate member **Pa-bc** is interpreted as a submarine channel deposit because of its restricted occurrence.

The uniform presence of epidote, chlorite and local amphibole in the formation suggests a significant volcanic component to the source provenance. This volcanic setting for the source area is reinforced by the extensive volcanic material in clasts of many of the breccias and conglomerates. Extensive volcanic rocks may also reflect a tectonically active setting.

Geochemistry

Table III-1 (Appendix III) lists lithogeochemical analyses for several samples from this unit. Some of these analyses were previously published along with analyses of volcanic rocks immediately west of Toobally Lake (Pigage and MacNaughton, 2004). Hornfelsing and possible addition of a detrital clastic component to these samples suggests that the analyses may not be fully amenable to interpreting tectonic setting using discriminant diagrams. Samples from basalt clasts in the basaltic conglomerate member are more likely to be representative of the original volcanic rock. Slightly higher LOI (loss on ignition) values for the analyses indicate some alteration and possible mobility of elements. Given these caveats, it still remains useful to look at various discriminant diagrams.

Figure 19 plots the major oxides from Table III-1 (Appendix III) in a Harker diagram. All samples consisting dominantly of volcanic rocks (except for sample C-417058) contain less than 51% SiO_2. Outside of the SiO_2 content, sample C-417058 cannot be uniquely distinguished from the other samples. This suggests that C-417058 may contain detrital or vein quartz, which has only slightly diluted the amounts of the other plotted oxides. Figure 19 further illustrates that the three green volcanic breccia samples contain higher CaO contents than the other samples; the reason for this difference is unknown.

In Figure 20 several elements commonly used in discriminant diagrams are plotted against LOI (loss on ignition) to test for immobility. Figure 20 infers that

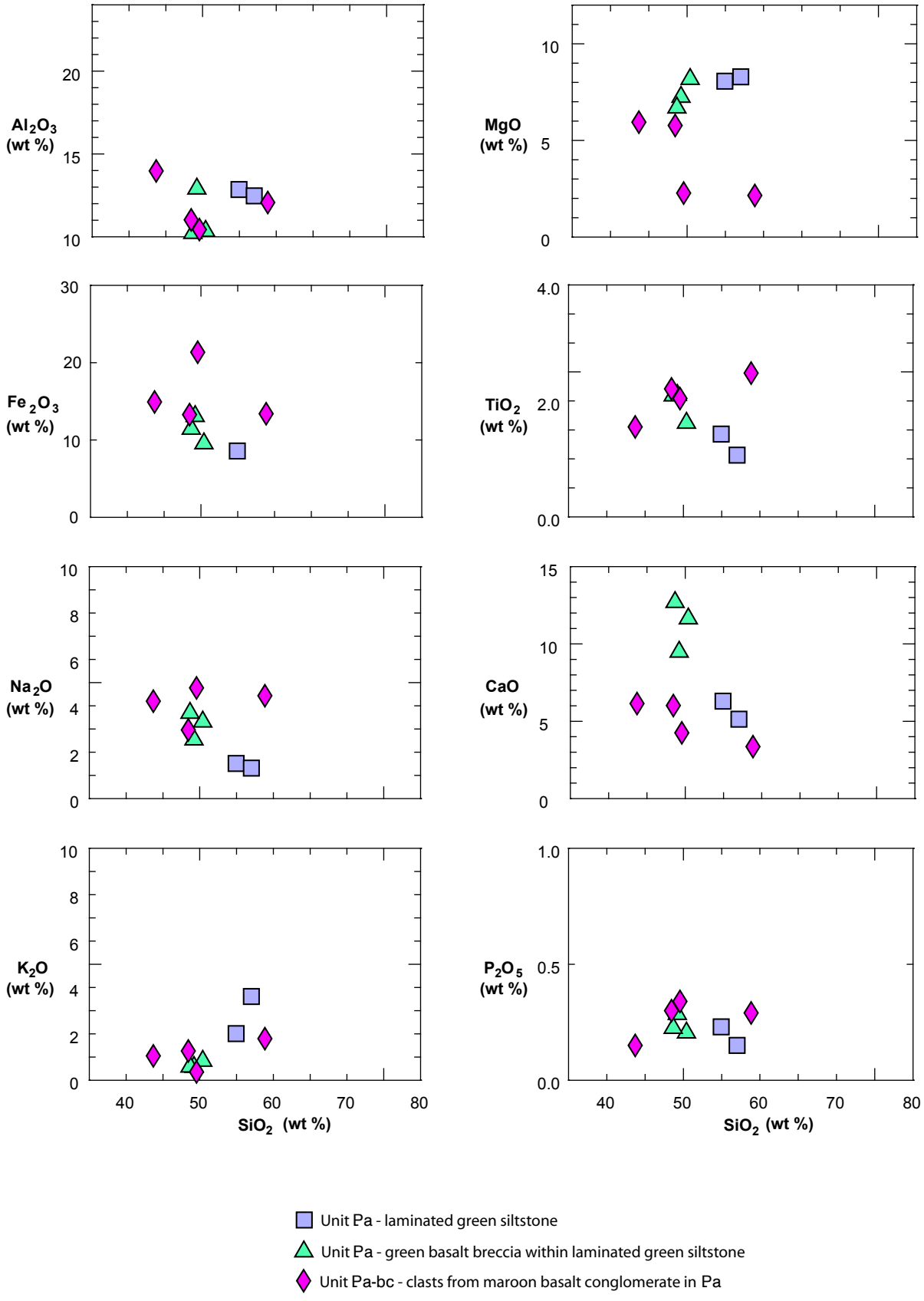


Figure 19. *Harker diagram of major oxides vs SiO_2 for different lithologies in Unit* ***Pa****. Analyses listed in Table III-1 (Appendix III).*

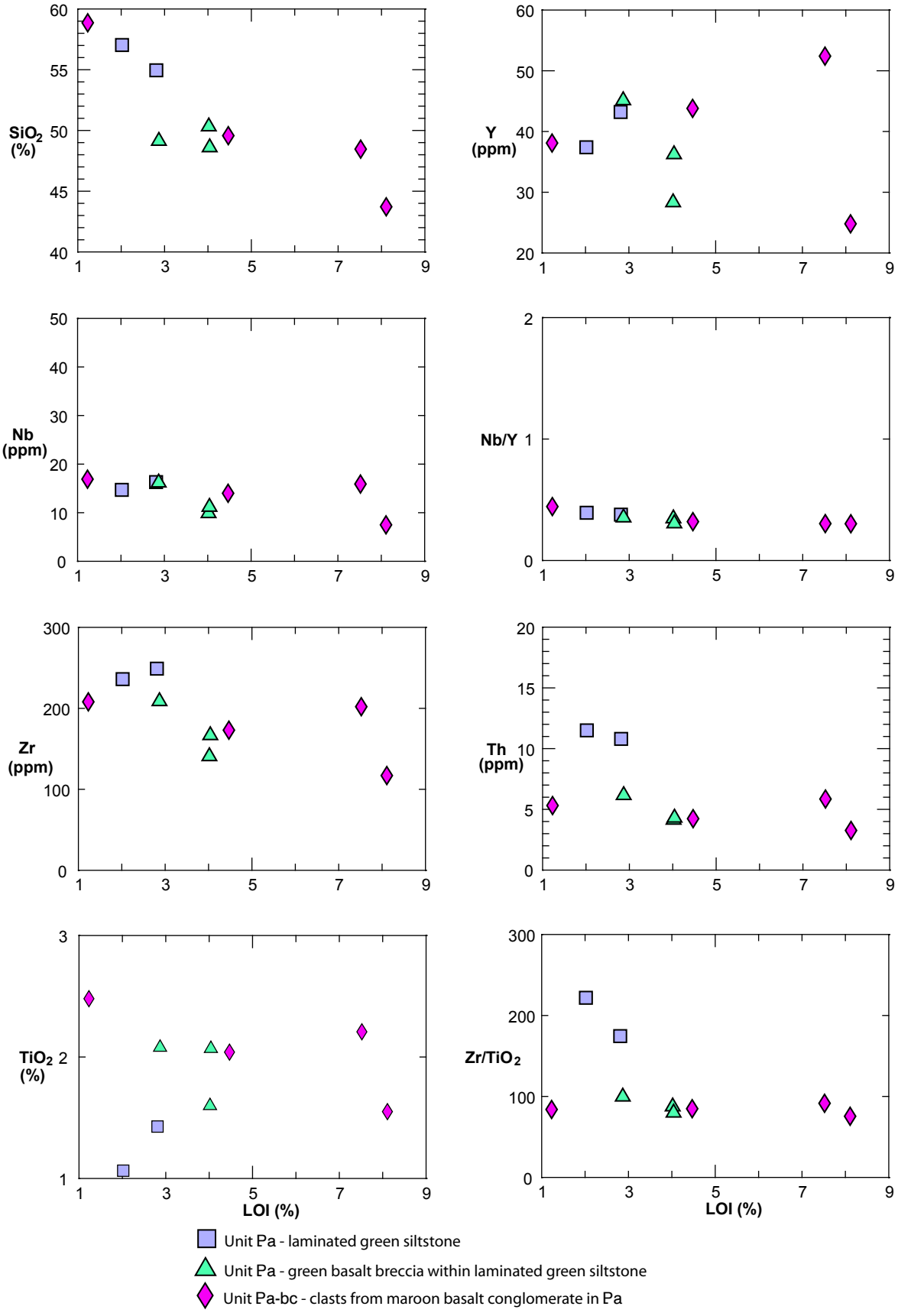


Figure 20. *Bivariate plots of elements and element ratios vs LOI (loss on ignition). Increasing LOI approximately indicates increasing alteration and metamorphism. Analyses from Table III-1 (Appendix III).*

increasing LOI corresponds to an increasing extent of alteration and/or metamorphism. Systematic linear increasing or decreasing patterns for the plotted elements with increasing LOI are not obvious. Therefore alteration and metamorphism have not significantly affected the validity of the various discriminant diagrams utilizing the analyses in Table III-1 (Appendix III).

Volcanic rock samples plot in the subalkaline basalt field in a Zr/Ti - Nb/Y diagram (Fig. 21a; Pearce, 1996; modified from Winchester and Floyd, 1977). In contrast, the samples from the volcaniclastic siltstone plot in the andesite/basalt field. Displacement of these samples to higher Zr/Ti values may be related to addition of detrital zircon. All samples have a general oceanic island basalt (OIB) signature in multi-element diagrams normalized to primitive mantle (Fig. 21b). The two volcaniclastic siltstone samples have element ratios very similar to those delineated for the basalt clast samples. All samples are slightly enriched in heavy rare earth elements (HREE), slightly depleted in light rare earth elements (LREE) and show a significant negative Nb anomaly relative to OIB.

Tectonic discriminant diagrams do not delineate an incisive tectonic domain for the analyzed basalts (Fig. 22). In the Pearce-Cann (1973) Ti-Zr-Y diagram (Fig. 22a) the basaltic clast and breccia samples cluster in the corner of fields B, C and D, and the volcaniclastic siltstone samples plot in the calc-alkali basalt field C. Displacement of the volcaniclastic siltstone samples into field C is consistent with addition of detrital zircon. In the Th-Hf-Ta diagram (Fig. 22b) of Wood (1980), the samples all plot within the (calc-alkaline) volcanic arc field. Similarly in the Nb-Zr-Y diagram (Fig. 22c), the samples plot in the combined volcanic arc and within plate tholeiite field (Meschede, 1986). However in the Ti-V diagram (Fig. 22d) of Shervais (1982), the samples all plot in the midocean ridge basalt (MORB) to back-arc MORB and alkaline fields and are well away from the volcanic arc fields.

Enrichment in Th/Yb ratio relative to the mantle array in Figure 22e (Pearce and Peate, 1995) is related to either crustal contamination or subducted slab metasomatism. Offset of the samples from Table III-1 (Appendix III) away from the mantle array supports crustal contamination and/or influx of a detrital crustal component. Because several of the analyses were for individual clasts that did not contain any detrital component, crustal contamination of the magma during ascent is the preferred inference.

In summary, these various diagrams indicate samples are subalkaline basalts with an oceanic island basalt (OIB) geochemical affinity. The volcanic rocks have been affected by crustal contamination, which is attributed to contamination of the magma during ascent rather than to influx of detrital crustal material. Although some of the discriminant diagrams suggest a volcanic arc setting, other diagrams are more consistent with an oceanic to back-arc basin setting. Their geochemistry is permissive with a continental rift setting; their subalkaline composition is indicative of rifting where the source for the basaltic melt is mantle beneath attenuated continental crust.

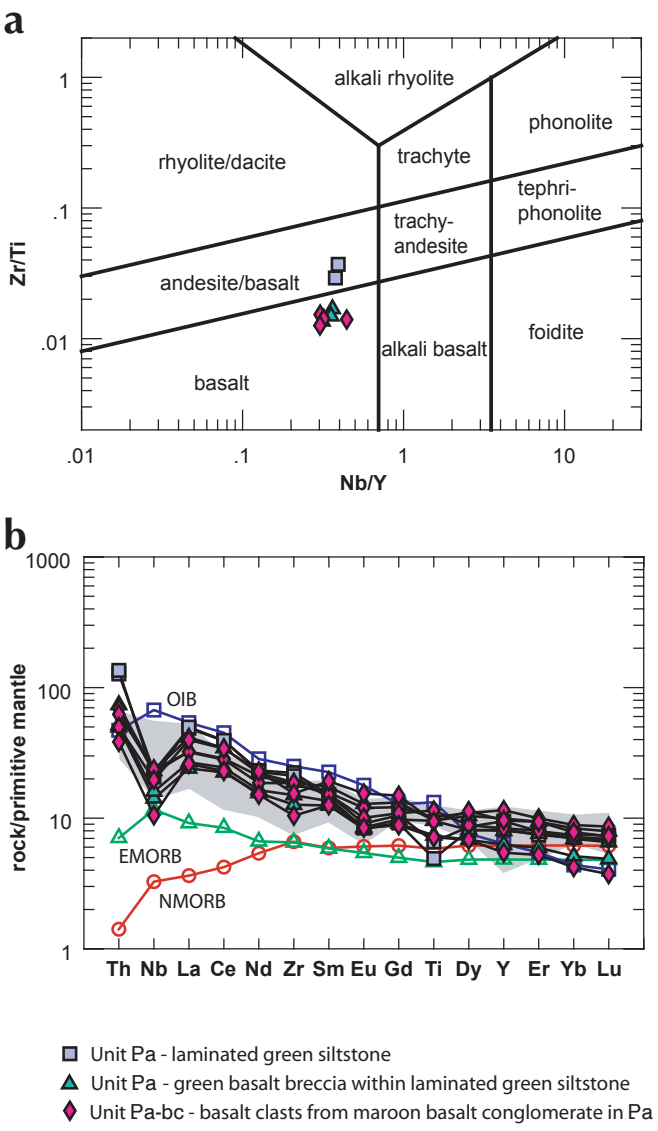


Figure 21. *Compositional diagrams for analyses in Table III-1 (Appendix III).* ***(a)*** *Zr/Ti - Nb/Y diagram from Pearce (1996), modified from Winchester and Floyd (1977);* ***(b)*** *multielement diagram normalized to primitive mantle (Sun and McDonough, 1989). EMORB (enriched midocean ridge basalt), NMORB (normal midocean ridge basalt), and OIB (oceanic island basalt); reference analyses are included. Shaded area indicates composition for analyses of Little Dal basalt in northeastern Yukon (Dudas and Lustwerk, 1997).*

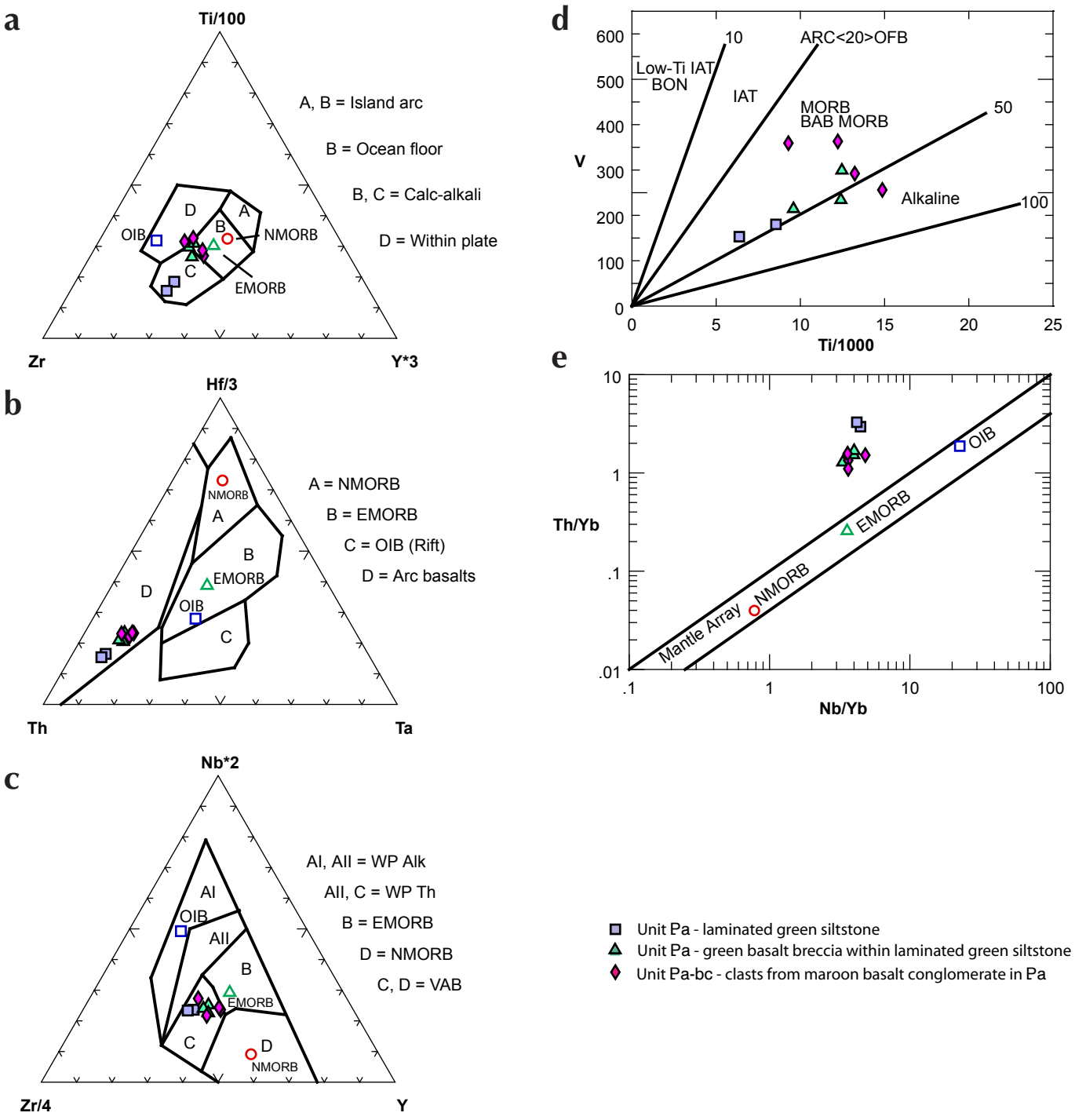


Figure 22. *Tectonic discriminant diagrams for analyses in Table III-1 (Appendix III), Unit* Pa. ***(a)*** *Ti-Zr-Y plot from Pearce and Cann (1973);* ***(b)*** *Hf-Th-Ta from Wood (1980);* ***(c)*** *Nb-Zr-Y from Meschede (1986);* ***(d)*** *V-Ti from Shervais (1982), IAT=island arc tholeiite, BON-boninite, BAB=back-arc basin, OFB=ocean floor basalt;* ***(e)*** *Th/Yb-Nb/Yb from Pearce and Peate (1995). EMORB, NMORB, and OIB as in Figure 21. WP Alk = within plate alkalic; WP Th = within plate tholeiitic, VAB = volcanic arc basalt; MORB = midocean ridge basalt.*

Age and correlation

Unit Pa corresponds to Unit 1 of Douglas and Norris (1959). More recently, Allen *et al.* (2001) described this formation as Unit 3 and subunit 3a. Douglas and Norris correlated this unit with the Proterozoic Apekunni Formation of southern Alberta based on lithologic similarity.

The volcaniclastic laminated argillite-siltstone unit is pervasively moderately hornfelsed. Hornfelsing is interpreted to be caused by intrusion of the nearby 650 Ma Pool Creek syenite (Pigage and Mortensen, 2004). Consequently, a minimum age for this succession is 650 Ma. This age is consistent with the unit being unconformably overlain by Cambrian-Ordovician Crow Formation containing an Ibexian (Middle Ordovician) conodont assemblage.

Samples were collected from large limestone clasts in three locations and an interbedded limestone locality (Table IV-1, Appendix IV) for possible microfossils. The limestone clast samples were barren. The limestone bed outcrop yielded nine conodont elements with a suggested Middle Ordovician age. Because of the intrusive and stratigraphic relations described above, this age is suspect and is considered to result from contamination of the sample with glacial float (Sunblood Formation?) during sample collection. Attempts to isotopically date ($^{39}Ar/^{40}Ar$) basalt clasts from the basaltic conglomerate member were unsuccessful (Villeneuve, pers. comm., 2004; sample 00TLA009, Appendix II).

Detrital zircon age dating was completed on two samples of unit Pa: one from a dolomitic sandstone (05LP025) and one from a laminated siltstone (05LP026). Tables I-3a and I-3b, Appendix I contain the zircon ages for samples 05LP025 and 05LP026, respectively. Figures I-7 and I-8 illustrate Concordia and probability distribution plots for the two samples. Figure I-9 is a composite diagram of the probability distribution for the two samples.

Both samples show a large number of zircon ages ranging between 1000 Ma and 1500 Ma as well as having muted peaks at 1800 Ma and older than 2500 Ma. Seven ages from the two samples are less than 1000 Ma (654 ± 25 Ma, 722 ± 41 Ma, 831 ± 12 Ma, 908 ± 20 Ma, 946 ± 12 Ma, 983 ± 26 Ma, 994 ± 69 Ma). Although these seven younger ages do not form a single cluster, the presence of several grains in this age range suggests the minimum depositional age for Unit Pa is younger than 1000 Ma and may be as young as 654 Ma (excluding the error range). This minimum age is consistent with Unit Pa displaying a contact metamorphic effect from the Pool Creek syenite.

The distribution of detrital zircon ages >1000 Ma for Unit Pa can be readily explained by the presence of two source provenances contributing zircons to the samples. The zircon ages >2500 Ma and zircon ages in the age range 1600-2400 Ma correspond to zircon ages present in North American basement in Alberta and Northwest Territories just to the east and northeast of the map area (Figure I-6). The zircon ages ranging from 1000-1500 Ma have previously been noted by Rainbird *et al.* (1992; 1997) as being typical for Mackenzie Mountains Supergroup strata. They attributed these zircon ages to transport of zircons sourced in exposed rocks of the Grenville orogen by large northwest-directed drainages during Mackenzie Mountains Supergroup deposition. Zircons in Unit Pa either denote this drainage pattern still existed during Pa deposition or zircons have been recycled from eroded Mackenzie Mountains Supergroup strata.

The depositional age of Unit Pa inferred above is consistent with the depositional ages of the lower Winderemere Supergroup (sequence C). Windermere-age volcanic units in the northern Cordillera include the Little Dal basalt, the Mount Harper volcanics and the Gataga volcanics. The age of the Little Dal basalt is inferred as 779 Ma by correlation with the geochemically similar Tsezotene sills in the Mackenzie Mountains Supergroup (LeCheminant and Heaman, 1994; Dudas and Lustwerk, 1997). The age of zircons from a thin rhyolite flow in the upper part of the Mount Harper volcanics is 751 +18/-26 Ma (Roots and Parrish, 1988). In northeastern British Columbia, Ferri *et al.* (1999) have dated the Windermere Gataga volcanics as 689 ± 4.6 Ma. These various primary zircon ages are potentially represented among the younger detrital zircon ages from the Unit Pa samples. The present level of information for Unit Pa only constrains the depositional age and correlation to being within the lower Windermere Supergroup.

Toobally Formation (PT)

Introduction

Reconnaissance traverses along the west shore of Toobally Lake (NTS 95D/8) in 2003 identified a previously unrecognized massive diamictite for which the name Toobally Formation was proposed (Pigage and MacNaughton, 2004). The stratotype for the Toobally Formation consists of exposures within the valley cut by an unnamed stream that flows eastward into Toobally Lake roughly along grid reference line UTM 6 698 000N, zone 9, with a reference section along another stream slightly further south at 649 320E/6 694 834N, zone 9. The basal contact of the Toobally Formation is structural and consists of the unexposed east-verging Toobally fault. The top of the unit is not exposed; it appears to be overlain by mafic volcanic flows and volcaniclastic sedimentary rocks of the Crow Formation. The stratotype valley contains the northernmost exposure of the Toobally Formation; all exposures along strike to the north consist of Crow Formation strata. The minimum thickness of the formation along the type valley is 1800 m assuming structural continuity and a uniform west dip of 45 degrees.

Composition

The Toobally Formation consists almost entirely of a monotonous succession of polymictic, matrix-supported conglomerates to pebbly mudstones (Fig. 23). The matrix consists of dark brown to dark grey, brown-, buff-, or orange-weathering silty shale to siltstone and accounts for 50 to 80% of total rock volume. Conglomerate clasts are most commonly within the granule to pebble size range; cobbles are rarely present. In one locality a very large block of finely laminated dolostone is present. Clasts are angular to subrounded and show no preferred orientation (Fig. 24). Clast compositions include quartzitic metasandstone, calcareous sandstone, lithic sandstone, mudstone, massive lime mudstone and dolomudstone, laminated lime mudstone, massive grainstone, and rare vesicular to amygdaloidal basalt. Abundant subangular, monocrystalline quartz sand grains are also disseminated in the silty matrix (Fig. 25).



Figure 24. *Randomly oriented carbonate clasts in matrix-supported conglomerates of Toobally Formation, field station 03LP015. Circle encloses two carbonate clasts with different orientations.*



Figure 23. *Polymictic, matrix-supported conglomerates to pebbly mudstones, Toobally Formation, field station 03LP006.*

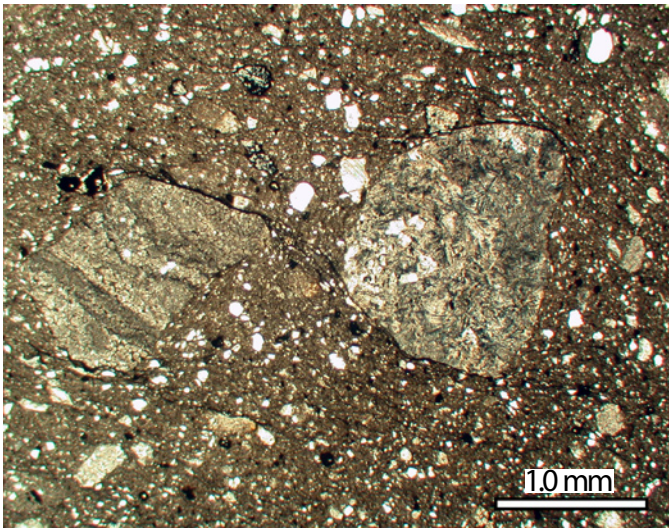


Figure 25. *Thin section photo of Toobally Formation. Subangular clasts of siltstone, volcanic rock and abundant monocrystalline quartz. Plane light. Field station 03LP007. Scale bar is 1.0 mm.*

The unit is overwhelmingly massive with bedding being observed in only one locality (Fig. 26). At this locality, normally graded to massive beds less than 10 cm thick are preserved. In another area, a gradational change upward from a silty mudstone to a siltstone matrix was observed within an unbedded succession of pebbly mudstone. In both localities, bedding orientation is consistent with the regional westward dip of the overlying Crow Formation. The formation contains a moderately developed, pervasive slaty cleavage which becomes more intense in an eastward direction as the Toobally fault is approached.

The Toobally Formation is cut by scattered dark green, orange-weathering, fine-grained, diabase to gabbro dykes and sills ranging from less than 10 cm thick to greater than 10 m thick. Locally, the dykes and sills are extensively altered to a pale grey, orange-weathering, pyritic quartz-carbonate-sericite assemblage. The chemistry of the dykes and sills is similar to that of the overlying volcanic rocks of the Crow Formation, and they are therefore considered to be feeders for these volcanic rocks. Whole rock analyses for the dykes and sills are presented in Table III-2 (Appendix III). Table III-2 also contains an analysis for one large vesicular basalt clast contained within the diamictite (Fig. 27). Large LOI (loss on ignition) in the analyses indicates the samples are altered to varying extents. Compositional and discriminant diagrams (Figs. 28, 29) using immobile elements show the sills and dykes are alkalic within plate basalts with a general OIB (oceanic island basalt) signature. Figure 29e suggests the samples cooled from a magma derived directly from the mantle with no significant crustal contamination. Compositions are consistent with a rift or extensional tectonic setting. Similar compositions have been noted in several places along strike within the lower Paleozoic North American miogeocline (Goodfellow *et al.*, 1995).

In a stream valley outcrop (UTM 649 705E/ 6 698 302N, zone 9) about 1.3 km upstream from the west edge of Toobally Lake, the conglomeratic mudstone is overlain by an orange-weathering, unfossiliferous, microcrystalline to very finely crystalline, thinly bedded dolostone at least 20 m thick (Fig. 30). Beds within the dolostone are 10 to 40 cm thick. Internally the dolostone beds display parallel lamination, low-angle cross-lamination or ripple cross-lamination (Fig. 31). Rare, bedding-parallel stylolites are also present. The contact between the dolostone and the underlying conglomeratic mudstone is sharp and stained red. Immediately above the contact, the dolostone is highly fractured and generally harder than further upsection, suggesting it has been silicified. Bedding within the dolostone is oriented to the northeast, whereas the regional bedding dip is to the west. Pigage and MacNaughton (2004) suggested the dolostone was actually a large clast within the Toobally Formation, with 1400 m of Toobally Formation occurring structurally upsection from the clast.



Figure 26. *Rare primary sedimentary layering in Toobally Formation, field station 03LP010.*



Figure 27. *Rare basalt clast in matrix-supported conglomerate of Toobally Formation, field station 03LP007.*

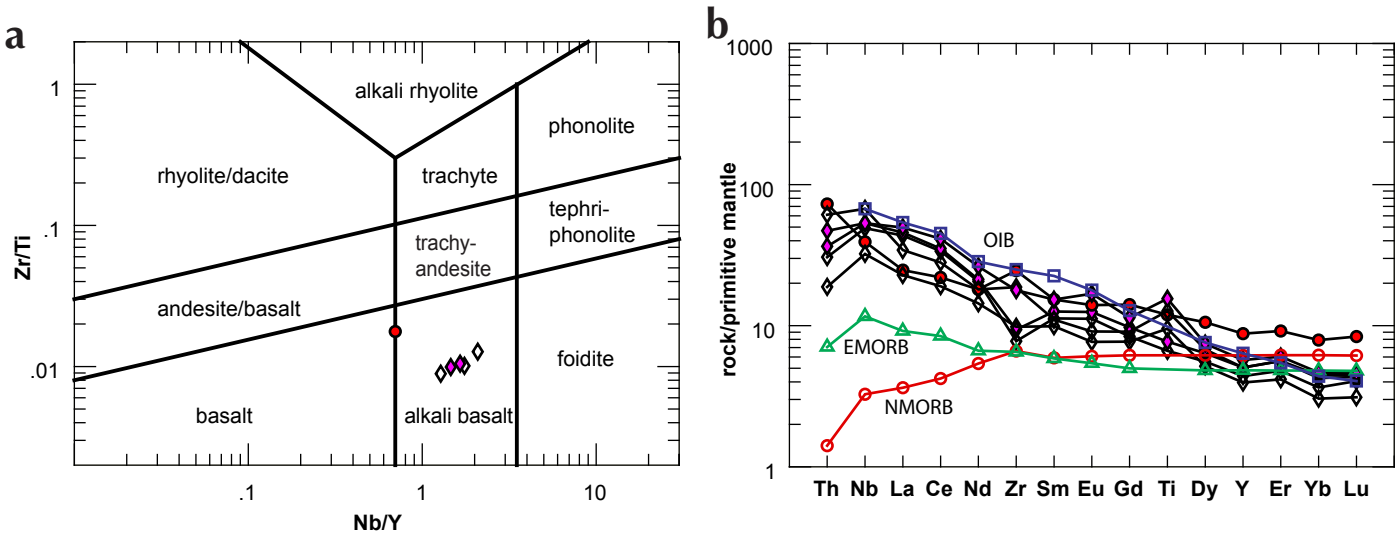


Figure 28. *Compositional diagrams for analyses in Table III-2 (Appendix III), dykes and clast in Toobally Formation.* ***(a)*** *Zr/Ti - Nb/Y diagram from Pearce (1996), modified from Winchester and Floyd (1977);* ***(b)*** *multielement diagram normalized to primitive mantle (Sun and McDonough, 1989). EMORB (enriched midocean ridge basalt), NMORB (normal ocean ridge basalt) and OIB (oceanic island basalt) reference analyses are included.*

Depositional environment

The Toobally Formation was interpreted by Pigage and MacNaughton (2004) as being produced by relatively viscous, sediment-gravity flows, probably debris flows. Thick accumulations of debris flows associated with turbidites are typical of marine slope to toe-of-slope settings. The lack of primary features such as ripples or small scale bedding further indicates a low energy, deeper water depositional environment.

An alternative interpretation for the deposition of the Toobally Formation would be that it represents a sedimentary intrusive breccia unit, similar to a mud volcano or dewatering pipe. Cecile and Campbell (1977) described intrusive sedimentary breccias in the lower Proterozoic Goulburn Group near Bathurst Inlet, Nunavut. Intrusion of the breccias was interpreted to be related to intrusion and stoping of overlying strata by overpressured intrastratal fluids to a Goulburn paleosurface, forming sedimentary mud volcanoes on the paleosurface. This interpretation is attractive because the depositional age is not the same as the age of the clasts and the matrix forming the intrusive unit. Primary features of the Goulburn intrusive units included small euhedral crystals of dolomite and quartz and flow-banding textures parallel to the intrusive margins of the breccia units. Deposition as a sedimentary intrusive breccia was not considered appropriate for the Toobally Formation because rare bedding in the Toobally Formation is consistent with a regional bedding orientation (not a marginal flow-banding orientation). Further, the unit is devoid of any euhedral crystals (which would suggest crystallization from low temperature connate fluids).

Age and correlation

Fossils have not been recognized within the Toobally Formation (Table IV-2, Appendix IV). The upper contact of the formation is structurally 2900 m beneath a Lower Ordovician fossil locality (Pyle, 2004) originally reported by Gabrielse and Blusson (1969) as lower Cambrian. A minimum age for deposition of the Toobally Formation is therefore earliest Ordovician.

A maximum possible depositional age for the Toobally Formation is more difficult to infer and could range from Neoproterozoic to Ordovician, depending on geology-based assumptions on the nature of the contact between the Toobally and Crow formations. Pigage (2006) illustrated three possible stratigraphic-structural interpretations for the map pattern of the Toobally and Crow formations (Fig. 32). The following discussion assumes that the Crow Formation has a depositional age of upper Cambrian to Lower Ordovician (see next section on the Crow Formation). Figures 32a and 32b infer that the Toobally Formation is older than the Crow Formation — Proterozoic to possibly Cambrian. An unconformity is required at the base of the Crow Formation volcanic horizon 2, immediately above the Toobally Formation, to account for the volcanic unit being uninterrupted along strike to the north. In Figure 32a, the lateral contact between the Toobally Formation and lower Crow Formation is an early, east-trending, pre-

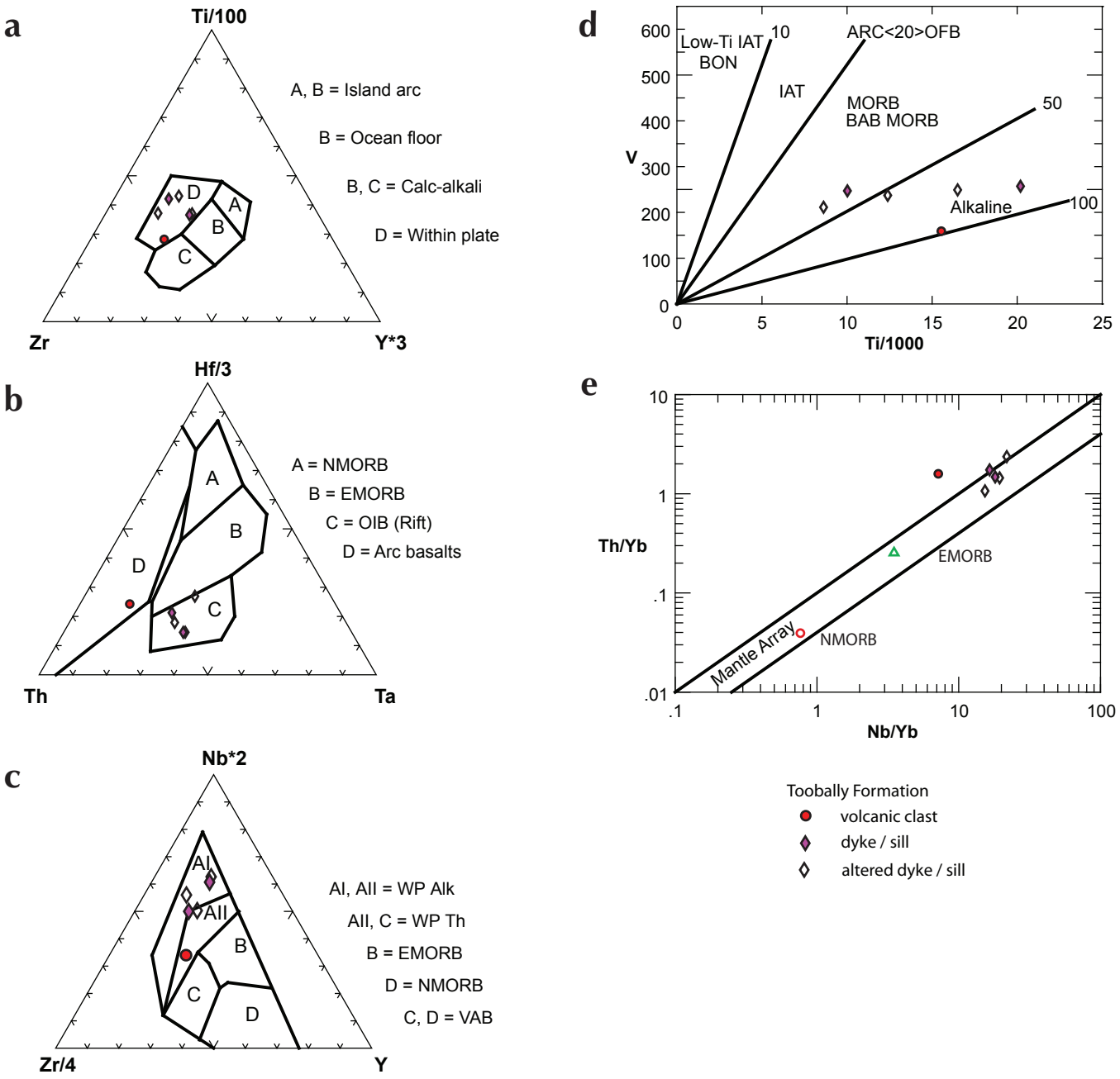


Figure 29. *Tectonic discriminant diagrams for analyses in Table III-2 (Appendix III), dykes and clast in Toobally Formation.* ***(a)*** *Ti-Zr-Y plot from Pearce and Cann (1973);* ***(b)*** *Hf-Th-Ta from Wood (1980);* ***(c)*** *Nb-Zr-Y from Meschede (1986);* ***(d)*** *V-Ti from Shervais (1982), IAT, OFB, BON, BAB as in Figure 22;* ***(e)*** *Th/Yb-Nb/Yb from Pearce and Peate (1995). EMORB, NMORB and OIB as in Figure 28.*

unconformity fault with the unconformity at the top of the Toobally Formation being internal to the Crow Formation in the northern part of map sheet 95D/8.

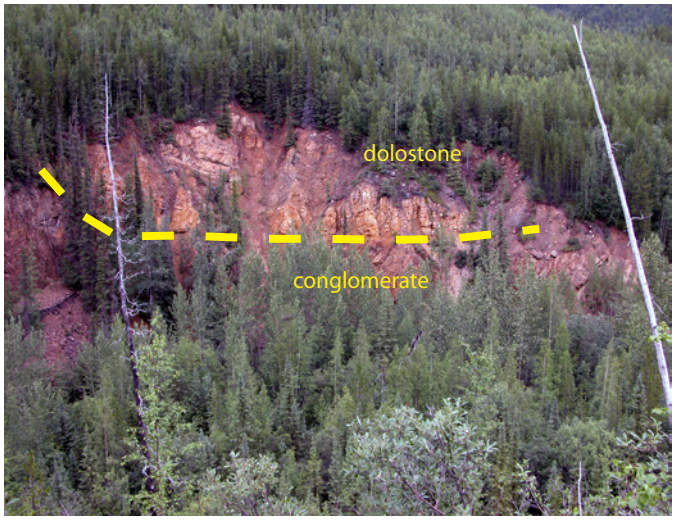


Figure 30. *Laminated dolostone clast within pebbly conglomerate mudstones of Toobally Formation. View looking north, field station 03LP014. Cliff face is about 20 m high.*



Figure 31. *Closeup view of laminated dolostone clast, field station 03LP014.*

Such a fault would have a minimum displacement of 1800 m, the stratigraphic thickness of the lower Crow Formation immediately north of the Toobally Formation. In Figure 32b, the unconformity at the top of the Crow Formation has erosional relief, cutting down through the Toobally Formation in a northward direction. In this interpretation the unconformity is cut out by the Toobally fault immediately north of the Toobally Formation.

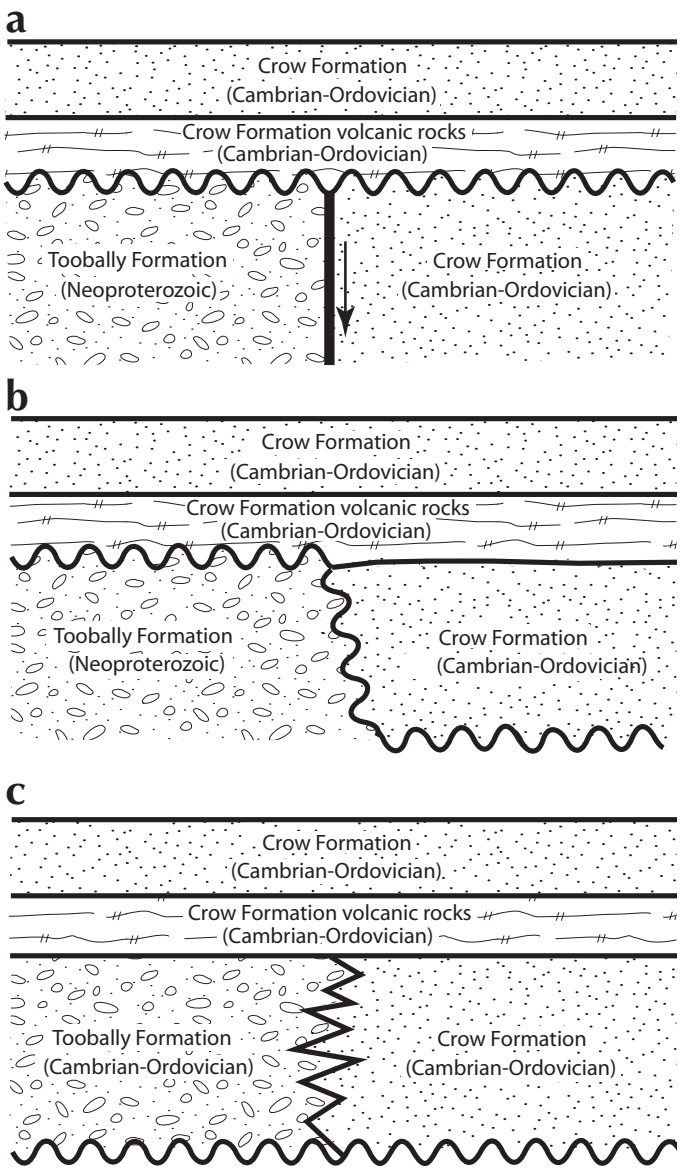


Figure 32. *Interpreted stratigraphic and structural relations between Toobally Formation and Crow Formation. In* ***(a)*** *and* ***(b),*** *Toobally Formation is Neoproterozoic and lower Crow Formation is Cambrian. In* ***(c),*** *Toobally Formation and Crow Formation are Cambrian-Ordovician.*

In contrast, Figure 32c considers the Toobally Formation to be laterally correlative with the lower Crow Formation. In this case the transition between Toobally and Crow formations is a lateral facies change and the Toobally Formation is also Cambrian-Ordovician in age. The major unconformity at the base of the Crow Formation in map sheet 95C/5 is cut out by the Toobally fault in map sheet 95D/8.

One sample from the Toobally Formation was submitted for detrital zircon U-Pb geochronology (sample 03LP010, Table I-4, Appendix I). The distribution of detrital zircon ages for this sample contains a northern Canada sequence B Mesoproterozoic signature. The formation, therefore, is either correlative with Mackenzie Mountains Supergroup or has a source provenance containing extensive Mackenzie Mountains Supergroup exposures. The youngest detrital zircon age is about 650 Ma (two zircon dates). The detrital zircon age distribution supports but does not constrain the Toobally Formation to a Neoproterozoic age of deposition.

In this report, the preferred depositional age of the Toobally Formation is considered to be late (post 650 Ma) Neoproterozoic. The Toobally Fomation is therefore older than the Crow Formation and is separated from the lower Crow Formation by an interpreted unconformity. The juxtaposition of the Crow Formation and Toobally Formation along strike in map area 95D/8 is considered to be associated with a growth fault that was active during lower Crow Formation deposition. The bottom contact of the volcanic unit overlying the Toobally Formation is also an unconformity; north of the interpreted normal (growth) fault, this unconformity is internal to the Crow Formation.

Pigage and MacNaughton (2004) noted that the Toobally Formation resembles Neoproterozoic glacial diamictites such as the Shezal Formation (Eisbacher, 1978, 1981), Ice Brook Formation (Aitken, 1991) or Mount Vreeland Formation (McMechan, 2000). Although massive, the diamictites in these other formations are visibly interbedded with rhythmically bedded marine and nonmarine sedimentary rocks. Glacially striated clasts were not encountered in the Toobally Formation. Glacial features such as dropstones and lonestones also were not encountered. Despite these difficulties, they tentatively correlated the Toobally Formation with the Ice Brook Formation and considered it to be Neoproterozoic in age on the basis of lithologic similarities. As part of these similarities they included the very large dolostone clast being similar to the cap carbonate rocks associated with the Ice Brook Formation.

SUCCESSION 2 (CAMBRIAN-ORDOVICIAN)

Succession 2 unconformably overlies the Proterozoic siliciclastic and volcaniclastic sedimentary rocks of succession 1 (Fig. 3) and the Neoproterozoic Pool Creek syenite. Succession 2 sedimentary rocks indicate a generally shallow water depositional environment in the east, transitional to a deeper water depositional environment in the west. The age of succession 2 ranges from upper Cambrian to latest Lower Ordovician (Ibexian). In the western part of the map area, succession 2 consists of two sedimentary units, the Crow Formation and the Rabbitkettle Formation. In the Pool Creek map sheet, the Rabbitkettle Formation is absent and succession 2 consists entirely of the Crow Formation. Basaltic volcanic rocks occur at four separate intervals within the Crow Formation. These volcanic rocks have previously been informally called Toobally volcanics and Gusty volcanics (Goodfellow *et al.*, 1995).

Crow Formation (new) (ЄOc)

Introduction

Scattered outcrops of interbedded greyish red to white, locally subarkosic sandstone, conglomerate and maroon siltstone overlie the northern end of the Pool Creek nepheline syenite, Unit Pa and the Toobally Formation. Isolated occurrences of interbedded, locally calcareous, tan sandstone and greyish red to maroon siltstone occur in the core of the north-trending anticline in the southwest corner of the Pool Creek map sheet and continue southwest into the southeast corner of map sheet 95D/8. Extensive exposures of interbedded greyish red to white, variably subarkosic sandstone, conglomerate, maroon siltstone, minor limestone or dolostone and basalt pillow lavas and lapilli tuffs occur in stream valleys and ridges on the west half of map sheet 95D/8. All these exposures constitute the Crow Formation, newly described in this report.

The formation is named after the Crow River which has its headwaters in the south-central part of the Pool Creek map area. Exposures of the Crow Formation occur on the east side of the south-trending valley containing the headwaters of the Crow River. The proposed type locality for the formation occurs in the same stream valley as the type locality for the Toobally Formation in map sheet 95D/8, extending from UTM 647 536E/6 697 626N, zone 9, upstream to UTM 641 495E/6 699 105N, zone 9. Extensive exposures of variably arkosic quartz sandstone interbedded with maroon siltstone and basalt flows and volcaniclastic rocks occur in the stream valley, especially on the north side. Two additional reference areas further

extend the stratigraphic limits of this formation and enhance exposures. The first additional reference area is a series of exposures on the north side of the stream, centred at UTM 653 380E/6 702 440N, zone 9. Outcrops encompass the lowest exposed portions of the Crow Formation in the hangingwall of the east-verging Toobally fault. The second reference area consists of a series of exposures of Crow Formation resting unconformably on the Pool Creek nepheline syenite located along the ridge crest from UTM 343 605E/6 701 480N, zone 10 to UTM 342 300E/6 704 340N, zone 10.

Upper and lower contacts of the Crow Formation are not exposed. It is overlain by the Sunblood Formation. In the Pool Creek map sheet, the Crow Formation unconformably overlies either the Proterozoic Pool Creek syenite or Unit Pa. This is consistent with the absence of hornfelsing in the Crow Formation maroon argillites immediately overlying the nepheline syenite. Clasts of the Pool Creek syenite were not noted in the lowermost exposures of the Crow Formation in the immediate vicinity of the underlying syenite. In the south part of map sheet 95D/8, the Crow Formation unconformably overlies the Toobally Formation. In the northern part of the same map sheet, the base of the formation is structural, consisting of the east-verging Toobally fault. Immediately west of the Toobally fault, the lower part of the Crow Formation is laterally along strike with the Toobally Formation to the south.

The overall thickness of the Crow Formation changes dramatically from east to west across the map area. The minimum interpreted thickness in the north Pool Creek map area at its easternmost exposure is 300 m. In the west part of map sheet 95D/8, the interpreted thickness where the Crow Formation overlies the Toobally Formation is 4250 m. In the area where the formation is floored by the Toobally fault, it has a minimum thickness of 5700 m. These thickness estimates in map sheet 95D/8 infer that Crow Formation exposures all occur within the same structural panel with no thrust fault repetitions.

The upper contact of the formation is demonstrably diachronous, ranging from latest Early Ordovician (Ibexian to Whiterockian) in the Pool Creek map sheet to Early Ordovician (Tremadocian) in map sheet 95D/8 (see Table IV-3; Appendix IV). Depositional age of the lower contact is speculative with possible ages ranging from Neoproterozoic to Ordovician. It is most likely that the lower contact of the Crow Formation is also diachronous because of the dramatic differences in total thickness from west to east. The major regional unconformity at the base of the Crow Formation in the Pool Creek map sheet is tentatively correlated with the regional late Cambrian sub-Franconian unconformity recognized by Gabrielse *et al.* (1973), making the lower age limit of the formation upper Cambrian.

Composition

The dominant lithology is a poorly sorted, thick-bedded to massive, coarse- to fine-grained, pebbly, variably subarkosic sandstone with subangular to subround monocrystalline quartz clasts and weathered clasts of plagioclase and/or K-feldspar, and detrital muscovite. Minor amounts of sandstone, siltstone and volcanic rock also occur as clasts. Locally scattered through the sandstone are well-rounded quartz pebbles up to 2 cm across (1-3%) consisting largely of monocrystalline quartz (Fig. 33). The sandstone is typically indistinctly bedded with bed thicknesses ranging from 20 to 70 cm. Very locally, the sandstone contains trough cross-beds (Fig. 34), ripples (Fig. 35),

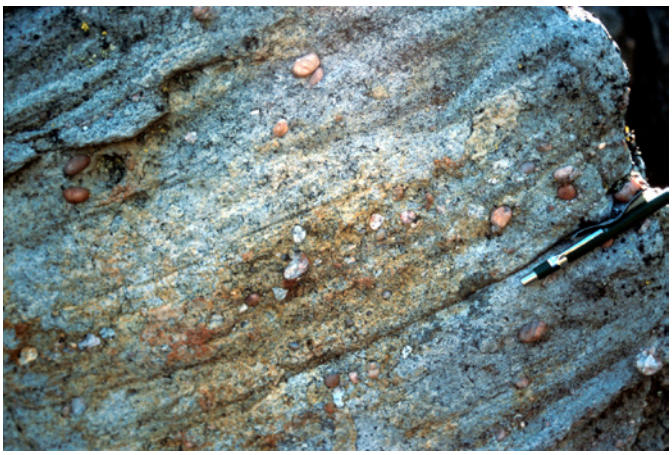


Figure 33. *Crow Formation sandstone with scattered monocrystalline quartz pebbles, field station 01LP044. Mechanical pencil for scale.*



Figure 34. *Trough cross-beds in quartz sandstones of Crow Formation, field station 01TLA152. Swiss army knife (circle) for scale. Photo by T. Allen.*

or desiccation cracks (Fig. 36). The number of quartz pebbles locally increases, and the sandstone grades into a pebbly conglomerate (Fig. 37). Both matrix- and clast-supported variants of the pebbly conglomerate occur. Conglomerate interbeds typically range up to 40 cm thick. Contacts are gradational, but only locally are graded. Minor amounts of detrital muscovite are common. Minor clasts of bedded siltstone and volcanic rocks are locally also present. Quartz clasts in the sandstones exhibit distinct epitaxial quartz overgrowths reducing the porosity (Fig. 38).

Interbedded with the pebbly sandstone are lesser intervals of white to light grey, noncalcareous, clast-supported, cobble conglomerate (Fig. 39). Cobbles are well-rounded and consist dominantly of white quartz sandstone with lesser grey quartz sandstone and



Figure 37. *Pebbly conglomerate interval within Crow Formation, field station 01LP044. Mechanical pencil (circled) for scale.*



Figure 35. *Ripple marks on bedding plane, subarkosic sandstone, Crow Formation, field station 05LP079.*

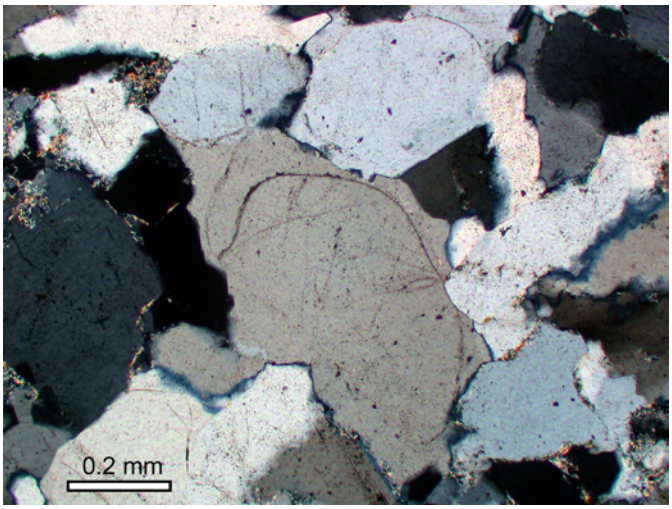


Figure 38. *Thin section photo of epitaxial quartz overgrowths on rounded quartz clasts in sandstone, Crow Formation, field station 02LP120, crossed nicols. Scale bar is 0.2 mm.*



Figure 36. *Desiccation cracks on bedding plane in fine-grained, subarkosic sandstone, Crow Formation, field station 05LP080.*



Figure 39. *Clast-supported conglomerate, Crow Formation, field station 01TLA033. Predominant clasts are white, pink and grey quartz sandstones. Photo by T. Allen. Swiss army knife (circle) for scale.*

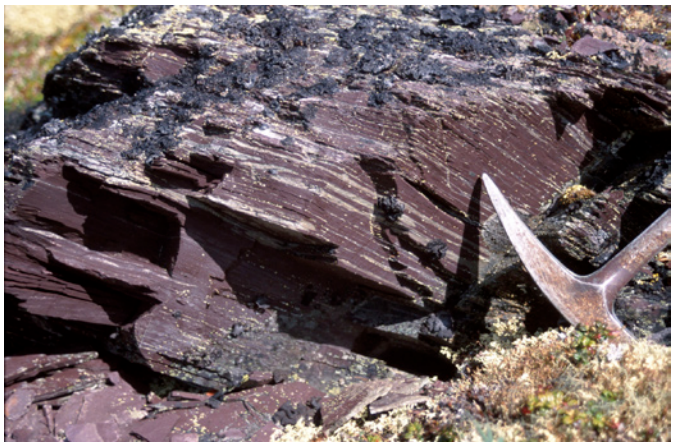


Figure 40. *Maroon silty argillite, Crow Formation, field station 01TLA036. Hammer for scale.*



Figure 41. *Interbedded massive, calcareous, fine-grained sandstone and maroon, calcareous, laminated silty argillite, Crow Formation, field station 01TLA017. Photo by T. Allen. Swiss army knife (circle) for scale.*

minor pink quartz sandstone. Matrix for the cobbles is a medium- to coarse-grained quartz sand. In one location the conglomerate has a minimum thickness of 9 m. Imbrication of the cobbles is not visible. These conglomerate interbeds are present only within the Pool Creek map sheet; they do not occur in map sheet 95D/8.

Minor amounts of dark maroon, silty argillite (Fig. 40) are interbedded with the above coarse siliciclastic rocks. Argillite weathers into small plates. It is not hornfelsed. Commonly, it contains abundant fine detrital mica on bedding plane surfaces. Thicknesses range from a few centimetres to greater than 6 m. Locally, the silty argillite contains thin finely parallel bedded intervals which are grey to green. This lithology also locally contains desiccation cracks on bedding plane surfaces.

Exposures in the southwest corner of the Pool Creek map sheet typically consist of alternating maroon, parallel-laminated silty argillite and fine-grained, brown-weathering sandstone (Fig. 41). Argillite beds are commonly 1 to 2 cm thick. Interbedding of sandstone and argillite occurs on a scale of 1 cm to 2-3 m. Locally, both lithologies are calcareous or dolomitic.

Dolostone and limestone interbeds are scattered through the upper part of the formation in map sheet 95D/8. One prominent 200 m-thick carbonate horizon, about 530 m below the top of the formation, outcrops along the stream forming the type area (UTM 642 780E/6 698 745N, zone 9). On the north side of the creek, it is a thin-bedded, medium grey limestone with irregular bedding planes (Fig. 42) and abundant feeding trace fossils (Fig. 43). Beds range from 3 to 20 cm thick. Locally, fine laminae are preserved in the lower part of the limestone horizon (Fig. 44). On the south side of the creek, the same limestone is overlain by a



Figure 42. *Bedded limestone, Crow Formation, field station 04LP037. Hammer for scale. View looking northwest. Beds dip moderately to left (west).*



Figure 43. *Trace fossils on bedding plane, bedded limestone, Crow Formation, field station 04LP037.*

tan-weathering dolostone. A 3 m-thick, massive, brown-weathering dolostone was also encountered lower in the stratigraphic section immediately upsection from the prominent basalt (horizon 2) overlying the Toobally Formation (UTM 645 990E/6 698 400N, zone 9). This dolostone is extensively recrystallized with botryoidal textures (Fig. 45). Carbonate horizons do not occur within Crow Formation in the Pool Creek map sheet.

Volcanic horizons – composition and geochemistry

Crow Formation west of Toobally Lake contains pillow basalts and interbedded lapilli tuffs occurring at four stratigraphic levels. No volcanic rocks occur in the formation in the Pool Creek map sheet. These horizons are informally called horizons 1 (oldest) through 4 (youngest), with successively younger horizons outcropping farther to the west in the map area. The most prominent of these horizons (horizon 2) is about 890 m thick and immediately overlies the Toobally Formation. This particular horizon has been mapped laterally along strike for a distance of slightly greater than 15 km. Horizon 1 was encountered in two outcrop areas on the west side of Toobally Lake. From outcrops along the northern stream it has an estimated thickness of 260 m. The two inferred horizon 1 outcrops are separated by a lateral distance of about 4.8 km. Horizon 3 was encountered in the valley containing the type area of the Crow Formation. Approximately 150 m thick, it differs lithologically from the other horizons in containing abundant nepheline(?) phenocrysts ranging up to 3 cm across. Horizon 3 was only intersected in this stream valley; it may actually constitute a dyke or sill rather than an extrusive flow. The uppermost horizon 4 was encountered in the general Gusty Lakes area in the northwest part of map sheet 95D/8. It is approximately 150 m thick.

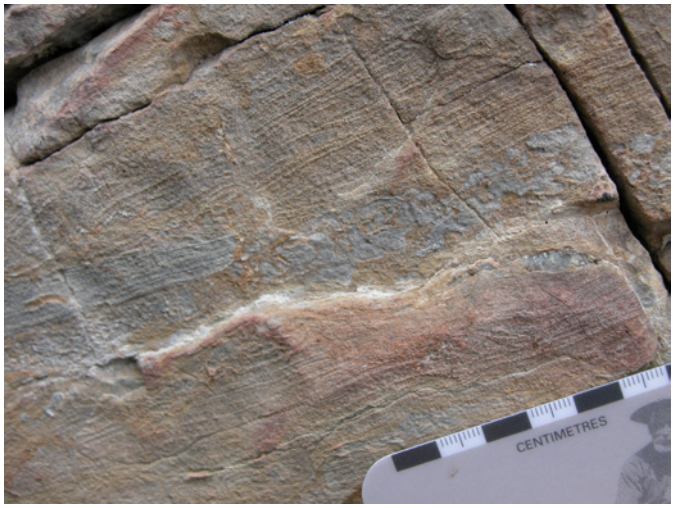


Figure 44. *Closeup of laminae in limestone, Crow Formation, field station 04LP037. Younging direction in photo is up. Truncations visible in centre part of photo.*

The volcanic horizons consist of thick-bedded to massive lapilli tuffs (Fig. 46) interbedded with dark purplish green, amygdaloidal to vesicular, massive or pillow basalt flows (Fig. 47). Amygdules are infilled by chlorite, calcite and quartz. Plagioclase and clinopyroxene microphenocrysts and glomerocrysts are scattered in a groundmass of randomly oriented plagioclase microlites (Fig. 48) with interstitial epidote, calcite, chlorite and opaque minerals. Several samples contain serpentine or chlorite pseudomorphs of former olivine microphenocrysts (Fig. 49). The matrix mineralogy

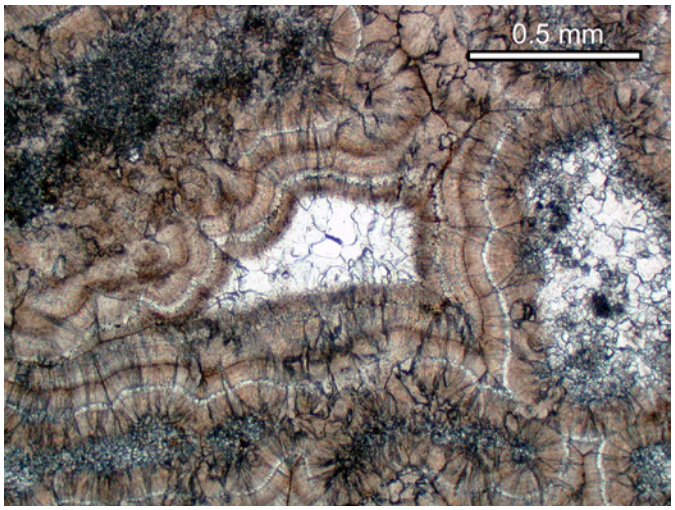


Figure 45. *Thin section photo of botryoidal dolomite crystals in brown dolostone, Crow Formation, field station 05LP039, plane light. Scale bar is 0.5 mm.*

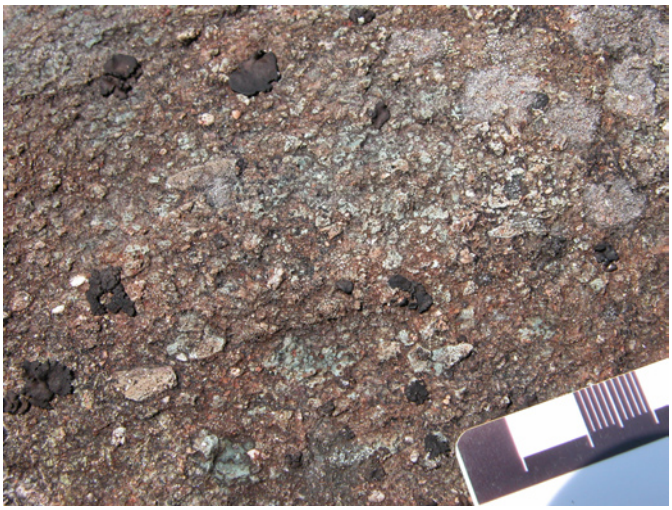


Figure 46. *Closeup of lapilli tuff, volcanic horizon 2, Crow Formation, field station 03LP029. Major divisions on scale are 1 cm.*



Figure 47. *Pillow in volcanic horizon 1, Crow Formation, field station 05LP005. View looking north. Hammer for scale.*

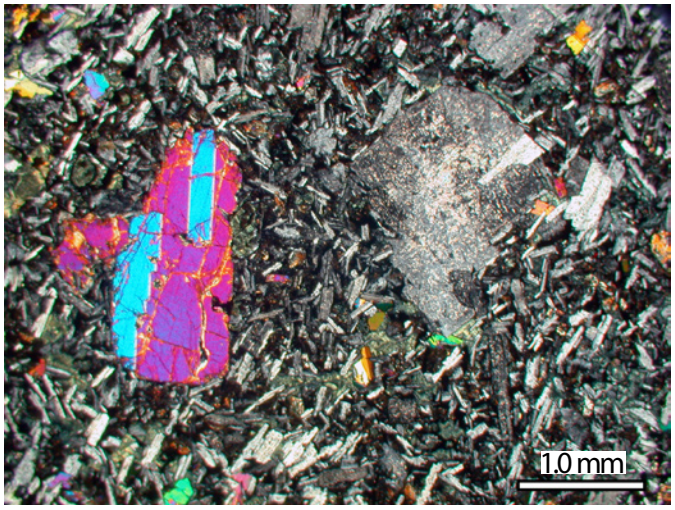


Figure 48. *Thin section photo of plagioclase phenocryst and rare clinopyroxene phenocryst in groundmass consisting of plagioclase microlites, epidote, chlorite and opaque minerals. Slight sericitic dusting in plagioclase. Volcanic horizon 2, Crow Formation, field station 04LP058, crossed nicols. Scale bar is 1.0 mm.*

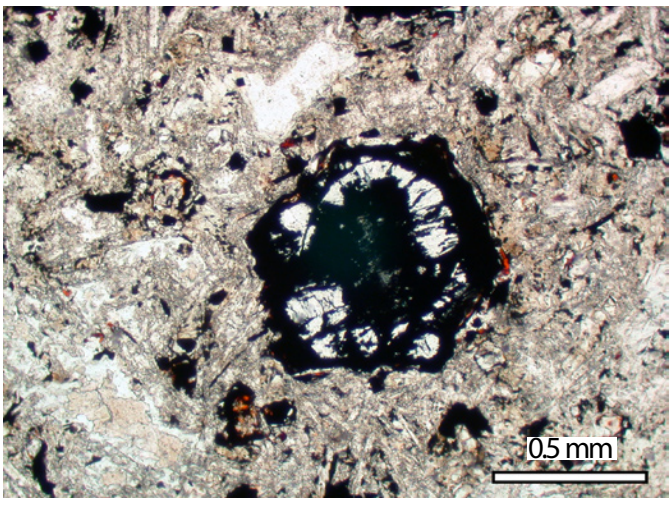


Figure 49. *Thin section photo of hexagonal olivine(?) phenocryst now pseudomorphed by chlorite with extensive iron oxide rim. Microlites in matrix are pseudomorphed by sericite; lesser anhedral aggregates of carbonate minerals. Volcanic horizon 2, Crow Formation, field station 05LP060, plane light. Scale bar is 0.5 mm.*

indicates low temperature metamorphic replacement and alteration. Locally, malachite staining occurs on fractures. One outcrop from horizon 4 near Gusty Lakes (field station 04LP060, UTM 639 391E/6 707 717N, zone 9) contains aggregates of fine- to medium-grained chalcopyrite (up to 5 mm across) disseminated in the matrix.

Table III-3 (Appendix III) contains whole rock geochemical analyses for the Crow Formation volcanic rocks, and Table III-2 contains analyses for dykes and sills in the Toobally Formation which are considered to be subvolcanic feeder dykes for the Crow Formation volcanic rocks. The low temperature metamorphism and alteration are reflected by dramatically increased LOI (loss on ignition) in some of the analyses. All analyzed samples are alkali basalts with an overall OIB (oceanic island basalt) geochemical signature (Fig. 50). The samples plot as rift-related, within plate tectonic assemblages (Fig. 51). Similar lower Paleozoic basalts occur in various parts of the miogeocline of the Northern Cordillera (Goodfellow *et al.*, 1995). Figure 50b contains an envelope for Ordovician basalts of the Menzie Creek formation near Faro (Pigage, 2004a) showing a very similar geochemical signature. Figure 51e indicates minimal crustal component or contamination within the basalt magma.

Correlation

Crow Formation was locally differentiated in the earlier La Biche River geology map as unit 2 (Douglas and Norris, 1959) or Pcg boulder conglomerate (possibly Hadrynian; Douglas, 1976). In the Coal River geology map, this unit was labeled as unit 4 (Gabrielse and Blusson, 1969). Gabrielse and Blusson differentiated 4a from 4b predominantly by the increased occurrence of pebbly sandstone, dolostone and bioclastic limestone in the latter. Gabrielse and Blusson (1969) differentiated two of the volcanic horizons in the Crow Formation as units 3 and 7. These particular horizons were also informally designated as the Toobally and Gusty volcanics, respectively, by Goodfellow *et al.* (1995).

Age and correlation

In the Coal River geology map, the Crow Formation was previously assigned an early Cambrian age based on trilobites and 'Scolithus' tubes noted in the limestones and sandstones about 530 m below the top of the formation west of Toobally Lake (Gabrielse and Blusson, 1969). Resampling of this same outcrop for conodonts (Table IV-3, Appendix IV) resulted in a revised Early Ordovician (Tremadocian) age (Pyle, 2004). Conodont samples from the lowermost Sunblood Formation immediately above the Crow Formation in the same area also have a Tremadocian age, resulting in a Tremadocian age for the upper contact of the formation in map sheet 95D/8. Two samples from the Crow Formation in the Pool Creek area contained conodonts indicating an age range of Late Blackhillsian (Ibexian) to Early Whiterockian (Rangerian) (Table IV-3, Appendix IV). The upper contact

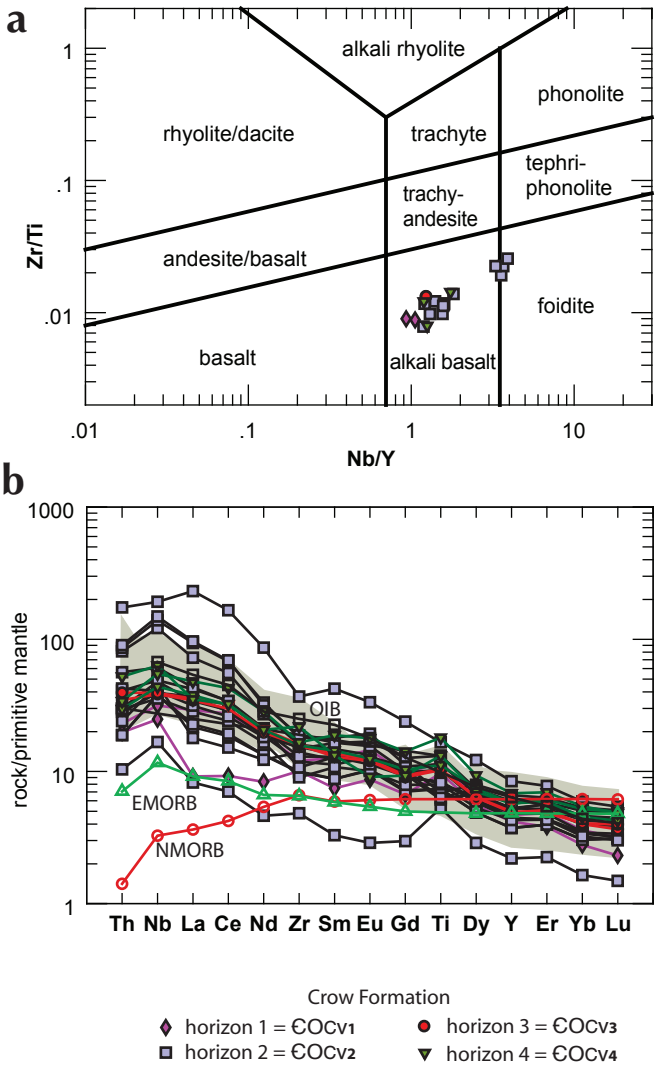


Figure 50. *Compositional diagrams for analyses in Table III-3 (Appendix III), Crow Formation volcanic horizons 1-4.* ***(a)*** *Zr/Ti - Nb/Y diagram from Pearce (1996), modified from Winchester and Floyd (1977).* ***(b)*** *multielement diagram normalized to primitive mantle (Sun and McDonough, 1989). EMORB (enriched midocean ridge basalt), NMORB (normal midocean ridge basalt) and OIB (oceanic island basalt) reference analyses are included. Shaded area indicates composition for analyses of Menzie Creek Formation in Anvil District, Yukon (Pigage, 2004a).*

of the Crow Formation, therefore, is diachronous and youngs to the east.

Detrital zircons from seven samples of the Crow Formation (three samples in map sheet 95C/5 and four samples in map sheet 95D/8) were analyzed for isotopic age dates. Detailed tables of the zircon dates are presented in Appendix I, Tables I-5a through I-5g. The total range of detrital zircon ages is between 470 ± 9 Ma and 3274 ± 11 Ma with the preponderance of detrital zircon ages from all samples being between 1800 Ma and 2100 Ma. All samples also contain a lesser number of Archean ages ranging from 2500 Ma to 3300 Ma. Two samples have a modest number of zircon dates between 470 Ma and 500 Ma, one date at 724 Ma and two dates near 1200 Ma. The young dates from samples 02LCP120 and 05LP011 indicate the Crow Formation in this immediate area has a maximum stratigraphic age of upper Cambrian.

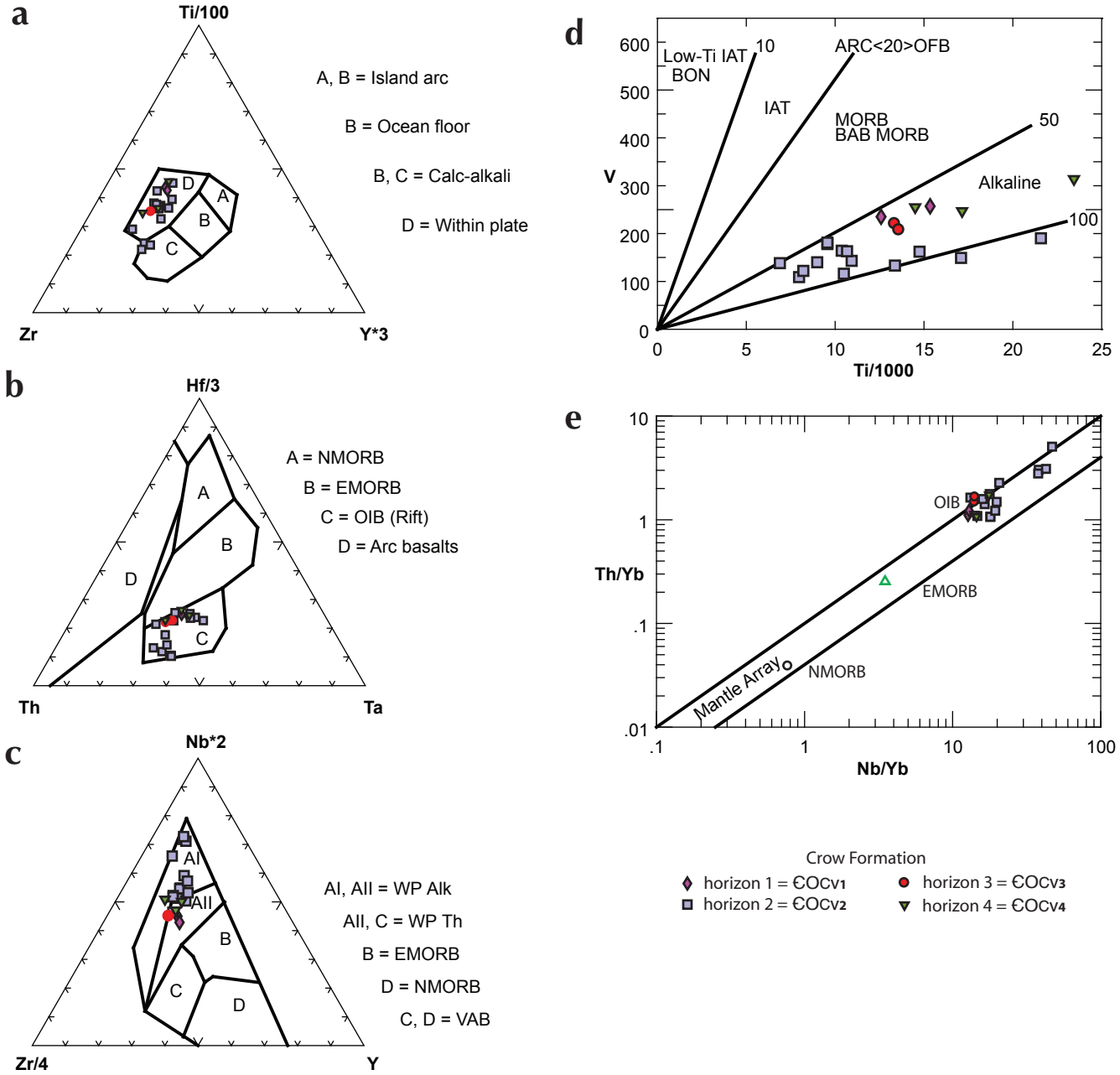


Figure 51. *Tectonic discriminant diagrams for analyses in Table III-3 (Appendix III), Crow Formation volcanic horizons.* ***(a)*** *Ti-Zr-Y plot from Pearce and Cann (1973);* ***(b)*** *Hf-Th-Ta from Wood (1980);* ***(c)*** *Nb-Zr-Y from Meschede (1986);* ***(d)*** *V-Ti from Shervais (1982), IAT, OFB, BON, BAB as in Figure 22;* ***(e)*** *Th/Yb-Nb/Yb from Pearce and Peate (1995). EMORB, NMORB and OIB as in Figure 50.*

Crow Formation is correlative with Sauk III strata as described by Aitken (1993). Correlative units include Road River Group, Skoki Formation, Rabitkettle Formation and Kechika Formation (Pyle and Barnes, 2000).

Depositional environment

The occurrence of poorly sorted, fine- to coarse-grained, locally cross-bedded sandstones interbedded with pebbly sandstones and cobble conglomerates indicates a shallow water depositional environment. The common presence of interbedded maroon siltstones and argillites, locally with desiccation cracks, indicates a shallow water to subaerial depositional setting. The local occurrence of herringbone cross-bedding further indicates an intertidal paleogeography. Locally, a marine setting is substantiated by the presence of carbonate and calcareous clastic rocks, both with conodont microfossils. Subarkosic compositions for many of the sandstones suggest an immature clastic succession derived largely from an eroding igneous plutonic domain. However, the overwhelming dominance of monocrystalline quartz clasts in the sandstones suggests a more mature provenance.

The detrital zircon ages delineated in Appendix I are consistent with Archean Slave Province and the adjacent Wopmay orogen being the source provenance for the vast majority of the detrital zircons in the Crow Formation (Hoffman, 1989). A Wopmay-Slave source area would suggest a southwest- to west-directed transport direction for the clastic rocks of the Crow Formation. Several trough cross-bed orientations were measured in Crow Formation sandstones during 2004-2005 field work (Table 1a). Figure 52 contains a rose diagram indicating downslope direction for measured cross-beds after correction for nonhorizontal beds. The majority of the cross-bed dip azimuths are consistent with a west to southwest transport direction during deposition. In contrast, the one measured ripple crest (Table 1b; Fig. 35) has a northeast azimuth upon rotation of bedding to horizontal.

The upper part of the Crow Formation is time-correlative with the lower Early to Middle Ordovician carbonate platform to basinal shale transition in central Yukon (Abbott *et al.*, 1986) and a similar transition between MacDonald platform and Kechika trough in northeastern British Columbia (Pyle and Barnes, 2000). The extensive coarse siliciclastic sedimentary rocks represented by the Crow Formation indicates an erosional and depositional environment that presumably had a very localized paleogeographic high.

Table 1a. *Cross-bedding in Crow Formation, rotated to horizontal bedding.*

	Bedding		Cross-bedding		Rotated Cross-bedding	
Station	Strike	Dip	Strike	Dip	Strike	Dip
04LP031	151	33	179	46	216	22
05LP011	205	7	154	12	119	9
05LP030	130	35	144	57	160	24
05LP042	215	61	205	42	54	21
05LP050	165	45	155	71	144	24
05LP050	166	49	164	67	160	18
05LP053	163	36	144	46	104	16
05LP055	225	18	253	24	298	12
05LP069	186	20	214	48	228	31
05LP069	186	20	180	44	176	24
05LP070	201	30	188	36	146	9
05LP071	209	22	182	39	158	21
05LP071	209	22	240	29	286	15
05LP071	209	22	191	28	149	10
05LP073	189	25	202	34	230	11
05LP073	189	25	184	27	139	3
05LP078	200	42	235	38	313	23

Table 1b. *Ripple crest in Crow Formation, rotated to horizontal bedding.*

	Bedding		Ripple Crest		Rotated Ripple Crest	
Station	Strike	Dip	Azimuth	Plunge	Azimuth	Plunge
05LP079	180	40	206	16	30	3

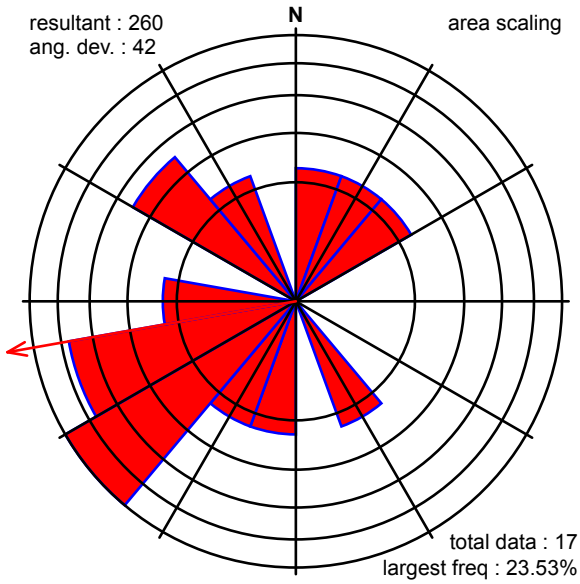


Figure 52. *Rose diagram of paleocurrent directions derived from 17 cross-bedding measurements in Crow Formation. Cross-bedding planes rotated to present orientation by unfolding bedding to horizontal orientation.*

Rabbitkettle Formation (ЄOR)

Introduction

The Rabbitkettle Formation (Gabrielse *et al.*, 1973) is exposed for a distance of 980 m along an east-trending stream valley in the westernmost part of map sheet 95D/8 (UTM 640 930E/6 699 070N, zone 9). The formation consists predominantly of a thin-bedded, brownish grey siltstone. The uppermost part of the siltstone contains distinctive interbeds of nodular, medium grey limestone. The interpreted thickness of the Rabbitkettle Formation along the stream is 700 to 750 m. It occurs as a stratigraphic tongue extending into the Crow Formation; the Rabbitkettle siltstones are both overlain and underlain by Crow Formation sandstones with interbedded basalts. Both upper and lower contacts are not exposed, but are considered conformable. The Rabbitkettle Formation thins rapidly and disappears to the south as it was not observed near Spruce Creek. It also was not observed in the east half of the map sheet 95D/8 or in the Pool Creek map sheet.



Figure 53. *Stream outcrop of slightly calcareous, moderately soft shale to silty shale (Rabbitkettle Formation), field station 04LP035. View looking south. Bedding dips to right.*

Composition

The dominant lithology is a thin-bedded, brownish grey, slightly dolomitic to noncalcareous siltstone which forms small cliff outcrops along the stream valley (Fig. 53). Bedding is delineated by thin striping (1-10 mm) resulting from lesser dark grey siltstone interbeds. Locally, the siltstone contains thin (0.5-3 cm) intervals of pale tan-weathering sandstone which locally delineates abundant primary soft deformation features like slump folds and truncation surfaces (Fig. 54). The same outcrop also contains a matrix-supported, brown-grey, orange-weathering conglomerate at least 3 m thick (Fig. 55). Clasts consist of randomly oriented, subangular limestone blocks typically up to 20 cm across and constituting 10-40% of the conglomerate. One large limestone clast has a diameter of over 2 m.

Outcrops of the upper part of the siltstone contain distinctive interbeds (5-20%) of medium grey, fine-grained, nodular limestone (Fig. 56). Typically the nodular beds are 2 to 5 cm thick and weather recessively to form



Figure 54. *Internal unconformity delineated by truncated sandstone beds in grey shale to siltstone (Rabbitkettle Formation), field station 04LP034. Pencil for scale is 15 cm long.*



Figure 55. *Closeup view of matrix-supported, subangular, randomly oriented limestone clasts in sandstone matrix (Rabbitkettle Formation), field station 04LP034. Pencil is 15 cm long.*



Figure 56. *Closeup view of limestone nodules coalescing to form beds in brown, calcareous siltstone outcrop (Rabbitkettle Formation), field station 04LP032. Bedding dips to right (west). View looking south.*

a "holey" outcrop pattern. Locally the nodules become extensive enough to form continuous limestone interbeds.

Age, correlation and depositional environment

In the type area at the headwaters of the Rabbitkettle River, Northwest Territories, the Rabbitkettle Formation is greater than 1200 m thick (Gabrielse *et al.*, 1973) and consists of interbedded limestones, silty limestones and siltstones. It is characterized by a wavy banding of silty layers and a 'swiss-cheese' texture resulting from the recessive weathering of limestone boudins in a more resistant network of silty beds. Although unfossiliferous in the type area, fossils collected regionally from the Rabbitkettle Formation encompass upper Cambrian (Franconian) through Lower Ordovician (Gabrielse *et al.*, 1973; Tipnis *et al.*, 1978; Cecile, 1982). The formation in the type area is bounded by unconformities at both its lower and upper contacts. The lower unconformity is angular and marks a major stratigraphic break since, regionally, the Rabbitkettle Formation overlies strata as old as the Precambrian-lower Cambrian Hyland Group (Gabrielse *et al.*, 1973).

The Rabbitkettle Formation in the map area constitutes only the uppermost part of the Rabbitkettle as defined and mapped farther to the north and west. Conodont collections (Tables IV-3 and IV-4, Appendix IV) from the underlying Crow Formation and the overlying Sunblood Formation in this area are both Lower Ordovician (Tremadocian). Crow Formation is correlative with the Rabbitkettle Formation as mapped regionally and indicates a major facies transition from calcareous, fine-grained, basinal to slope clastic rocks of the Rabbitkettle Formation to coarse quartzose clastic rocks of the Crow Formation in an eastward direction. This facies transition is local in areal extent since Crow Formation does not occur along strike to the north and south of southeast Yukon. Mapping by Gabrielse and Blusson (1969) confirmed that the Rabbitkettle Formation increases dramatically in thickness west and north of the present map area. The regional sub-Franconian unconformity noted at the base of the Rabbitkettle Formation (Gabrielse *et al.*, 1973) is considered to occur at the base of the Crow Formation.

Correlative strata include the Broken Skull Formation and Franklin Mountain Formation, both consisting of Cambrian-Ordovician carbonate rocks of the Mackenzie platform northeast of this map area. In northern British Columbia, correlative strata include the Cambrian-Ordovician Kechika Formation, occurring as a basinal slope facies west of the Skoki Formation of the MacDonald carbonate platform.

SUCCESSION 3 (ORDOVICIAN-SILURIAN)

Succession 3 is composed of Sunblood Formation overlain by interbedded sandstones, shales and bioturbated siltstones of Unit OSs. Unit OSs has a limited occurrence and is absent west, south and east of the map areas (Gabrielse and Blusson, 1969).

Sunblood Formation (OSu)

Introduction

The Sunblood Formation (Kingston, 1951) consists of medium to dark grey, tan- to tannish grey-weathering, fine-grained, interbedded dolostones and limestones. It is a resistant unit and locally forms cliffs over 30 m high (Fig. 57). The interpreted thickness of the Sunblood Formation in map sheet 95C/5 ranges from 150 to 550 m (Pigage and Allen, 2001). It increases in thickness to the west with an interpreted thickness of greater than 2000 m in the western part of map sheet 95D/8 (Pigage, 2006). The lower contact is poorly exposed, and the upper contact was observed in two areas in map sheet 95C/5.



Figure 57. *Large cliffs of tan-weathering dolostone (Sunblood Formation), field station 04LP050. Bedding dips to left (west). View looking north.*

The Sunblood Formation is interpreted to conformably overlie the Crow Formation. In the northern part of the map areas it is conformably(?) overlain by Unit OSs, an assemblage of sandstone, dolomitic siltstone and shale. In the southern part of map sheet 95C/5, Sunblood carbonate rocks are unconformably(?) overlain by thin-bedded, dark grey, cherty dolostones correlated with the Silurian Nonda Formation.

Two exposures of carbonate rocks in an area of very poor exposure in the southwest part of map sheet 95C/5 have been included in Sunblood Formation. One outcrop consists of medium to dark grey, tan-weathering, bioturbated, sandy dolostone. The other outcrop consists of dark grey, thick-bedded to massive, locally bioturbated limestone with beds ranging from 1 to 40 cm thick. These carbonate rock exposures occur on either side of the northeast-trending anticline cored by the Crow Formation.

Composition

Dolostone is the predominant lithology; limestone intervals within the dolostone range up to 60 m thick. Both limestone and dolostone are essentially monomineralic, with only very minor amounts of opaque minerals and quartz. Beds typically range between 5 cm and 1 m in thickness.

Dolostone and limestone intervals typically have a mottled appearance caused by bioturbation with irregular lighter grey patches scattered in the darker grey matrix (Fig. 58). Bedding planes in mottled outcrops are slightly irregular (Fig. 59). Locally, the carbonate rocks are finely laminated with millimetre-scale beds. Laminae exhibit primary depositional textures including erosional truncation of laminae (Fig. 60) and disharmonic slump fold structures. The thinly laminated variant of the

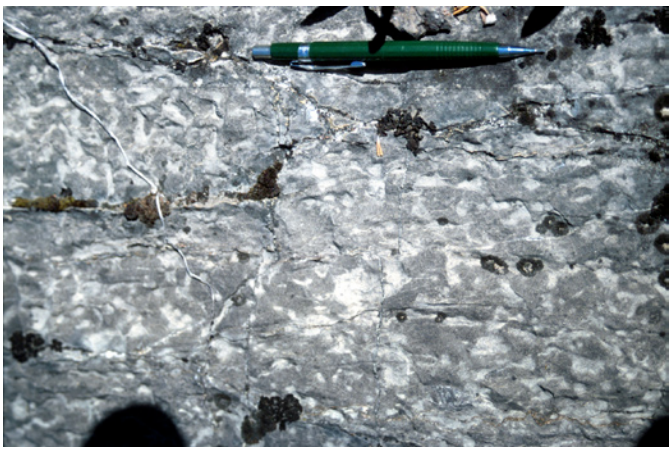


Figure 58. *Fossil burrowing pattern on surface perpendicular to primary bedding, Sunblood Formation, field station 01LP057. Bedding is parallel to pencil.*

Sunblood Formation contains no visible fossils. Mottled, irregular bedded outcrops locally contain visible crinoid ossicles, star crinoid ossicles and shell fragments. Fossils are destroyed during recrystallization of limestone to dolostone (Fig. 61). In the northwest corner of the Pool Creek map sheet (UTM 337 790E/6 708 695N, zone 10) dolostone beds near the top of the Sunblood Formation contain irregular black chert nodules (up to 5 cm thick and 15 cm long; Fig. 62) elongate in the bedding plane.

In one outcrop, Sunblood dolostones contain a fine-grained, 1.5 to 2.0 m-thick, dark green basalt sill (Fig. 63). The centre of the sill is amygdaloidal with 1 cm-diameter vesicles infilled with calcite. Table III-4 contains a geochemical analysis of this basalt sill (station 01LP093, Appendix III).

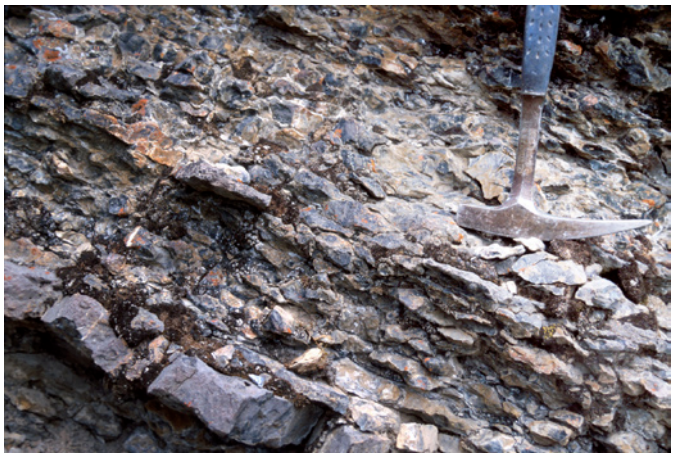


Figure 59. *Fossiliferous, recessive limestone, Sunblood Formation, field station 01LP050. Bedding dips down gently to the right.*



Figure 60. *Parallel-laminated limestone, Sunblood Formation, field station 01LP050.*

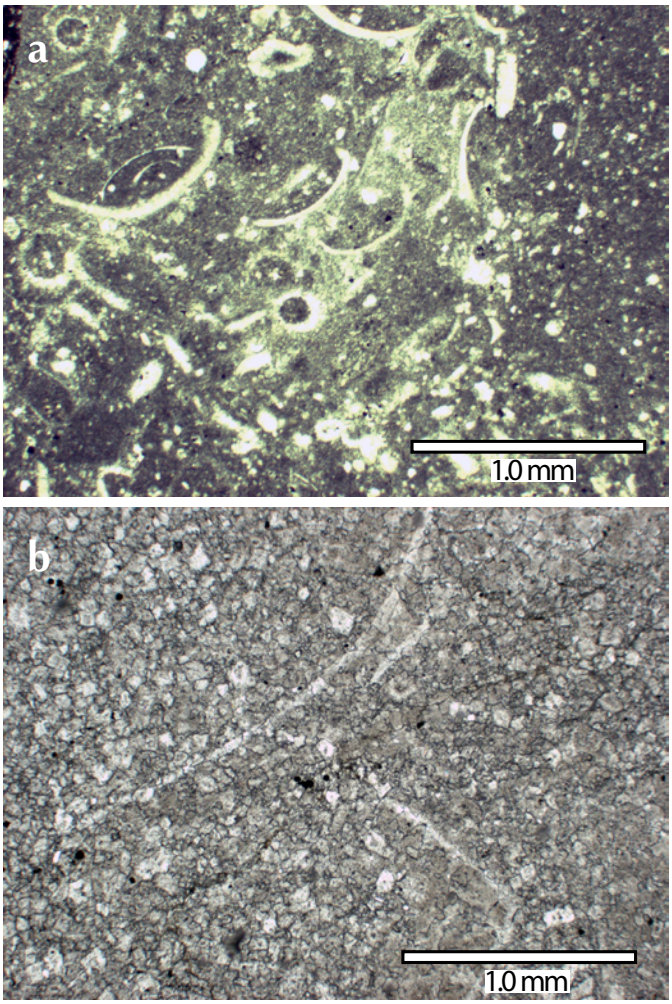


Figure 61. *Sunblood Formation thin sections, plane view.* ***(a)*** *Fossiliferous limestone, plane light, field station 01LP071; scale bar is 1.0 mm.* ***(b)*** *Poorly fossiliferous dolostone, plane light, field station 01LP070; scale bar is 1.0 mm.*



Figure 62. *Thin-bedded, tan weathering, fine-grained, grey dolostone with black chert nodules up to 5 cm across, Sunblood Formation, field station 00LP051. Chert nodule to right of scale card.*



Figure 63. *Basaltic sill in Sunblood Formation, field station 01LP093.*

Age, correlation and depositional environment

Conodont samples indicate the lower contact of the formation is diachronous, ranging in age from Tremadocian in map sheet 95D/8 to upper Lower Ordovician to lower Middle Ordovician in map sheet 95C/5 (see Table IV-4, Appendix IV). The Tremadocian age is earlier than the age of the bottom of the Sunblood Formation in its type area. Two conodont samples from near the top of the unit in the southern part of the map area have a lower Whiterockian age. In contrast, two samples from the top of the formation in the central and northwestern parts of the map area have an age range of upper Middle Ordovician to lower Upper Ordovician (Rocklandian). These latter two samples have ages which are younger than the upper contact of the Sunblood Formation in its type area. This indicates that the uppermost part of the Sunblood Formation, as mapped in the Pool Creek and 95D/8 map sheets, includes carbonate rocks differentiated as the Esbattoine Formation overlying the Sunblood Formation farther to the north and east.

Sunblood Formation is exposed in Northwest Territories and Yukon over a wide area north and west of the map area. The Sunblood carbonate rocks were deposited in a shallow, dominantly sublittoral (0-100 m depth) environment on a carbonate platform up to 100 km wide (Ludvigson, 1975). The formation is bounded on the southwest by deeper water, dark grey to black shale facies (Road River Group) of Selwyn basin.

Ordovician-Silurian sandstone, siltstone and conglomerate (OSs)

Introduction

Unit **OSs** occurs as scattered outcrops of sandstone and pebbly sandstone with lesser interbeds of pebble to cobble conglomerate, bioturbated dolomitic siltstone and dark grey silty shale (Fig. 64). It has an interpreted thickness of 160 to 200 m. The lower contact with Sunblood Formation is marked by an abrupt change from dolostone to sandstone. The upper contact is not exposed but is marked by a rapid change to black, silty, graptolitic shales and limestones of the Road River Group.

Composition

The predominant lithology consists of quartz-rich, noncalcareous to slightly calcareous, light grey, thick-bedded quartzose to arkosic sandstone. The sandstone weathers with a tan to orange-brown surface coating. Small black shale, quartz sandstone, K-feldspar, plagioclase, volcanic rock and chert clasts occur in minor amounts locally (Fig. 65). Fine to medium sand clasts are typically subround to round and consist predominantly of monocrystalline quartz. Sandstones that are more quartzose have epitaxial quartz growth around the quartz clasts. Beds range from 10 cm to 2 m in thickness. Cross-beds and horizontal feeding worm burrows occur locally.

The sandstone contains intervals up to 1 m thick with white, blue and lesser pale green quartz pebbles in a quartz sand matrix. Marginal contacts of the pebbly intervals are both sharp and gradational. The pebbles are typically matrix-supported, although occasionally they are extensive enough to be clast-supported. Minor



Figure 64. *Thick-bedded, quartzose sandstone with interbeds of recessive-weathering dolomitic siltstone and recessive dark grey silty shale, Unit* ***OSs****, field station 00LP064. Photo by T. Allen.*

chalky white K-feldspar clasts and very minor volcanic rock clasts are sometimes interspersed with the quartz pebbles. In one talus slope, some float pieces consisted of pebble conglomerate which was visually identical to the conglomerates described for the Crow Formation. Pebbles consisted of white quartz sandstone up to 5 cm across. This conglomerate was not found in outcrop and was noted only in one area.

The sandstone also contains recessive intervals up to 2 m thick of light grey, tan-weathering, bioturbated, dolomitic siltstone to fine sandstone (Fig. 66). The siltstone contains minor, discontinuous dark grey shaly partings. Dark grey to black, noncalcareous shale forms a third lithotype occurring in minor amounts as thin beds forming intervals up to 2 m thick.

Dolomitic siltstone and dark grey to black shale lithotypes decrease in abundance in a northwest to southeast direction. Outcrops along the Beaver River in the central part of the map area consist entirely of quartz sandstone, and approximately 50% of the unit in the northwest corner of the map sheet consists of dolomitic siltstone and interbedded grey shale.

Age, correlation and depositional environment

The **OSs** unit was not differentiated in the La Biche River regional mapping (Douglas, 1976). It was recognized and mapped during exploration geology in the 1980s (unit OSq in Cathro, 1983 and unit 3 in Burt, 1983). Allen *et al.* (2001) described **OSs** as unit 6 in their earlier study. Immediately to the west, Gabrielse and Blusson (1969) mapped the same unit as Unit 10 in the Coal River map sheet.

Unit **OSs** does not contain diagnostic fossils for determining an age of deposition. It is considered to be Ordovician to Silurian because it overlies the Ordovician Sunblood Formation and underlies the Silurian Road River Group (see next section). It represents a transitional depositional environment between platform carbonate sedimentation (Sunblood Formation) and euxinic, basinal siliciclastic sedimentation (Road River Group).

Cecile and Norford (1979) informally recognized a 180 m-thick interval of interbedded shale and quartzite with minor dolostone (unit OR_5 in the Road River Formation) in northeastern British Columbia which may be an equivalent unit. Recently unit OR_5 has been formally designated by Pyle and Barnes (2000) as the Ware Member of the Ospika Formation, Road River Group. It ranges in age from late Middle Ordovician (middle Caradoc) to Late Ordovician (Ashgill).

An abundance of bioturbation and horizontal worm burrows indicates the depositional environment contained abundant nutrients and was below wave base. This unit signifies a westward progradation of clastic facies overlying Sunblood carbonate rocks. Restriction of this unit to the northwest corner and western portion of the Pool Creek map sheet and northeastern part of map sheet 95D/8 suggests the source of the clastic debris for this formation was further to the north.

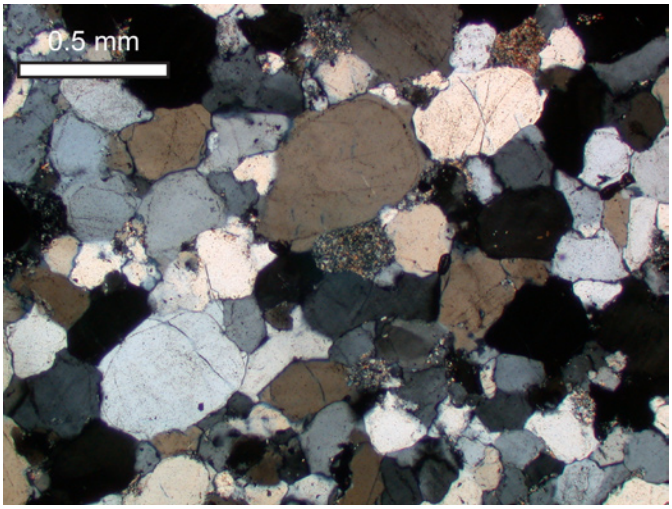


Figure 65. *Thin section photo of arkosic sandstone, unit* ***OSs****, field station 01TLA019. Sericitic plagioclase grain in centre of photo. Epitaxial quartz overgrowths on subround quartz clasts, crossed nicols. Scale bar is 0.5 mm.*



Figure 66. *Tan-weathering, recessive, bioturbated dolomitic siltstone, Unit* ***OSs****, field station 00LP064. Photo by T. Allen.*

SUCCESSION 4 (SILURIAN-DEVONIAN)

Succession 4 consists of black shales and carbonate rocks overlying shallow water siltstone and sandstone and platform carbonate rocks of succession 3. Formations in succession 4 have a facies polarity, with deep water shales occurring in map sheet 95D/8 and the northwest portion of map sheet 95C/5 and carbonate rocks occurring in the south part of map sheet 95C/5. Units within this succession include the Nonda Formation, Road River Group, undivided Muncho-McConnell-Stone formations, and Dunedin Formation.

The various formations of succession 4 consisting predominately of dolostone could not be differentiated in the southwest part of the Pool Creek map sheet because of sparse outcrop. In this region, therefore, the Nonda, Muncho-McConnell-Stone and Dunedin formations have been mapped as a single map unit SDc (Silurian-Devonian carbonate).

Nonda Formation (SN)

Introduction

Exposures of dark grey, fetid, locally nodular dolostone at two localities in the central part of the Pool Creek map sheet have been assigned to the Nonda Formation (Norford *et al.*, 1966) based on their general stratigraphic position and lithologies. Similar strata are not exposed in map sheet 95D/8. The lower contact with the underlying Sunblood Formation thick-bedded dolostones is sharp. The upper contact with medium grey to buff-weathering, thick dolostones of the undivided Muncho-McConnell-Stone formations is exposed in cliffs overlooking a tributary of the Beaver River near UTM 350 330E/6 698 270N, zone 10. In the northern exposures where formation contacts are most tightly constrained, interpreted thickness of the Nonda Formation is 90 m. In the southern exposures where contact locations are less tightly constrained, the estimated thickness is 200 m.

Composition

In the north-central Pool Creek map sheet (UTM 350 200E/6 698 500N, zone 10), the Nonda Formation is a finely crystalline, dark grey, fetid, thin-bedded dolostone with interbeds and lenses of black chert (Fig. 67). Beds are typically 3 to 10 cm thick. Overall the outcrop has a bedded chert aspect with dolostone and chert beds being separated by black, shaly partings. Chert beds constitute up to 50% of the unit. Beds are locally undulatory. Commonly, the formation has dark grey, medium-grained, ovoid dolostone concretions up to 20 cm in diameter. Locally the unit contains fossil debris, including crinoid ossicles. In plan view, the chert nodules have a polygonal distribution on the bedding plane (Fig. 68).

In the south-central Pool Creek map area (UTM 350 100E/6 686 500N, zone 10) the dolostone is dark grey, fetid, and fine to medium crystalline. The outcrop consists of interbedded massive and bioclastic intervals ranging from 50 cm to 2 m in thickness (Fig. 69). Fossils include crinoid ossicles and corals. The major similarity with more northern outcrops is the dark grey, fetid character of the dolostone.

Age, correlation and depositional environment

The type area for the Nonda Formation is in northeastern British Columbia (Norford *et al.*, 1966). Both upper and lower contacts are unconformable in the type area. Norford *et al.*, (1966) further indicated the Nonda Formation represents the westernmost



Figure 67. *Thin-bedded dolostone with irregular, black chert beds and nodules, Nonda Formation, field station 01LP102.*



Figure 68. *Irregular chert nodule pattern on bedding plane of thin-bedded dolostone, Nonda Formation, field station 01LP103. Pencil for scale.*



Figure 69. *Interbedded dark grey, massive dolostone and dark grey, bioclastic dolostone (centre), Nonda Formation, field station 01TLA042. Photo by T. Allen.*

exposures of MacDonald platform carbonate rocks, with a rapid westward transition to carbonaceous graptolitic shales and siltstones of the Road River Group. A recent stratigraphic study by Pyle and Barnes (2001) in northeastern British Columbia has documented in more extensive detail the platform carbonate succession (Nonda Formation) to basinal shale succession (Road River Group) occurring in an east to west direction. Fossil assemblages from the early study indicated an upper Llandovery age for the Nonda Formation (Norford *et al.*, 1966). Conodont assemblages delineated a lower to middle Llandovery age (Pyle and Barnes, 2001). Samples collected for fossil control in the Pool Creek map area resulted in conodont assemblages with a wide-ranging age of Middle Ordovician to Middle Devonian, thus not providing any tighter constraints than previously published age ranges for the Nonda Formation. The upper Middle Ordovician age of the uppermost Sunblood Formation from this study would suggest that the lower contact of the Nonda Formation is unconformable (Fig. 4), with a depositional hiatus occurring between the two formations.

Nonda Formation has not been previously delineated in the Pool Creek map area; rather, it was included within a Middle Devonian and older carbonate succession (Douglas, 1976). Gabrielse and Blusson (1969) did recognize and map Nonda Formation within the same carbonate succession in the Coal River map sheet immediately to the west.

These correlations and age ranges indicate a platform carbonate to basin facies transition occurring in a northward direction in the northern part of the Pool Creek map area during Llandovery time. This facies change marks a major transgression of Selwyn basin deep water siliciclastic facies from the west during early Silurian.

Road River Group (SDRR-a and SDRR-b)

Introduction

The Road River Formation was first described and defined in northern Yukon (Jackson and Lenz, 1962). In the type area it consisted of two members: a lower limestone unit (upper Cambrian to Lower Ordovician; Norford, 1964) and an upper shale, limestone and chert unit (Ordovician to Lower Devonian; Jackson and Lenz, 1962; Lenz, 1966, 1972). In southern Yukon, Gabrielse *et al.* (1973) restricted the Road River Formation to include only the upper recessive carbonaceous shale-dominated portion of the original formation; the lower limestone member was excluded from the Road River Formation and assigned to the Rabbitkettle Formation. More recently, Fritz (1985) and Gordey and Anderson (1993) raised the Road River Formation to formal group status. Gordey and Anderson (1993) retained the exclusion of Rabbitkettle Formation from the Road River Group. This discrepancy over what is included within the Road River Group has not been resolved, and reflects differences in mapping practices between northern and southern Yukon. Pyle and Barnes (2000) have followed the definition proposed by Gabrielse *et al.* (1973) in describing their detailed sections in northeastern British Columbia. More extensive discussion concerning the current status and usage of Road River may be found in Morrow (1999).

In Pool Creek and 95D/8 map areas, Road River Group forms recessive scree slopes and scattered outcrops, largely along Beaver River. Two lithofacies have been differentiated for the Road River Group in the map area. Facies A (SDRR-a) is the predominant lithofacies and outcrops in the northwest part of the Pool Creek map area and the northeast part of map sheet 95D/8. It consists of intimately interbedded shale, siltstone, sandstone, limestone and bedded chert. Exposures of Facies B (SDRR-b) in the map areas are restricted to the northwest corner of the Pool Creek map sheet. There it consists of black, siliceous, silty shale.

Lower and upper contacts of the Road River Group are not exposed. The lower contact is assumed to be unconformable based on age constraints for Road River Group in the map area. A 1984 drill program completed by Utah Mines Ltd. in the Pool Creek map sheet drilled several diamond drill holes through the upper contact with the overlying Dunedin Formation (Burt, 1985). This contact appeared to be gradational with interbedding

of limestone, dolostone, chert, shale and siltstone. Interpreted thickness of the unit ranges from 950 to 1000 m depending on the area being considered.

Composition

*Road River Group – Facies A (**SDRR-a**)*

Facies A (**SDRR-a**) is a highly varied unit consisting of silty shale, siltstone, sandstone, argillaceous limestone, siliceous shale, dolostone and bedded chert, all interbedded on a scale of less than one metre to tens of metres. All lithotypes are dark grey to black and commonly contain visible graptolites.

The predominant lithology is a dark grey to black, brown- to grey-weathering, finely planar laminated siltstone interbedded with lesser silty shale (Fig. 70). Both siltstone and shale commonly contain fine detrital micas visible on the bedding surfaces. Locally, the shale weathers with a yellow jarositic surface coating. Pyrite nodules up to 3 cm across occur sporadically. Many outcrops are dolomitic; fewer are calcareous or noncalcareous. Locally dolomitic carbonate concretions up to 0.5 m thick occur scattered along a single stratigraphic horizon.

Interbedded with the siltstone and shale are lesser intervals of dark grey to black, finely crystalline, argillaceous limestone (Fig. 71). Limestone beds are 30-60 cm thick with 1-2 cm shaly partings every 10-15 cm. The limestone beds rarely contain discontinuous black chert beds and lenses.

Black bedded chert occurs as a minor lithotype interbedded with the other lithologies. Chert beds are 5 to 10 cm thick with 1 to 3 cm thick shaly partings (Fig. 72). Bedded chert intervals are up to 8 m thick. Locally bedded cherts also contain elongate buff dolostone nodules.

Locally, dark grey, argillaceous, noncalcareous to slightly dolomitic fine-grained sandstone (Fig. 73) is interbedded with siltstone and silty shale. Detrital micas are readily visible on bedding surfaces. Sandstones are massive to planar-laminated. Typically, they contain thin interbeds of shaly siltstone up to 5 cm thick.

*Road River Group – Facies B (**SDRR-b**)*

In the northwest corner of the Pool Creek map sheet, a separate Facies B lithotype can be differentiated within the Road River Group (**SDRR-b**). Facies B is a pale grey-weathering, black, siliceous, noncalcareous, poorly fossiliferous, silty shale (Fig. 74). Exposures typically weather to smooth thin plates, which break between the fingers with difficulty. Graptolites are not present within this facies. It does contain sparse straight cephalopod



Figure 70. *Planar-laminated, dolomitic, dark grey to black siltstone, Road River Group-facies A, field station 01TLA066. Photo by T. Allen. Hammer head (circled) at bottom of photo for scale.*



Figure 71. *Dark grey, bedded limestone, Road River Group-facies A, field station 01LP063. Hammer for scale. Photo by T. Allen.*



Figure 72. *Bedded chert interval within Road River Group-facies A, field station 01TLA066. Photo by T. Allen.*



Figure 73. *Interbedded resistant, fine-grained sandstone and recessive, platy, silty shale, Road River Group-facies A, field station 00LP055. Hammer (circled) for scale. Photo by T. Allen.*



Figure 74. *Slumped outcrop of* ***SDRR-b****, siliceous, pale grey-weathering silty shale, Road River Group, field station 00LP045.*

macrofossils up to 10 cm long. In the Pool Creek map sheet, Facies B appears to conformably overlie Facies A.

Age, correlation and depositional environment

Graptolite and conodont fossil collections from Facies A in the Pool Creek area (Table IV-6, Appendix IV) have age ranges extending from Late Ordovician to Early Devonian. Two of the graptolite samples have more restricted ranges of Telychian and Wenlock (both early Silurian). One of the conodont samples has a restricted range of Llandovery (early Silurian).

Fossils from Facies B (see Table IV-6, Appendix IV) were assigned a broadly Silurian age and were correlated with similar fossils from the Silurian siltstone in northeastern British Columbia (Norford, 2001). Recent fossil collections from Silurian siltstone in British Columbia suggest an Upper Ordovician to a Lower Devonian (Emsian) range (Ferri *et al.*, 1996) for that unit. More recently, the Silurian siltstone has been formally designated as the Kwadacha Formation within the Road River Group (Pyle and Barnes, 2000).

Road River Group in the map area is therefore considered to range from lower Silurian (Telychian) to Lower Devonian (Emsian). The upper age of deposition is not well constrained by fossils. However, the upper contact of Road River Group with Dunedin Formation appears to be conformable with interbedding of lithologies, and the overlying Dunedin Formation does contain two-hole crinoid fossils (Emsian to Eifelian). Therefore, it is reasonable that Road River deposition extended into Lower Devonian.

This age range for Road River Group is more restricted than the age range for Road River Group in other areas of Selwyn basin and Kechika trough further to the west. In northeastern British Columbia, the Road River Group ranges from Lower Ordovician-Arenigian to Middle Devonian (Pyle and Barnes, 2002). Similarly Gordey and Anderson (1993) have graptolite faunas starting in Lower Ordovician-lower Arenigian for Road River Group carbonaceous shales in central Yukon. In both of these areas, the Road River shales are overlying calcareous shales older than Sunblood Formation. The lower contact of the Road River Group is therefore regionally diachronous and becomes younger in an eastward direction.

Outcrops presently grouped as Road River Group in the map area have previously been divided into several poorly constrained shale units. Douglas and Norris's (1959) unit 4 locally includes Road River Group and Besa River Formation. Road River Group also corresponds to parts of Psh (Paleozoic shale) and OSD (Ordovician-Silurian-Devonian limestone or shale) in the compilation map by Douglas (1976). Outcrops assigned to Road River Group in this report correspond to parts of units 7, 8 and 10 in the previous study by Allen *et al.* (2001).

The depositional environment represented by the Road River Group is a relatively deep, euxinic, quiet basin. Bedded cherts are probably biogenic, formed from radiolarian detritus. Intervals of sandstone represent influxes of siliciclastic material into the shale basin, presumably from an eastern provenance. The age range of the Road River Group in the Pool Creek map sheet corresponds to the age range for the Nonda and Muncho-McConnell-Stone formations immediately to the south and east, and therefore Road River Group is correlative with these units. Proposed unconformities at the base and top of the Nonda Formation would suggest that

the Road River Group contains internal, unrecognized unconformities.

Muncho-McConnell and Stone formations undivided (SDMMS)

Introduction

Thick-bedded dolostones of the undivided Muncho-McConnell (Taylor and MacKenzie, 1970) and Stone (Taylor and MacKenzie, 1970) formations form prominant cliffs locally greater than 300 m high along the Beaver River and associated tributaries in the east-central part of the Pool Creek map sheet. They overlie the Nonda Formation and underlie the Dunedin Formation. The lower contact of the dolostone is exposed in cliffs overlooking a tributary flowing into the Beaver River (near UTM 350 330E/6 698 270N, zone 10); the contact appears conformable in this location. The upper contact is poorly exposed but moderately constrained along the Beaver River (UTM 357 680E/6 696 680N, zone 10) where it is conformably overlain by fossiliferous dolostones of the Dunedin Formation. Interpreted thickness based on these contact locations is approximately 1080 m. The dolostone cliffs form a moderately northeast- to east-dipping, homoclinal succession through the central and southern parts of the Pool Creek map sheet. It is structurally repeated along several west-verging reverse faults with small amounts of displacement.

Composition

The undivided Muncho-McConnell-Stone formations consist entirely of a dark to light grey, buff-weathering, thick-bedded, fine to medium crystalline dolostone (Fig. 75). Beds range from 10 cm to greater than 7 m in thickness; generally they are 1 to 2 m thick. Locally, these thicker beds are internally fine planar parallel-laminated with thin laminae spaced 2 mm to 1 cm apart. Bedding contacts are sometimes undulatory with a relief of up to 30 cm. The dolostone contains minor small convex vugs, typically up to 1 cm across, which are generally lined with small white dolomite crystals. Fossils are not visible.

Age, correlation and depositional environment

Douglas (1976) mapped this unit as a Middle Devonian and older carbonate unit. It correlates with unit 13 as mapped by Gabrielse and Blusson (1969) in the Coal River map sheet immediately to the west. Based on its stratigraphic location, equivalent units in northeastern British Columbia are the Muncho-McConnell, Wokkpash, and Stone formations (Taylor and MacKenzie, 1970). In northeast British Columbia, the Stone Formation is separated from the Muncho-McConnell Formation by the intervening Wokkpash Formation sandstones. No sandstones were noted anywhere through the entire dolostone succession in the Pool Creek map area. This thick carbonate accumulation in the map area is therefore presented as an undivided succession of dolostones forming part of the lower to middle Paleozoic MacDonald carbonate platform. Correlative marine shales and sandstones farther west are represented by the Road River Group of Selwyn basin. Sparse fossils from the Muncho-McConnell, Wokkpash and Stone formations in British Columbia indicate an age range from Lower to Middle Devonian. The few productive samples from the map area containing conodonts do not further restrict the age of the dolostones (Table IV-8, Appendix IV).



Figure 75. *Large outcrop along the Beaver River of thick-bedded dolostone, undivided Muncho-McConnell-Stone formations, field station 01LP115. Person for scale (circle) on right side of photo.*

Unconformities are recognized at the base of each of the Muncho-McConnell, Stone and Dunedin formations (Taylor and MacKenzie, 1970; Morrow and Geldsetzer, 1992). These unconformities have regional extent and divide the MacDonald and Mackenzie carbonate platforms into successive stratigraphic packages of laterally equivalent formations separated by discontinuities. From oldest to youngest, these are the Delorme sequence (Muncho-McConnell Formation), Bear Rock-Stone sequence (Wokkpash and Stone formations), and the Hume-Dunedin sequence (Dunedin Formation). In the map area, similar unconformities cannot be confirmed anywhere in the succession because of the lack of fossil control and the lack of variation in the dolostones. An unconformity at the base of the undivided

Muncho-McConnell-Stone formations is inferred (see Fig. 4) on the basis of the regional age of the correlated Muncho-McConnell Formation.

Dunedin Formation (DD-l and DD-d)

Introduction

Conformably overlying the Road River Group or the Muncho-McConnell-Stone formations is a succession of dolostones and limestones constituting the Dunedin Formation (Taylor and MacKenzie, 1970). Two facies have been mapped within this unit, a predominantly dolostone facies (DD-d) and a limestone facies (DD-l). There is a systematic change in facies from the northwest to the southeast, with the DD-l facies occurring dominantly in the northwest corner of the Pool Creek map sheet, and the DD-d facies occurring in the north-central and eastern parts of the Pool Creek map sheet. In both areas the lower contact is conformable and is marked by the first appearance of abundant, medium-bedded, fossiliferous carbonate rocks. Drill holes on the BEAV property (Burt, 1985) locally detail interbedding of black shales, dolostones and limestones over a 5–10 m interval at the lower contact with the Road River Group. Near UTM 357 680E/6 696 680N, zone 10, the lower contact with the Muncho-McConnell-Stone formations is delineated by the first appearance of bedded, fossiliferous, grey dolostone, which is interbedded with the typical thick-bedded, cream dolostones of the underlying Muncho-McConnell-Stone formations. The upper contact is marked by a sharp transition to the fine-grained siliceous shales of the Besa River Formation. Interpreted thickness of the unit from cross-sections ranges from 120 to 750 m.

The Dunedin Formation was not encountered above the Muncho-McConnell-Stone formations in two areas within the same structural panel along the Beaver River (UTM 351 780E/6 698 900N, zone 10 and UTM 354 930E/6 694 270N, zone 10). The local absence of the fossiliferous Dunedin in this structural panel is interpreted as being stratigraphic rather than structural.

Composition

Dunedin Formation – Facies DD-l

Excellent riverbank exposures of lithofacies DD-l are located at UTM 341 400E, 6 707 250N, zone 10 in the northwest part of the Pool Creek map sheet. The lithofacies consists dominantly of dark grey to black, medium- to thick-bedded, argillaceous, micritic limestone with thin dark grey shale or light grey siltstone interbeds (Fig. 76). Locally, the limestone beds contain thin nodules or discontinuous beds of black chert. Sparse grainstones up to 10 cm thick contain fossil debris consisting of crinoid columns with single and twin axial canals. The uppermost 20 m of the unit is more resistant and forms steep cliff outcrops (Fig. 77). Limestone beds within the uppermost resistant unit are 2 to 150 cm thick with thin, recessive, medium to dark grey, calcareous shale or siltstone interbeds.

Dunedin Formation – Facies DD-d

Lithofacies DD-d occurs as scattered outcrops in the north-central and eastern parts of the Pool Creek map sheet. The most continuous exposures through the unit occur at UTM 348 000E/6 703 000N, zone 10. This facies generally is a dark grey to black, fine-grained, medium dark grey-weathering, fetid dolostone (Fig. 78). It is medium- to thick-bedded with beds ranging from 5 to 50 cm thick. Bedding is crudely undulatory. Locally the dolostone is internally laminated on a millimetre scale. The dolostone contains lenses and discontinuous beds of black chert (Fig. 79), with chert representing 5–20% of any particular outcrop. Commonly, the chert beds contain fossil hash consisting dominantly of crinoid columns.

Interbedded with the micritic dolostone are intervals of massive to thick-bedded, medium grey, pale grey-weathering, fine- to medium-grained, highly fossiliferous dolostone (Figs. 78 and 80). Beds range in thickness from 20 cm to greater than 1 m. Intervals of this fossiliferous dolostone range up to 10 m thick; their extent and thickness increase in an eastward direction within the Pool Creek map sheet.

In the eastern part of map sheet 95C/5, the lower contact of the Dunedin Formation where it overlies the



Figure 76. *Closeup view of argillaceous, micritic limestone, Dunedin Formation, field station 00LP060. Light bands going across photo are thin siltstone intervals; bedding dips gently from upper left to lower right. Pervasive slaty cleavage goes from lower left to upper right in photo.*

Muncho-McConnell-Stone formations is delineated by the lowermost bed of dark grey dolostone with abundant two-hole crinoid ossicles interbedded with the thick-bedded, creamy dolostones typical of the Muncho-McConnell-Stone formations; interbedding of the two lithologies is on a scale of 10 m. Internal beds in the fossiliferous dolostone are typically up to 1 m thick; vugs up to 10 cm across are abundant.

Age, correlation and depositional environment

The age range for the Dunedin Formation is restricted to Emsian (upper Lower Devonian)-Eifelian (lower Middle Devonian) by the common presence of crinoids with twin



Figure 77. *Resistant uppermost limestone interval in Dunedin Formation, field station 00LP056. Tree at edge of Beaver River immediately beneath light-coloured circle (caused by sun shining into lens) is about 4 m high. Limestone beds are undulating. Photo by T. Allen.*



Figure 78. *Cliff outcrop of dark grey dolostones, Dunedin Formation, field station 01TLA082. View looking north. Medium grey dolostone in centre (at hammer) is fossiliferous grainstone. Photo by T. Allen.*



Figure 79. *Closeup of black chert lens within dark grey dolostone, Dunedin Formation, field station 01LP076.*

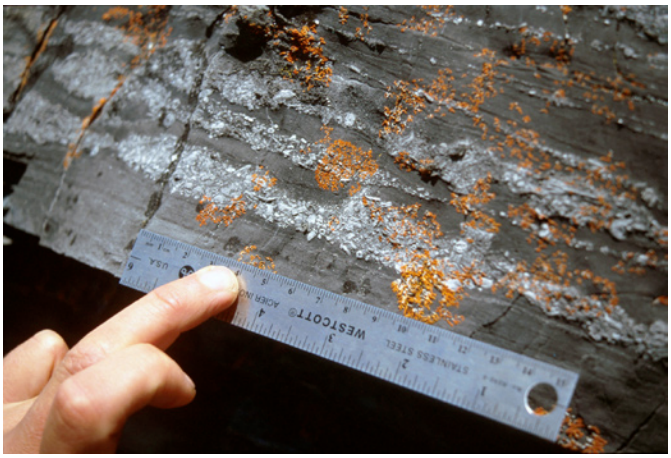


Figure 80. *Closeup of fossiliferous grainstone in dark grey dolostone, Dunedin Formation, field station 01TLA082. Photo by T. Allen.*

axial canals (Gasterocoma(?) bicaula Johnson & Lane?) throughout the unit. Conodont-bearing samples collected in the map areas are consistent with this age range (Table IV-9, Appendix IV).

Douglas and Norris (1959) and Douglas (1976) mapped this unit as part of the Middle Devonian and earlier carbonate succession (unit 3 or Pc). Allen *et al.* (2001) originally designated it as unit 10. More recently, (Pigage and Allen, 2001), the limestone lithofacies was designated as Dl, and the dolostone lithofacies was designated as Dfd. Dunedin Formation is correlative with the Hume, Nahanni and Headless formations of the Mackenzie platform. Morrow (1978) extensively studied the Dunedin Formation in northeastern British Columbia. Regionally the lower contact is unconformable (Morrow, 1978). It is the major formation in the transgressive Hume-Dunedin sequence (Morrow and Geldsetzer, 1992). The correlative marine shale occurring north and west of the above transitional and platform carbonate formations is the Besa River Formation (Morrow, 1978).

Morrow (1978) documented that stratigraphic facies within the Dunedin Formation delineate transgression and inundation during Dunedin deposition. In southeast Yukon, the Dunedin Formation extends further west and northwest than the undivided Muncho-McConnell-Stone formations (Fallas *et al.*, 2005). The increasing thickness of fossiliferous grainstones in the unit to the east and southeast is consistent with a facies change to an increasingly shallow water platform edge in an east to southeast direction.

SUCCESSION 5 (DEVONIAN-LOWER CARBONIFEROUS)

The base of succession 5 is marked by a major transgression with deposition of deep water shales of the Besa River Formation over carbonate lithologies of the Devonian Dunedin Formation. Besa River Formation shales are in turn overlain by shallow water to tidal to alluvial deposits of the Mattson Formation.

Besa River Formation (DCBR)

Introduction

Outcrops of dark grey to black silty shale, limestone and bedded chert overlying the carbonate rocks of the Dunedin Formation and underlying the sandstones of the Mattson Formation are assigned to the Besa River Formation (Kidd, 1963). The lower contact is exposed in the cliffs where Pool Creek drains into the Beaver River (UTM 357 870E/6 697 190N, zone 10). The upper contact with the Mattson Formation is placed at the base of the first substantial quartz sandstone bed within black shales; this contact is poorly exposed on a north-trending ridge in the north-central part of the map area (UTM 347 300E/6 707 000N, zone 10). This upper contact is consistent with that proposed by Richards (1989) for parts of southeastern Yukon. The Besa River Formation occurs in several structural panels in the Pool Creek map area, separated by west-verging reverse faults. In map sheet 95D/8, it occurs as a west-dipping succession in the central part of the map area. Interpreted thickness for the unit ranges from 250 to 1000 m.

Composition

The dominant lithology is a black, silty, siliceous, finely parallel-laminated shale (Fig. 81) which constitutes some 60–75% of the unit. Typically, the shale weathers light



Figure 81. *Carbonaceous shales of the Besa River Formation, field station 01TLA123. Photo by T. Allen.*

grey to off-white; locally, it weathers with patchy rust brown and yellowish jarositic surface coatings. Former pyrite nodules up to 1 cm across now form holes with rust brown iron oxide coatings. Weathered surfaces locally have small selenite crystals growing on them. The shale weathers into small plates which sound like broken dishes when walked on. Typically it is noncalcareous, although locally it is calcareous or dolomitic. Beds are typically 5–20 cm thick and are separated by 1–10 mm recessive shaly partings. Ovoid, finely laminated, dark grey to black limestone concretions up to 2 m thick (Fig. 82) are restricted to specific stratigraphic horizons.

Noncalcareous, rusty-weathering, black bedded chert (Fig. 83) is interbedded with the silty shales. Chert beds range from 2–15 cm thick with 1–3 cm shaly partings between them. Thicker chert beds are internally planar-laminated on a millimetre scale. Bedded cherts commonly constitute 20–30% of a larger outcrop. Bedded cherts may grade laterally to siliceous shales; in this case, the shales retain the bedded aspect, even though they can be readily scratched with a metal nail.

Dark grey to black, parallel-laminated, silty limestone beds (Fig. 84) up to 1.5 m thick are also interbedded with the other lithologies. Limestone beds are locally nodular; one nodule had a black chert core.

Age, correlation and depositional environment

Besa River Formation is equivalent to the upper part of Douglas and Norris's (1959) map unit 4 for the La Biche River map (95C). Richards (1989) discussed stratigraphic correlation of Besa River Formation with eastern shale and carbonate formations through facies relations in southeastern Mackenzie Mountains. Bamber *et al.* (1968) noted that Dunedin Formation laterally changes to Besa River Formation in a northward direction in northeastern British Columbia.

The Besa River Formation regionally ranges from Middle Devonian to Middle Mississippian (late Visean) (Richards, 1989). Both upper and lower contacts are diachronous, with the age of the lower contact becoming older and the age of the upper contact becoming younger from east to west (Bamber and Mamet, 1978). Macrofossils were not found in the Besa River Formation in the map area. Conodont collections from limestone interbeds within the formation resulted in age assignments of Devonian to early Carboniferous (Table IV-10, Appendix IV; McCracken, pers. comm., 2003).

Besa River Formation was deposited in a quiet, deeper water marine basin.



Figure 82. *Large limestone concretion in siliceous shales of the Besa River Formation, field station 00LP057. Hammer (circled) in centre of photo for scale. Photo by T. Allen.*



Figure 83. *Bedded chert in Besa River Formation, field station 00LP058. Photo by T. Allen.*



Figure 84. *Dark grey limestone bed in Besa River Formation, field station 01LP139. Hammer adjacent to limestone interval.*

Mattson Formation (CM, CM-a, CM-b)

Introduction

Mattson Formation (Patton, 1958) is exposed in several north-trending structural panels in the map area. It consists dominantly of fine- to medium-grained sandstone with lesser interbedded carbonaceous shale and limestone. The lower contact with the underlying Besa River Formation is gradational with interbedding of shale and sandstone lithologies. This contact is best exposed in a north-trending ridge north and east of the Beaver River (UTM 347 500E/6 707 000N, zone 10). At the upper contact, the Mattson Formation is unconformably overlain by the undivided Triassic Grayling and Toad formations in the Pool Creek map sheet and the Permian Fantasque Formation in map sheet 95D/8. Two members, a lower CM-a and upper CM-b, are differentiated in the northern Pool Creek map sheet. The Mattson Formation is undivided in map sheet 95D/8 and the southwest part of the Pool Creek map sheet. Interpreted thickness of the formation ranges from 1850 to 2850 m in 95C/5, with the lower member ranging in thickness from 250 to 350 m. In 95D/8 the entire formation has an interpreted thickness of 1450 m.

Composition

Mattson Formation – lower member (CM-a)

The lower member CM-a is characterized by interbedded carbonaceous shale and dark to light grey, fine- to medium-grained, thick-bedded, noncalcareous, well-indurated, well-sorted sandstone on a scale of 5 to 15 m. In Figure 85, this interbedding is visible as intervals

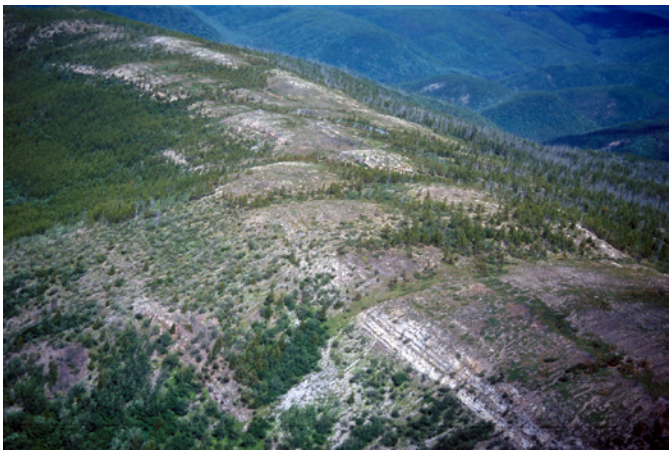


Figure 85. *Helicopter view of interbedded sandstone and carbonaceous shale, lower member a, Mattson Formation, field stations 01TLA098, 01TLA099. View looking north. Photo by T. Allen. Four sandstone horizons with interbedded shale intervals are visible. Each sandstone interval is about 10 m thick.*

of resistant sandstone with recessive intervals of black, noncalcareous, carbonaceous shale of similar thickness. Sandstone bands contain beds ranging from 10 to 200 cm in thickness. Beds are locally faintly parallel-laminated; more commonly they are massive (Fig. 86). Internally, the sandstone-rich intervals contain 20 to 100 cm-thick interbeds of black, noncalcareous shale.

Sandstones are composed dominantly of subround to subangular quartz grains. Minor constitutents include up to 5% randomly oriented grains of organic material up to 5 mm across, 1–3% coarse detrital muscovite, and locally 1–5% orange oxidized pyrite. Quartz grains are monocrystalline and typically show small silica overgrowths which substantially reduce porosity (Fig. 87). Bright orange to orange-brown Liesegang rings typically occur as a surface-coating weathering pattern on fractures (Fig. 88). Load casts are visible on bedding planes of sandstone overlying shale. Locally, feeding traces parallel to bedding are visible on bedding surfaces.



Figure 86. *Massive sandstone,* ***CM-a****, Mattson Formation, field station 01LP084. Bedding dips gently from upper left to lower right in photo, parallel to fractures.*

Black shale interbeds in the lower member are identical in appearance to the underlying Besa River Formation. Typically, they weather as recessive slopes containing abundant light grey silty shale chips. Locally, thin stratigraphic horizons within the shale weather with bright orange and red surface coatings.

*Mattson Formation – upper member (**CM-b**)*

The upper member **CM-b** consists of interbedded sandstone and argillaceous sandstone with lesser limestone intervals. Sandstones generally weather to tan, orange or yellowish-brown (Fig. 89). The lower part is thin- to medium-bedded with beds ranging between 1 to 30 cm thick; the upper part contains thick-bedded, friable, noncalcareous, fine-grained quartz sandstones

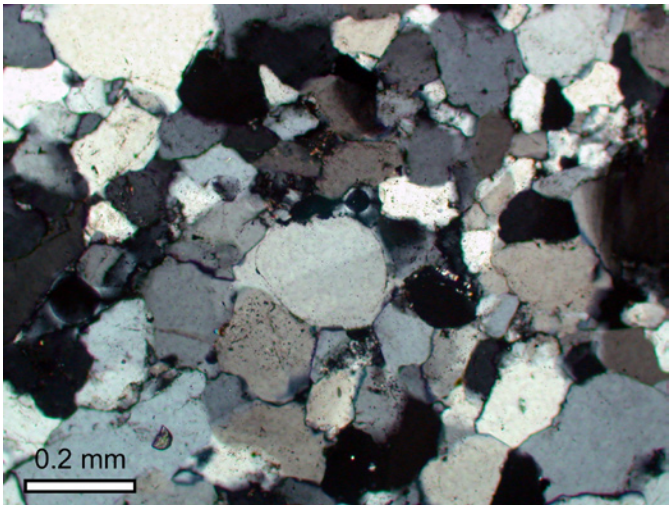


Figure 87. *Thin section photo of epitaxial quartz overgrowths on subround quartz clasts,* ***CM-a****, Mattson Formation, field station 01TLA095, crossed nicols. Scale bar is 0.2 mm.*



Figure 88. *Liesegang ring weathering pattern along fractures,* ***CM-a****, Mattson Formation, field station 01LP085. Bedding in photo is horizontal.*



Figure 89. *Thick-bedded, tan- to orange-weathering sandstone,* ***CM-b****, Mattson Formation, field station 01TLA147. Bedding dips gently to right away from viewer. Field assistant (circled) on left side of photo. Photo by T. Allen.*

with some beds ranging up to 5 m thick. Quartz grains are subangular to subround. Sandstones commonly are rippled or contain load casts. Tan-brown weathering limestone interbeds in the upper member are medium grey, medium-fine crystalline, argillaceous, and thin-bedded with beds 2–15 cm thick. Locally, limestones are sandy enough to be considered calcareous sandstones.

*Mattson Formation – undivided (**CM**)*

Exposures of undivided Mattson Formation consist entirely of light to dark grey, fine- to medium-grained, noncalcareous, massive, thick-bedded, quartz sandstone (Fig. 90). Bedding is indistinct and difficult to recognize. Trace amounts of black organic material and detrital muscovite are dispersed among the quartz clasts. Trace chert clasts (Fig. 91) weather with a chalky white appearance in hand sample. Quartz clasts have epitaxial quartz overgrowths reducing porosity in the sandstones.

Age, correlation and depositional environment

Douglas and Norris (1959) and Douglas (1976) informally divided the Mattson Formation into three members during their mapping. Their lower Mattson is characterized by thin-bedded, orange- to red-weathering quartz sandstones. The transition to the middle Mattson is marked by the appearance of thick, friable, cross-bedded, pale tan to buff quartz sandstones. The base of the upper Mattson is located at the first appearance of significant limestones within the Mattson quartz sandstones. This informal subdivision of the Mattson Formation into three members is difficult to apply in the Pool Creek area because the thick, friable channel sandstones typifying the middle Mattson are not present. Recent mapping

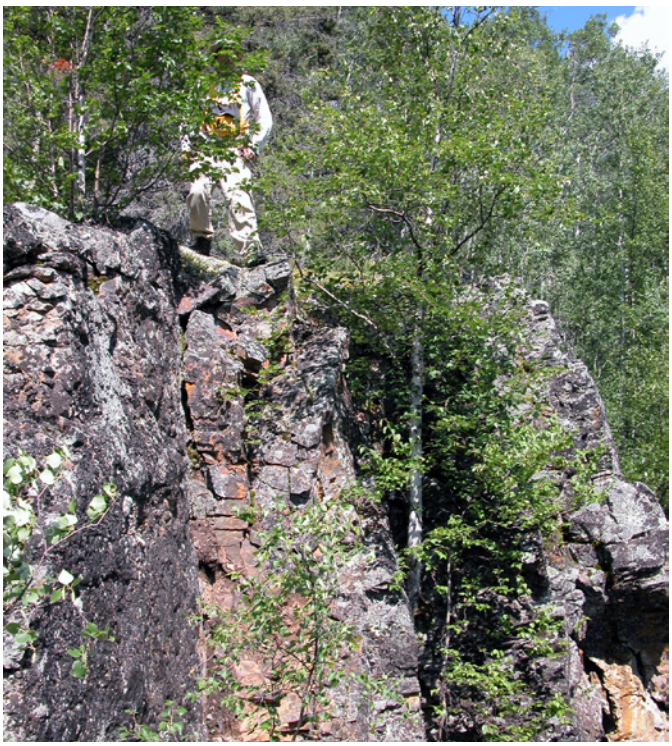


Figure 90. *Vertical beds of quartz sandstone,* ***CM****, undivided Mattson Formation, field station 03LP012. Field assistant at top of outcrop.*

in the mapsheets immediately east of Pool Creek have recognized two informal units, a lower Mattson member and a combined middle-upper Mattson member (Fallas, *et al.*, 2004).

The lower member (CM-a) in this report corresponds to unit DMs as mapped by Douglas (1976). It also lies entirely within the lower Mattson member of Douglas and Norris (1959). The division between lower and middle-upper Mattson units occurs within the upper CM-b member as mapped for this study. Currie *et al.* (1998) separated out a succession of medium to dark brown, fine-grained, silty limestones and dolostones at the top of the Mattson Formation as a new Permian Tika map unit. The Tika map unit has not been recognized in the map area. The Mattson Formation correlates with the Stoddart Formation (Rutgers, 1958) of northeastern British Columbia.

The Mattson Formation is interpreted as being deposited in fluvially dominated, wave- and tide-influenced lobate deltas prograding southwestward over the Besa River Formation (Richards *et al.*, 1993). Sand in the Mattson Formation has a northern sedimentary source. In the map area, the interbedding of sandstone and shale for the lower Mattson Formation (CM-a) indicates a marine offshore environment with sandstone intervals delineating local prograding of shallow water facies over deeper water fine siliciclastic facies.

Mattson Formation ranges in age from upper Visean to Serpukhovian in the Lower Carboniferous (Patton, 1958). One conodont sample from this area (see Table IV-11, Appendix 4) resulted in a Visean to Serpukhovian age for the upper Mattson member (CM-b).

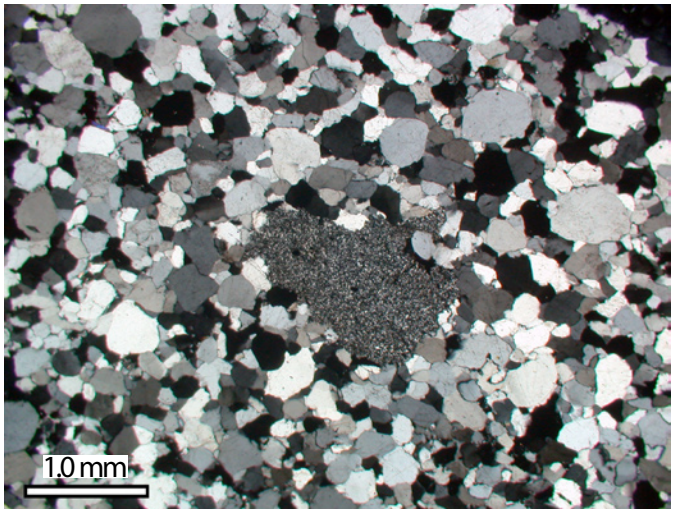


Figure 91. *Thin section photo of subangular quartz clasts with slightly larger chert clast, undivided Mattson Formation, field station 04LP022, crossed nicols. Scale bar is 1.0 mm.*

SUCCESSION 6 (PERMIAN)

Succession 6 consists of siliceous shales and limestones of the Permian Fantasque Formation. It is preserved only in one structural panel forming the immediate footwall to the Toobally fault in map sheet 95D/8. Within that structural panel all stratigraphic units dip uniformly to the west.

Fantasque Formation (PF)

Introduction

Fantasque Formation (Harker, 1961) in the map areas consists of siliceous shale with one thick interbed of thin-bedded, dark grey limestone. The formation disconformably overlies the Mattson Formation and is in turn disconformably overlain by the undivided Grayling and Toad formations. Both upper and lower contacts are unexposed. Interpreted thickness of the formation is approximately 1700 m, with the limestone interbed being approximately 800 m thick. The best outcrop exposures in map sheet 95D/8 are located along a west-draining stream (UTM 651 523E/6 696 340N, zone 9). Other scattered subcrop exposures occur along the shoreline on Toobally Lake.

Composition

*Fantasque Formation – shale lithofacies (**PF-s**)*

The predominant lithology (PF-s) is a dark brown-weathering, dark grey to black, hard, noncalcareous, siliceous shale (Fig. 92). The shale is internally bedded on a scale of 5 to 20 cm. Thin, locally discontinuous, nodular limestone beds occur scattered through the shale



Figure 92. *Dark brown-weathering, siliceous shales, Fantasque Formation, field station 04LP013. Bedding dips into the hillslope down to the left. View looking north. Field assistant for scale.*

succession; limestone nodules within these beds typically form concretions up to 50 cm across.

Fantasque Formation – limestone lithofacies (PF-l)

The limestone interbed (PF-l) occurs in scattered subcrops and outcrops along the east margin of the large Toobally Lake in map sheet 95D/8. It is dominated by medium to dark grey, light grey-weathering, finely crystalline, thin-bedded limestone (80%) with lesser (20%) dark grey, silty shale interbeds (Fig. 93). Limestone beds are irregular and range in thickness from 1 to 30 cm, most commonly 1 to 10 cm. Beds typically are massive to parallel-laminated; locally they are bioturbated. The limestone gives off a fetid strong sulphur odor with weak HCl acid. Upper and lower contacts of the limestone are not exposed. Exposures of the limestone on the east shoreline of Toobally Lake are landslide or slump blocks from higher up the hillside on the east.

Age, correlation and depositional environment

Regionally, the Fantasque Formation was named by Harker (1961) with a type area on the lower Beaver River, east of the present map area. It correlates with unit 9 of Douglas and Norris (1959). Both upper and lower contacts are regionally unconformable (Douglas and Norris, 1959). Lithological facies have been regionally interpreted as a slope to basinal depositional environment (Henderson *et al.*, 1993). Depositional facies shallow in a general easterly direction.

Samples collected for conodonts (Table IV-12, Appendix IV) from the limestone interbed were barren. One sample from a limestone nodule stratigraphically and structurally underlying the limestone interbed (field station 04LP013) contained a broadly Permian conodont assemblage (Pyle, 2004). Farther east in map sheet 95C, the Fantasque unconformably overlies the lower Permian Tika map unit (B. Richards, pers. comm., 2002) and is in turn unconformably overlain by Triassic or Cretaceous strata. It is assumed to be Permian in age, although fossils have not been collected from the unit. Henderson *et al.* (1993) reported an age range of upper Artinskian through Wordian (early Permian through middle late Permian) for the Fantasque Formation regionally. Occurrences of the Fantasque Formation in map sheet 95C have been documented only for the southern part of the map sheet. It apparently was removed by post-Permian erosion in the northern part of the map sheet.



Figure 93. *Thinly bedded, dark grey limestone, Fantasque Formation, field station 03LP009. Bedding dips steeply down to left in photo. View looking north.*

SUCCESSION 7 (TRIASSIC)

Dark grey, soft, recessive Triassic shales with lesser interbedded thin, tan-weathering sandstones constitute succession 7 in the map area. Exposures within the map area occur only on the west side of Toobally Lake in map sheet 95D/8. Other areas of the map sheets are interpreted as containing succession 7 strata based on exposures in adjacent map sheets, and the overall lack of outcrop. Structurally, the Triassic shales are preserved in synclinal fold keels and in the immediate footwall of thrust faults in the map area. Since outcrop control is sparse, Triassic siliciclastic sedimentary rocks in the immediate area have generally been mapped as consisting of undivided Grayling and Toad formations (Kindle, 1944; Fallas and Lane, 2001).

Grayling and Toad formations (undivided) (ʞGT)

Introduction

Kindle (1944) first described the Grayling and Toad formations along the Grayling and Liard rivers in northeastern British Columbia. The Lower Triassic Grayling Formation in the type area consisted of soft, laminated, friable grey shales with lesser interbeds of hard, ripple-marked sandstone. It had a measured thickness of 183 m and a total thickness of nearly 305 m. Overlying the Grayling Formation, the Toad Formation consisted of brown and black platy shales and siltstones, sandstones and limestones. Exposed thickness of the formation ranged between 245 m and 730 m. Fossils from the top of the Toad Formation indicated a late Middle Triassic age.

Brady (1959) and Douglas (1976) inferred recessive Triassic strata in La Biche River map sheet (95C) by extending known occurrences in British Columbia northward into Yukon. The presence of Triassic siliciclastic strata in southeastern map sheet 95C (Mount Martin map area, 95C/1) was confirmed by Fallas and Lane (2001) as part of the Central Foreland project. Fallas and Lane tentatively assigned the Triassic strata to the Grayling and Toad formations on the basis of lithologic similarity and general stratigraphic position and estimated a combined stratigraphic thickness of 350–400 m in map sheet 95C/1. Two detailed sections of exposed Triassic strata in map sheets 95C/1 and 95C/2 were subsequently measured and described by MacNaughton (2002a). He suggested a total stratigraphic thickness of approximately 300 m for Triassic strata in one of his measured sections. Palynology studies in map sheet 95C/4 have confirmed the presence of Triassic strata overlying Mattson Formation in that map sheet as well (Utting, pers. comm., 2004; Fallas *et al.*, 2004).

Limited exposures immediately east of the Pool Creek map area indicate Grayling and Toad formations lie unconformably on Lower Carboniferous Mattson Formation and are in turn unconformably overlain by dark shales of the Cretaceous Garbutt Formation (Fallas *et al.*, 2004). The lower contact of the Grayling and Toad formations was interpolated at the break in slope where resistant beds of the Mattson Formation dip eastward underneath a generally flat river valley which is assumed to be underlain by the recessive Triassic units and Cretaceous Garbutt Formation. This contact was not confirmed through ground observations in the Pool Creek map sheet (95C/5).

In the Larsen Lake map sheet (95C/4) immediately south of Pool Creek, Triassic strata have been confirmed to overlie Mattson Formation in one of the structural panels in the southeast part of the map sheet (Fallas *et al.*, 2004). Triassic strata have been inferred to extend northward into the Pool Creek map sheet in the structural panel immediately to the west on the basis of airborne magnetic patterns in the second vertical derivative. Helicopter flying of this map area (95C/5) during 2001 was unable to visually confirm the presence of Grayling-Toad strata in the area.

Composition

Limited exposures of soft, phyllitic, noncalcareous, greenish-grey, silty shale overlying the siliceous shales of the Fantasque Formation are documented on the west side of Toobally Lake in map sheet 95D/8 (Fig. 94). Mica is locally visible on the slaty cleavage surfaces of the shale. Thin beds of greenish-grey, very fine-grained sandstone constitute less than 10% of the exposure. The sandstone preserves small load casts and possible gutter casts. Both the shale and sandstone are locally concretionary. The sandstone also contains poorly preserved horizontal burrows with external scratch ornamentation.

Age, correlation and depositional setting

Pollen analysis by MacNaughton and Utting (2002) of Triassic strata in La Biche River (NTS 95C) map area consistently denoted a Griesbachian age (Lower Triassic). This age is consistent with type area Grayling Formation. Lithologically, however, Triassic strata in La Biche River (NTS 95C) map area are more consistent with type area Toad Formation. Because of limited exposures, Fallas and Lane (pers. comm., 2003) did not recommend subdividing the Triassic strata into separate Grayling and Toad



Figure 94. *Poorly exposed subcrop of undivided Triassic Grayling and Toad formations, field station 03LP008.*

formations in the La Biche River (NTS 95C) map area. Palynological studies for this unit in map sheet 95D/8 identified Early Triassic pollen with abundant Middle and Late Devonian reworked spores (Utting, 2006). The confirmed age of the Triassic strata indicate upper and lower contacts are both unconformable (Fig. 5).

MacNaughton (2002a) recognized five facies associations within these Triassic strata and assigned them to depositional environments on a wave-dominated shelf ranging from relatively distal, sand-poor settings below storm wave-base to high-energy, proximal sand-rich, mid- to upper shoreface settings. These lithologies overall indicate a shallow marine depositional environment. The exposures in map sheet 95D/8 constitute the westernmost mapped exposures of Triassic Grayling and Toad formations in southeast Yukon to date.

SUCCESSION 8 (PALEOCENE)

Paleocene sediments (ℙssc) and Paleocene basalt (ℙb)

Introduction

In the northwest corner of the Pool Creek map area (UTM 336 500E/6 706 900N, zone 10), a 160+ m-thick succession of horizontal, tan, noncalcareous, poorly consolidated siltstones, sandstones and conglomerates underlies an east-west ridge length of approximately 5 km (Fig. 95). In one small area, the sedimentary rocks are conformably overlain by a 15 to 20 m-thick, dark brown, massive basalt flow. Conglomerate immediately beneath the basalt flow is baked and therefore more resistant to erosion, resulting in an inverted topography as poorly consolidated sedimentary rocks have been removed from other areas by erosion. These sedimentary rocks were first recognized and mapped during exploration work on the TRANZ quartz claims (Cathro, 1983). I.R. Smith described and sampled the sediments in detail for paleomagnetic studies (Smith, pers. comm., 2002); much of the following is based on his detailed study.

Composition

The predominant lithology in the lower portion of the unit is a medium-coarse, poorly indurated, pale tan sandstone containing scattered pebbles and small cobbles. Overall, the sandstone units coarsen upwards. Bedding within most of these sandstone intervals is obscured by colluvium. Marginal contacts are often diffuse and irregular (wavy). The sandstones contain thinner interbeds of clay siltstone to mudstone and highly variable 'red beds'. Siltstone intervals consist of well-sorted clayey siltstone to mudstone, which are discontinuous across the section, occurring as thin lenses up to 20 m long. One interval, up to 4 m thick, contains abundant organic material, much of which is coalified. Two red bed intervals consist dominantly of a dark red-stained, matrix-supported conglomerate with a strongly to moderately cemented sand-silt matrix. Lesser discontinuous interbeds within the conglomerate include well-sorted siltstone, sandstone and fine conglomerate. Typically these interbeds are not red-stained or cemented. Marginal contacts are gradational or sharp and are usually irregular.

The uppermost sedimentary lithology in this sequence is a coarse, clast-supported, pebble to cobble conglomerate (Fig. 96) up to 21 m thick. The dominant clast lithology is grey quartzite (>70%); other clast types include black chert, grey chert, bedded grey chert, vein



Figure 95. *Ridge of Paleocene subaerial sediments (**Pssc**) capped by basalt flow (**Pb**), field station 01LP016. View looking southeast. Recent mudflow emanated from area immediately in front of ridge and traveled downslope to Beaver River. Photo by T. Allen.*



Figure 96. *Closeup view of baked conglomerate immediately beneath the basalt flow, unit **Pssc**, field station 01LP016. Hammer for scale.*

quartz, light grey shale and coarse quartz sandstone. The conglomerate contains several small, discontinuous interbeds of well-sorted clayey siltstone or silty sandstone to sandstone. Clasts tend to be well-rounded and do not have any striations on their surfaces. Both inverse and normal graded beds are present. Up to to 14 m of the conglomerate (immediately beneath the basalt flow) is baked to form a very resistant, hard rock. In this baked interval, the clasts have a red surface coating.

Capping the sequence in one small area of the ridge is an aphanitic, medium dark grey, brown-weathering basalt flow up to 20 m thick. The flow is massive to slightly vesicular. Locally it is columnar-jointed (Fig. 97), with upper parts of the columns leaning slightly eastward (azimuth 125). The bottom contact of the basalt is sharp and essentially horizontal. Locally, clasts from the underlying conglomerate are entrained within the lowest part of the flow, and basalt infills hollows between large clasts in the conglomerate.

In thin section, the basalt contains microphenocrysts of olivine and plagioclase in a fine-grained, trachytic matrix consisting largely of oriented plagioclase microlites up to 0.2 mm long (Fig. 98) with lesser biotite, carbonate minerals, olivine and opaque minerals. Plagioclase phenocrysts up to 4 mm long are indistinctly concentrically zoned and are locally broken so zoning patterns are incomplete.

Table III-4 (Appendix III) contains a lithogeochemical analysis (sample 01LP016) for the basalt. The basalt plots as an alkali basalt following both the major element classification scheme of Irvine and Barager (1971; Fig. 99b) and the trace element scheme of Winchester and Floyd (1977) as modified by Pearce (1996; Fig. 99a). A multi-element ratio diagram of typically immobile elements shows enrichment of all elements except Ti relative to OIB (oceanic island basalt) (Fig. 99c). Light REE and Th are significantly enriched. Nb shows relative depletion; this Nb signature is typical for crustal contamination.

Age, correlation and depositional environment

The presence of columnar jointing in the basalt, occurrence of red beds and coal in the sedimentary package, and the widespread presence of gravels and sands with interbedded discontinuous silts and sands all indicate a subaerial, fluvial depositional environment, probably a clastic braided river environment. Imbrication and bar forms and columnar leaning in the basalt all indicate a paleoflow direction of east to east-southeast.

A whole rock sample of the basalt flow was dated with $^{39}Ar/^{40}Ar$ methods as 56.7 ± 0.7 Ma (2σ) (Villeneuve,

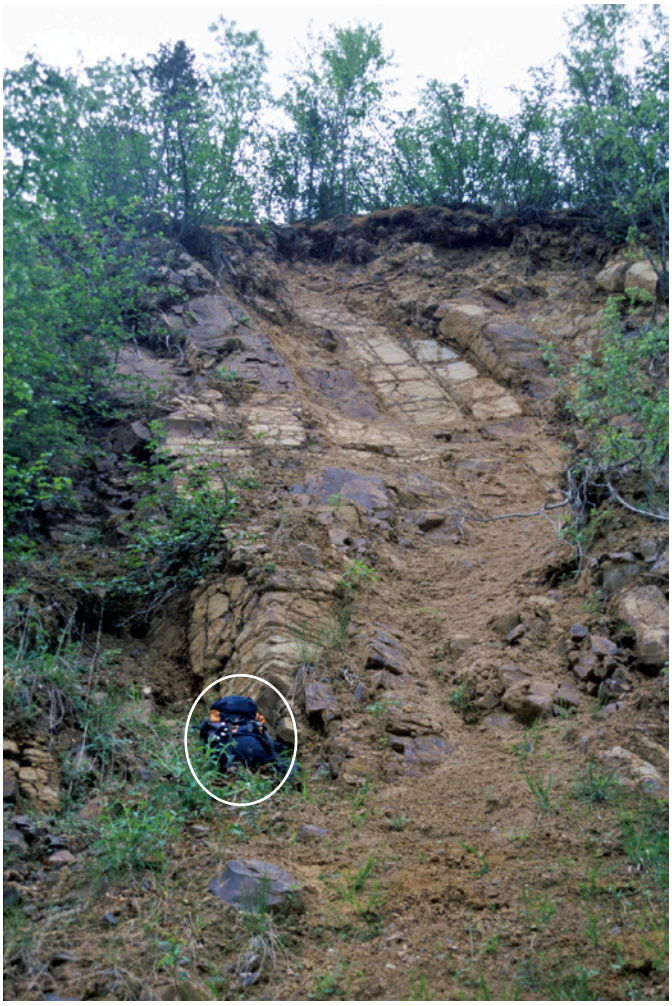


Figure 97. *View looking south of brown basalt flow, unit lPb, field station 01LP016. Backpack (circle) for scale.*



Figure 98. *Thin section photo of unit lPb. Plagioclase phenocrysts in trachytic matrix of plagioclase microlites with lesser opaque minerals, olivine, biotite and carbonate minerals. Olivine microphenocryst in lower right corner of photo, crossed nicols. Scale bar is 1.0 mm.*

pers. comm., 2003) Appendix II details operating conditions for the age dating analysis. The basalt flow is Late Paleocene. This radiometric age also is a minimum age for the ℙssc sedimentary succession underlying the basalt flow.

The basalt flow has normal polarity (Smith, pers. comm., 2003), and therefore most likely corresponds to polarity chron C25n (Cande and Kent, 1995). Polarity measurements for the underlying sedimentary succession were inconclusive, except for one interval which had a fairly convincing reversed signature (Smith, pers. comm., 2003). Presumably this would correspond either to one of the five reversed cryptochrons in C25 or the reversed interval between C25n and C26n. The maximum age of the sediments, therefore, would be 58.7 Ma which also corresponds to Late Paleocene.

Pollen analysis of coal samples from unit ℙssc returned a broadly Tertiary age (Smith, pers. comm., 2003), consistent with radiometric and paleomagnetic results. The entire sedimentary and igneous succession represents dominantly coarse clastic deposition from a braided river flowing from west to east in Late Paleocene.

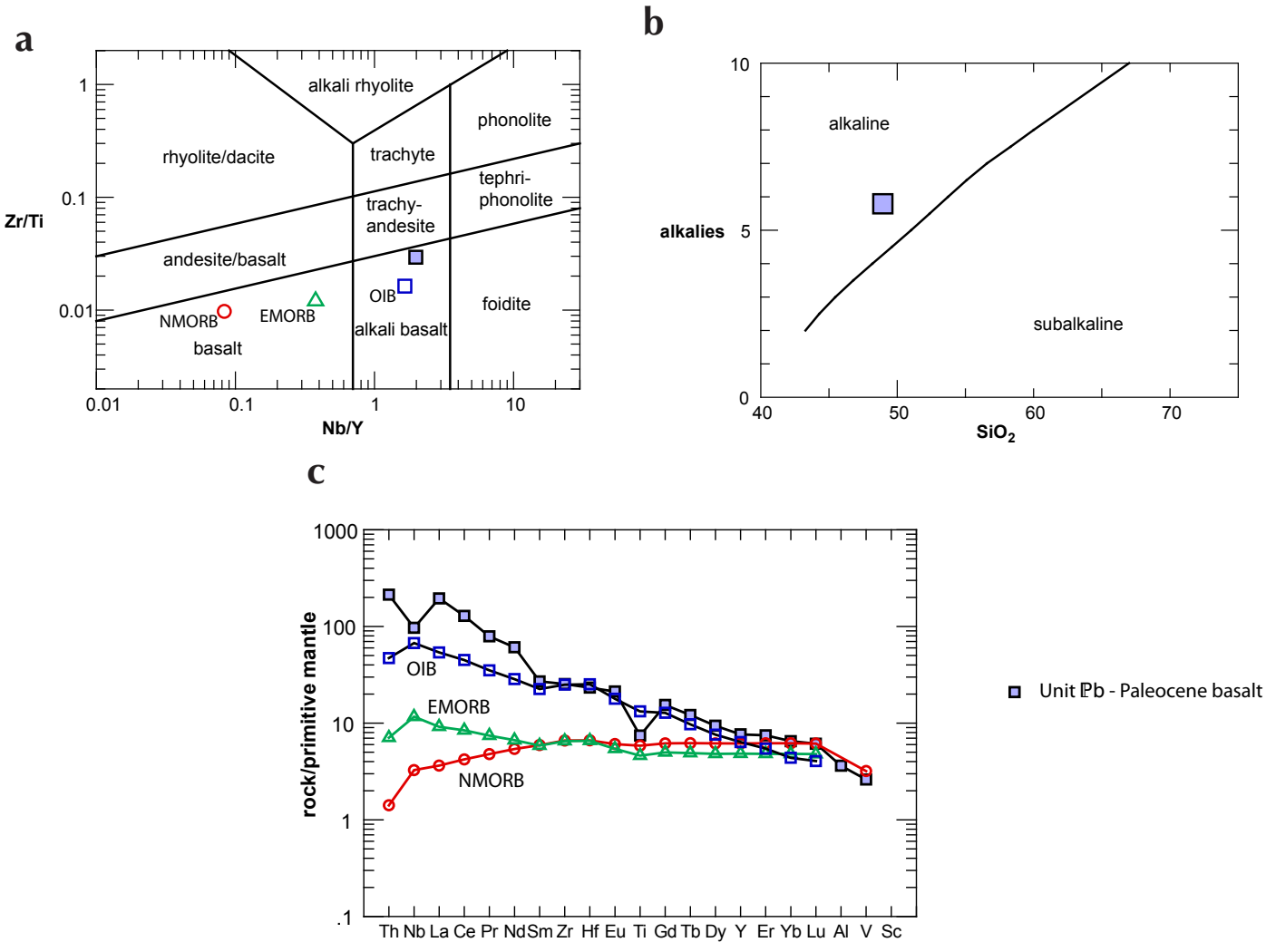


Figure 99. *Compositional diagrams for Paleocene basalt (ℙb), field station 01LP016.* **(a)** *Zr/Ti-Nb/Y diagram from Pearce (1996), modified from Winchester and Floyd (1977);* ***(b)*** *total alkalies vs SiO_2 diagram from Irvine and Barager (1971);* ***(c)*** *multielement diagram normalized to primitive mantle (Sun and McDonough, 1989). EMORB (enriched midocean ridge basalt), NMORB (normal midocean ridge basalt) and OIB (oceanic island basalt) reference analyses are included.*

IGNEOUS ROCKS

INTRODUCTION

Pool Creek map area contains four intrusive bodies clustered in the northwest part of the Pool Creek map sheet, about 6 km south of the Beaver River. Two of these are coarsely crystalline, medium-level syenite intrusions, and two are aphanitic high-level felsic intrusions (possibly extrusive?) with abundant quartz phenocrysts and numerous inclusions. Although the syenite intrusions are spatially adjacent to each other, they have widely different crystallization ages of 650 Ma (Neoproterozoic) and 52 Ma (Eocene). The aphanitic igneous bodies have not been isotopically dated; they are tentatively correlated with the Eocene Ting alkalic suite (52-54 Ma) which is located in the southwest corner of NTS 95C/12, approximately 3 km north of the northern edge of map sheet 95C/5.

More detailed discussion of mineralogy, contact relations, geochemistry and isotopic age dating for the igneous bodies is presented in the following sections. Much of this information has been previously published in Pigage and Mortensen (2004).

NEOPROTEROZOIC POOL CREEK NEPHELINE SYENITE (PPCsy)

Introduction

Excellent exposures of an unfoliated nepheline syenite (Fig. 100), informally called the Pool Creek syenite (Harrison, 1982), occur on the one ridge above treeline in the west-central part of the Pool Creek map area (UTM 343 801E/6 698 828N, zone 10). The syenite typically weathers as rounded knobs with abundant feldspar grain scree around outcrops. Locally, the syenite is intensely weathered and clay-altered along linear zones up to 5 to 10 m wide and extending along trend for tens of metres. These intensely altered zones have cream-coloured weathered surfaces with local rust-coloured zones. Scattered thin, dark purplish pink, fine-grained, nearly vertical dykes (Fig. 101) intrude the syenite. Pink and dark green compositionally banded (1-5 cm scale) dykes (Fig. 102) containing purple fluorite along fractures are also locally associated with the syenite. Both sets of dykes also occur as sills and dykes intrusive into the Precambrian unit Ps. The Pool Creek syenite is intrusive into hornfelsed quartzites and pelites of Ps (Fig. 103) along its south margin. Along its east margin, the syenite is unconformably overlain by the Crow formation, which contains no visual evidence of hornfelsing.



Figure 100. *Closeup view of typical outcrop of unfoliated nepheline syenite, Pool Creek syenite, field station 00LP025.*

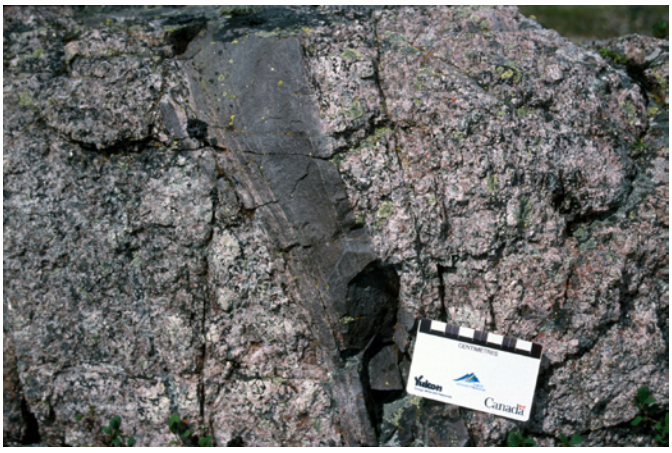


Figure 101. *Vertical, fine-grained intrusive dykes in Pool Creek nepheline syenite, field station 02LP122.*

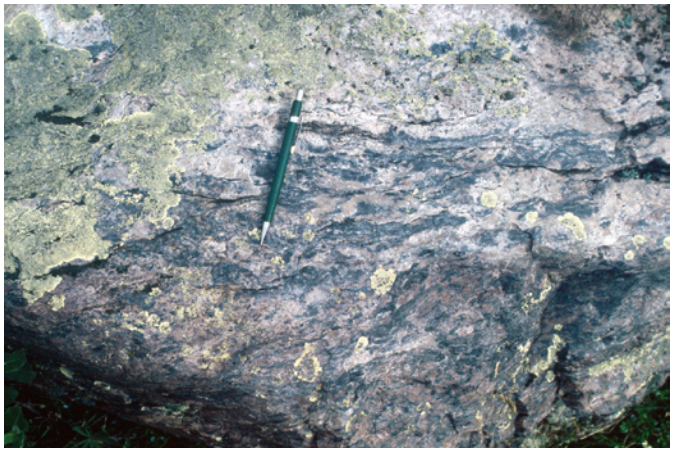


Figure 102. *Banded gneissic dykes in Pool Creek nepheline syenite and Unit* **Ps**, *field station 00LP023.*



Figure 103. *Pool Creek syenite intrusive into hornfelsed pelites of unit* **Ps**, *field station 02LP111.*

Mineralogy

The Pool Creek nepheline syenite consists dominantly of medium to coarsely crystalline, randomly oriented, pink K-feldspar (50-60%) laths intergrown with lesser subhedral to euhedral, strongly sericitized nepheline (20-25%). Primary nepheline has not been identified in thin section or hand sample; its former presence is deduced from abundant euhedral, 0.2-1.5 cm sericite pseudomorphic aggregates (Fig. 104) and the quartz undersaturated chemistry presented in Table III-5 (Appendix III). Sericite pseudomorphs have a striking pale green colour in outcrop. Growth relations between the pseudomorphs and K-feldspar indicate the nepheline and K-feldspar crystallized at approximately the same time. Minor apatite, opaque minerals, plagioclase and dark brown biotite occur in interstitial, symplectic aggregates. In some instances these aggregates appear to be replacing earlier unknown mafic minerals. K-feldspar laths have disseminated fine pinkish opaque dust, coarse lamellar twinning, and abundant fine, perthitic flame exsolution lamellae. Microcline grid twinning was not observed. Individual feldspar crystals range up to 4 cm long, although lengths of 0.5 to 1.0 cm are more typical.

Geochemistry

Table III-5 (Appendix III) presents the geochemistry for several samples of Pool Creek syenite and associated dykes. Pool Creek syenite is a foid syenite to foid monzosyenite (Pigage and Mortensen, 2004). Tectonic discrimination diagrams by Pearce *et al.* (1984) indicate the syenite intrusion is not subduction- or collision-related; rather it is a within plate intrusion (Pigage and Mortensen, 2004).

Age

The Pool Creek syenite was originally considered Cretaceous? (Douglas, 1976) on the basis of correlation with the Tertiary trachytes in the same general area. This correlation was reinforced by the occurrence of the radiometrically dated Eocene Ting alkalic complex immediately to the north (Harrison, 1982) of the Pool Creek syenite in map sheet 95C/12. Several radiometric U-Pb dates of zircons from the Pool Creek syenite and associated dykes all cluster around 650 Ma, corresponding to a Neoproterozoic-Cryogenian age (Pigage and Mortensen, 2004; Gradstein *et al.*, 2004).

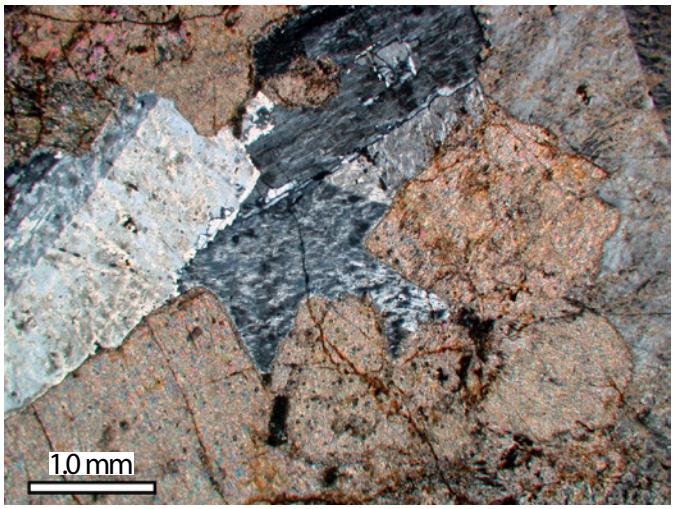


Figure 104. *Microscope thin section photo of sericitized nepheline and K-feldspar constituting the major constituents of the Pool Creek syenite, field station 00LP025, crossed nicols. Scale bar is 1.0 mm.*

EOCENE BIOTITE SYENITE (Ebsy)

Introduction

One stream traverse immediately west of the Pool Creek syenite encountered a distinctive, medium-coarse-grained, unfoliated biotite syenite intrusion (UTM 341 000E/6 700 800N, zone 10). The biotite syenite weathers crumbly grey to off-white. Spectacular cliffs up to 80 m high (Fig. 105) are exposed in the streamcut. Marginal contacts of the syenite were not observed.

Mineralogy and geochemistry

The syenite (Fig. 106) consists of K-feldspar (40%) and plagioclase (25%) with hornblende (25%), biotite (10%), and accessory opaque minerals, sphene, apatite and clinopyroxene. Clinopyroxene has a faint green colour in plane light. Hornblende is strongly pleochroic from pale brown to dark brown. Locally, small fringe areas of hornblende grains have a deep bluish green colour. Biotite pleochroism ranges from pale tan-brown to deep walnut-brown. All grains are equant with equigranular texture. Feldspars have a moderate sericite dusting. K-feldspar displays an incipient microcline grid twinning. Mafic clinopyroxene and hornblende grains are locally altered to a fine-grained, medium-green aggregate. Table III-5 (Appendix III) contains chemistry for one sample of the biotite syenite.

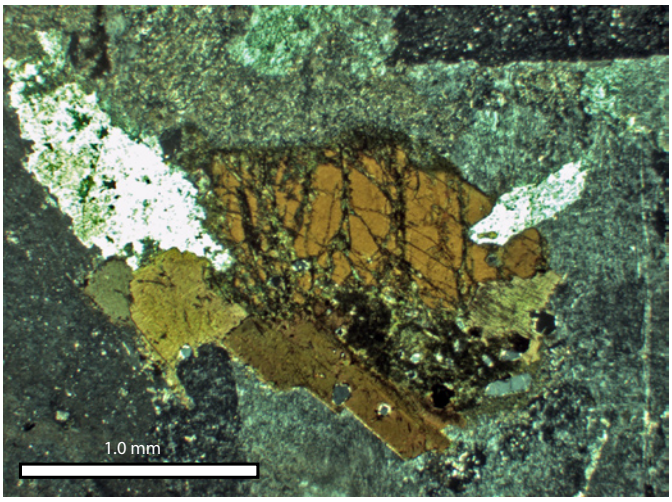


Figure 106. *Thin section photo of euhedral biotite and hornblende in a matrix of K-feldspar and plagioclase, field station 01LP033, crossed-nicols. Scale bar is 1.0 mm.*



Figure 105. *Stream cliff outcrops of Eocene biotite syenite, field station 01LP034. View looking north.*

Age

The biotite syenite intruded Cambrian through Middle Devonian sedimentary rocks, indicating a post-Devonian intrusion age. Isotopic dating of zircons from the syenite resulted in five concordant fractions giving an early Eocene crystallization age of 51.8 ± 0.2 Ma (Pigage and Mortensen, 2004).

EOCENE(?) IGNEOUS BRECCIA (Eib)

Introduction

Two fine-grained, igneous breccia bodies were mapped in the Pool Creek map sheet. The eastern body was observed during the present mapping program; the western body is based on earlier exploration mapping (Culbert, 1981). In addition, numerous dykes, too small to map at 1:50 000 scale, occur in the area.

Mineralogy and geochemistry

The igneous breccia consists of a dark grey, aphanitic porphyry with numerous small (1-2 mm) quartz phenocrysts ('eyes') and local small white to pink feldspar phenocrysts (Fig. 107). The unit typically weathers to a pale tan or dark maroon. Abundant rounded to subangular inclusions (Fig. 108) up to 10 cm across consist dominantly of clear quartz sandstone with minor dark green basalt, siltstone and coarse-grained pink syenite.

Table III-5 (Appendix III) contains chemical analyses of two samples of the igneous breccia. The analyses are considered suspect because of the extensive number of quartz sandstone inclusions. In addition, Table III-6 (Appendix III) lists 36-element ICP analyses for this unit.

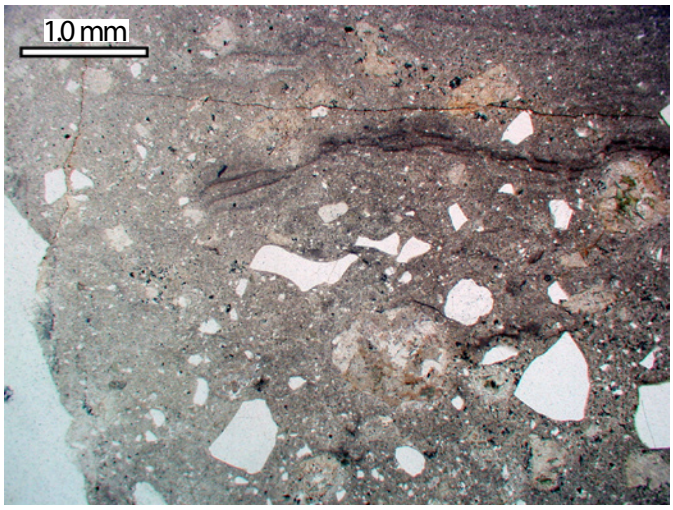


Figure 107. *Thin section photo of broken quartz and feldspar crystals in an aphanitic matrix of an igneous breccia, field station 00TLA026, plane light. Flow banding present locally. Scale bar is 1.0 mm.*

Age

Textures in the igneous breccia indicate they are high-level intrusive to extrusive igneous bodies. The map pattern in Culbert (1981) suggests the igneous breccia crosscuts the Eocene biotite syenite and is therefore younger than that unit.

Attempts to isotopically date zircons from the unit were not successful (Pigage and Mortensen, 2004). About 12 km to the north, the Ting Creek alkalic intrusion contains similar explosive lithofacies (Harrison, 1982). K-Ar dating of biotite from the Ting Creek intrusion resulted in ages of 54.1 ± 1.9 Ma, 53.0 ± 1.8 Ma and 52.4 ± 1.8 Ma (Stevens, *et al.*, 1982). These dates overlap with or are slightly younger than those of the Eocene biotite syenite. Fallas *et al.* (2004) inferred the intrusions are part of a suite informally termed the Ting suite. The igneous breccia is tentatively considered Eocene and slightly younger than the biotite syenite. It is considered to be distinct from the younger syenitic bodies dated at approximately 40 Ma which occur east and south of the Pool Creek area (Francis, pers. comm., 2001; Fallas *et al.*, 2004).



Figure 108. *Rounded to subangular quartz sandstone and basalt clasts within igneous breccia, field station 00TLA026.*

STRUCTURAL GEOLOGY

INTRODUCTION

The map area contains structural features related to two contractional deformation events, one pre-late Cambrian and the other post-Triassic/pre-Paleocene. Evidence for the early D_1 deformation event is restricted to Proterozoic sedimentary rocks in the north-central part of the Pool Creek map sheet. Structural features related to the second post-Triassic/pre-Paleocene D_2 deformation event in the map area consist dominantly of reverse faults and associated open to tight folds. Structural styles for these D_2 deformation features can be related to the different lithofacies present in the map area (Pigage, 2003).

Additionally, lateral separation of the Toobally Formation from the Crow Formation by a Cambrian to Ordovician east-trending normal fault with a suggested displacement of at least 1800 m indicates early Paleozoic rifting. This rifting is consistent with occurrences of Ordovician alkali basalts at several stratigraphic levels within the Crow Formation.

PRE-LATE CAMBRIAN DEFORMATION D_1

Proterozoic sedimentary rocks in the Pool Creek area contain northwest- and southeast-plunging open folds and steep faults that are truncated by the overlying Crow Formation. Bedding within unit Ps south of the Pool Creek syenite outlines a gently northwest-plunging anticline (Fig. 109a). Pi axis for the best-fit girdle to the bedding measurements for this anticline has an orientation of 314/15. Bedding within unit Pa, in contrast, defines an open, southeast-plunging syncline with a pi axis orientation of 113/19 (Fig. 109b). The similar trends for these two fold structures suggest they are related to the same deformation event. No associated axial planar structural cleavage or foliation was observed during the field work. The map pattern for the Crow Formation indicates the syncline in unit Pa is not present in the Crow Formation, which unconformably overlies unit Pa. The folds also appear to be truncated by the steep faults within and between units Ps and Pa.

The D_1 deformation event is loosely constrained to a pre-Crow Formation deposition and post-Unit Pa deposition time interval. Truncation of the fold axial traces by the steep faults indicates that the D_1 folding deformation event also pre-dates the faults. Detrital zircon ages and the general stratigraphic discussion for unit Pa suggested a broad correlation of unit Pa with lower

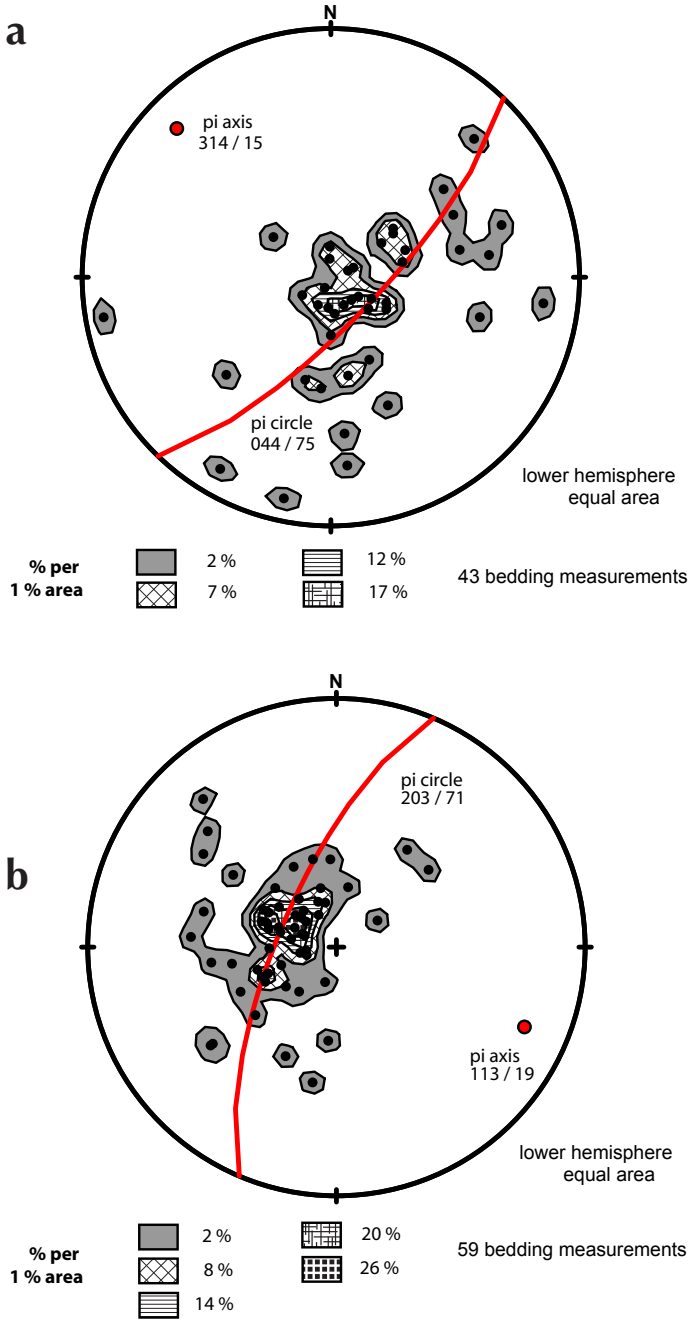


Figure 109. *Equal-area stereonet plot of poles to bedding in Units* ***Ps*** *and* ***Pa****. The spread in bedding poles outlines northwest- to southeast-trending fold patterns.* ***(a)*** *Proterozoic deformation – poles to bedding – Unit* ***Ps*** *south of Pool Creek syenite.* ***(b)*** *Proterozoic deformation – poles to bedding – Unit* ***Pa****.*

Windermere strata. Two detrital zircon dates of 650 Ma from unit Pa would further constrain deformation to be younger than 650 Ma.

Alternatively, D_1 folding could be a very local feature related to intrusion of the Pool Creek syenite. In that case, timing of deformation would be approximately 650 Ma and unrelated to regional orogenic events.

The faults mapped in the Proterozoic units south of the Pool Creek syenite have been interpreted on the basis of geomorphic erosional features, local occurrences of breccia, rapid changes in bedding orientation, and the apparent discontinuous nature of the D_1 fold-surface axial traces. These faults have variable trends. They are unconformably overlain by and covered by the Crow Formation.

Brecciated fragments of syenite within the gully immediately south of the Pool Creek syenite indicate that the interpreted southeast-trending fault post-dates intrusion of the syenite (650 Ma), which provides a maximum age for the faulting. Truncation of the faults by Crow Formation restricts the minimum age for the faulting to before deposition of the Crow Formation (at least before Early Ordovician; more probably late Cambrian). This early faulting, therefore, is restricted to the time interval between 650 Ma and 501 Ma. Faulting is also late- or post-D_1 folding because the faults appear to truncate the fold axial traces. The above time interval for faulting is consistent with the timing constraints suggested for the D_1 folding deformation.

POST-TRIASSIC/PRE-LATE PALEOCENE DEFORMATION D_2

Cambrian-Ordovician through Triassic strata contain folds and faults related to a D_2 deformation event loosely constrained by the stratigraphic units in the map area to the time interval between Triassic and late Paleocene. Deformation D_2 must be post-Triassic Grayling-Toad formations because these formations are folded and faulted. In contrast, the late Paleocene sediments and basalt in the northwestern part of the Pool Creek map area are flat-lying and do not exhibit the fold patterns present in the underlying Road River Group sedimentary rocks, constraining D_2 deformation to being pre-late Paleocene. All folds and faults and their associated cleavages and lineations in the map areas, with the exception of the southeast-trending folds and faults discussed above, are associated with the D_2 deformation.

The map area has been divided into three structural domains (Fig. 110) separated by the major Toobally and Beaver River thrust faults. The eastern domain A is characterized largely by an east- to northeast-dipping homoclinal succession of stratigraphic units in the hanging wall of the Beaver River thrust with box folds to open folds being developed locally. The western domain C, in the hanging wall of the Toobally fault, is characterized by a west-dipping homoclinal succession of stratigraphic units. Between these two major thrusts, stratigraphic units in domain B are structurally repeated through both faulting and folding.

The west-verging Beaver River thrust (Brady, 1959) juxtaposes Proterozoic sedimentary and intrusive rocks in the hanging wall with Paleozoic or Mesozoic sedimentary rocks in the footwall. Stratigraphic throw of the Beaver River thrust in the vicinity of cross-section A-B (Plate 1) is approximately 4700 m. Relative displacement along the Beaver River thrust decreases rapidly to the north; the fault has been interpreted as dying out in carbonaceous shales of the Besa River Formation at the north edge of the Pool Creek map area.

Sedimentary rocks in domain A, in the immediate hanging wall of the Beaver River thrust, are deformed into a large, north-trending, box-fold anticline with a broad, nearly horizontal hinge zone and a steeply to moderately dipping east limb. The west limb of the anticline is truncated by the Beaver River thrust. The sharp hinge of the east limb of the anticline is best-developed north of the Beaver River where the Sunblood Formation has nearly vertical bedding. South of the Beaver River, the east limb has moderate dips and the box-fold style is less well-developed. Fold intensity in the hanging wall decreases away from the thrust.

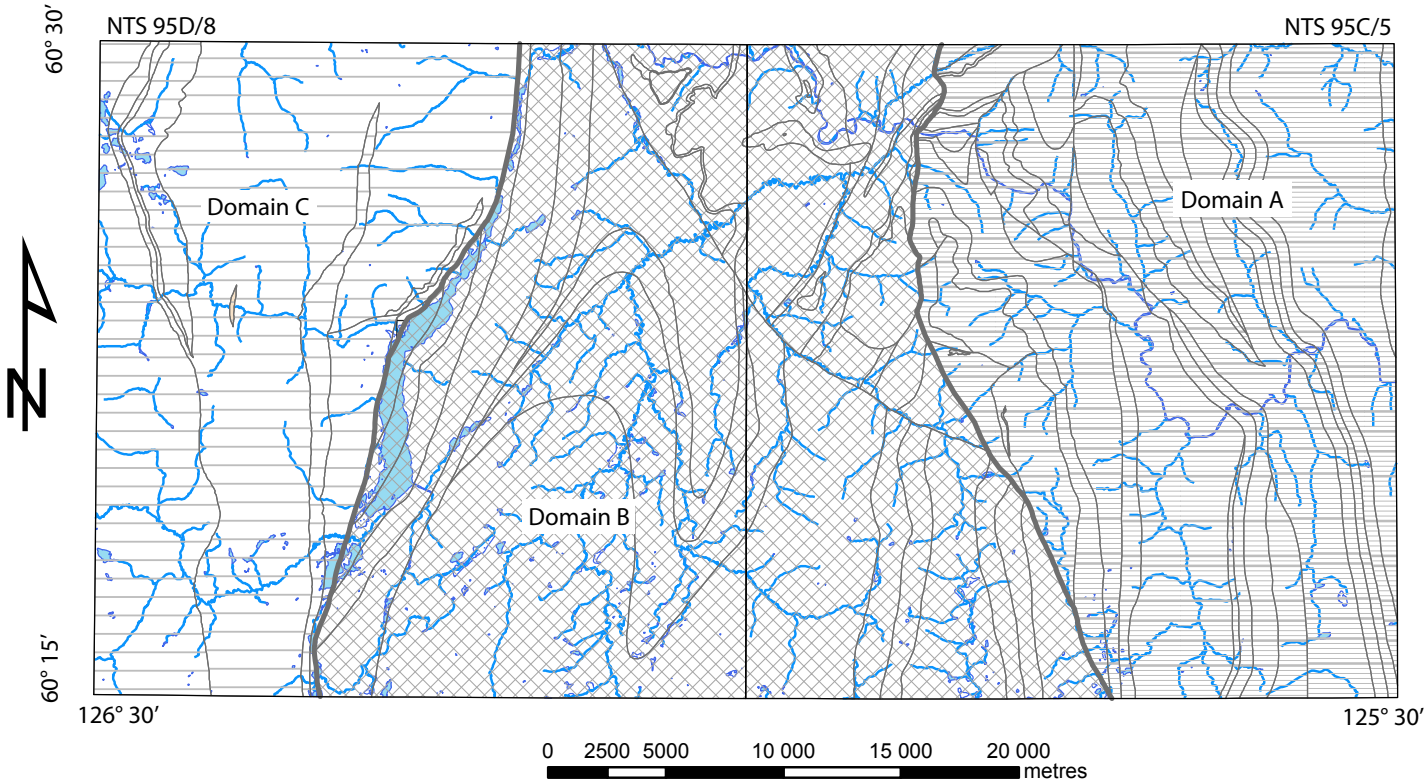


Figure 110. *Structural domains A, B and C for map areas.*

Folds farther east within domain A are open with shallowly dipping limbs. When visible in outcrop they typically consist of small, gentle kink-flexures (Fig. 111). These minor folds trend north to northeast and plunge gently towards the north and the south. Deformation fabrics are generally not observed, although a steeply dipping, north-trending slaty cleavage or spaced fracture cleavage is visible locally. Lineations consist largely of intersection lineations between bedding and the dominant cleavage, although minor fold axes are visible in a few instances. Figure 112a is an equal-area stereonet plot of poles to bedding in domain A, and Figure 112b is a similar plot for measured lineations and poles to the dominant cleavage. Figure 112a illustrates the dominant east dip for bedding. The spread of poles to bedding indicates a dominant gentle north plunge to folds within domain A. Figure 112b confirms the steeply dipping, north-trending cleavage pattern. Measured lineations plunge gently both south and north, although a greater number of lineations plunge north.

Structural repetition of the stratigraphic units in domain A is largely caused by west-verging steep reverse faults spaced every 2.5 to 10 km. Grayling and Pool Creek faults (Brady, 1959; Fallas *et al.*, 2004) are west-verging reverse faults that are recognized largely because of the structural repetition of the Muncho-McConnell-Stone, Dunedin, Besa River and Mattson formations.

One east-verging reverse fault was recognized in the north-central part of the Pool Creek map area. This fault appears to die out to the south and continues into map sheet 95C/12 to the north.

Domain B contains overturned, asymmetric, east-verging folds, box folds, open folds, and a west-verging thrust fault, all north- to northeast-trending. The thrust fault has a small displacement, placing lower Paleozoic strata on middle Paleozoic strata. Fold intensity decreases in a westward direction away from the Beaver River thrust. Folds on the western margin of the Pool Creek map area become open and gentle. Farther west, the folds are box folds with sharp angular hinge zones and a broad flat core zone. Similarly, axial planar slaty cleavage to spaced fracture cleavage is most strongly developed in the immediate footwall of the Beaver River thrust and decreases in intensity westward away from the thrust. The spread of poles to bedding in Figure 113a indicates that bedding has both east and west dips in the domain, and folds dominantly have a gentle north plunge. Figure 113b confirms the steeply dipping, north-trending cleavages. Measured lineations plunge gently north, with a few aberrant lineations plunging west.

The Toobally-Crow fault (Fallas *et al.*, 2004) trends northwest from the Beaver River thrust to the north-trending, west-verging thrust fault interpreted within domain B. This fault has been interpreted as restricted to domain B since it does not appear to cut the Beaver River thrust. Folds north of the Toobally-Crow fault have a box-fold style with sharp hinges, a wide flat fold crest, and straight, moderately dipping limbs. South of the fault, folds have been interpreted as upright, open folds with rounded hinge zones; the absence of extensive outcrop in the southern area makes it difficult to definitively interpret fold style. The Toobally-Crow fault has oblique displacement with both normal (south side down) and right-lateral strike-slip components.

The immediate footwall to the Beaver River thrust north of the Toobally-Crow fault contains a tight to open, strongly asymmetric, northeast-trending, east-verging syncline cored by Besa River Formation. The west limb of this syncline is steep to overturned, and the east limb is moderately dipping. An axial planar slaty cleavage is well-developed in the hinge zone of the fold (Fig. 76). To the north, this synclinal keel can be traced into map sheet 95C/12 where it forms a very open syncline with fold limbs having gentle dips of 10 to 20 degrees as outlined by the sandstones of the Mattson Formation (Fallas *et al.*, 2005). This synclinal fold is truncated by the Toobally-Crow fault to the south.

Immediately east of Toobally Lake, a north-trending fault has been interpreted as juxtaposing Besa River Formation on the west against lower Paleozoic strata on the east. This fault is not exposed. It can be interpreted as either a west-verging reverse fault or a west-side-down normal fault. The reverse fault interpretation is preferred in this report.

The Toobally fault (Gabrielse and Blusson, 1969) forms the boundary between domains B and C and is the dominant structure within map sheet 95D/8. The inferred trace of the fault trends north to northeast in the major valley containing the Toobally Lakes. Gabrielse and Blusson (1969) estimated a maximum stratigraphic throw of approximately 3960 m (13 000 ft) with the east side down. In this report it is interpreted as an east-verging reverse fault placing lower Paleozoic strata on Triassic sediments. Stratigraphic throw of the Toobally fault along



Figure 111. *Small-scale kink/box folds with east vergence in Road River Group silty shales, field station 01TLA064. View looking south. Photo by T. Allen.*

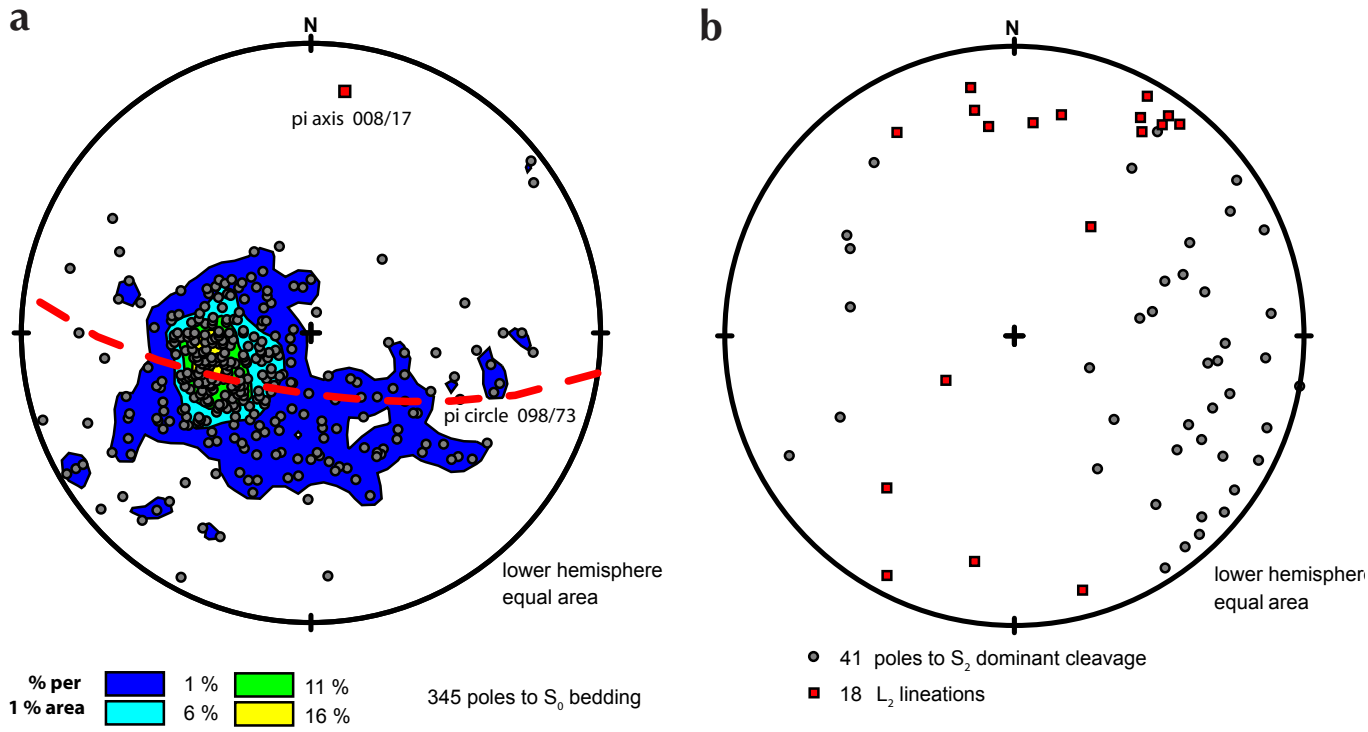


Figure 112. *Equal-area stereonet plots of structural elements in domain A, deformation D_2.* ***(a)*** *poles to bedding, calculated great circle girdle and pi axis for bedding poles;* ***(b)*** *measured lineations and poles to cleavage associated with D_2 deformation, domain A.*

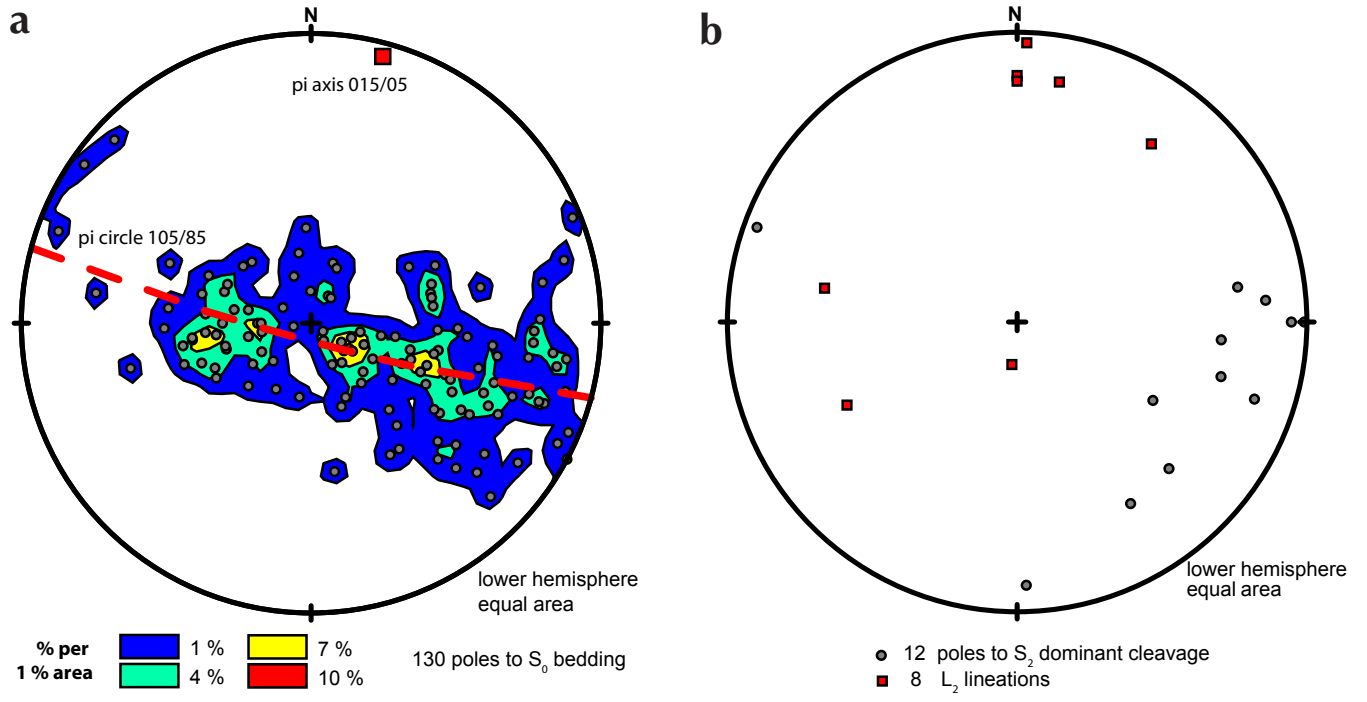


Figure 113. *Equal-area stereonet plots of structural elements in domain B, deformation D_2.* ***(a)*** *poles to bedding, calculated great circle girdle and pi axis for bedding poles;* ***(b)*** *measured lineations and poles to cleavage associated with D_2 deformation, domain B.*

section G-H is approximately 14 000 m (46 000 ft), assuming no structural repetition of the Crow Formation in the hanging wall of the fault.

Figure 114 illustrates stereonets with poles to bedding, poles to the dominant foliation, and lineations measured in domain C. The hanging wall of the Toobally fault is a west-dipping homoclinal succession of Cambrian through Ordovician sedimentary and volcanic rocks. Strata in the immediate hanging wall and footwall of the fault have a moderately well-developed slaty to spaced fracture cleavage. The intensity of this cleavage dies out to the west and east with increasing distance from the fault. Figure 114b indicates deformation structures in domain C are approximately north trending.

On a more regional scale, the map area is situated in a zone where structural style changes from south to north. To the south, contractional deformation is dominated by west-verging reverse faults with lesser folding. To the north, contractional deformation is predominantly reflected by open to tight folds interspersed with east-verging reverse faults. Tight folds generally have the same east vergence sense as the interspersed reverse faults.

This change in structural style broadly occurs at the same geographic location as the major facies change from Silurian-Devonian MacDonald platform carbonate rocks in the south to correlative Selwyn basin shales in the north. In the area dominated by carbonate rocks, the dominant structural element consists of west-verging reverse faults. In the area where shales of Road River Group are present instead of the carbonate rocks, open to tight folds become the dominant structural element. The crudely parallel orientation of structures in these two structural domains suggests that the folds and reverse faults are broadly contemporaneous and are manifestations of the same deformation event. These differences are related to differences in lithologic competency between a stratigraphic succession dominated by carbonate rocks and one containing substantial shale intervals (Pigage, 2003). This south to north transition in stratigraphic facies is broadly correlated with the Liard line (Cecile and Norford, 1993 – see discussion below).

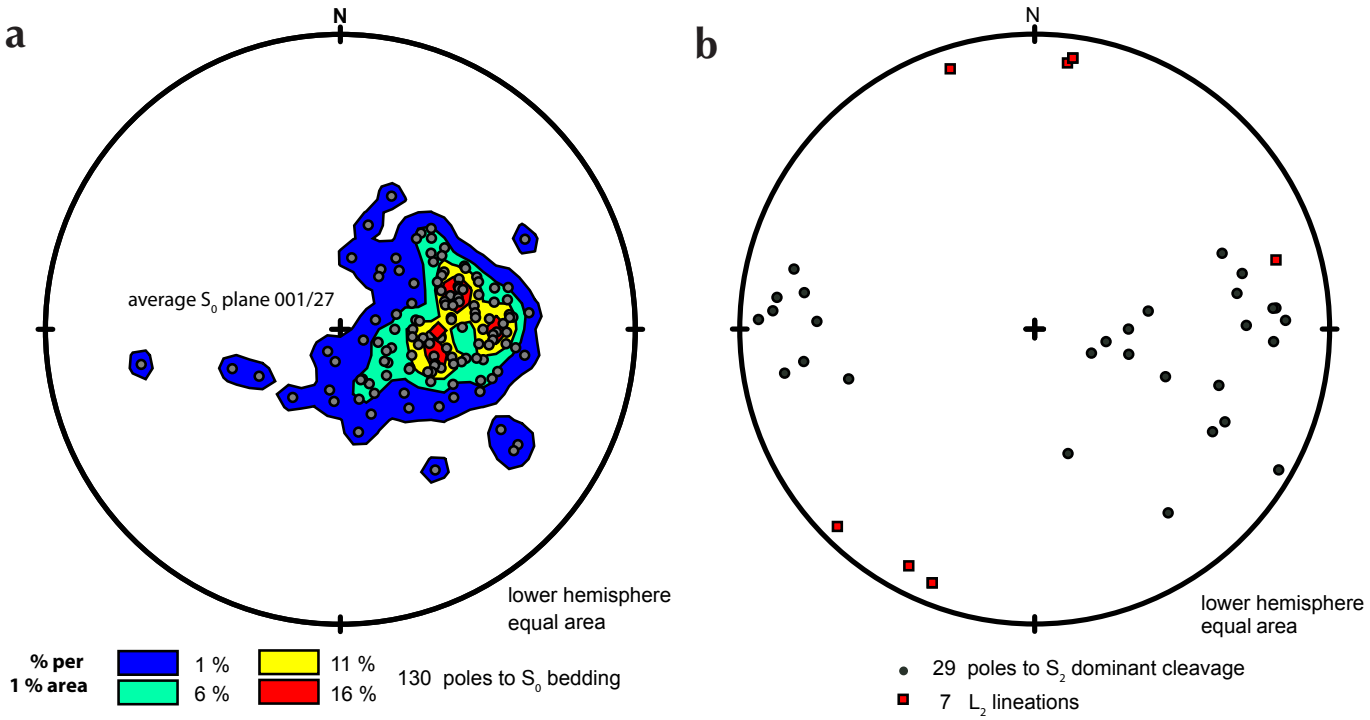


Figure 114. *Equal-area stereonet plots of structural elements in domain C, deformation D_2.* ***(a)*** *poles to bedding;* ***(b)*** *measured lineations and poles to cleavage associated with D_2 deformation, domain C.*

BEAVER RIVER STRUCTURE

The differing structural style between the southeast and northwest portions of the map area has been previously noted (Morrow and Miles, 2000). Morrow and Miles hypothesized the different styles were caused because the map area straddled a major northeast-trending crustal discontinuity which they termed the 'Beaver River Structure'. This discontinuity was active during the Laramide orogeny and was expressed as the 'Beaver Fault' (a strike slip fault with some 20 km of displacement) as mapped by Douglas (1976). It was hypothesized as being related to a Precambrian crustal feature which was reactivated at different times during the Phanerozoic.

Detailed mapping as part of this program showed that several fold and fault structures in the northern part of the map area are continuous across the earlier proposed trace of the 'Beaver Fault'. The 'Beaver Fault' and therefore the 'Beaver River Structure' as hypothesized from the earlier 250 000-scale geology map do not exist. The dramatic difference in stratigraphic successions in the area of the 'Beaver Fault' is instead caused by the rapid facies change from the Silurian-Devonian MacDonald platform carbonate rocks to the Silurian-Devonian Selwyn basin shales and cherts. The northeast-trend of this facies change may be inherited from earlier fault scarps associated with the Liard line (see below).

LIARD LINE

The Liard line is a northeast-trending feature that marks a major Ordovician-Devonian erosional and depositional pinchout (Cecile and Norford, 1993). It forms the southern boundary for the Liard depression, an area of continued subsidence and thick sediments during Ordovician through Devonian time (Fig. 115). South of the line, Ordovician through early Devonian strata are eroded or not deposited beneath Devonian strata. The carbonate to shale facies transition is offset approximately

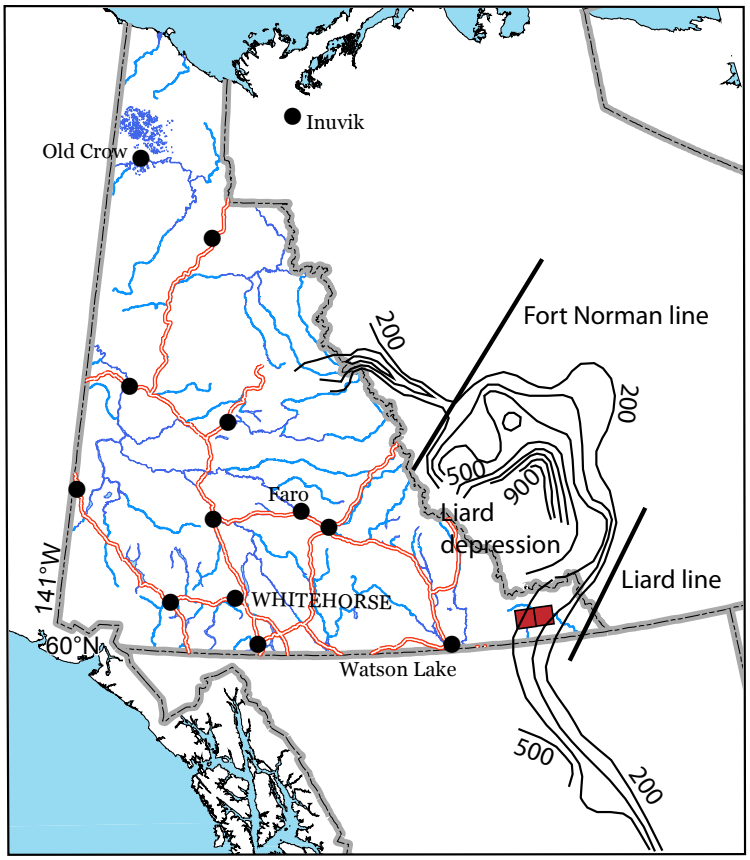


Figure 115. *Isopach map of Tippecanoe sequence strata (Ordovician-Silurian) showing Liard depression and approximate position of Liard line and Fort Norman line bounding the depression. Modified from Cecile and Norford (1993). Contour interval = 100 m. 95D/8 and 95C/5 map areas shown in southeast Yukon.*

200 km to the northeast across the Liard line. Cecile *et al.* (1997) hypothesized that the Liard line represented a major Proterozoic transfer fault, initiated during rifting to form Laurentia, which has been periodically reactivated during lower Paleozoic time to form the Meilleur River embayment and the Liard depression.

Lithofacies relations in the Pool Creek map area broadly support the existence of the Liard line with a positive topographic high area existing to the south in early Paleozoic time. Proterozoic sedimentary rocks exposed in the hanging wall of the Beaver River thrust are unconformably overlain by the Cambrian-Ordovician Crow Formation. As previously discussed, the Crow Formation contains subaerial to shoreline lithofacies indicating a local paleogeographic high during deposition. At the same time as this unit was being deposited, units farther to the north and to the south defined a carbonate platform to shale basin lateral facies variation from east to west. Further support is suggested by the superimposed incidence of undersaturated alkaline intrusions in Neoproterozoic and Eocene, possibly related to the presence of the Liard line (Pigage and Mortensen, 2004).

The general orientation of the platform carbonate to shale basin transition off the north end of MacDonald platform is south to north. The suggested offset of the northerly to northwesterly trending shale to platform carbonate transition approximately 200 km to the northeast in this area is consistent with a reactivated Proterozoic basement fault. It is uncertain whether the fault has dominantly strike-slip or vertical movement. A positive topographic feature for pre-Devonian strata to the south suggests a large component of vertical displacement along such a proposed fault.

EARLY PALEOZOIC NORMAL FAULTING

The Toobally Formation in map sheet 95D/8 is on trend with lower Crow Formation in the immediate hanging wall of the Toobally fault. Detrital zircon studies and some fossil control for these two formations indicate Toobally Formation is Neoproterozoic and Crow Formation is Cambrian-Ordovician. The contact between them is interpreted as an east-trending normal fault with at least 1800 m of displacement. The normal faulting is inferred to have occurred in late Cambrian or Early Ordovician during Crow Formation depositional time because the lower Crow Formation is offset by the fault and the upper Crow Formation unconformably overlies the fault.

STRATIGRAPHIC AND TECTONIC DISCUSSION

The various formations of the Pool Creek and 95D/8 map sheets have been presented above in the context of eight major stratigraphic successions ranging from Proterozoic to Paleocene with a combined thickness on the order of 5000 to 15 000 m. Lower early to middle Paleozoic stratigraphic successions are best preserved, with later strata being only locally preserved. Each succession contains one or more formations with related lithologic facies and depositional environments. In many cases these successions are separated by unconformities, often marking significant hiatuses. Internally, the successions also locally contain unconformities.

The sedimentary successions record vertical and lateral changes in the depositional environment through time. Variations in the sedimentary depositional environments recorded by the formations are caused by an interplay of tectonics, eustasy and climate (Catuneanu, 2003). In a broad sense, consideration of the stratigraphy in this manner is comparable to that of higher order stratigraphic sequences (Catuneanu, 2003). Table 2 lists the different

Table 2. *Depositional Environments and Transgression/Regression cycles.*

Succession	Sequence (Sloss, 1963)	Formation	Age Range	Depositional Environment	Transgression/Regression/ Orogeny/Rifting
8		PssC/Pb	Paleocene	subaerial fluvial	isolated volcanism and intrusion
Unconformity					regression and orogeny
7	Absaroka	Grayling-Toad	Early Triassic	shallow marine	
Unconformity					regression followed by transgression
6	Absaroka	Fantasque	Permian	shallow marine	
Unconformity					regression followed by transgression
5	Kaskaskia	Mattson	Lower Carboniferous	delta complex just to east	regression-shallowing upward from Besa River
5		Besa River	Devonian-Lower Carboniferous	deeper water marine shale basin	
?					transgression
4	Kaskaskia	Dunedin	Middle Devonian	shallow marine carbonate platform	regression?/transgression
4		Nonda-Muncho-McConnell-Stone/Road River	Silurian-Devonian	shallow marine carbonate platform and deeper water shale basin	lateral northwest-facing facies transition from shallow water carbonate platform to basinal shale deeper water
Unconformity					regression/transgression
3	Tippecanoe	OSs	Ordovician-Silurian?	shallow marine sea	regression?/clastic sediment influx
3		Sunblood	Ordovician	shallow marine carbonate platform	isolated volcanism
					transgression
2	Sauk	Rabbitkettle/ Crow	Cambrian/ Ordovician	shoreline slopes west to marine shale basin	lateral west-facing facies transition from subaerial to deeper water (volcanism/rifting)
Unconformity					regression/orogeny/ transgression
1		Toobally	Proterozoic	deeper water marine slope	glaciation? Pool Creek syenite intrusion/ rifting
1		Pa	Proterozoic	deeper water marine slope/ submarine channel	volcanism (rifting?)
?					regression and transgression?
1		Ps	Proterozoic	deeper water marine slope	intruded by Pool Creek syenite

successions with a brief indication of depositional environment and interpreted transgressions, regressions, rifting and orogenies. Lower Paleozoic successions can be reasonably correlated with the cratonic sequences suggested by Sloss (1963). Upper Paleozoic and later successions, with their more extensive hiatuses, limited areal distribution, and significant transgressions and regressions not correlated with the craton sequences, denote increasing influence of Cordilleran deformation which overshadows the cratonic sequence stratigraphy. This deviation from the craton sequences outlined by Sloss (1963) starts with succession 4, corresponding to the Kaskaskia sequence.

SUCCESSION 1

Succession 1 is Neoproterozoic and older, and has a maximum depositional age (unit Ps) of about 1700 Ma. Given the above age constraints, succession 1 is a possible correlative with any of sequences A, B or C. Unit Pa in succession 1 has a maximum age of deposition of 654 Ma and has been tentatively broadly correlated with lower Windermere Supergroup. The Toobally Formation has a maximum depositional age of 650 Ma. Strata in this succession delineate a relatively deep water, offshore, slope to base-of-slope marine depositional environment. The lower boundary of this succession is not exposed. Unit Pa in this succession records distal to proximal volcanic activity (rifting?) that occurred during deposition. The Toobally Formation is correlated with lower Windermere glacial diamictites in the northern Cordillera.

The upper boundary of succession 1 and lower boundary of succession 2 are marked by an absence of geological information encompassing at least 100 million years. Within this time interval at least one episode of orogeny, regression and transgression is inferred because of the folding of Ps and Pa units, extensive erosion or nondeposition of latest Proterozoic (Windermere) and lower Cambrian sediments, and subsequent deposition of succession 2 during upper Cambrian and Lower Ordovician. The latest unconformity associated with this hiatus is correlated with the regional sub-Franconian unconformity (Gabrielse *et al.*, 1973) within the northern Canadian Cordillera.

SUCCESSION 2

The Crow and Rabbitkettle formations (succession 2) consist of coarse and fine siliciclastic sediments unconformably deposited on the clastic formations of succession 1 during upper Cambrian(?) to Middle Ordovician time. This succession is correlated with the Sauk sequence of Sloss (1963). The source provenance for the Crow Formation is dominated by mature quartz sandstone, possibly similar to unit Ps in succession 1. Locally, coarse-grained conglomerates within the Crow Formation suggest a proximal clastic source. Deposition is in a shallow marine to subaerial setting. The Crow Formation is not present regionally. Both to the north (Abbott *et al.*, 1986) and south (Pyle and Barnes, 2001), same-age rocks denote a relatively stable marine carbonate platform to marine shale basin transition, with subaerial depositional environments being much farther east. For these reasons it is inferred that the deposition of the Crow Formation is related to a local paleogeographic high caused by proximal faulting (i.e., tectonic control). This tectonic control is correlated with the Liard line as described by Cecile and Norford (1997), and therefore represents reactivation of a major Proterozoic fault in the early Laurentian continental margin. Rifting intervals during deposition of the Crow Formation are inferred because of the multiple alkaline basalt volcanic horizons within the formation and the recognition of a late Cambrian to Early Ordovician, east-trending normal fault in map sheet 95D/8. Only the uppermost basalt horizon in the Crow Formation has been constrained to a definitive age of Tremadocian (Lower Ordovician). Earlier volcanic horizons are considered upper Cambrian to Ordovician.

SUCCESSION 3

The Sunblood Formation and unit OSs overlying the Crow Formation in succession 3 delineate a shallow marine carbonate platform depositional environment. Inferred water depths for the carbonate platform indicate transgression at the base of succession 3 relative to the Crow Formation. A diachronous age range for the base of succession 3, with younging in an eastward direction, confirms transgression in Early Ordovician towards the craton. Strata in succession 3 are correlated with the Tippecanoe sequence of Sloss (1963). The paleogeographic high inferred for the underlying succession 2 is not apparent since the Sunblood Formation has a widespread uniform distribution. Regional studies (Abbott *et al*, 1986; Pyle and Barnes, 2001) show the shallow water carbonate platform to deep water marine shale basin transition occurs approximately 200 km west of this map area. Minor basaltic sills within the Sunblood Formation suggest some rifting and volcanism during this time of deposition; rifting also occurred in the Misty Creek embayment to the north (Cecile *et al.*, 1997), and alkalic volcanism was widespread in the Cordillera (Goodfellow *et al.*, 1995).

Unit OSs records an influx of siliciclastic sediments occurring at the top of this succession. It is uncertain from unit OSs whether this influx is caused by a regional regression or a paleogeographic drainage change related to local tectonic activity.

SUCCESSION 4

The lower contact of succession 4 delineates a major transgression relative to succession 3. In the map area, this succession contains a sharp lateral transition from a shallow carbonate platform (Nonda Formation, Muncho-McConnell-Stone formations, Dunedin Formation) to a deeper water siliciclastic marine basin (Road River Group). The polarity of this facies transition is northwest, with the shale basin occurring north of the carbonate platform that marks the northern extent of the MacDonald carbonate platform. This basin-to-platform transition, therefore, has shifted some 200 km eastward from its paleogeographic location with the underlying succession 3. The position of this transition is relatively stable during most of the Silurian to Middle Devonian depositional interval represented by succession 4. During the Middle Devonian, the carbonate platform depositional environment prograded northwest, resulting in Dunedin Formation carbonate rocks being deposited onto deeper water Road River Group sediments. This progradation may be related to a regional regression. Succession 4 is correlated with the Kaskaskia sequence of Sloss (1963).

SUCCESSION 5

The lower contact of the Besa River Formation in succession 5 delineates a major transgression, with deposition of deep water marine shales of the Besa River Formation over shallow water carbonate sediments of Dunedin Formation. The transgression delineated by the Besa River Formation is followed by a regression indicated by the prograding delta lithofacies of the Mattson Formation overlying the Besa River Formation.

Regionally, Besa River Formation occurs east of the correlative Earn Group. Earn Group deposition is marked by a major change from an earlier passive continental margin to local extensional tectonics, with coarse clastics being sourced from the local outer portion of the miogeocline (Gordey *et al.*, 1987). The source area for Earn Group, therefore, is not from the craton but from the west.

SUCCESSION 6

Succession 6 is separated from succession 5 by a major regressive unconformity followed by transgression, with deposition of Permian Fantasque Formation strata in a shallow marine depositional environment. Fantasque Formation is only locally preserved in the map area, indicating extensive post-Permian erosion. Missing strata indicate a major erosional period or depositional hiatus occurring sometime during the missing Late Carboniferous to Triassic interval. In a regional context, Permian strata in the Canadian Cordillera consist mainly of shallow marine to basinal siliciclastic sedimentary rocks (Gordey *et al.*, 1991).

SUCCESSION 7

Similar to the boundary between successions 5 and 6, Triassic Grayling and Toad formations of succession 7 define a major regression and subsequent transgression separating them from succession 6. Triassic assemblages are also only locally preserved in the area of interest. The Triassic units are recessive and outcrop very poorly. Both upper and lower contacts are profound regional unconformities. Within the Canadian Cordillera, Triassic strata comprise a westward-thickening marine succession of siliciclastic sedimentary and carbonate rocks derived from the east (Gordey *et al.*, 1991).

SUCCESSION 8

No Jurassic or Cretaceous strata have been recognized within the map area. The Canadian Cordillera during this time interval reflects the Mesozoic and early Cenozoic orogeny and sedimentation related to collision of suspect terranes with ancestral North America (Yorath, 1991). Deposition within the miogeocline consisted of siliciclastic sediments deposited east of a prograding and advancing paleogeographic and structural high generated by the collision of ancestral North America with suspect terranes to the west.

The subaerial fluvial nature of Paleocene sediments constituting succession 8 is consistent with this increase in base level during the latter part of the collisional orogeny. As with successions 6 and 7, succession 8 is only very locally preserved.

ECONOMIC GEOLOGY

MINERAL POTENTIAL

With only six Yukon MINFILE occurrences, Pool Creek and 95D/8 map sheets have had limited mineral exploration (Deklerk, 2008). Quartz claim staking and exploration programs were completed largely in the 1970s and 1980s. Several different types of mineralized targets, including intrusion-related uranium and REEs, SEDEX zinc-lead, intrusion-related veins and barite veins, are identified through the reported exploration. Geologic location of the map area at the southeast margin of Selwyn basin further identifies Mississippi Valley-type zinc-lead and Irish-type zinc-lead exploration models as being appropriate.

The Kidd, Vista and Sid quartz claims were staked in 1976 over an airborne radiometric anomaly (Yukon MINFILE 95C 051). Subsequently, the MGM claims were staked over lapsed portions of the above claims. Hand trenching, soil sampling, geological mapping and drilling of several short IEX drill holes outlined areas of higher rare earth elements, thorium and uranium associated with the Pool Creek nepheline syenite. Mineralization occurs both in the nepheline syenite and in associated skarns in Unit Ps intruded by the syenite. Although significant high-grade mineralized zones were not encountered in the exploration program, several anomalies remain incompletely tested.

Union Oil Ltd. reported four vertical barite veins cutting through the dolostones of the Muncho-McConnell-Stone formations on the TROUT claims northeast of Beaver River (Yukon MINFILE 95C 023). Two chip samples grading 77% and 88% BaSO4 were collected as part of the same exploration program. No further work has been completed on this target, and the geological setting of the veins is uncertain.

Selwyn basin, a major lead-zinc province in western Canada, contains SEDEX massive sulphide-barite mineralization in Cambrian, Silurian and Devonian carbonaceous shales (Abbott *et al.*, 1986). Mapping as part of this report has confirmed that the map area is located at the southeast margin of Selwyn basin and contains stratigraphy that is mineralized in areas to the northwest. Exploration programs by Utah Mines Ltd. (Yukon MINFILE 95C 068, BEAV claims) and ZX Joint Venture (Yukon MINFILE 95C 069, TRANZ claims) evaluated SEDEX targets in the northwestern corner of the Pool Creek map area. Both programs reported zinc and lead soil geochemistry anomalies in areas underlain by Road River Group carbonaceous shales. A large ferricrete gossan overlooking the Beaver River on the TRANZ claims (Fig. 116) was also anomalous in nickel and cobalt (Cathro, 1983). Although significant SEDEX mineralization has not yet been discovered, the map area remains prospective, partly because areas of relevant stratigraphy



Figure 116. *Large outcrop of ferricrete, field station 00LP041. Photo taken by T. Allen.*

(Road River Group, Besa River Formation) are extensively covered with overburden.

The northern part of the Pool Creek map area contains the Silurian-Devonian facies change from shales of Selwyn basin (north) to dolostones of the MacDonald platform (south). In northeastern British Columbia, platform carbonate rocks immediately east of a similar transition between shales of Kechika trough and carbonate rocks of MacDonald platform host several showings of Mississippi Valley-type lead-zinc mineralization (MacQueen and Thompson, 1978). The largest of these is the Robb Lake deposit, containing a geological resource of 6.5 million tonnes at 7.11% combined lead and zinc, (2.4 m mining width, 5% cut-off grade; Nelson and Paradis, 1999). Robb Lake occurs in Muncho-McConnell Formation. Geological elements are appropriate for similar-style mineralization in Pool Creek area, although nothing has been discovered to date.

HYDROCARBON POTENTIAL

Pointed Mountain, Kotaneelee and Beaver River gas fields in southeastern Yukon and southwestern Northwest Territories are Canada's most northerly producing fields. The gas fields are located in stratigraphic traps related to karsting, diagenetic dolomitization and subsequent burial of Middle Devonian carbonate rocks (Morrow *et al.*, 1990). Similar stratigraphy exists at surface or close to surface in the Pool Creek area. Manetoe facies dolomitization (Morrow *et al.*, 1990) has been identified in Larsen Lake map area immediately south of Pool Creek map area. Potential exists, therefore, for oil or gas reservoirs in structural or stratigraphic traps.

Black carbonaceous mudstones and limestones from surface outcrops were collected and tested using Rock-Eval/TOC pyrolysis for potential as hydrocarbon source rocks. Programmed pyrolysis using the Rock-Eval 6 system provides information on the type, maturity and quantity of organic matter present in the sample (Espitalié *et al.*, 1977). Samples were prepared and analyzed at the Organic Geochemistry Laboratory of the Geological Survey of Canada Calgary. Table V-3 (Appendix V) presents results for the analyses. Appendix V describes operating conditions during analysis.

Most analyzed samples are shales or siltstones from the Besa River Formation and Road River Group. Sample size ranges from 10 to 100 mg. In all samples, PC (pyrolysable carbon) is negligible. TOC (total organic carbon) and RC (residual carbon) are nearly identical. All samples in the Pool Creek and 95D/8 map areas are therefore overmature with little remaining oil or gas generative capacity. Tmax for the samples may not be meaningful because S2 values are less than 0.2 mg HC/g Rock (Peters, 1986).

CAI (conodont alteration index) values for conodont collections from the Pool Creek map area range from 2 to 4. A few samples studied for palynology indicate TAI (thermal alteration index) values greater than 5. These two thermal indicators substantiate the higher temperatures denoted by the Rock-Eval analyses.

The Eocene biotite syenite intrusion in the west-central part of the Pool Creek map sheet represents a possible source of the higher temperatures indicated by the Rock-Eval results. On a more regional scale, the Eocene intrusions and high CAI and TAI values may both be symptoms of higher geothermal gradient at the particular structural level represented by the present erosion surface.

Assuming no structural complications, source rock potential in the Pool Creek map area would generally decrease even more with increasing depth because of increasing temperature related to the geothermal gradient. Organic-rich rocks in the Pool Creek map area have been subjected to temperatures which have essentially destroyed their capability of generating oil or gas locally. Any hydrocarbon reservoir in these rocks would have to form by extensive lateral migration into the map areas from a source area which has not been subjected to the local higher temperatures. Inspection of coarser grained siliciclastic sediments in the Pool Creek map area indicated that these sediments do not have significant porosity or permeability because of epitaxial quartz growth. Similarly, carbonate rock outcrops in the map area do not exhibit Manetoe facies-type alteration. From these different lines of reasoning, it is inferred that reservoir potential in map sheets 95C/5 and 95D/8 is very limited.

OVERALL SUMMARY

The Pool Creek and NTS 95D/8 map sheets contain eight successions of sedimentary rocks, ranging from Proterozoic to Paleocene in age with a total thickness of 5000 to 15 000 m. Lower to middle Paleozoic strata are best preserved, with younger strata being only locally preserved. Proterozoic strata have been tentatively correlated with Pinguicula Group and Windermere Supergroup. The newly defined Cambrian-Ordovician Crow Formation documents shallow-water to subaerial siliciclastic sedimentation related to a local paleogeographic high. Silurian-Devonian strata contain the transition from the MacDonald carbonate platform northward to the Selwyn marine basin. Units older than Jurassic are part of a regional west- to southwest-facing marine passive margin of ancestral North America. Poor preservation of sedimentary successions younger than Jurassic is linked to Cordilleran deformation caused by accretion of exotic terranes to the western margin of North America.

Intrusive igneous activity in the Neoproterozoic and Eocene occurred in close proximity in the map area: the Proterozoic Pool Creek syenite and an Eocene biotite syenite are less than 1 km apart. Extrusive volcanic rocks are dated stratigraphically or with isotopic age dating as Proterozoic, Cambrian-Ordovician, Paleocene and Eocene. Stratigraphic constraints on extrusive activity are locally poorly known. Proterozoic and Paleozoic volcanic rocks are basalts; Paleocene and Eocene volcanic rocks include both rhyolite and basalt.

The map area contains structural features related to two contractional deformation events, one pre-late Cambrian and the other post-Triassic. Evidence for the early deformation event is restricted to southeast-trending open folds in Proterozoic sedimentary rocks in the north-central part of the Pool Creek map sheet. Deformation features related to the second post-Triassic deformation event in the map areas consist dominantly of reverse faults and associated open to tight folds. Faults and folds trend north to northeast. The western part of the area is a dominantly homoclinal succession dipping west. The eastern part of the the map area is a dominantly homoclinal succession dipping east. Structural styles for the post-Triassic deformation can be related to the different lithofacies present in the map area. Sedimentology and igneous activity are considered related to periodic reactivation of the Liard line, a major Precambrian transfer fault located proximally to the south.

One east-trending extensional fault has been recognized in map sheet 95D/8. Faulting is constrained to late Cambrian or Early Ordovician by stratigraphic ages of units offset and overlying the fault. Early Paleozoic normal faulting is consistent with alkali basalt volcanism in the Crow Formation. Extension is correlated with rifting associated with reactivation of the Liard line located immediately to the south of the map areas.

Previous mineral exploration has not resulted in the discovery of major mineral deposits in the area. Mineral deposit models appropriate for the geology include barite vein deposits, SEDEX zinc-lead deposits, Mississippi Valley-type zinc-lead deposits, Irish-type zinc-lead deposits and intrusion-related uranium deposits. Thermal maturation indices confirm the sediments are overmature for hydrocarbon generation. Clastic units have epitaxial quartz overgrowths that have reduced porosity and permeability. The closest hydrocarbon fields are gas fields hosted in Manetoe facies dolomite; Manetoe facies was not recognized at surface in the map area.

ACKNOWLEDGEMENTS

Jordin Barclay, Annie Daigle, Kristen Kennedy, Jesse Kirkby, Andre Lebel, Janis Lloyd, Andrew McNeill and Kyle McWilliam assisted in the field. Tammy Allen spent two years working with the project as senior assistant geologist. Rob MacNaughton measured a detailed stratigraphic section through part of unit Pa in the area, and Rod Smith completed regional and detailed studies on the recent Cenozoic and glacial history. Helicopter support was provided by Talon Helicopters (2000), Wildcat Helicopters (2001), Mustang Helicopters (2002), and Trans North Air (2003-2005). Northern Rockies Air Charter provided fixed wing support in 2003-2005. Logistical support (2000-2002) was provided by the Central Foreland NATMAP project under the supervision of Larry Lane, Research Scientist, Geological Survey of Canada, Calgary. Yukon Geological Survey supported continuation of the field work in map sheet 95D/8 after completion of the NATMAP field program.

Extensive discussions concerning map details with Karen Fallas, Rob MacNaughton and Larry Lane were illuminating. Rob MacNaughton offered stratigraphic consultation. Rod Smith provided detailed stratigraphic information on the Paleocene sediments and reviewed the section on the glacial history of the area. Charlie Roots reviewed the sections concerned with age and correlation of the Neoproterozoic strata. Grant Abbott provided consistent encouragement for the project. The manuscript was reviewed by Mike Cecile.

SELECTED REFERENCES

Abbott, J.G., 1997. Geology of the Upper Hart River area, Eastern Ogilvie Mountains, Yukon Territory (116A/10, 116A/11). Exploration and Geological Services Division, Yukon, Indian and Northern Affairs Canada, Bulletin 9, 92 p.

Abbott, J.G., Gordey, S.P. and Tempelman-Kluit, D.J., 1986. Setting of stratiform, sediment-hosted lead-zinc deposits in Yukon and northeastern British Columbia. *In:* Mineral Deposits of Northern Cordillera, J.A. Morin (ed.), Canadian Institute of Mining and Metallurgy, Special Volume 37, p. 1-18.

Aitken, J.D., 1991. The Ice Brook Formation and post-Rapitan, Late Proterozoic glaciation, Mackenzie Mountains, Northwest Territories. Geological Survey of Canada, Bulletin 404, 43 p.

Aitken, J.D., 1993. Cambrian and Lower Ordovician Sauk Sequence, Subchapter 4B. *In:* Sedimentary Cover of the Craton in Canada, D.F. Stott and J.D. Aitken (eds.), Geology of Canada, no. 5, Geological Survey of Canada, p. 96-124.

Aitken, J.D. and McMechan, M.E., 1991. Middle Proterozoic assemblages, Chapter 5. *In:* Geology of the Cordilleran Orogen in Canada, H. Gabrielse and C.J. Yorath (eds.), Geology of Canada, no. 4, Geological Survey of Canada, p. 97-124.

Allen, T.L. and Pigage, L.C., 2000. Geological map of Pool Creek (NTS 95C/5), southeastern Yukon (1:50 000 scale). Exploration and Geological Services Division, Yukon Region, Indian and Northern Affairs Canada, Open File 2000-11.

Allen, T.L., Pigage, L.C. and MacNaughton, R.B., 2001. Preliminary geology of the Pool Creek map area (95C/5), southeastern Yukon. *In:* Yukon Exploration and Geology 2000, D.S. Emond and L.H. Weston (eds.), Exploration and Geological Services Division, Yukon, Indian and Northern Affairs Canada, p. 53-72.

Bamber, E.W. and Mamet, B.L., 1978. Carboniferous biostratigraphy and correlation, northeastern British Columbia and southwestern District of Mackenzie. Geological Survey of Canada, Bulletin 266, 19 p.

Bamber, E.W., Taylor, G.C. and Procter, R.M., 1968. Carboniferous and Permian stratigraphy of northeastern British Columbia. Geological Survey of Canada, Paper 68-15, 25 p.

Bostock, H.S., 1966. Notes on glaciation in central Yukon Territory. Geological Survey of Canada, Paper 65-36, 18 p.

Bradley, D.C., McClelland, W.C., Wooden, J.L., Till, A.B., Roeske, S.M., Miller, M.L., Karl, S.M. and Abbott, J.G., 2007. Detrital zircon geochronology of some Neoproterozoic to Triassic rocks in interior Alaska. *In:* Tectonic growth of a collisional continental margin: crustal evolution of southern Alaska, K.D. Ridgway, J.M. Trop, J.M.G. Glen and J.M. O'Neill (eds.), Geological Society of America, Special Paper 431, p. 155-189.

Brady, W.B., 1959. The geology of the Liard River area, Northwest Territories, Yukon Territory and British Columbia. Union Oil Company of California, NEB #28-1-5-4.

Burt, P., 1983. Geological, geochemical and geophysical report on work performed during June and July of 1983 on the BEAV 1 to 180 claims. Unpublished mineral assessment report #091486. Energy, Mines and Resources, Yukon Government, 46 p.

Burt, P., 1985. Diamond drilling report of work performed during June, July and August 1984 on the BEAV 1 to 180 claims. Unpublished mineral assessment report #091613. Energy, Mines and Resources, Yukon Government, 11 p.

Cande, S.C. and Kent, D.V., 1995. Revised calibration of the geomagnetic polarity timescale for the Late Cretaceous and Cenozoic. Journal of Geophysical Research, vol. 100, p. 6093-6095.

Catuneanu, O., 2003. Sequence stratigraphy of clastic systems. Geological Association of Canada, Short Course Notes, vol. 16, 248 p.

Cathro, R.J., 1983. Report on geological and geochemical surveys conducted July 12-August 17, 1982, TRANZ 1-14 claims – YA68631-YA68644, Watson Lake M.D., Yukon, claim sheet 95C/5, Latitude 60°28'N; Longitude 125°56'W. Unpublished mineral assessment report #091459. Energy, Mines and Resources, Yukon Government, 9 p.

Cecile, M.P., 1982. The Lower Paleozoic Misty Creek embayment, Selwyn Basin, Yukon and Northwest Territories. Geological Survey of Canada, Bulletin 335, 78 p.

Cecile, M.P. and Campbell, F.H.A., 1977. Large-scale stratiform and intrusive sedimentary breccias of the lower Proterozoic Goulburn Group, Bathurst Inlet, N.W.T. Canadian Journal of Earth Sciences, vol. 14, p. 2364-2387.

Cecile, M.P., Morrow, D.W. and Williams, G.K., 1997. Early Paleozoic (Cambrian to Early Devonian) tectonic framework, Canadian Cordillera. Bulletin of Canadian Petroleum Geology, vol. 45, p 54-74.

Cecile, M.P. and Norford, B.S., 1979. Basin to platform transition, Lower Paleozoic strata of Ware and Trutch map areas, northeastern British Columbia. Geological Survey of Canada, Paper 79-1A, p. 219-226.

Cecile, M.P. and Norford, B.S., 1993. Ordovician and Silurian, Subchapter 4C. *In:* Sedimentary Cover of the Craton in Canada, D.F. Stott and J.D. Aitken (eds.), Geology of Canada, no. 5, Geological Survey of Canada, p. 125-149.

Coney, P.J., Jones, D.L. and Monger, J.W.H., 1980. Cordilleran suspect terranes. Nature, vol. 288, p. 329-333.

Culbert, R.R., 1981. Geochemical report on the THOR 1-22 mineral claims, Watson Lake Mining District. Unpublished mineral assessment report #090846. Energy, Mines and Resources, Yukon Government, 14 p.

Currie, L.D., Kubli, T.E., McDonough, M.R. and Hodder, D.N., 1998. Geology of the Babiche Mountain and Chinkeh Creek map areas, southeastern Yukon Territory and southwestern Northwest Territories. Geological Survey of Canada, Current Research 1998-A, p. 39-48.

Dalrymple, R.W. and Narbonne, G.M., 1996. Continental slope sedimentation in the Sheepbed Formation (Neoproterozoic, Windermere Supergroup), Mackenzie Mountains, N.W.T. Canadian Journal of Earth Sciences, vol. 33, p. 848-862.

Deklerk, R. (compiler), 2008. Yukon MINFILE 2008 - A database of mineral occurrrencs. Yukon Geological Survey, <www.geology.gov.yk.ca/databases_gis.html>.

Douglas, R.J.W., 1976. Geology of La Biche River map area (95C), District of Mackenzie. Geological Survey of Canada, "A" Series Map 1380A (scale 1:250 000).

Douglas, R.J.W. and Norris, D.K., 1959. Fort Liard and La Biche map-areas, Northwest Territories and Yukon 95B and 95C. Geological Survey of Canada, Paper 59-6, 23 p.

Dudas, F.O. and Lustwerk, R.L., 1997. Geochemistry of the Little Dal basalts: continental tholeiites from the Mackenzie Mountains, Northwest Territories, Canada. Canadian Journal of Earth Sciences, vol. 34, p. 50-58.

Duk-Rodkin, A., Barendregt, R.W., Tarnocai, C. and Phillips, F.M., 1996. Late Tertiary to late Quaternary record in the Mackenzie Mountains, Northwest Territories, Canada: stratigraphy, paleosols, paleomagnetism and chlorine-36. Canadian Journal of Earth Sciences, vol. 33, p. 875-895.

Duk-Rodkin, A., Barendregt, R.W., Froese, D.G., Weber, F., Enkin, R., Smith, I.R., Zazula, G.D., Waters, P. and Klassen, R., 2004. Timing and extent of Plio-Pleistocene glaciations in north-western Canada and east-central Alaska. *In:* Quaternary Glaciations – Extent and Chronology, Part II, J. Ehlers and P.L. Gibbard (eds), Elsevier, p. 313-345.

Eisbacher, G.H., 1978. Re-definition and subdivision of the Rapitan Group, Mackenzie Mountains. Geological Survey of Canada, Paper 77-35, 21 p.

Eisbacher, G.H., 1981. Sedimentary tectonics and glacial record in the Windermere Supergroup, Mackenzie Mountains, northwestern Canada. Geological Survey of Canada, Paper 80-27, 40 p.

Espitalié, J., Laporte, J.L., Madec, M., Marquis, F., Leplat, P., Paulet, J. and Boutefeu, A., 1977. Methode rapide de caracterisation des roches meres de leur potential petrolier et de leur degree d'evolution. Revue de l'Institute Francais du Petrole, vol. 32, p. 23-42.

Fallas, K.M. and Lane, L.S., 2001. Geology of the Mount Martin, Fisherman Lake and Mount Flett map areas, Yukon Territory and Northwest Territories. Geological Survey of Canada, Current Research 2001-A5, 11 p.

Fallas, K.M., Pigage, L.C. and MacNaughton, R.B. (compilers), 2004. Geology, southwest La Biche River (95C/SW), Yukon Territory and British Columbia. Geological Survey of Canada, Open File 4664 (scale 1:100 000, 2 sheets).

Fallas, K.M., Pigage, L.C. and Lane, L.S. (compilers), 2005. Geology, La Biche River northwest (95C/NW), Yukon and Northwest Territories. Geological Survey of Canada, Open File 5018 (scale 1:100 000, 1 sheet).

Fedo, C.M., Sircombe, K.N. and Rainbird, R.H., 2003. Detrital zircon analysis of the sedimentary record. *In:* Zircon, J.M. Hanchar and P.W.O. Hoskins (eds.), Reviews in Mineralogy and Geochemistry, Mineralogical Society America, p. 277-303.

Ferri, F., Rees, C. and Nelson, J., 1996. Geology and mineralization of the Gataga Mountain area, northern Rocky Mountains (94L/10, 11, 14 and 15). *In:* Geological Fieldwork 1995, B. Grant and J.M. Newell (eds.), British Columbia Ministry of Energy, Mines and Petroleum Resources, Paper 1996-1, p. 137-154.

Ferri, F., Rees, C., Nelson, J. and Legun, A., 1999. Geology and mineral deposits of the northern Kechika Trough between Gataga River and the 60th parallel. British Columbia Ministry of Energy and Mines, Bulletin 107, 122 p.

Fritz, W.H., 1985. The basal contact of the Road River Group-a proposal for its location in the type area and in other selected areas in Northern Canadian Cordillera. Geological Survey of Canada, Paper 85-1B, p. 205-215.

Gabrielse, H. and Blusson, S.L., 1969. Geology of Coal River map-area, Yukon Territory and District of Mackenzie (95D). Geological Survey of Canada, Paper 68-38, 22 p.

Gabrielse, H., Blusson, S.L. and Roddick, J.A., 1973. Geology of Flat River, Glacier Lake and Wrigley Lake map-areas, District of Mackenzie and Yukon Territory. Geological Survey of Canada, Memoir 366, (Parts I and II), 421 p.

Gehrels, G.E., Dickinson, W.R., Ross, G.M., Stewart, J.H. and Howell, D.G., 1995. Detrital zircon reference for Cambrian to Triassic miogeoclinal strata of western North America. Geology, vol. 23, p. 831-834.

Gehrels, G.E., Johnsson, M.J. and Howell, D.G., 1999. Detrital zircon geochronology of the Adams argillite and Nation River Formation, east-central Alaska, U.S.A., Journal of Sedimentary Research, vol. 69, p. 135-144.

Gehrels, G.E. and Ross, G.M., 1998. Detrital zircon geochronology of Neoproterozoic to Permian miogeoclinal strata in British Columbia and Alberta, Canadian Journal of Earth Sciences, vol. 35, p. 1380-1401.

Goodfellow, W.D., Cecile, M.P. and Leybourne, M.I., 1995. Geochemistry, petrogenesis and tectonic setting of lower Paleozoic alkalic and potassic volcanic rocks, Northern Canadian Cordilleran miogeocline. Canadian Journal of Earth Sciences, vol. 32, p. 1236-1254.

Gordey, S.P., Abbott, J.G., Tempelman-Kluit, D.J. and Gabrielse, H., 1987. "Antler" clastics in the Canadian Cordillera. Geology, vol. 15, p. 103-107.

Gordey, S.P. and Anderson, R.G., 1993. Evolution of the Northern Cordilleran miogeocline, Nahanni map area (105I), Yukon and Northwest Territories. Geological Survey of Canada, Memoir 428, 214 p.

Gordey, S.P., Geldsetzer, H.H.J., Morrow, D.W., Bamber, E.W., Henderson, C.M., Richards, B.C., McGugan, A., Gibson, D.W. and Poulton, T.P., 1991. Part A. Ancestral North America in Upper Devonian to Middle Jurassic assemblages, Chapter 8. *In:* Geology of the Cordilleran Orogen in Canada, H. Gabrielse and C.J. Yorath (eds), Geological Survey of Canada, Geology of Canada, no. 4, p. 219-281.

Gradstein, F., Ogg, J. and Smith, A., 2004. A Geologic Time Scale 2004. Cambridge University Press, Cambridge, United Kingdom, 589 p.

Harker, P., 1961. Summary account of Carboniferous and Permian formations, southwestern District of Mackenzie. Geological Survey of Canada, Paper 61-1, 9 p.

Harrison, J.C., 1982. Petrology of the 'Ting Creek' alkalic intrusion, southeast Yukon. Unpublished MSc thesis, University of Toronto, Ontario, 299 p.

Henderson, C.M., Bamber, E.W., Richards, B.C., Higgins, A.C. and McGugan, A., 1993. Permian; Subchapter 4F. *In:* Sedimentary Cover of the Craton in Canada, D.F. Stott and J.D. Aitken (eds), Geological Survey of Canada, Geology of Canada no. 5, p. 272-293.

Hoffman, P., 1989. Precambrian geology and tectonic history of North America. *In:* The Geology of North America - an overview, A.W. Bally and A.R. Palmer (eds.), Geological Society of America, Vol A, p. 447-512.

Irvine, T.N. and Barager, W.R.A., 1971. A guide to the chemical classification of the common volcanic rocks: Canadian Journal of Earth Sciences, vol. 8, p. 523-548.

Jackson, D.E. and Lenz, A.C., 1962. Zonation of Ordovician and Silurian graptolites in northern Yukon, Canada. American Association of Petroleum Geologists Bulletin, vol. 46, p. 30-45.

Jackson, L.E., Jr., Ward, B., Duk-Rodkin, A. and Hughes, O.L., 1991. The last Cordilleran ice sheet in southern Yukon Territory. Géographie physique et Quaternaire, vol. 45, no. 3, p. 341-354.

Jefferson, C.W. and Parrish, R.R., 1989. Late Proterozoic stratigraphy, U-Pb zircon ages, and rift tectonics, Mackenzie Mountains, northwestern Canada. Canadian Journal of Earth Sciences, vol. 26, p. 1784-1801.

Kidd, F.A., 1963. The Besa River Formation. Bulletin of Canadian Petroleum Geology, vol. 11, p. 369-372.

Kindle, E.D., 1944. Geological reconnaissance along Fort Nelson, Liard, and Beaver Rivers, northeastern British Columbia and southeastern Yukon. Geological Survey of Canada, Paper 44-16, 19 p.

Kingston, D.R., 1951. Stratigraphic reconnaissance along the upper South Nahanni River, NWT. American Association of Petroleum Geologists Bulletin, vol. 35, no. 11, p. 2409-2426.

LeCheminant, A.N. and Heaman, L.M., 1994. 779 Ma mafic magmatism in the northwestern Canadian shield and the northern Cordillera: A new regional time maker. *In:* Abstracts of the Eighth International Conference on Geochronology, Cosmochronology and Isotope Geology, M.A. Lanphere, G.B. Dalrymple and B.D. Turrin (eds.), United States Geological Survey, Circular 1107, p. 187.

Lenz, A.C., 1966. Upper Silurian and Lower Devonian paleontology and correlations, Royal Creek, Yukon Territory: a preliminary report. Bulletin of Canadian Petroleum Geology, vol. 14, p. 604-612.

Lenz, A.C., 1972. Ordovician to Devonian history of northern Yukon and adjacent District of Mackenzie. Bulletin of Canadian Petroleum Geology, vol. 20, p. 321-361.

Leslie, C.D., 2009. Detrital zircon geochronology and rift-related magmatism: Central Mackenzie Mountains, Northwest Territories. Unpublished MSc thesis, University of British Columbia, British Columbia, 224 p.

Ludvigsen, R., 1975. Ordovician formations and faunas, southern Mackenzie Mountains. Canadian Journal of Earth Sciences, vol. 12, p. 663-697.

Ludwig, K.R., 2003. User's manual for Isoplot 3.0: A geochronological toolkit for Microsoft Excel. Berkeley Geochronology Center Special Publication 4, 71 p.

MacNaughton, R.B., 2002a. Sedimentology of Triassic siliciclastic strata, Mount Martin and Mount Merrill map areas, Yukon Territory. Geological Survey of Canada, Current Research, 2002-A4, 10 p.

MacNaughton, R.B., 2002b. Report on one sample from Ordovician strata, Pool Creek map area, Yukon Territory, collected by Lee Pigage (Yukon Geology Program) and submitted for trace-fossil identification; NTS 95C/5. Geological Survey of Canada, Report No. 001-RBM-2002, 3 p.

MacNaughton, R.B. and Utting, J., 2002. The Triassic of the La Biche River map area (NTS 95C), southeastern Yukon Territory: preliminary sedimentology, biostratigraphy, and thermal maturity. Canadian Society of Petroleum Geologists, Diamond Jubilee Convention, Program and Abstracts, p. 214.

MacQueen, R.W. and Thompson, R.J., 1978. Carbonate-hosted lead-zinc occurrences in northeastern British Columbia with emphasis on the Robb Lake deposit. Canadian Journal of Earth Sciences, vol. 15, p. 1737-1762.

Mathews, W.H. (compiler), 1986. Physiography of the Canadian Cordillera. Geological Survey of Canada, Map 1701A (scale 1:5 000 000).

McCracken, A.D., 2003a. Report on 12 samples (Con. No. 1762) from Middle Ordovician and Devonian strata from British Columbia collected by A. Khudoley and L. Pigage and submitted by L. Lane (GSC-C). NTS 94G/12, 95C/04, 95C/05, 95C/11, 95C/12, 95C/13. Geological Survey of Canada, Report No. 6-ADM-2003, 8 p.

McCracken, A.D., 2003b. Report on one conodont sample (Con. No. 1674) from Middle Ordovician strata from southeastern Yukon Territory collected by R.B. MacNaughton (GSC-C) NTS 95C/05. Geological Survey of Canada, Report No. 7-ADM-2003, 4 p.

McMechan, M.E., 2000. Vreeland Diamictites - Neoproterozoic glaciogenic slope deposits, Rocky Mountains, northeast British Columbia. Bulletin of Canadian Petroleum Geology, vol. 48, p. 246-261.

Meschede, M., 1986. A method of discriminating between different types of mid-ocean ridge basalts and continental tholeiites with the Nb-Zr-Y diagram. Chemical Geology, vol. 56, p. 207-218.

Morrow, D.W., 1978. The Dunedin Formation: A transgressive shelf carbonate sequence. Geological Survey of Canada, Paper 76-12, 35 p.

Morrow, D.W., 1999. Lower Paleozoic stratigraphy of northern Yukon Territory and northwestern District of Mackenzie. Geological Survey of Canada, Bulletin 538, 202 p.

Morrow, D.W., Cumming, G.L. and Aulstead, K.L., 1990. The gas-bearing Devonian manetoe facies, Yukon and Northwest Territories. Geological Survey of Canada, Bulletin 400, 54 p.

Morrow, D.W. and Geldsetzer, H.H.J., 1992. Lower and Middle Devonian Assemblages. *In:* Geology of the Cordilleran Orogen in Canada, H. Gabrielse and C.J. Yorath (eds.), Geological Survey of Canada, Geology of Canada, no. 4, p. 196-210.

Morrow, D.W. and Miles, W.C., 2000. The Beaver River structure: A cross-strike discontinuity of possible crustal dimensions in the southern Mackenzie Fold Belt, Yukon and Northwest Territories, Canada. Bulletin of Canadian Petroleum Geology, vol. 48, no. 1, p. 19-29.

Nelson, J.L. and Paradis, S., 1999. The Robb Lake carbonate-hosted lead-zinc deposit, northeastern British Columbia: a Cordilleran MVT deposit. *In:* Geological Fieldwork 1998, B.C. Ministry of Energy and Mines, Paper 1999-1, p. 89-101.

Norford, B.S., 1964. Reconnaissance of the Ordovician and Silurian rocks of northern Yukon Territory. Geological Survey of Canada, Paper 63-39, 139 p.

Norford, B.S., 2001. Report on six collections from the Trutch and La Biche River map-areas, northern British Columbia and adjacent Yukon Territory submitted by Dr. L.S. Lane in 2001 (NTS 94G/04, 95C/05). Geological Survey of Canada, Report No. S-3 BSN 2001, 3 p.

Norford, B.S., 2002. Report on two lots of fossils from the LaBiche River map-area, southern Yukon Territory, collected by Mr. Lee Pigage and Ms. Tammy Allen in 2001 and submitted by Dr. L.S. Lane, 2001 (NTS 95C/5). Geological Survey of Canada, Report No. S-1-BSN-2002, 2 p.

Norford, B.S., Gabrielse, H. and Taylor, G.C., 1966. Stratigraphy of Silurian carbonate rocks of the Rocky Mountains, northern British Columbia. Bulletin of Canadian Petroleum Geology, vol. 14, p. 504-519.

Nowlan, G.S., 2001. Report on one sample from Yukon Territory collected by Larry Lane and submitted for microfossil analysis; NTS 095C/05; CON # 1627. Geological Survey of Canada, Report No. 010-GSN-2001, 1 p.

Nowlan, G.S., 2004. Report on eighteen samples from Cambrian, Ordovician, Silurian and possibly Devonian strata in the southeastern part of Yukon Territory submitted for conodont analysis by Larry Lane, Rob MacNaughton and Karen Fallas (Geological Survey of Canada Calgary) and Lee Pigage and Tammy Allen (Yukon Geological Survey); NTS 095C/05; CON #1657. Geological Survey of Canada, Report No. 002-GSN-2004, 10 p.

Nowlan, G.S., 2008. Report on six samples from Ordovician strata in the northern Toobally Lake and Coal River map areas, southeastern Yukon submitted for conodont analysis by Lee Pigage (Yukon Geological Survey); NTS 095 D/06; 095D08, Geological Survey of Canada, Report No. 003-GSN-2008, 5 p.

Patton, W.J.H., 1958. Mississippian succession in South Nahanni River area, Northwest Territories. *In:* Jurassic and Carboniferous of western Canada, A.J. Goodman (ed.), American Association of Petroleum Geologists, John Andrew Allan Memorial Volume, p. 309-326.

Pearce, J.A., 1996. A user's guide to basalt discrimination diagrams. *In:* Trace Element Geochemistry of Volcanic Rocks: Applications for Massive Sulphide Exploration, D.A. Wyman (ed.), Geological Association of Canada, Short Course Notes, vol. 12, p. 79-113.

Pearce, J.A. and Cann, J.R., 1973. Tectonic setting of basic volcanic rocks determined using trace element analyses. Earth and Planetary Science Letters, vol. 19, p. 290-300.

Pearce, J.A., Harris, N.B.W. and Tindle, A.G., 1984. Trace element discrimination diagrams for the tectonic interpretation of granitic rocks. Journal of Petrology, vol. 25, p. 956-983.

Pearce, J.A. and Peate, D.W., 1995. Tectonic implications of the composition of volcanic arc magmas. Annual Review of Earth Planetary Sciences, vol. 23, p. 251-285.

Peters, K.E., 1986. Guidelines for evaluating petroleum source rock using programmed pyrolysis. American Association of Petroleum Geologists Bulletin, vol. 70, p. 318-329.

Pigage, L.C., 2003. Structural styles in western La Biche River map area (NTS 95C), southeastern Yukon Territory, Canada (abstr.). Geological Association of Canada, Mineralogical Association of Canada, Society of Economic Geologists Joint Annual Meeting, Abstract Number 137.

Pigage, L.C., 2004a. Bedrock geology compilation of the Anvil District (parts of NTS 105K/2, 3, 5, 6, 7 and 11), central Yukon. Yukon Geological Survey, Bulletin 15, 103 p.

Pigage, L.C., 2004b. Preliminary geology of NTS 95D/8 (north Toobally Lakes area), southeast Yukon (1:50 000 scale). Yukon Geological Survey, Open File 2004-19.

Pigage, L.C., 2006. Stratigraphy summary for southeast Yukon (95D/8 and 95C/5). *In:* Yukon Exploration and Geology 2005, D.S. Emond, G.D. Bradshaw, L.L. Lewis and L.H. Weston (eds.), Yukon Geological Survey, p. 267-285.

Pigage, L.C. and Allen, T.L., 2001. Geological map of Pool Creek (NTS 95C/5), southeastern Yukon (1:50 000 scale). Exploration and Geological Services Division, Yukon Region, Indian and Northern Affairs Canada, Open File 2001-32.

Pigage, L.C. and MacNaughton, R.B., 2004. Reconnaissance geology of northern Toobally Lake (95D/8), southeast Yukon. *In:* Yukon Exploration and Geology 2003, D.S. Emond and L.L. Lewis (eds.)., Yukon Geological Survey, p. 199-219.

Pigage, L.C. and Mortensen, J.K., 2004. Superimposed Neoproterozoic and early Tertiary alkaline magmatism in the La Biche River area, southeast Yukon Territory. Bulletin of Canadian Petroleum Geology, vol. 52, p. 325-342.

Pyle, L., 2001. Eight samples submitted for conodont microfossil analysis, collected by Lee Pigage (Yukon Geological Survey), Pool Creek map sheet (NTS 95C/5). Report No. LJP01-01, 3 p.

Pyle, L., 2004. Seventeen samples submitted for conodont microfossil analysis, collected by Lee Pigage (Yukon Geological Survey), map sheet NTS 95D/8. Report No. LJP04-02, 12 p.

Pyle, L.J. and Barnes, C.R., 2000. Upper Cambrian to Lower Silurian stratigraphic framework of platform-to-basin facies, northeastern British Columbia. Bulletin of Canadian Petroleum Geology, vol. 48, p. 123-149.

Pyle, L.J. and Barnes, C.R., 2001. Ordovician-Silurian stratigraphic framework, Macdonald Platform to Ospika Embayment transect, northeastern British Columbia. Bulletin of Canadian Petroleum Geology, vol. 49, p. 513-535.

Pyle, L.J. and Barnes, C.R., 2002. Taxonomy, evolution and biostratigraphy of conodonts from the Kechika Formation, Skoki Formation and Road River Group (Upper Cambrian to Lower Silurian), northeastern British Columbia. National Research Council of Canada, monograph series, 227 p.

Rainbird, R., Heaman, L.M. and Young, G.M., 1992. Sampling Laurentia: Detrital zircon geochronology offers evidence for an extensive Neoproterozoic river system originating from Grenville orogen. Geology, vol. 20, p. 351-354.

Rainbird, R.H., McNicoll, V.J., Thériault, R.J., Heaman, L.M., Abbott, J.G., Long, D.G.F. and Thorkelson, D.J., 1997. Pan-continental river system draining Grenville Orogen recorded by U-Pb and Sm-Nd geochronology of Neoproterozoic quartzarenites and mudrocks, northwestern Canada. Journal of Geology, vol. 105, p. 1-17.

Renne, P.R., Swisher, C.C., Deino, A.L., Karner, D.B., Owens, T.L. and DePaolo, D.J., 1998. Intercalibration of standards, absolute ages and uncertainties in $^{40}Ar/^{39}Ar$ dating. Chemical Geology, vol. 145, p. 117-152.

Richards, B.C., 1989. Uppermost Devonian and Lower Carboniferous stratigraphy, sedimentation and diagenesis, southwestern District of Mackenzie and southeastern Yukon Territory. Geological Survey of Canada, Bulletin 390, 135 p.

Richards, B.C., Bamber, E.W., Higgins, A.C. and Utting, J., 1993. Carboniferous; Subchapter 4E. *In:* Sedimentary Cover of the Craton in Canada, D.F. Stott and J.D. Aitken (eds.), Geological Survey of Canada, Geology of Canada, no. 5, p. 202-271.

Roddick, J.C., 1988. The assessment of errors in $^{40}Ar/^{39}Ar$ dating. *In:* Radiogenic Age and Isotopic Studies, Report 2, Geological Survey of Canada, Paper 88-2, p. 7-16.

Roots, C.F. and Parrish, R.R., 1988. Age of the Mount Harper volcanic complex, southern Ogilvie Mountains, Yukon. *In:* Radiogenic age and isotopic studies: Report 2, Geological Survey of Canada, Paper 88-2, p. 29-35.

Ross, G.M., 1991. Tectonic setting of the Windermere Supergroup revisited. Geology, vol. 19, p. 1125-1128.

Ross, G.M. and Villeneuve, M., 2003. Provenance of the Mesoproterozoic (1.45 Ga) Belt basin (western North America): Another piece of the pre-Rodinia paleogeographic puzzle. Geological Society of America Bulletin, vol. 115, p. 1191-1217.

Ross, G.M., Villeneuve, M.E. and Theriault, R.J., 2001. Isotopic provenance of the lower Muskwa assemblage (Mesozoic, Rocky Mountains, British Columbia): new clues to correlation and source areas. Precambrian Research, vol. 111, p. 57-77.

Rutgers, A.T.C., 1958. Stoddart Formation of northeast British Columbia. *In:* Jurassic and Carboniferous of western Canada, A.J. Goodman (ed.), American Association of Petroleum Geologists, John Andrew Allan Memorial Volume, p. 327-330.

Scaillet, S., 2000. Numerical error analysis in $^{40}Ar/^{39}Ar$ dating. Chemical Geology, vol. 162, p. 269-298.

Shervais, J., 1982. Ti-V plots and the petrogenesis of modern and ophiolitic lavas. Earth and Planetary Science Letters, vol. 59, p. 101-118.

Slama, J., Kosler, J., Condon, D.J., Crowley, J.L., Gerdes, A., Hanchar, J.M., Horstwood, M.S.A., Morris, G.A., Nasdala, L., Norberg, N., Schaltegger, U., Schoene, B., Tubrett, M.N. and Whitehouse, M.J., 2008. Plesovice zircon - A new natural reference material for U-Pb and Hf isotopic microanalysis. Chemical Geology, vol. 249, p. 1-35.

Sloss, L.L., 1963. Sequences in the cratonic interior of North America. Geological Society of America Bulletin, vol. 74, p. 93-114.

Smith, I.R., 2000. Preliminary report on surficial geology investigations of La Biche River map area, southeast Yukon Territory. Geological Survey of Canada, Current Research 2000-B3, 9 p.

Smith, I.R., 2002. Surficial geology, Mount Merrill (95C/02), Yukon Territory – British Columbia. Geological Survey of Canada, Open File 4324, 1 map, scale 1:50 000.

Stacey, J.S. and Kramers, J.D., 1975. Approximation of terrestrial lead isotope evolution by a two-stage model. Earth and Planetary Science Letters, vol. 26, p. 207-221.

Stevens, R.D., Delabio, R.N. and Lachance, G.R., 1982. Age determinations and geological studies, K-Ar isotopic ages, Report 15, Geological Survey of Canada, Paper 81-2, p. 21-23.

Sun, S.S. and McDonough, W.F., 1989. Chemical and isotopic systematics of oceanic basalts; implications for mantle composition and processes. *In:* Magmatism in the ocean basins, A.D. Saunders and M.J. Norry (eds.), Geological Society of London, Special Publications, vol. 42, p. 313-345.

Taylor, G.C. and MacKenzie, W.S., 1970. Devonian stratigraphy of northeastern British Columbia. Geological Survey of Canada, Bulletin 186, 62 p.

Thorkelson, D.J., 2000. Geology and mineral occurrences of the Slats Creek, Fairchild Lake and "Dolores Creek" areas, Wernecke Mountains (106D/16, 106C/13, 106C/14), Yukon Territory. Exploration and Geological Services Division, Yukon Region, Indian and Northern Affairs Canada, Bulletin 10, 73 p.

Thorkelson, D.J., Abbott, J.G., Mortensen, J.K., Creaser, R.A., Villeneuve, M.E., McNicoll, V.J. and Layer, P.W., 2005. Early and Middle Proterozoic evolution of Yukon, Canada. Canadian Journal of Earth Sciences, vol. 42, p. 1045-1071.

Tipnis, R.S., Chatterton, B.D.E. and Ludvigsen, R., 1978. Ordovician conodont biostratigraphy of the southern District of Mackenzie, Canada. *In:* Western and Arctic Canadian biostratigraphy, C.R. Stelck and B.D.E. Chatterton (eds.), Geological Association of Canada, Special Paper 18, p. 39-91.

True North Gems Inc., 2006. True North Gems – Corundum Dome sampling returns high grade nickel to 15.85%, True North Gems Inc., Press Release, March 3, 2006. http://www.truenorthgems.com/newreleases/nr2006_Mar3.html.

Utting, J., 2000. Palynological study of 10 samples from the Lower Paleozoic and Proterozoic of Yukon; submitted by T. Allen, Mineral Resources Branch, Whitehorse, Yukon (NTS 95C/5, Pool Creek). Geological Survey of Canada, Report No. 8-JU-00, 4 p.

Utting, J., 2006. Palynological investigation of 2 outcrop samples of unknown age from Yukon, submitted by R.B. MacNaughton, Geological Survey of Canada (Calgary) and L. Pigage, Yukon Geological Survey (Map Sheet 095-D-08), Geological Survey of Canada, Report No. 04-JU-2006, 3 p.

Van Achterbergh, E., Ryan, C.G., Jackson, S.E. and Griffin, W.L., 2001. Data reduction software for LA-ICP-MS. *In:* Laser Ablation-ICP-Mass Spectrometry in the Earth Sciences: Principles and Applications, P.J. Sylvester (ed.), Mineralogical Association of Canada Short Course Series, v. 29, p. 239-243.

Villeneuve, M.E. and MacIntyre, D.G., 1997. Laser $^{40}Ar/^{39}Ar$ ages of the Babine porphyries and Newman Volcanics, Fulton Lake map area, west-central British Columbia. *In:* Radiogenic Age and Isotopic Studies, Report 10, Geological Survey of Canada, Current Research 1997-F, p. 131-139.

Villeneuve, M.E., Sandeman, H.A. and Davis, W.J., 2000. A method for the intercalibration of U-Th-Pb and $^{40}Ar/^{39}Ar$ ages in the Phanerozoic. Geochimica et Cosmochimica Acta, vol. 64, p. 4017-4030.

Vinci Technologies, 2001. Rock-Eval 6 user's guide, version 1.0, 40 p.

Walker, J.F., 1926. Geology and mineral deposits of Windermere map-area, British Columbia. Geological Survey of Canada, Memoir 148, 69 p.

Winchester, J.A. and Floyd, P.A., 1977. Geochemical discrimination of different magma series and their differentiation products using immobile elements. Chemical Geology, vol. 20, p. 325-343.

Wood, D.A., 1980. The application of a Th-Hf-Ta diagram to problems of tectonomagmatic classification and to establishing the nature of crustal contamination of basaltic lavas of the British Tertiary Volcanic Province. Earth and Planetary Science Letters, vol. 45, p. 326-336.

Yorath, C.J., 1991. Upper Jurassic to Paleogene assemblages, Chapter 9. *In:* Geology of the Cordilleran Orogen in Canada, H. Gabrielse and C.J. Yorath (eds.), Geological Survey of Canada, Geology of Canada, no. 4, p. 329-371.

Young, G.M., Jefferson, C.W., Delaney, G.D. and Yeo, G.M., 1979. Middle and Late Proterozoic evolution of the northern Canadian cordillera and shield. Geology, vol. 7, p. 125-128.

APPENDIX I. DETRITAL ZIRCON GEOCHRONOLOGY

INTRODUCTION

U-Pb geochronology of detrital zircon grains is an effective tool for determining stratigraphic correlation, possible provenance regions, maximum age of stratigraphic successions and regional paleogeographic reconstructions (Fedo *et al.*, 2003). Depositional age and stratigraphic correlation for some of the mapped units in 95C/5 and 95D/8 are problematic because of limited and poor exposure. Detrital zircon U-Pb isotopic analyses were completed for several formations as a potential means of more tightly constraining stratigraphic and paleogeographic reconstructions and ages. An integral part of this research was comparison of the zircon analytical results with reference studies of material from the Laurentian miogeocline ranging from Alaska to Mexico (Gehrels *et al.*, 1995; Gehrels and Ross, 1998).

Detrital zircon analyses were completed at the Arizona Laserchron Center (University of Arizona) under the supervision of George Gehrels and the Pacific Centre for Isotopic and Geochemical Research (University of British Columbia) under the supervision of James Mortensen.

ARIZONA LASERCHRON CENTER

Samples 02LP120, 02LP121, 04LP027, 04LP028

U-Pb geochronology of zircons was conducted by laser ablation multicollector inductively coupled plasma mass spectrometry (LA-MC-ICPMS). The analyses involve ablation of zircon with a New Wave DUV193 Excimer laser (operating at a wavelength of 193 nm) using a spot diameter of 25 to 50 microns. The ablated material is carried in helium into the plasma source of a Micromass Isoprobe, which is equipped with a flight tube of sufficient width that U, Th and Pb isotopes are measured simultaneously. All measurements are made in static mode, using Faraday detectors for ^{238}U, ^{232}Th, $^{208\text{-}206}Pb$ and an ion-counting channel for ^{204}Pb. Ion yields are 0.5-1.0 mv per ppm. Each analysis consists of one 20-second integration on peaks with the laser off (for backgrounds), 20 one-second integrations with the laser firing, and a 30-second delay to purge the previous sample and prepare for the next analysis. The ablation pit is ~15 microns in depth.

For each analysis, the errors in determining $^{206}Pb/^{238}U$ and $^{206}Pb/^{204}Pb$ result in a measurement error of ~1-2% (at 2-sigma level) in the $^{206}Pb/^{238}U$ age. The errors in measurement of $^{206}Pb/^{207}Pb$ and $^{206}Pb/^{204}Pb$ also result in ~1-2% (at 2-sigma level) uncertainty in age for grains that are >1.0 Ga. Uncertainty in the $^{206}Pb/^{207}Pb$ age is substantially larger for grains younger than 1.0 Ga due to low intensity of the ^{207}Pb signal. For most analyses, the cross-over in precision of $^{206}Pb/^{238}U$ and $^{206}Pb/^{207}Pb$ ages occurs at 0.8-1.0 Ga.

Common Pb correction is accomplished by using the measured ^{204}Pb and assuming an initial Pb composition from Stacey and Kramers (1975) (with uncertainties of 1.0 for $^{206}Pb/^{204}Pb$ and 0.3 for $^{207}Pb/^{204}Pb$). Measurement of ^{204}Pb is unaffected by the presence of ^{204}Hg because backgrounds are measured on peaks (thereby subtracting any background ^{204}Hg and ^{204}Pb), and because very little Hg is present in the argon gas.

Inter-element fractionation of Pb/U is generally ~20%, whereas fractionation of Pb isotopes is generally ~2%. In-run analysis of fragments of a large zircon crystal (generally every fifth measurement) with known age of 564 ± 4 Ma (2-sigma error) is used to correct for this fractionation. The uncertainty resulting from the calibration correction is generally 2-3% (2-sigma) for both $^{206}Pb/^{207}Pb$ and $^{206}Pb/^{238}U$ ages.

The analytical data are reported in Tables I-1 through I-5. Uncertainties shown in these tables are at the 1-sigma level, and include only measurement errors.

Interpreted ages are based on $^{206}Pb/^{238}U$ for <800 Ma grains and on $^{206}Pb/^{207}Pb$ for >800 Ma grains. This division at 800 Ma results from the increasing uncertainty of $^{206}Pb/^{238}U$ ages and the decreasing uncertainty of $^{206}Pb/^{207}Pb$ ages as a function of age. Analyses that are >10% discordant (by comparison of $^{206}Pb/^{238}U$ and $^{206}Pb/^{207}Pb$ ages) or >5% reverse discordant (in italics and with shading in Tables I-1 through I-5) are not considered further.

The resulting interpreted ages are shown on relative age-probability diagrams (from Ludwig, 2003). These diagrams show each age and its uncertainty (for measurement error only) as a normal distribution, and sum all ages from a sample into a single curve.

Table I-1. *Detrital zircon samples. PCIGR = Pacific Centre for Isotopic and Geochemical Research.*

Sample ID	Field Station	Unit	UTM E	UTM N	UTM Zone	Longitude	Latitude	Analytical Laboratory
04LP027-1	04LP027	Ps	344921	6695383	10N	-125.8119	60.3651	Arizona Laserchron
05LP024-1	05LP024	Ps	344571	6696860	10N	-125.8194	60.3782	PCIGR
05LP024-2	05LP024	Ps	344571	6696860	10N	-125.8194	60.3782	PCIGR
05LP025-1	05LP025	Pa	345730	6693686	10N	-125.7960	60.3502	PCIGR
05LP026-1	05LP026	Pa	346087	6693551	10N	-125.7894	60.3491	PCIGR
03LP010-1	03LP010	PT	649320	6694834	9N	-126.2928	60.3624	PCIGR
02LP120-1	02LP120	€Oc	343936	6700252	10N	-125.8335	60.4084	Arizona Laserchron
02LP121-1	02LP121	€Oc	343939	6700170	10N	-125.8334	60.4077	Arizona Laserchron
04LP028-1	04LP028	€Oc	343744	6701195	10N	-125.8378	60.4168	Arizona Laserchron
05LP003-1	05LP003	€Oc	653393	6702371	9N	-126.2133	60.4284	PCIGR
05LP011-1	05LP011	€Oc	649839	6699029	9N	-126.2802	60.3998	PCIGR
05LP034-1	05LP034	€Oc	643278	6688822	9N	-126.4065	60.3106	PCIGR
05LP069-1	05LP069	€Oc	645278	6705740	9N	-126.3580	60.4616	PCIGR

PACIFIC CENTRE FOR ISOTOPIC AND GEOCHEMICAL RESEARCH

Samples 03LP010, 05LP003, 05LP011, 05LP024-1, 05LP024-2, 05LP025, 05LP026

Detrital zircons were dated at the Pacific Centre for Isotopic and Geochemical Research (PCIGR) at the University of British Columbia using a New Wave 213 nm Nd-YAG laser fitted with a New Wave "Supercell" ablation chamber coupled with a Thermo Finnigan ELEMENT 2 single collector, double-focussing, magnetic sector, high resolution, inductively coupled mass spectrometer.

Zircons were separated from samples using conventional Wilfley table, heavy liquid and magnetic methods. A portion of each zircon concentrate was mounted in an epoxy puck with several grains of two zircon standards, Plesovice (Slama *et al.*, 2008) and KL (an internal UBC standard). The puck was polished to expose grain interiors, washed for 10 minutes with dilute nitric acid, and rinsed with ultraclean water before analysis.

Line scans rather than spot analyses were used to minimize elemental fractionation. Typically, analyses were completed using 35% laser power and 25 micron laser diameter. Background measurements were taken with the laser off for 25 seconds, followed by data collection with the laser on for approximately 47 seconds. Data reduction of the time-integrated signals was completed using GLITTER software (Van Achterbergh *et al.*, 2001). Corrections for mass and elemental fractionation were made by bracketing analyses of unknown grains with replicate analyses of standard zircon.

Isotopic ratios and interpreted ages are presented in Tables I-1 through I-5. All errors are reported at the 1-sigma level. The preferred age for zircons with dates less than 1000 Ma are based on the $^{206}Pb/^{238}U$ age; for zircons greater than 1000 Ma old, the preferred age is based on the $^{207}Pb/^{206}Pb$ age. Zircons with greater than 10% discordance, less than -5% reverse discordance, and with a 1-sigma error of greater than 10% are not considered further in our discussion and calculation of results.

Concordia and relative probability plots were prepared using Isoplot 3.0 (Ludwig, 2003).

Analytical results

Unit Ps

Unit Ps is a succession of hornfelsed siliciclastic siltstones and sandstones with minor conglomerate and calc-silicate rock exposed on one ridge in the Pool Creek map sheet. The only age constraint is that it is intruded by the Pool Creek syenite and associated dykes and must therefore be older than 650 Ma.

Detrital zircons were extracted from three samples (04LP027, 05LP024-1, 05LP024-2) for analysis (see Figure I-1). Figures I-2 through I-4 illustrate a concordia plot and a relative probability distribution plot for each of the samples. Figure I-5 is a composite probability distribution plot for the combined three samples. Actual analytical results are listed in Table I-1.

All three samples have a bimodal probability distribution with the major peak being in the Paleoproterozoic and a secondary, less well-defined peak being in the Archean. The Paleoproterozoic peak for each of the samples is slightly different, with the dominant Paleoproterozoic peaks being at 1793 Ma, 1823 Ma,

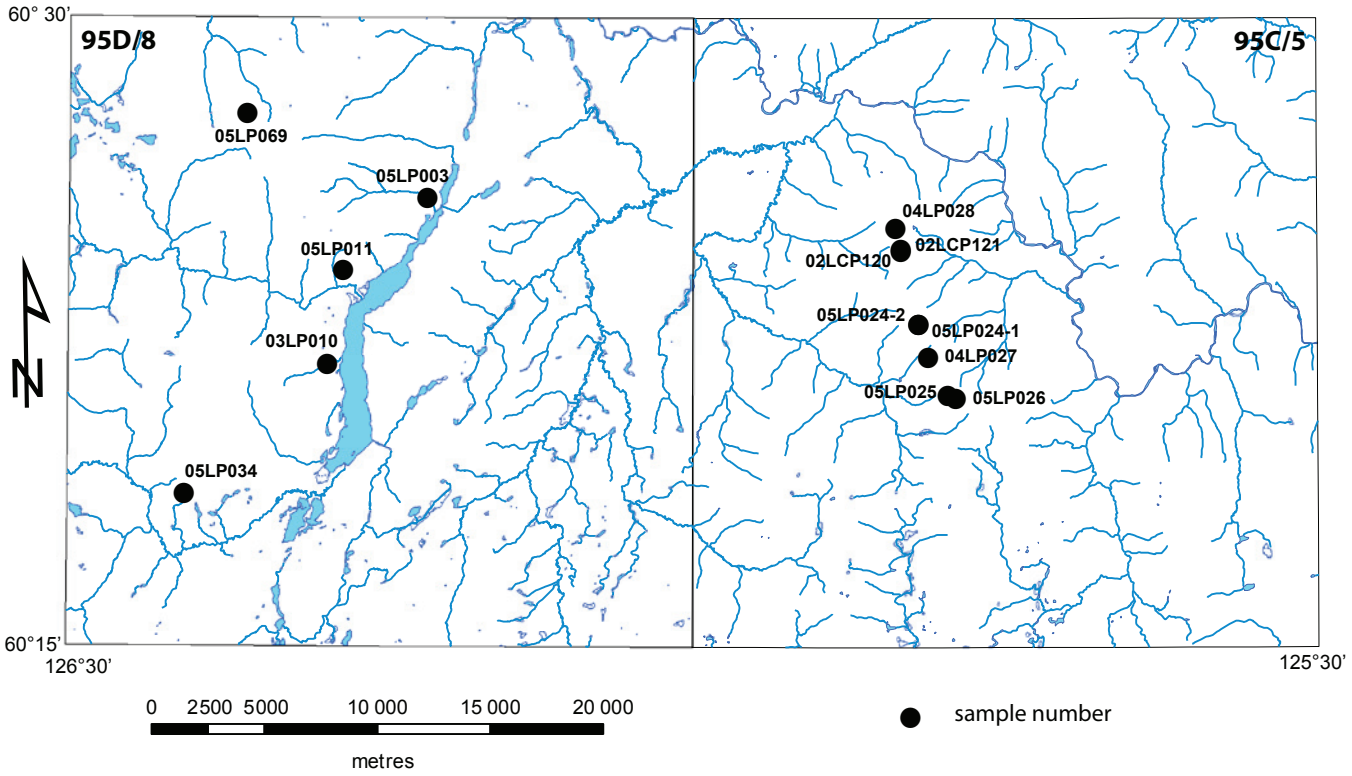


Figure I-1. *Location map for detrital zircon samples, NTS 95C/5 and NTS 95D/8.*

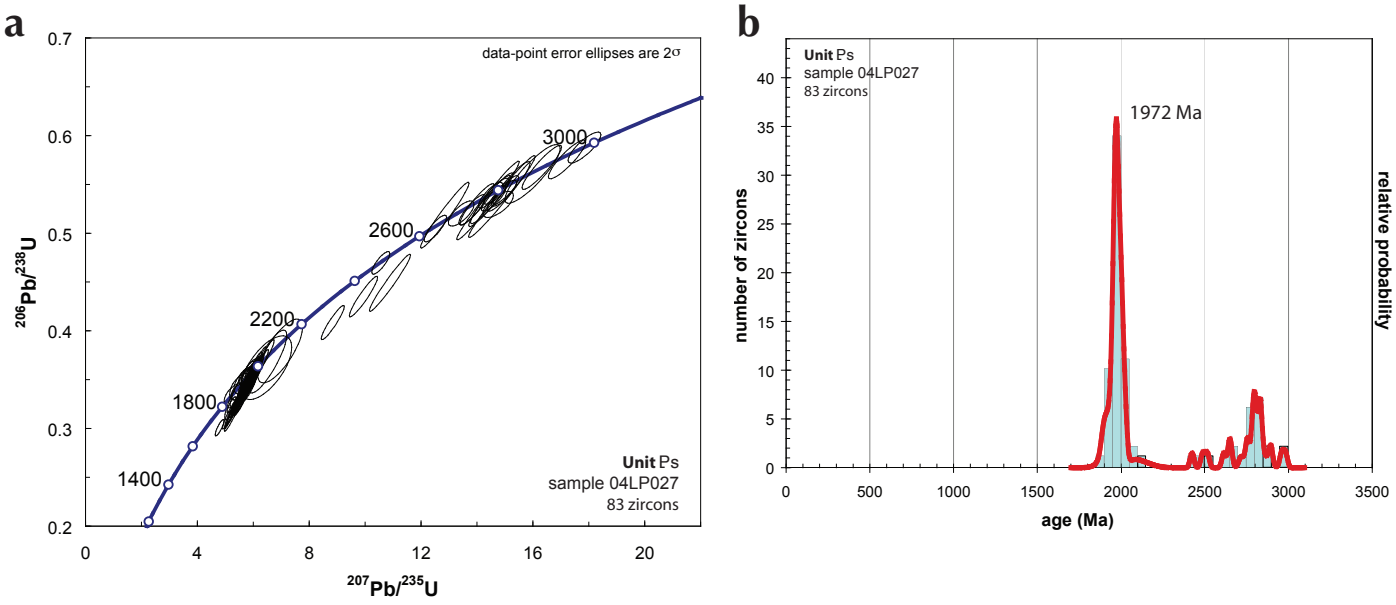


Figure I-2. *Detrital zircon Pb/U isotopic age dates, sample 04LP027 in Unit* **Ps**. ***(a)*** *Concordia diagram of individual concordant detrital zircons from sample 04LP027;* ***(b)*** *Probability distribution function and histogram of all concordant detrital zircon ages from sample 04LP027.*

and 1971 Ma depending on the sample. This pattern is essentially the same as the Precambrian through Triassic reference samples from the Northern Cordillera (Gehrels *et al.*, 1995). From Figure I-6, it can be seen that basement terranes in Northwest Territories and northern Alberta are suitable proximal source areas for the detrital zircon signature present within this unit. Recently, Thorkelson *et al.* (2005) published 10 detrital zircon analyses from the basal Pinguicula Group; these analyses also contain the same age ranges as illustrated in Figures I-2 through I-5.

The detrital zircon patterns do not provide any further constraints on the depositional age of Unit Ps. The maximum age of deposition is approximately 1700 Ma based on individual detrital zircon results.

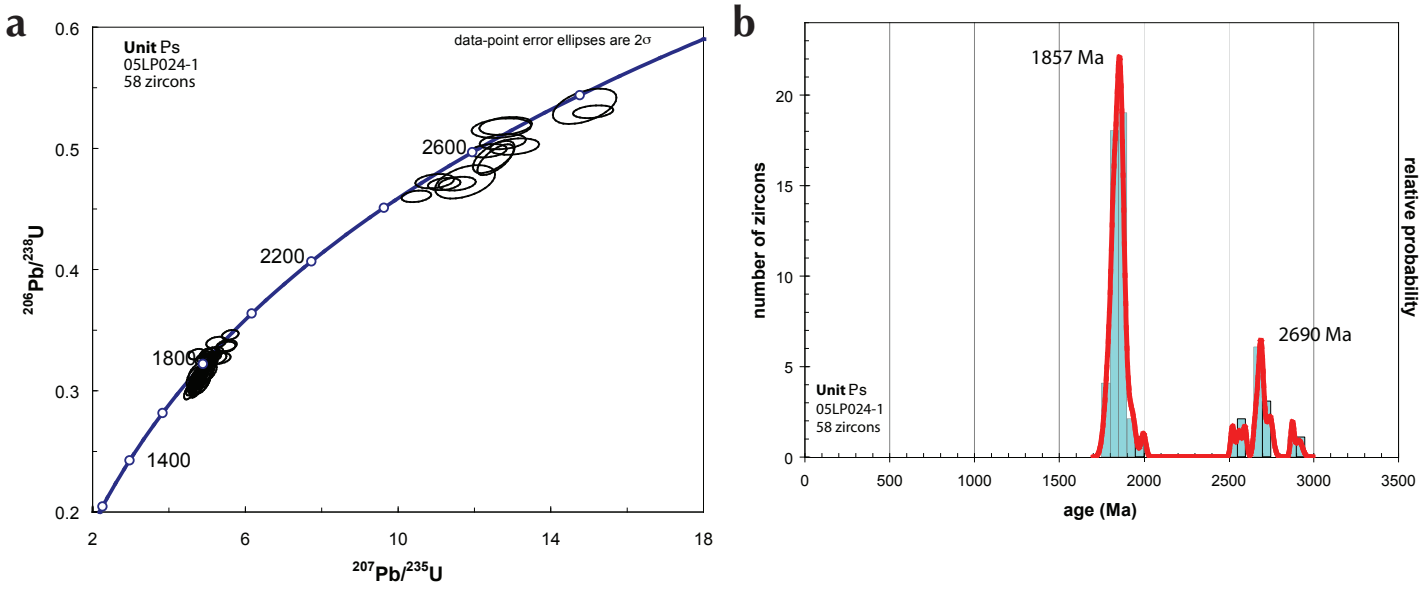


Figure I-3. *Detrital zircon Pb/U isotopic age dates, sample 05LP024-1 in Unit* ***Ps****.* ***(a)*** *Concordia diagram of individual concordant detrital zircons from sample 05LP024-1;* ***(b)*** *Probability distribution function and histogram of all concordant detrital zircon ages from sample 05LP024-1.*

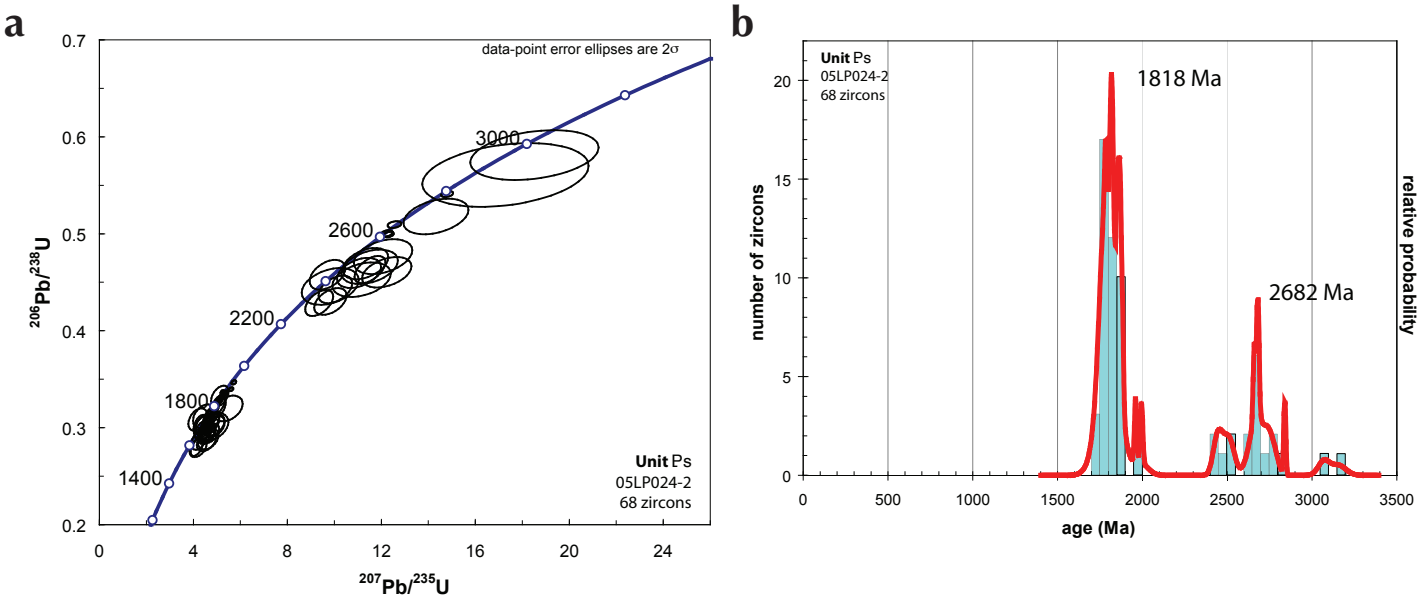


Figure I-4. *Detrital zircon Pb/U isotopic age dates, sample 05LP024-2 in Unit* ***Ps****.* ***(a)*** *Concordia diagram of individual concordant detrital zircons from sample 05LP024-2;* ***(b)*** *Probability distribution function and histogram of all concordant detrital zircon ages from sample 05LP024-2.*

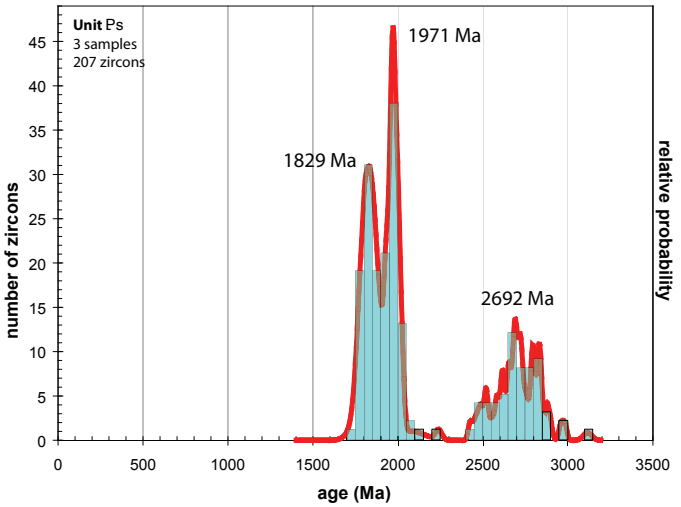


Figure I-5. *Probability distribution function and histogram of all concordant detrital zircon ages from composite of three samples in Unit* **Ps**.

Geologic arguments presented in the Stratigraphy section suggested a possible correlation with lowermost Pinguicula Group, with a resulting depositional age of about 1380 Ma, although a depositional age as young as the suggested age for Unit **Pa** cannot be ruled out.

Unit Pa

Unit **Pa** consists of laminated volcaniclastic argillites and siltstones with intimately interbedded sandstones unconformably underlying the Crow Formation. Minor volcanic conglomerates and breccias also occur locally. This unit outcrops in one area of the Pool Creek map sheet, south of the Pool Creek syenite. It is slightly metamorphosed; this metamorphism is thought to be related to intrusion of the 650 Ma Pool Creek syenite. At the same time, Unit **Pa** is considered younger than Unit **Ps** because Pool Creek syenite and associated dykes are not present in exposed portions of Unit **Pa**.

Detrital zircons from two samples (05LP025, 05LP026) were analyzed at the Pacific Centre for Isotopic and

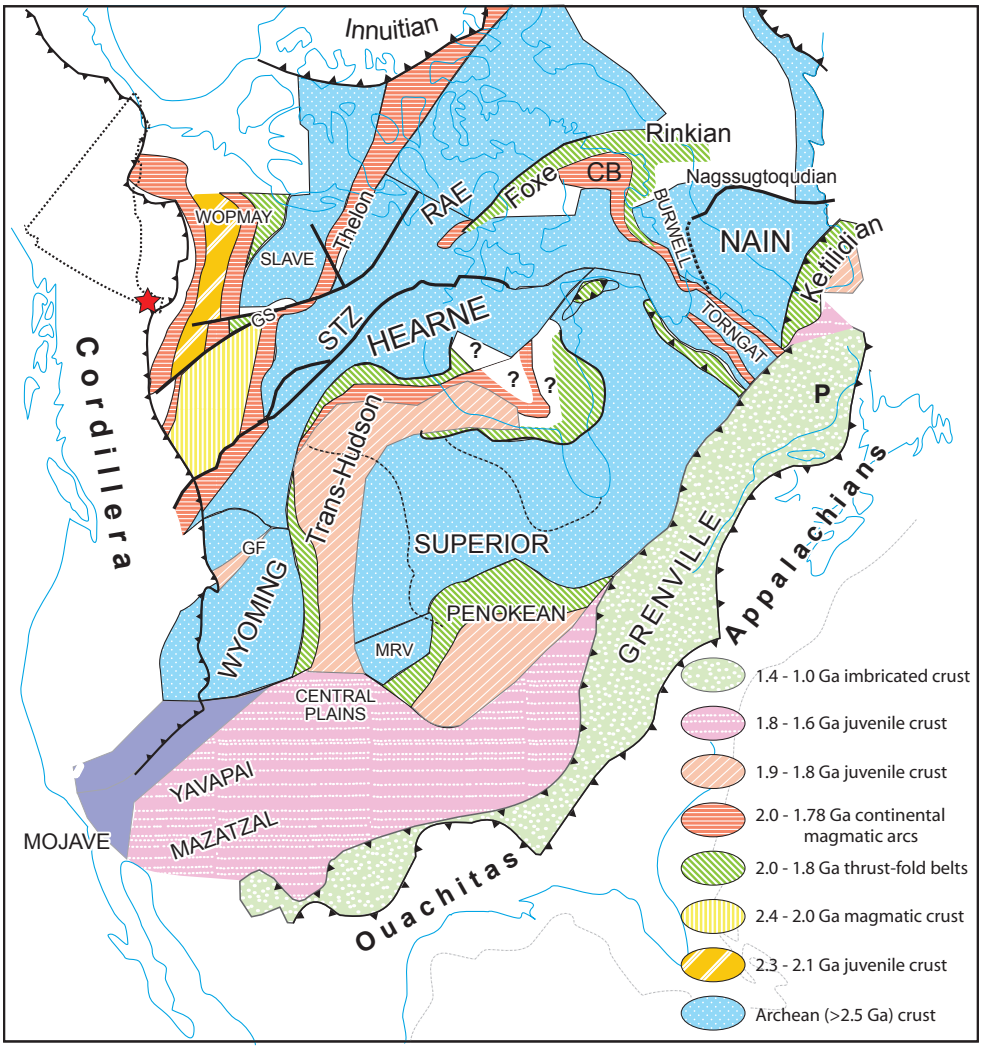


Figure I-6. *Tectonic framework for the Precambrian of North America. Modified from Ross and Villeneuve (2003). MRV-Minnesota River valley; P-Pinware terrane; STZ-Snowbird tectonic zone; GF-Great Falls tectonic zone; GS-Great Slave Lake shear zone; CB-Cumberland batholith. Location of map areas in Yukon shown by star in northwest corner of Figure.*

Geochemical Research. Table I-3 contains the resulting zircon ages. Figures I-7 and I-8 illustrate concordia and probability distribution plots for the two samples. Figure I-9 is a composite diagram of the probability distribution for all reasonably concordant zircon analyses from the two samples.

Both samples show a large number of zircon ages ranging between 1000 Ma and 1500 Ma as well as having muted peaks at 1800 Ma and older than 2500 Ma. Seven ages from the two samples are less than 1000 Ma (654 ± 25Ma, 722 ± 41 Ma, 831 ± 12 Ma, 908 ± 20 Ma, 946 ± 12 Ma, 983 ± 26 Ma, 994 ± 69 Ma). Although these seven younger ages do not form a single cluster, the presence of several grains in this age range suggests the minimum depositional age for Unit {a is younger than 1000 Ma and may be as young as 654 Ma (excluding the error range).

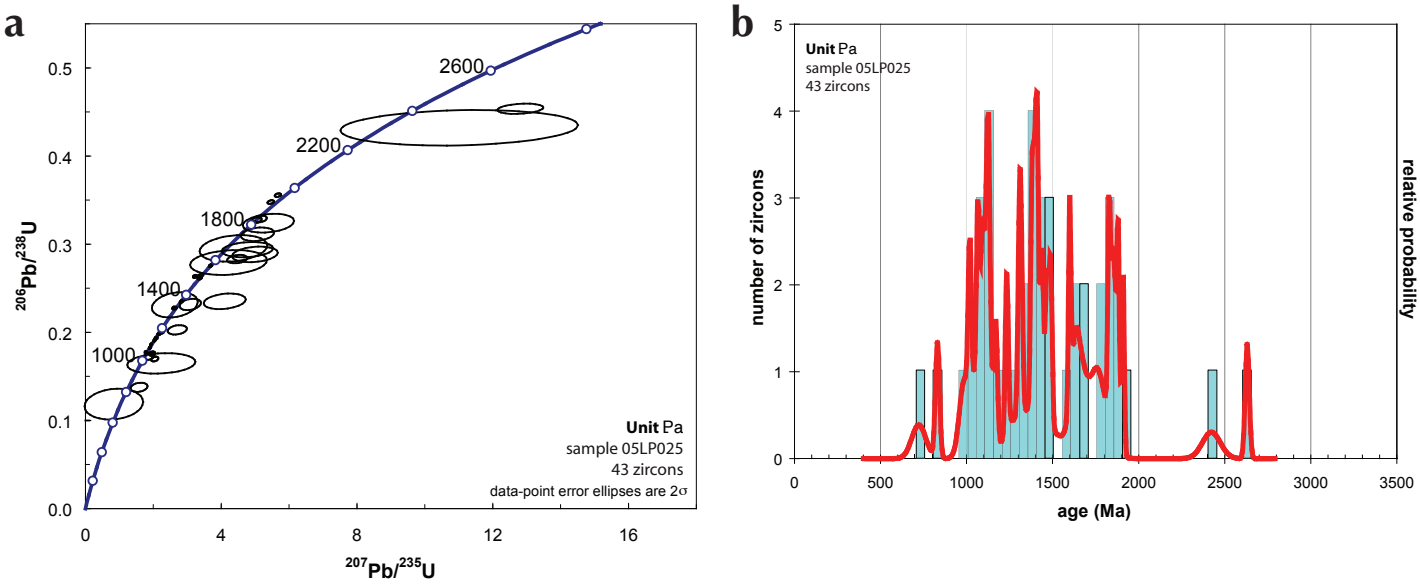


Figure I-7. *Detrital zircon Pb/U isotopic age dates, sample 05LP025 in Unit* Pa. ***(a)*** *Concordia diagram of individual concordant detrital zircons from sample 05LP025.* ***(b)*** *Probability distribution function and histogram of all concordant detrital zircon ages from sample 05LP025.*

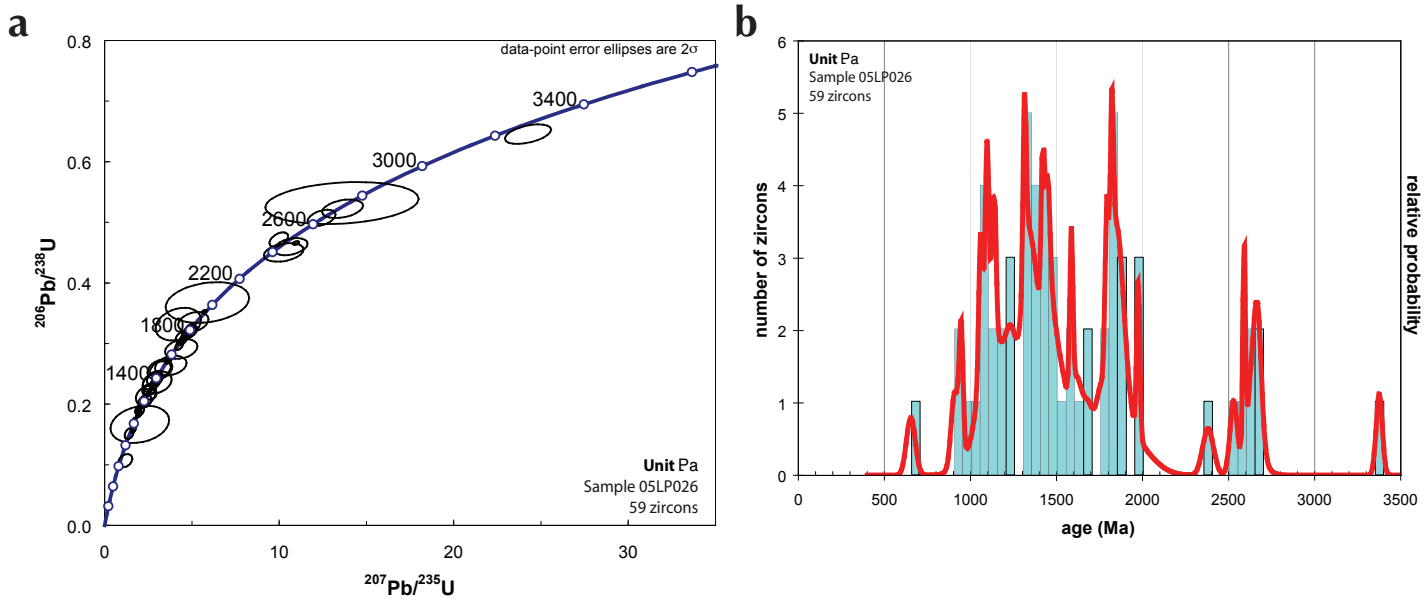


Figure I-8. *Detrital zircon Pb/U isotopic age dates, sample 05LP026 in Unit* Pa. ***(a)*** *Concordia diagram of individual concordant detrital zircons from sample 05LP026.* ***(b)*** *Probability distribution function and histogram of all concordant detrital zircon ages from sample 05LP026.*

This minimum age is consistent with Unit Pa displaying a contact metamorphic effect from the Pool Creek syenite.

The distribution of detrital zircon ages >1000 Ma for Unit Pa can be readily explained by the presence of two source provenances contributing zircons to the samples. The zircon ages >2500 Ma and zircon ages in the age range 1600-2400 Ma correspond to zircon ages present in North American basement in Alberta and Northwest Territories just to the east and northeast of the map area (Figure I-6). The zircon ages ranging from 1000-1500 Ma have previously been noted by Rainbird *et al.* (1992; 1997) as being typical for Mackenzie Mountains Supergroup strata. They attributed these zircon ages to transport of zircons sourced in exposed rocks of the Grenville orogen by large northwest-directed drainages during Mackenzie Mountains Supergroup deposition. Zircons in Unit Pa either denote this drainage pattern still existed during Pa deposition or zircons have been recycled from eroded Mackenzie Mountains Supergroup strata. In previous detrital zircon studies of Neoproterozoic and lower Paleozoic miogeoclinal strata in the northern Cordillera, this Grenville signature was present only in a Cambrian sample from east-central Alaska (Gehrels *et al.*, 1995; Gehrels *et al.*, 1999; Gehrels and Ross, 1998). More recent detrital zircon studies in Alaska and Northwest Territories have found additional Neoproterozoic and Lower Cambrian strata with this Grenville zircon signature (Bradley *et al.*, 2007; Leslie, 2009).

The depositional age of Unit Pa inferred above is consistent with the depositional ages of the lower Winderemere Supergroup (sequence C). Windermere age volcanic units in the northern Cordillera include the Little Dal basalt, the Mount Harper volcanics and the Gataga volcanics. The age of the Little Dal basalt is inferred as 779 Ma by correlation with the geochemically similar Tsezotene sills in the Mackenzie Mountains Supergroup (LeCheminant and Heaman, 1994; Dudas and Lustwerk, 1997). The age of zircons from a thin rhyolite flow in the upper part of the Mount Harper volcanics is 751 +18/-26 Ma (Roots and Parrish, 1988). In northeastern British Columbia, Ferri *et al.* (1999) have dated the Windermere Gataga volcanics as 689 ± 4.6 Ma. These various primary zircon ages are potentially represented among the younger detrital zircon ages from the Unit Pa samples. The present level of information for Unit Pa only constrains the depositional age and correlation to being within the lower Windermere Supergroup.

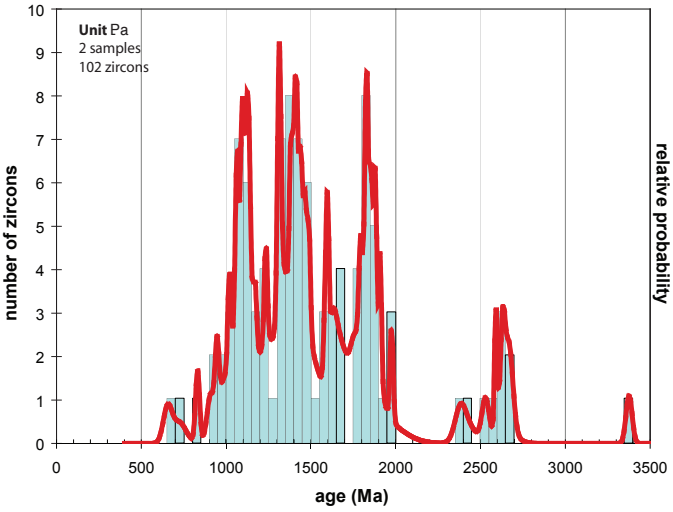


Figure I-9. *Probability distribution function and histogram of all concordant detrital zircon ages from composite of two samples in Unit Pa.*

Toobally Formation

The Toobally Formation outcrops along the west margin of Toobally Lake central to map sheet 95D/8. It consists of a diamictite with numerous rounded to subangular clasts in a mudstone to siltstone matrix. Detrital zircons were separated and analyzed from one sample (03LP010).

Table I-4 contains detrital zircon geochronology analyses from this sample. Figure I-10 illustrates the Concordia diagram and the probability distribution function for the sample. The youngest concordant detrital zircon age is approximately 650 Ma.

Pigage and MacNaughton (2004) first described the Toobally Formation and tentatively considered it to be Neoproterozoic based on correlation with other glacial diamictites in the Yukon and British Columbia. Subsequently, Pigage (2006) suggested an alternative interpretation, that the formation was a Cambrian-Ordovician channel unit deposited at the same time as the Crow Formation. The detrital zircon results presented here provide strong evidence in support of the original interpretation by Pigage and MacNaughton (2004). As with the samples from Unit Pa, detrital zircons from the Toobally Formation contain a northern Canada sequence B Mesoproterozoic signature. The formation is either correlative with Mackenzie Mountains Supergroup or has a source provenance containing extensive Mackenzie Mountains Supergroup exposures. The presence of 650 Ma detrital zircons in the sample would suggest the latter, indicating a maximum depositional age of 650 Ma.

The Toobally Formation is assigned to succession 1 (as discussed in this report). The presence of Ordovician Crow Formation along strike to the north of the Toobally Formation means that the contact between the Toobally

Formation and the Crow Formation immediately to the north is a normal fault.

Crow Formation

The Crow Formation forms extensive outcrops in the western half of map sheet 95D/8 and the west-central portion of map sheet 95C/5. It consists of interbedded greyish red to white, locally subarkosic sandstone, conglomerate and maroon siltstone with minor limestone, dolostone, basalt pillow lavas and lapilli tuffs. All fossil occurrences are Ordovician, ranging from Tremadocian to Darriwilian. The formation unconformably overlies the Pool Creek syenite, Unit Pa and the Toobally Formation in the map sheets. The uppermost portion of the Crow Formation is laterally equivalent to the Rabbitkettle Formation. Thickness ranges from 300 m to greater than 5700 m.

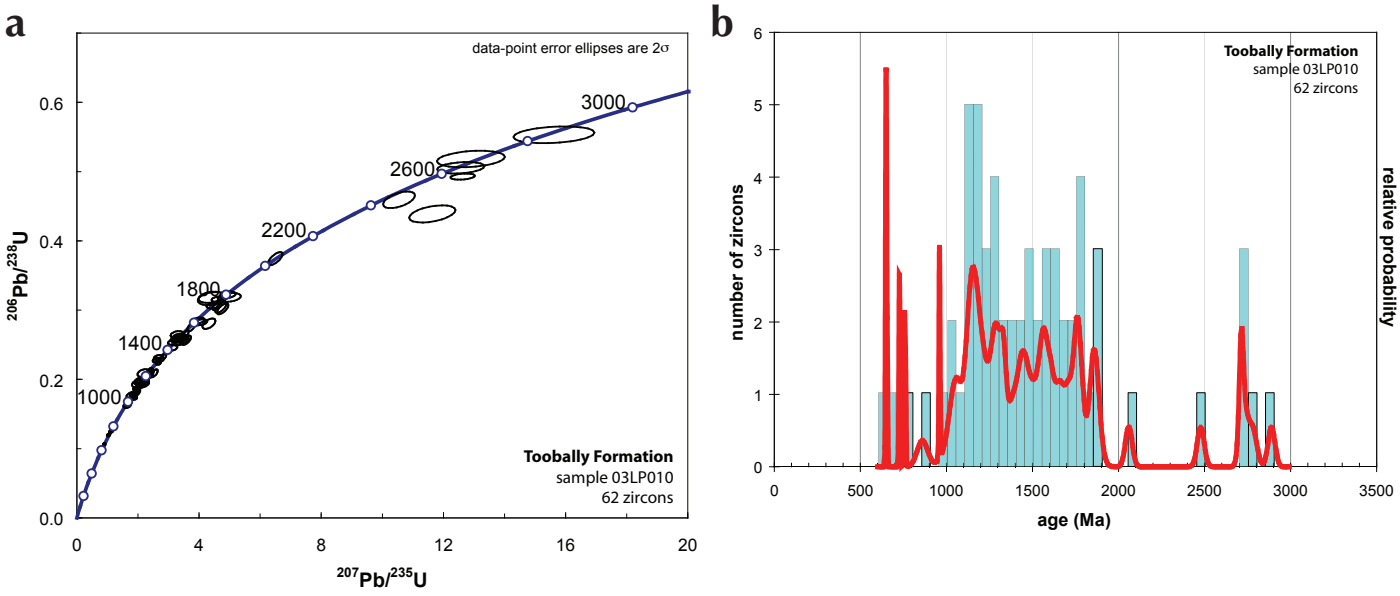


Figure I-10. *Detrital zircon Pb/U isotopic age dates, sample 03LP010 in Toobally Formation.* ***(a)*** *Concordia diagram of individual concordant detrital zircons from sample 03LP010.* ***(b)*** *Probability distribution function and histogram of all concordant detrital zircon ages from sample 03LP010.*

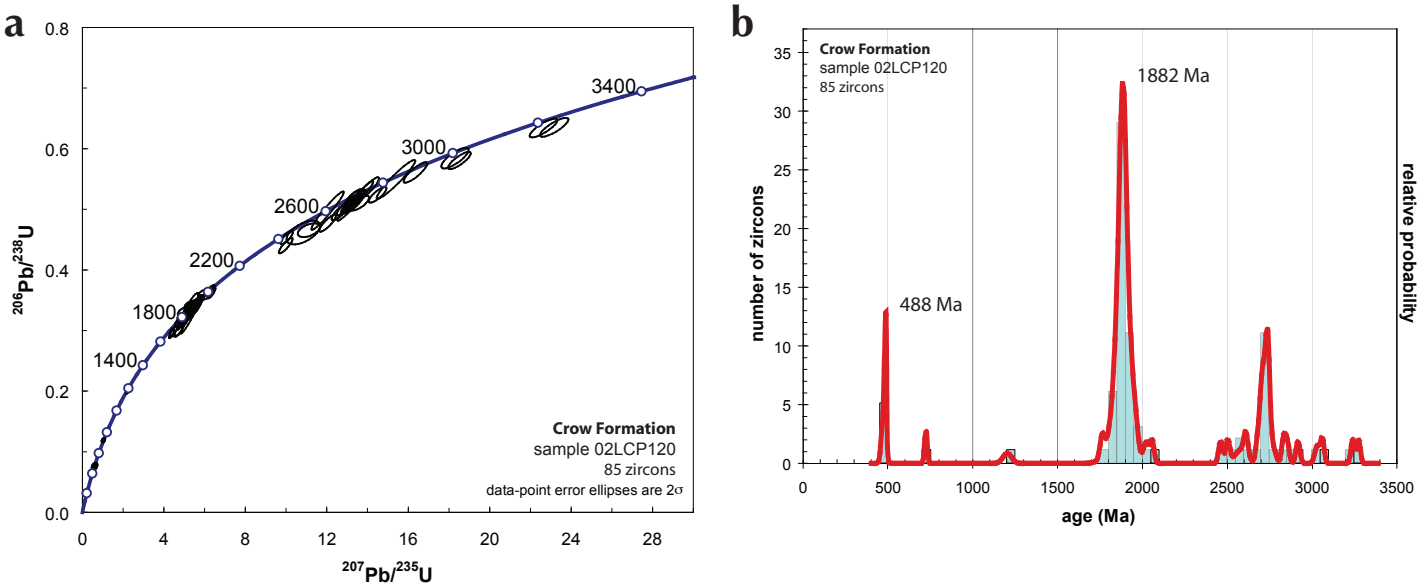


Figure I-11. *Detrital zircon Pb/U isotopic age dates, sample 02LP120 in Crow Formation.* ***(a)*** *Concordia diagram of individual concordant detrital zircons from sample 02LP120.* ***(b)*** *Probability distribution function and histogram of all concordant detrital zircon ages from sample 02LP120.*

Seven samples from the Crow Formation sandstones and conglomerates at different stratigraphic levels from map sheet 95D/8 (four samples) and map sheet 95C/5 (three samples) were collected for detrital zircon geochronology studies. Table I-5 contains the analytical results for the seven samples. Histograms and probability distributions for individual samples are displayed in Figures I-11 through I-17.

All samples show a largely bimodal distribution of ages with one peak being in the Paleoproterozoic (1700-2000 Ma) and a second, wider peak being in the Archean (>2500 Ma). This distribution pattern is similar to the reference distribution plots of Neoproterozoic and lower Paleozoic miogeocline sediments from the northern Cordillera (Gehrels *et al.*, 1995; Gehrels and Ross, 1998). Some of the samples have a few early Paleozoic to late Neoproterozoic detrital zircon ages ranging from 470 Ma to 725 Ma. One sample from the uppermost Crow Formation (05LP034) also contains a scattering of Mesoproterozoic ages ranging from 1022 Ma to 1500 Ma.

The distribution of ages points to provenance within the Archean and Paleoproterozoic terrains in Northwest

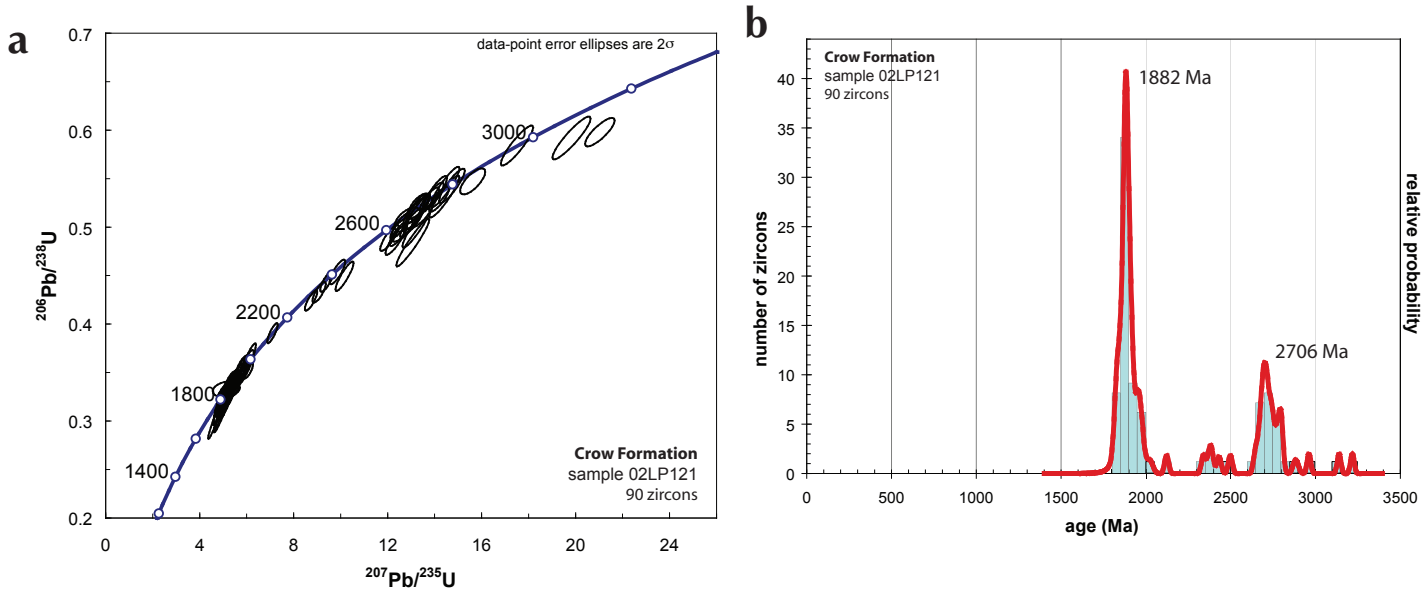


Figure I-12. *Detrital zircon Pb/U isotopic age dates, sample 02LP121 in Crow Formation.* ***(a)*** *Concordia diagram of individual concordant detrital zircons from sample 02LP121.* ***(b)*** *Probability distribution function and histogram of all concordant detrital zircon ages from sample 02LP121.*

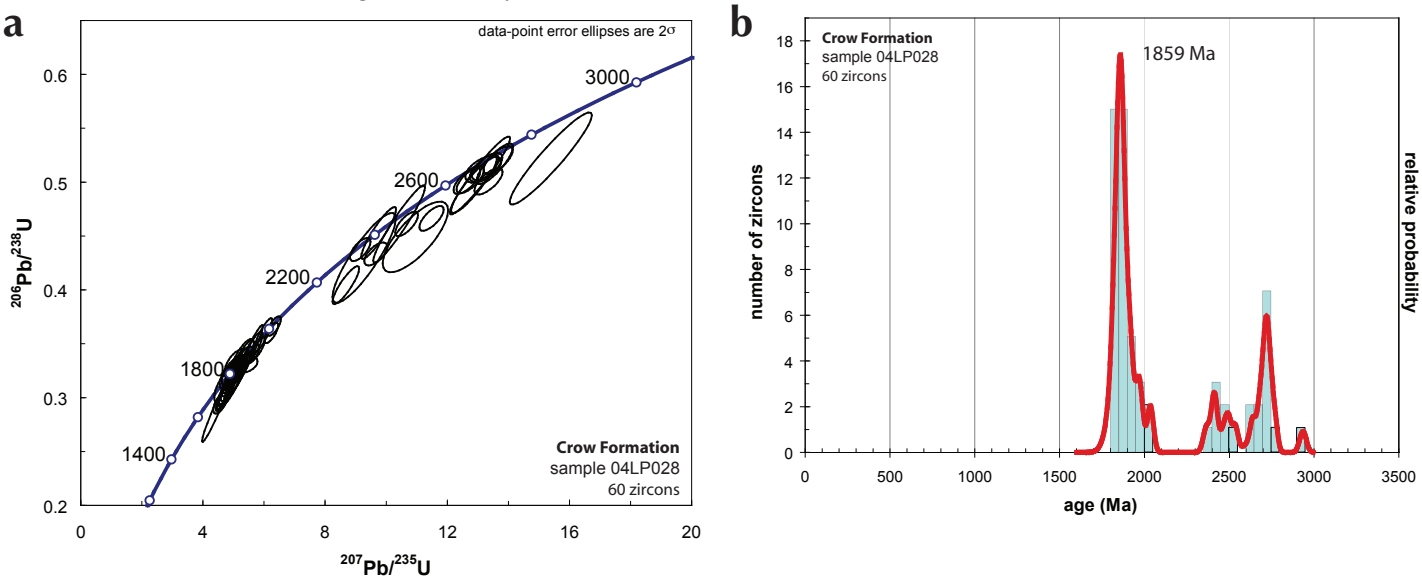


Figure I-13. *Detrital zircon Pb/U isotopic age dates, sample 04LP028 in Crow Formation.* ***(a)*** *Concordia diagram of individual concordant detrital zircons from sample 04LP028.* ***(b)*** *Probability distribution function and histogram of all concordant detrital zircon ages from sample 04LP028.*

Territories and Alberta (Fig. I-6), consistent with southwest- to west-directed paleocurrents from cross-bedding measurements in the Crow Formation (Fig. 52). The Mesoproterozoic ages from sample 05LP034 indicate exposure of Mackenzie Mountain Supergroup sediments in the source provenance for this particular sample. It is uncertain where the early Paleozoic and late Neoproterozoic detrital zircons are sourced. Appropriate-aged intrusive activity during this time period is not common in the northern Cordillera. Interestingly, the 650 Ma zircons of the Pool Creek syenite are not present in the Crow Formation, which unconformably overlies it. The large time interval represented by the unconformity beneath the Crow Formation has apparently resulted in the zircons from the syenite being transported elsewhere.

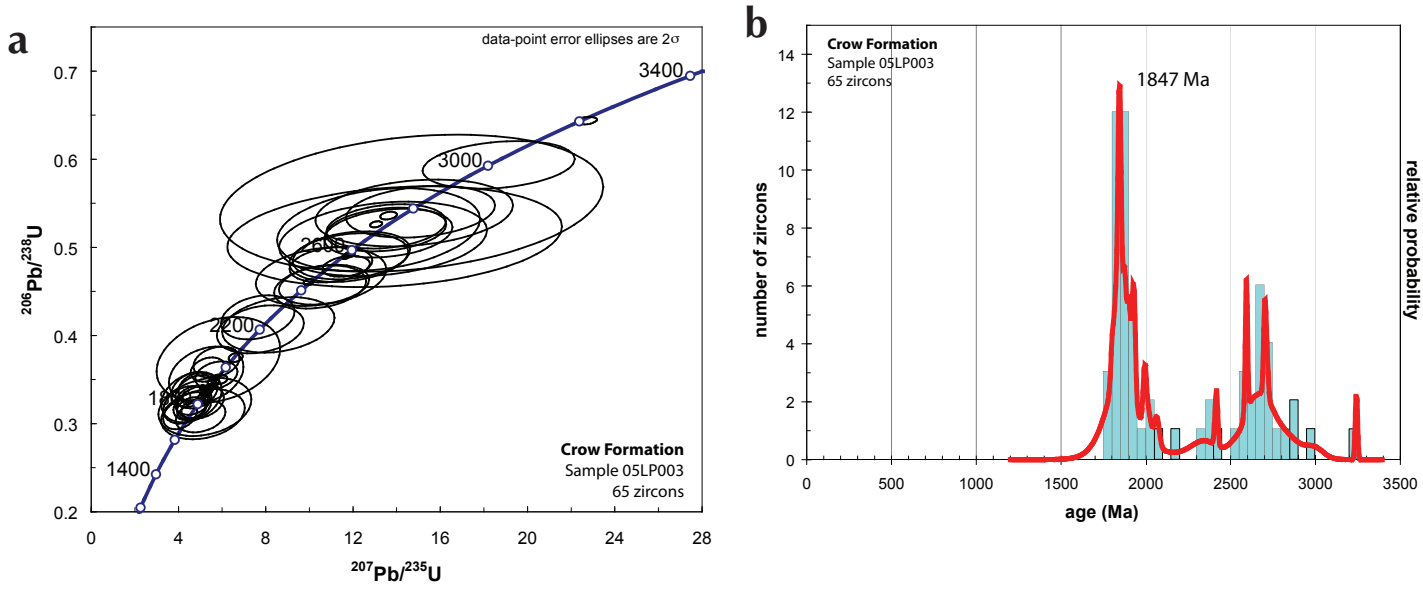


Figure I-14. *Detrital zircon Pb/U isotopic age dates, sample 05LP003 in Crow Formation.* ***(a)*** *Concordia diagram of individual concordant detrital zircons from sample 05LP003.* ***(b)*** *Probability distribution function and histogram of all concordant detrital zircon ages from sample 05LP003.*

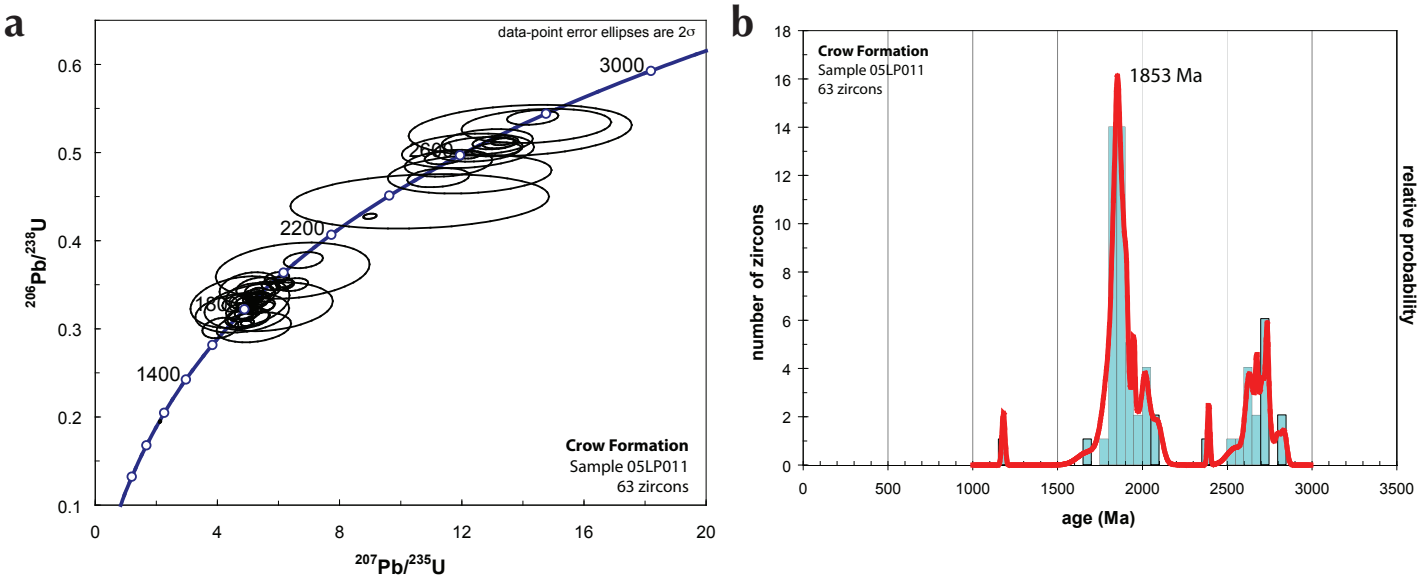


Figure I-15. *Detrital zircon Pb/U isotopic age dates, sample 05LP011 in Crow Formation.* ***(a)*** *Concordia diagram of individual concordant detrital zircons from sample 05LP011.* ***(b)*** *Probability distribution function and histogram of all concordant detrital zircon ages from sample 05LP011.*

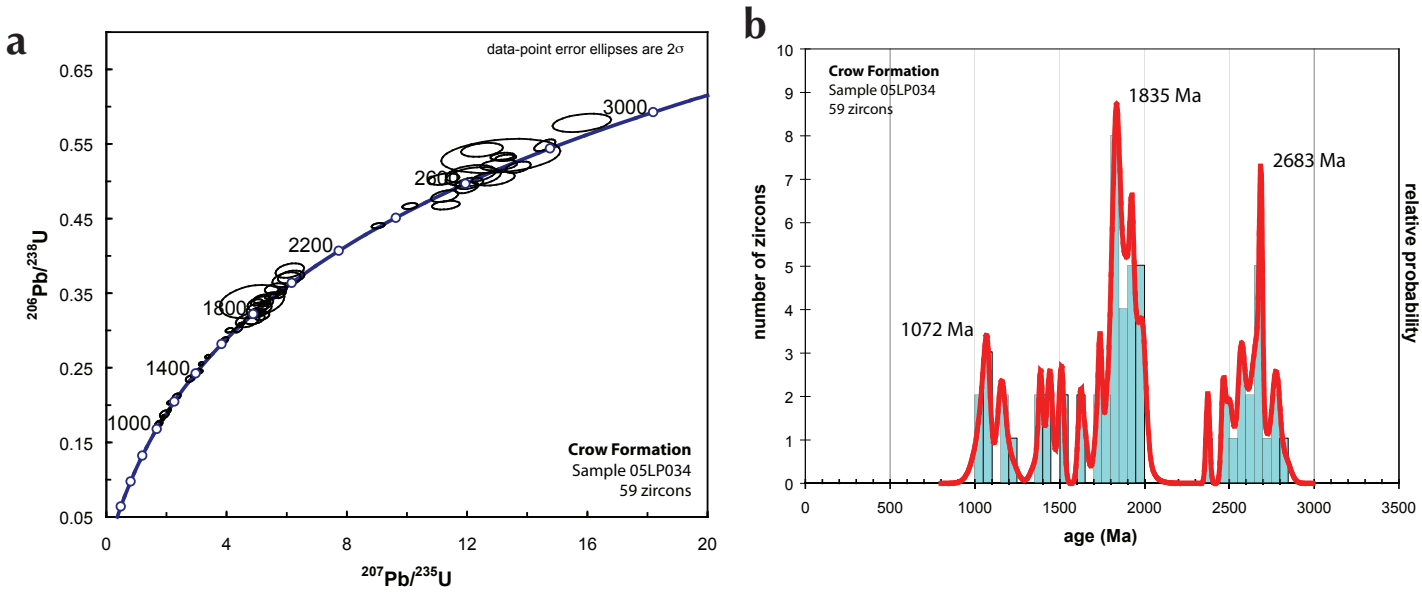


Figure I-16. *Detrital zircon Pb/U isotopic age dates, sample 05LP034 in Crow Formation.* ***(a)*** *Concordia diagram of individual concordant detrital zircons from sample 05LP034.* ***(b)*** *Probability distribution function and histogram of all concordant detrital zircon ages from sample 05LP034.*

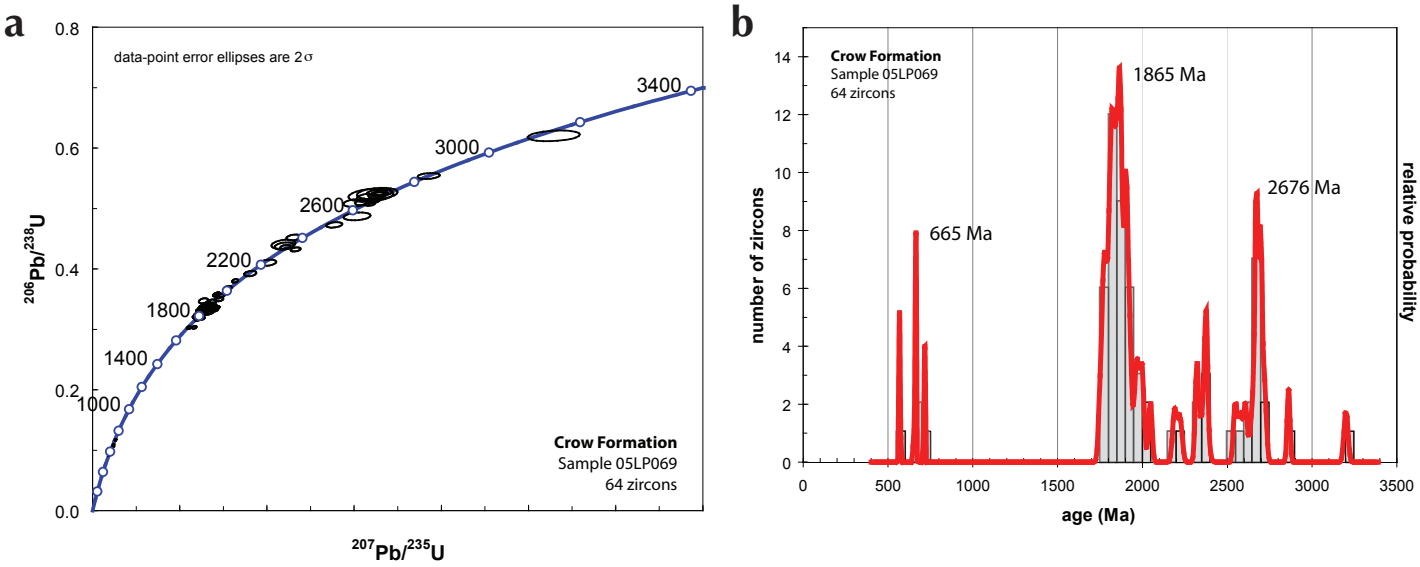


Figure I-17. *Detrital zircon Pb/U isotopic age dates, sample 05LP069 in Crow Formation.* ***(a)*** *Concordia diagram of individual concordant detrital zircons from sample 05LP069.* ***(b)*** *Probability distribution function and histogram of all concordant detrital zircon ages from sample 05LP069.*

Table I-2a. *Detrital Zircon U-Pb geochronologic analyses – Arizona Laserchron Center – Sample 04LP027 in Unit* ***Ps****.*

Isotopic ratios									Apparent ages (Ma)									
Sample	U (ppm)	$^{206}Pb/^{204}Pb$	U/Th	$^{207}Pb/^{235}U$	± (%) (1 sigma)	$^{206}Pb/^{238}U$	± (%) (1 sigma)	error corr.	$^{206}Pb/^{238}U$	± (Ma) (1 sigma)	$^{207}Pb/^{235}U$	± (Ma) (1 sigma)	$^{206}Pb/^{207}Pb$	± (Ma) (1 sigma)	BEST AGE	± (Ma) (1 sigma)	Error %	Discordance %
04LP027-95	*294*	*17527*	*1.1*	*3.78725*	*6.2*	*0.24520*	*6.0*	*0.98*	*1413.7*	*76.3*	*1590*	*49*	*1832*	*23*	*1832*	*23*	*1.3*	*22.8*
04LP027-99	*442*	*11142*	*1.3*	*4.41987*	*2.2*	*0.28078*	*2.0*	*0.90*	*1595.3*	*27.7*	*1716*	*18*	*1867*	*18*	*1867*	*18*	*1.0*	*14.6*
04LP027-28	*309*	*16422*	*1.0*	*4.14388*	*3.6*	*0.26032*	*3.5*	*0.98*	*1491.5*	*47.1*	*1663*	*30*	*1887*	*13*	*1887*	*13*	*0.7*	*21.0*
04LP027-79	382	30274	1.3	4.79694	1.3	0.30086	1.1	0.85	1695.6	17.0	1784	11	1890	13	1890	13	0.7	10.3
04LP027-48	*452*	*9172*	*1.2*	*4.47791*	*2.1*	*0.28009*	*1.9*	*0.93*	*1591.8*	*27.2*	*1727*	*17*	*1895*	*13*	*1895*	*13*	*0.7*	*16.0*
04LP027-89	62	5324	1.7	5.52003	2.7	0.34286	1.6	0.59	1900.4	26.7	1904	24	1907	40	1907	40	2.1	0.3
04LP027-78	127	43856	2.3	5.22406	1.3	0.32416	1.0	0.82	1810.0	16.3	1857	11	1909	13	1909	13	0.7	5.2
04LP027-18	46	14713	1.1	5.38410	3.2	0.33380	1.6	0.48	1856.7	25.0	1882	28	1911	51	1911	51	2.7	2.8
04LP027-68	81	9491	1.6	5.60036	3.1	0.34502	2.8	0.90	1910.8	46.4	1916	27	1922	25	1922	25	1.3	0.6
04LP027-77	77	29254	1.5	5.48753	2.1	0.33760	1.0	0.48	1875.1	16.3	1899	18	1924	33	1924	33	1.7	2.5
04LP027-19	69	19120	3.5	5.44695	3.5	0.33507	3.2	0.90	1862.9	51.0	1892	30	1925	27	1925	27	1.4	3.2
04LP027-100	*150*	*5642*	*1.4*	*4.04795*	*3.3*	*0.24853*	*3.0*	*0.92*	*1430.9*	*39.0*	*1644*	*27*	*1928*	*23*	*1928*	*23*	*1.2*	*25.8*
04LP027-69	127	7187	1.4	5.77395	2.1	0.35395	1.1	0.51	1953.5	18.0	1943	18	1931	32	1931	32	1.7	-1.2
04LP027-64	*395*	*9424*	*1.0*	*4.28636*	*5.0*	*0.26266*	*4.9*	*0.99*	*1503.4*	*65.7*	*1691*	*41*	*1932*	*13*	*1932*	*13*	*0.7*	*22.2*
04LP027-10	*379*	*8844*	*2.0*	*4.65788*	*3.4*	*0.28478*	*3.3*	*0.98*	*1615.4*	*46.7*	*1760*	*28*	*1936*	*13*	*1936*	*13*	*0.7*	*16.6*
04LP027-5	*280*	*23608*	*0.8*	*4.31051*	*1.8*	*0.26337*	*1.7*	*0.92*	*1507.0*	*22.7*	*1695*	*15*	*1937*	*13*	*1937*	*13*	*0.7*	*22.2*
04LP027-43	285	65218	0.6	5.16310	2.1	0.31472	2.0	0.94	1763.9	30.1	1847	18	1941	13	1941	13	0.7	9.1
04LP027-54	77	5981	1.4	5.72455	2.9	0.34853	1.6	0.54	1927.6	26.3	1935	25	1943	44	1943	44	2.3	0.8
04LP027-46	157	11297	1.8	5.86277	2.2	0.35683	1.7	0.76	1967.1	27.9	1956	19	1944	25	1944	25	1.3	-1.2
04LP027-97	69	37050	1.3	5.92242	1.4	0.35870	1.1	0.76	1976.0	18.2	1965	12	1952	17	1952	17	0.9	-1.2
04LP027-66	338	112653	2.5	5.72516	1.7	0.34599	1.6	0.91	1915.4	26.3	1935	15	1956	13	1956	13	0.7	2.1
04LP027-73	94	105469	1.6	5.76839	2.4	0.34840	2.1	0.88	1927.0	34.6	1942	20	1957	20	1957	20	1.0	1.5
04LP027-21	172	87493	1.4	5.30947	2.5	0.32065	2.4	0.96	1792.9	37.9	1870	22	1958	13	1958	13	0.7	8.4
04LP027-29	220	104605	2.4	5.72075	3.5	0.34515	3.4	0.98	1911.4	56.4	1935	30	1959	13	1959	13	0.7	2.4
04LP027-11	345	21474	2.3	5.29657	1.2	0.31904	1.0	0.82	1785.0	15.6	1868	10	1962	13	1962	13	0.7	9.0
04LP027-42	231	80277	1.3	5.75524	1.4	0.34644	1.2	0.85	1917.6	19.2	1940	12	1963	13	1963	13	0.7	2.3
04LP027-25	277	46497	1.2	5.89447	2.0	0.35462	1.9	0.93	1956.6	31.7	1960	18	1964	13	1964	13	0.7	0.4
04LP027-61	242	245117	1.4	5.59157	3.9	0.33650	3.8	0.98	1869.8	61.5	1915	33	1964	13	1964	13	0.7	4.8
04LP027-17	255	26739	0.9	5.61467	3.0	0.33771	2.9	0.96	1875.6	47.2	1918	26	1965	14	1965	14	0.7	4.5
04LP027-53	243	28033	1.1	6.02859	2.0	0.36254	1.8	0.92	1994.2	30.5	1980	17	1965	14	1965	14	0.7	-1.5
04LP027-27	380	49118	3.3	5.57464	4.3	0.33505	4.3	0.99	1862.8	69.2	1912	37	1966	13	1966	13	0.7	5.2
04LP027-37	120	30804	1.5	5.65910	1.4	0.33994	1.2	0.82	1886.4	19.1	1925	12	1967	14	1967	14	0.7	4.1
04LP027-48	337	63745	1.5	5.81268	1.4	0.34925	1.2	0.86	1931.0	19.9	1948	12	1967	13	1967	13	0.7	1.8
04LP027-83	*206*	*77493*	*1.5*	*4.98793*	*2.6*	*0.29952*	*2.5*	*0.96*	*1688.9*	*37.0*	*1817*	*22*	*1968*	*13*	*1968*	*13*	*0.7*	*14.2*

$^{206}Pb/^{204}Pb$ is measured ratio.

Analyses in italics/shaded are excluded due to >10% error in critical age, >10% discordance, or >5% reverse discordance.

All errors are at the 1-sigma level, and include only random uncertainties.

Best age = $^{206}Pb/^{238}U$ ages for analyses younger than 1.0 Ga and $^{206}Pb/^{207}Pb$ ages for analyses older than 1.0 Ga.

U concentration and U/Th are calibrated by comparison with NBS SRM 610 and have uncertainty of ~25%.

Decay constants: $^{235}U=9.8485x10^{-10}$, $^{238}U=1.55125x10^{-10}$, $^{238}U/^{235}U=137.88$.

Isotope ratios are corrected for Pb/U fractionation by comparison with standard zircon with an age of 564 ± 4 Ma (2-sigma).

Initial Pb composition interpreted from Stacey and Kramers (1975), with uncertainties of 1.0 for $^{206}Pb/^{204}Pb$ and 0.3 for $^{207}Pb/^{204}Pb$.

Table I-2a. *(continued) Detrital Zircon U-Pb geochronologic analyses – Arizona Laserchron Center – Sample 04LP027 in Unit* ***Ps****.*

Isotopic ratios									Apparent ages (Ma)									
Sample	U (ppm)	$^{206}Pb/^{204}Pb$	U/Th	$^{207}Pb/^{235}U$	± (%) (1 sigma)	$^{206}Pb/^{238}U$	± (%) (1 sigma)	error corr.	$^{206}Pb/^{238}U$	± (Ma) (1 sigma)	$^{207}Pb/^{235}U$	± (Ma) (1 sigma)	$^{206}Pb/^{207}Pb$	± (Ma) (1 sigma)	BEST AGE	± (Ma) (1 sigma)	Error %	Discordance %
04LP027-88	187	70554	1.8	5.82583	1.2	0.34970	1.0	0.82	1933.2	16.7	1950	11	1968	13	1968	13	0.7	1.8
04LP027-52	54	10291	1.1	5.91510	2.2	0.35494	1.2	0.55	1958.1	20.9	1964	20	1969	33	1969	33	1.7	0.6
04LP027-75	208	54326	0.9	5.80915	1.9	0.34866	1.7	0.93	1928.2	29.0	1948	16	1969	13	1969	13	0.7	2.1
04LP027-15	177	123791	3.2	5.67885	1.3	0.34050	1.0	0.76	1889.1	16.4	1928	11	1970	15	1970	15	0.8	4.1
04LP027-8	333	95579	1.1	5.40936	1.4	0.32380	1.2	0.86	1808.3	18.9	1886	12	1973	12	1973	12	0.6	8.3
04LP027-39	162	44309	2.0	5.70325	1.5	0.34144	1.3	0.87	1893.6	21.3	1932	13	1973	13	1973	13	0.7	4.0
04LP027-13	338	50288	1.2	5.74550	1.2	0.34384	1.0	0.81	1905.1	16.5	1938	11	1974	13	1974	13	0.7	3.5
04LP027-20	239	183446	1.7	5.72697	3.7	0.34233	3.6	0.98	1897.9	59.5	1935	32	1976	12	1976	12	0.6	4.0
04LP027-4	229	41412	0.7	5.53668	2.0	0.33060	1.8	0.93	1841.3	29.3	1906	17	1978	12	1978	12	0.6	6.9
04LP027-6	254	51691	1.9	5.27695	2.4	0.31473	2.3	0.96	1763.9	35.0	1865	20	1980	13	1980	13	0.7	10.9
04LP027-40	240	73387	1.8	5.66336	1.9	0.33768	1.8	0.93	1875.5	29.3	1926	17	1980	13	1980	13	0.7	5.3
04LP027-87	*317*	*51683*	*1.4*	*5.14846*	*2.4*	*0.30704*	*1.6*	*0.68*	*1726.1*	*24.4*	*1844*	*20*	*1980*	*31*	*1980*	*31*	*1.6*	*12.8*
04LP027-55	97	96595	1.3	6.01350	1.7	0.35834	1.6	0.91	1974.3	27.0	1978	15	1981	13	1981	13	0.7	0.3
04LP027-1	313	54362	1.2	5.50496	1.3	0.32791	1.1	0.83	1828.3	16.7	1901	11	1982	12	1982	12	0.6	7.8
04LP027-57	119	20090	3.2	5.96372	3.4	0.35520	3.3	0.97	1959.4	55.3	1971	29	1982	15	1982	15	0.8	1.1
04LP027-26	165	50504	1.1	5.79013	3.8	0.34442	3.8	0.98	1907.9	62.3	1945	33	1985	13	1985	13	0.7	3.9
04LP027-76	170	24872	1.3	5.93913	1.3	0.35306	1.0	0.76	1949.2	16.8	1967	12	1986	15	1986	15	0.8	1.9
04LP027-45	139	57809	1.6	5.83304	1.7	0.34513	1.0	0.59	1911.3	16.5	1951	15	1994	24	1994	24	1.2	4.1
04LP027-82	138	61522	1.7	5.77848	1.3	0.34197	1.0	0.78	1896.1	16.4	1943	11	1994	14	1994	14	0.7	4.9
04LP027-96	203	117694	2.8	5.73621	1.2	0.33945	1.0	0.82	1884.0	16.3	1937	11	1994	12	1994	12	0.6	5.5
04LP027-2	172	69184	2.5	5.70507	1.4	0.33703	1.2	0.87	1872.4	20.2	1932	12	1997	12	1997	12	0.6	6.2
04LP027-22	156	72927	1.6	5.86426	3.6	0.34584	3.5	0.97	1914.7	57.2	1956	31	2000	16	2000	16	0.8	4.3
04LP027-56	257	43175	0.9	5.48884	1.3	0.32361	1.1	0.84	1807.3	17.5	1899	11	2000	12	2000	12	0.6	9.6
04LP027-38	183	31093	2.6	5.84527	2.4	0.34455	2.1	0.89	1908.5	35.0	1953	21	2001	19	2001	19	0.9	4.6
04LP027-70	126	18532	1.6	5.97519	2.4	0.35210	2.2	0.92	1944.6	36.8	1972	21	2001	16	2001	16	0.8	2.8
04LP027-30	175	137214	1.6	6.03810	1.5	0.35568	1.3	0.88	1961.7	22.3	1981	13	2002	12	2002	12	0.6	2.0
04LP027-35	179	116822	1.6	5.69381	2.4	0.33512	2.3	0.96	1863.2	37.5	1930	21	2003	12	2003	12	0.6	7.0
04LP027-86	199	63205	0.4	5.67494	2.6	0.33378	2.5	0.96	1856.7	40.5	1928	23	2005	13	2005	13	0.6	7.4
04LP027-72	505	28990	2.0	5.85355	1.6	0.34389	1.4	0.89	1905.4	23.1	1954	14	2007	12	2007	12	0.6	5.1
04LP027-33	*374*	*9937*	*0.9*	*5.11797*	*1.9*	*0.30031*	*1.8*	*0.92*	*1692.8*	*26.1*	*1839*	*16*	*2009*	*13*	*2009*	*13*	*0.6*	*15.7*
04LP027-49	172	79848	1.8	6.16911	2.5	0.36001	2.4	0.96	1982.2	40.1	2000	21	2019	12	2019	12	0.6	1.8
04LP027-71	227	143744	2.9	6.44891	1.9	0.37523	1.7	0.93	2053.9	30.3	2039	16	2024	12	2024	12	0.6	-1.5
04LP027-24	249	90408	1.2	5.86864	1.7	0.34126	1.6	0.91	1892.7	25.8	1957	15	2025	12	2025	12	0.6	6.5
04LP027-65	*454*	*9973*	*0.8*	*5.51948*	*2.2*	*0.32044*	*2.1*	*0.94*	*1791.9*	*32.1*	*1904*	*19*	*2028*	*13*	*2028*	*13*	*0.6*	*11.6*

$^{206}Pb/^{204}Pb$ is measured ratio.

Analyses in italics/shaded are excluded due to >10% error in critical age, >10% discordance, or >5% reverse discordance.

All errors are at the 1-sigma level, and include only random uncertainties.

Best age = $^{206}Pb/^{238}U$ ages for analyses younger than 1.0 Ga and $^{206}Pb/^{207}Pb$ ages for analyses older than 1.0 Ga.

U concentration and U/Th are calibrated by comparison with NBS SRM 610 and have uncertainty of ~25%.

Decay constants: $^{235}U=9.8485x10^{-10}$, $^{238}U=1.55125x10^{-10}$, $^{238}U/^{235}U=137.88$.

Isotope ratios are corrected for Pb/U fractionation by comparison with standard zircon with an age of 564 ± 4 Ma (2-sigma).

Initial Pb composition interpreted from Stacey and Kramers (1975), with uncertainties of 1.0 for $^{206}Pb/^{204}Pb$ and 0.3 for $^{207}Pb/^{204}Pb$.

Table I-2a. *(continued) Detrital Zircon U-Pb geochronologic analyses – Arizona Laserchron Center – Sample 04LP027 in Unit* ***Ps****.*

Isotopic ratios									Apparent ages (Ma)									
Sample	U (ppm)	$^{206}Pb/^{204}Pb$	U/Th	$^{207}Pb/^{235}U$	± (%) (1 sigma)	$^{206}Pb/^{238}U$	± (%) (1 sigma)	error corr.	$^{206}Pb/^{238}U$	± (Ma) (1 sigma)	$^{207}Pb/^{235}U$	± (Ma) (1 sigma)	$^{206}Pb/^{207}Pb$	± (Ma) (1 sigma)	BEST AGE	± (Ma) (1 sigma)	Error %	Discordance %
04LP027-16	220	114504	6.3	6.51427	4.3	0.36850	3.6	0.84	2022.3	62.0	2048	38	2074	41	2074	41	2.0	2.5
04LP027-23	90	19936	0.9	6.46118	5.8	0.36233	3.7	0.64	1993.2	63.1	2041	51	2089	78	2089	78	3.7	4.6
04LP027-63	26	3532	1.7	6.96003	4.7	0.37940	3.5	0.75	2073.5	62.3	2106	42	2139	55	2139	55	2.6	3.1
04LP027-67	299	107255	1.1	8.84264	1.9	0.40847	1.8	0.93	2207.9	32.7	2322	17	2424	12	2424	12	0.5	8.9
04LP027-98	148	18899	1.8	10.56017	1.2	0.46965	1.0	0.82	2482.0	20.8	2485	12	2488	12	2488	12	0.5	0.2
04LP027-50	486	20518	1.4	9.94100	2.1	0.43508	2.0	0.94	2328.6	38.1	2429	19	2515	12	2515	12	0.5	7.4
04LP027-9	247	24365	3.0	10.88869	2.8	0.44922	2.7	0.97	2391.8	53.2	2514	26	2614	12	2614	12	0.5	8.5
04LP027-58	122	286227	2.1	12.85089	2.7	0.51856	2.7	0.97	2693.1	58.3	2669	26	2650	12	2650	12	0.5	-1.6
04LP027-91	449	513816	1.6	12.51237	1.3	0.50484	1.1	0.84	2634.6	23.8	2644	12	2651	12	2651	12	0.5	0.6
04LP027-74	*209*	*7125*	*0.8*	*6.36478*	*4.7*	*0.25581*	*4.5*	*0.97*	*1468.4*	*59.5*	*2027*	*41*	*2657*	*19*	*2657*	*19*	*0.7*	*44.7*
04LP027-81	309	10178	1.8	13.43821	1.4	0.52021	1.0	0.73	2700.1	22.2	2711	13	2719	16	2719	16	0.6	0.7
04LP027-32	*277*	*20170*	*0.6*	*10.81952*	*2.1*	*0.41794*	*2.0*	*0.94*	*2251.1*	*37.1*	*2508*	*19*	*2723*	*12*	*2723*	*12*	*0.4*	*17.3*
04LP027-90	*618*	*15644*	*2.2*	*9.69914*	*1.7*	*0.37376*	*1.5*	*0.90*	*2047.0*	*26.1*	*2407*	*15*	*2727*	*12*	*2727*	*12*	*0.4*	*24.9*
04LP027-94	75	35620	1.1	13.82904	1.4	0.52407	1.2	0.86	2716.4	26.8	2738	13	2754	12	2754	12	0.4	1.4
04LP027-60	87	37226	0.9	14.00262	1.8	0.52955	1.6	0.92	2739.5	36.4	2750	17	2757	12	2757	12	0.4	0.6
04LP027-3	89	48473	0.7	14.48381	1.2	0.53891	1.0	0.82	2778.9	22.6	2782	12	2784	11	2784	11	0.4	0.2
04LP027-7	*299*	*14378*	*0.8*	*11.88089*	*2.6*	*0.44148*	*2.5*	*0.96*	*2357.3*	*49.4*	*2595*	*24*	*2786*	*11*	*2786*	*11*	*0.4*	*15.4*
04LP027-62	272	118552	4.3	14.39588	3.2	0.53355	3.1	0.98	2756.4	69.3	2776	30	2791	11	2791	11	0.4	1.2
04LP027-80	139	23488	0.5	14.69871	1.3	0.54301	1.0	0.80	2796.0	22.7	2796	12	2796	12	2796	12	0.4	0.0
04LP027-92	119	56558	1.6	14.48402	2.0	0.53447	1.9	0.94	2760.3	42.2	2782	19	2798	12	2798	12	0.4	1.3
04LP027-36	152	49252	1.2	14.49739	2.2	0.53437	2.1	0.95	2759.8	47.2	2783	21	2800	12	2800	12	0.4	1.4
04LP027-85	154	323438	0.8	14.59694	1.2	0.53576	1.0	0.82	2765.7	22.5	2789	12	2806	11	2806	11	0.4	1.4
04LP027-41	103	71274	0.7	14.92814	1.5	0.54079	1.4	0.89	2786.8	31.0	2811	15	2828	11	2828	11	0.4	1.5
04LP027-93	202	15701	0.9	15.23674	1.8	0.55145	1.6	0.92	2831.2	37.1	2830	17	2829	12	2829	12	0.4	-0.1
04LP027-12	359	218140	0.8	14.96726	1.2	0.54101	1.0	0.82	2787.7	22.6	2813	12	2831	11	2831	11	0.4	1.5
04LP027-31	223	34127	1.3	14.89293	3.3	0.53758	3.2	0.98	2773.3	71.9	2808	31	2834	12	2834	12	0.4	2.1
04LP027-47	94	6699	0.8	14.75689	1.5	0.52952	1.0	0.68	2739.4	22.9	2800	14	2843	18	2843	18	0.6	3.6
04LP027-59	127	5561	1.0	15.98661	2.5	0.56078	2.2	0.87	2869.8	50.8	2876	24	2880	20	2880	20	0.7	0.4
04LP027-44	169	249646	1.6	16.32223	1.8	0.56749	1.6	0.92	2897.5	37.8	2896	17	2895	11	2895	11	0.4	-0.1
04LP027-34	126	26867	1.9	17.22209	1.6	0.57562	1.4	0.89	2930.9	33.2	2947	15	2959	12	2959	12	0.4	0.9
04LP027-51	114	16389	1.0	17.84677	1.3	0.58772	1.1	0.82	2980.2	26.3	2982	13	2982	12	2982	12	0.4	0.1
04LP027-84	*163*	*31200*	*0.9*	*12.09018*	*3.3*	*0.38040*	*3.2*	*0.97*	*2078.1*	*56.7*	*2611*	*31*	*3056*	*12*	*3056*	*12*	*0.4*	*32.0*
															83 zircons			

$^{206}Pb/^{204}Pb$ is measured ratio.

Analyses in italics/shaded are excluded due to >10% error in critical age, >10% discordance, or >5% reverse discordance.

All errors are at the 1-sigma level, and include only random uncertainties.

Best age = $^{206}Pb/^{238}U$ ages for analyses younger than 1.0 Ga and $^{206}Pb/^{207}Pb$ ages for analyses older than 1.0 Ga.

U concentration and U/Th are calibrated by comparison with NBS SRM 610 and have uncertainty of ~25%.

Decay constants: $^{235}U=9.8485x10^{-10}$, $^{238}U=1.55125x10^{-10}$, $^{238}U/^{235}U=137.88$.

Isotope ratios are corrected for Pb/U fractionation by comparison with standard zircon with an age of 564 ± 4 Ma (2-sigma).

Initial Pb composition interpreted from Stacey and Kramers (1975), with uncertainties of 1.0 for $^{206}Pb/^{204}Pb$ and 0.3 for $^{207}Pb/^{204}Pb$.

Table I-2b. *Detrital Zircon U-Pb geochronologic analyses – Pacific Centre for Isotopic and Geochemical Research – Sample 05LP024-1 in Unit* ***Ps***.

Analysis No.	Age estimates with 1 sigma uncertainty (Ma)										Isotopic Ratios with absolute errors							
	$^{207}Pb/^{235}U$ Ma	$^{207}Pb/^{235}U$ ± 1σ Error	$^{206}Pb/^{238}U$ Ma	$^{206}Pb/^{238}U$ ± 1σ Error	$^{207}Pb/^{206}Pb$ Ma	$^{207}Pb/^{206}Pb$ ± 1σ Error	Preferred Age Ma	± 1σ Error	Error %	Discordancy %	$^{207}Pb/^{235}U$ Ratio	$^{207}Pb/^{235}U$ 1σ Error	$^{206}Pb/^{238}U$ Ratio	$^{206}Pb/^{238}U$ 1σ Error	Rho	$^{207}Pb/^{206}Pb$ Ratio	$^{207}Pb/^{206}Pb$ 1σ Error	Th/U Ratio
2431	2661	18.18	2637.4	11	2695.2	12.06	2695.2	12.1	0.4	2.1	12.7448	0.2461	0.5055	0.0026	0.26	0.1847	0.0014	0.33063
2432	1821.8	9.27	1845.4	5.64	1818.2	10.8	1818.2	10.8	0.6	-1.5	5.0145	0.0549	0.3314	0.0012	0.32	0.1112	0.0007	0.26148
2433	2478	14.07	2441.5	8.69	2521.3	10.9	2521.3	10.9	0.4	3.2	10.4779	0.1590	0.4604	0.0020	0.28	0.1664	0.0011	0.32186
2434	2658.3	23.61	2685.2	14.07	2681.3	14.91	2681.3	14.9	0.6	-0.1	12.7082	0.3187	0.5167	0.0033	0.26	0.1831	0.0017	0.66047
2435	1824	14.87	1813.5	8.03	1862.7	15.59	1862.7	15.6	0.8	2.6	5.0278	0.0883	0.3249	0.0017	0.29	0.1139	0.0010	0.20863
2436	1854.7	19.53	1823.7	10.33	1931.2	19.74	1931.2	19.7	1.0	5.6	5.2128	0.1195	0.3270	0.0021	0.28	0.1183	0.0013	0.18269
2437	1801.7	19.17	1755.2	9.71	1767.7	20.1	1767.7	20.1	1.1	0.7	4.8967	0.1113	0.3129	0.0020	0.28	0.1081	0.0012	0.18761
2438	2540.7	14.5	2486.1	9.01	2593.8	11.05	2593.8	11.1	0.4	4.2	11.2090	0.1743	0.4706	0.0021	0.28	0.1737	0.0012	0.32831
2439	1833.2	18.54	1840.5	9.84	1865.2	19	1865.2	19.0	1.0	1.3	5.0824	0.1111	0.3304	0.0020	0.28	0.1141	0.0012	0.32548
2440	2519.8	17.58	2496.5	10.59	2559.3	12.83	2559.3	12.8	0.5	2.5	10.9609	0.2071	0.4730	0.0024	0.27	0.1702	0.0013	0.34078
2441	1898.4	16.33	1868.2	8.74	1881.7	16.55	1881.7	16.6	0.9	0.7	5.4863	0.1043	0.3362	0.0018	0.28	0.1151	0.0011	0.06212
2442	1827.4	14.46	1845.1	8.03	1863.5	15.48	1863.5	15.5	0.8	1.0	5.0481	0.0862	0.3314	0.0017	0.29	0.1140	0.0010	0.31053
2443	1858.6	17.15	1885.8	9.36	1867.1	17.66	1867.1	17.7	0.9	-1.0	5.2365	0.1053	0.3398	0.0019	0.28	0.1142	0.0011	0.39676
2444	2822.2	13.54	2742.5	9.08	2873.9	10.15	2873.9	10.2	0.4	4.6	15.1101	0.2148	0.5303	0.0022	0.29	0.2059	0.0013	0.59459
2445	1916.8	13.72	1916.1	7.86	1995.7	14.25	1995.7	14.3	0.7	4.0	5.6043	0.0893	0.3461	0.0016	0.30	0.1227	0.0010	0.30894
2446	2632.3	15.06	2605.8	9.67	2687.2	11.55	2687.2	11.6	0.4	3.0	12.3627	0.1982	0.4981	0.0023	0.28	0.1838	0.0013	0.38708
2447	1842.1	15.24	1829.3	8.32	1858.2	16.34	1858.2	16.3	0.9	1.6	5.1364	0.0921	0.3281	0.0017	0.29	0.1136	0.0010	0.21813
2448	1816.8	17.44	1826.4	9.37	1860	18.48	1860.0	18.5	1.0	1.8	4.9852	0.1028	0.3275	0.0019	0.29	0.1137	0.0012	0.28550
2449	1877.8	16.77	1822.7	8.78	1840.5	17.43	1840.5	17.4	0.9	1.0	5.3555	0.1050	0.3268	0.0018	0.28	0.1125	0.0011	0.25669
2450	*1554.3*	*14.39*	*1380.6*	*7*	*1835.2*	*18.25*	1835.2	18.3	*1.0*	*24.8*	*3.6218*	*0.0655*	*0.2388*	*0.0014*	*0.31*	*0.1122*	*0.0011*	*0.39527*
2451	1809.9	17.67	1818.2	9.45	1797.9	19.1	1797.9	19.1	1.1	-1.1	4.9448	0.1034	0.3258	0.0019	0.28	0.1099	0.0012	0.44418
2452	1808.3	10.9	1787.4	6.38	1850.7	13.18	1850.7	13.2	0.7	3.4	4.9353	0.0637	0.3195	0.0013	0.32	0.1132	0.0008	0.17339
2453	2568.7	16.1	2487.6	10.06	2655.5	12.91	2655.5	12.9	0.5	6.3	11.5512	0.1990	0.4709	0.0023	0.28	0.1803	0.0014	0.65876
2454	*1682.1*	*20.14*	*1593.6*	*10.1*	*1799.5*	*23.1*	1799.5	23.1	*1.3*	*11.4*	*4.2416*	*0.1040*	*0.2804*	*0.0020*	*0.29*	*0.1100*	*0.0014*	*0.40523*
2455	1770.9	14.96	1839.4	8.48	1785.7	17.24	1785.7	17.2	1.0	-3.0	4.7206	0.0843	0.3302	0.0018	0.30	0.1092	0.0010	0.29241
2456	1901.5	16.95	1873.8	9.21	1933.7	17.69	1933.7	17.7	0.9	3.1	5.5056	0.1086	0.3373	0.0019	0.29	0.1185	0.0012	0.13122
2457	1815.3	12.05	1791.9	6.93	1863.1	14.46	1863.1	14.5	0.8	3.8	4.9761	0.0709	0.3205	0.0014	0.31	0.1139	0.0009	0.31965
2458	2666.4	20.62	2692.9	12.85	2674.2	15.08	2674.2	15.1	0.6	-0.7	12.8188	0.2806	0.5185	0.0030	0.27	0.1823	0.0017	0.30774
2459	2683.4	19	2620.2	11.85	2744.5	14.37	2744.5	14.4	0.5	4.5	13.0520	0.2630	0.5015	0.0028	0.27	0.1903	0.0017	0.52305
2460	1848.4	16.51	1846.3	9	1810.8	18.22	1810.8	18.2	1.0	-2.0	5.1740	0.1004	0.3316	0.0019	0.29	0.1107	0.0011	0.39431
05LP024-1L1	1810.8	12.67	1751.9	16.05	1890.8	21.24	1890.8	21.2	1.1	5.8	4.9501	0.0743	0.3123	0.0033	0.70	0.1157	0.0014	0.19338
05LP024-1L2	2808	21.71	2761.3	25.05	2913.1	20.23	2913.1	20.2	0.7	4.4	14.8861	0.3397	0.5347	0.0060	0.49	0.2110	0.0027	0.19232

Analyses in italics/shaded are excluded due to >10% error in critical age, >10% discordance, or >5% reverse discordance.

All errors are at the 1-sigma level, and include only random uncertainties.

Best age = $^{206}Pb/^{238}U$ ages for analyses younger than 1.0 Ga and $^{206}Pb/^{207}Pb$ ages for analyses older than 1.0 Ga.

Isotope ratios are corrected for Pb/U fractionation by comparison with standard zircons Plesovice and FC1.

Table I-2b. *(continued) Detrital Zircon U-Pb geochronologic analyses – Pacific Centre for Isotopic and Geochemical Research – Sample 05LP024-1 in Unit* ***Ps****.*

Analysis No.	Age estimates with 1 sigma uncertainty (Ma)										Isotopic Ratios with absolute errors							
	$^{207}Pb/^{235}U$ Ma	$^{207}Pb/^{235}U$ ± 1σ Error	$^{206}Pb/^{238}U$ Ma	$^{206}Pb/^{238}U$ ± 1σ Error	$^{207}Pb/^{206}Pb$ Ma	$^{207}Pb/^{206}Pb$ ± 1σ Error	Preferred Age Ma	± 1σ Error	Error %	Discordancy %	$^{207}Pb/^{235}U$ Ratio	$^{207}Pb/^{235}U$ 1σ Error	$^{206}Pb/^{238}U$ Ratio	$^{206}Pb/^{238}U$ 1σ Error	Rho	$^{207}Pb/^{206}Pb$ Ratio	$^{207}Pb/^{206}Pb$ 1σ Error	Th/U Ratio
05LP024-1L3	1773	12.93	1701.9	15.75	1863.8	21.57	1863.8	21.6	1.2	6.8	4.7323	0.0730	0.3021	0.0032	0.68	0.1140	0.0014	0.35813
05LP024-1L4	1779	12.4	1709.6	15.72	1842.3	21.31	1842.3	21.3	1.2	5.3	4.7665	0.0704	0.3037	0.0032	0.71	0.1126	0.0013	0.13587
05LP024-1L5	1773.2	11.72	1742.2	15.88	1822.7	21.01	1822.7	21.0	1.2	3.6	4.7335	0.0662	0.3103	0.0032	0.74	0.1114	0.0013	0.19007
05LP024-1L6	1765.1	11.63	1733	15.83	1829.2	20.98	1829.2	21.0	1.1	4.4	4.6878	0.0651	0.3084	0.0032	0.75	0.1118	0.0013	0.08517
05LP024-1L7	1764.7	12.53	1741.5	16.06	1823.1	21.51	1823.1	21.5	1.2	3.8	4.6856	0.0702	0.3102	0.0033	0.70	0.1115	0.0013	0.18303
05LP024-1L8	1795.4	15.29	1721.9	16.42	1851.7	23.02	1851.7	23.0	1.2	5.0	4.8601	0.0882	0.3062	0.0033	0.60	0.1132	0.0015	0.09351
05LP024-1L9	1800.8	12.27	1752.9	16.11	1853.7	21.22	1853.7	21.2	1.1	4.1	4.8918	0.0712	0.3125	0.0033	0.72	0.1134	0.0013	0.20385
05LP024-1L10	1754	13.18	1711.7	15.98	1810.5	21.98	1810.5	22.0	1.2	4.3	4.6261	0.0730	0.3041	0.0032	0.67	0.1107	0.0014	0.24344
05LP024-1L11	1782.2	12.72	1729.2	16.05	1838.1	21.59	1838.1	21.6	1.2	4.5	4.7849	0.0725	0.3077	0.0033	0.70	0.1124	0.0014	0.11663
05LP024-1L12	2646.7	14.56	2573.7	22.43	2700.7	19.22	2700.7	19.2	0.7	3.4	12.5533	0.1944	0.4907	0.0052	0.68	0.1853	0.0022	0.14933
05LP024-1L13	2585	25.53	2494.2	24.63	2742.4	22.71	2742.4	22.7	0.8	7.4	11.7545	0.3207	0.4724	0.0056	0.44	0.1900	0.0027	0.13821
05LP024-1L14	1773.5	12.52	1709.8	15.91	1841.9	21.52	1841.9	21.5	1.2	5.4	4.7352	0.0707	0.3037	0.0032	0.71	0.1126	0.0014	0.17974
05LP024-1L15	1781.3	13.22	1744.9	16.32	1825.3	21.95	1825.3	22.0	1.2	3.4	4.7793	0.0752	0.3109	0.0033	0.68	0.1116	0.0014	0.21395
05LP024-1L16	1837.1	11.91	1807.7	16.62	1894	20.98	1894.0	21.0	1.1	3.8	5.1062	0.0716	0.3237	0.0034	0.75	0.1159	0.0014	0.04145
05LP024-1L17	1788.4	12.3	1743.4	16.2	1859	21.38	1859.0	21.4	1.2	5.0	4.8199	0.0705	0.3105	0.0033	0.72	0.1137	0.0014	0.12714
05LP024-1L18	1767.1	13.94	1726.9	16.39	1819.1	22.49	1819.1	22.5	1.2	4.0	4.6995	0.0783	0.3072	0.0033	0.65	0.1112	0.0014	0.11720
05LP024-1L19	1810.5	13.19	1740.5	16.35	1891.1	21.76	1891.1	21.8	1.2	6.1	4.9481	0.0773	0.3100	0.0033	0.69	0.1157	0.0014	0.06501
05LP024-1L20	1832.7	13.52	1794.2	16.84	1838.2	22.02	1838.2	22.0	1.2	1.3	5.0799	0.0810	0.3209	0.0035	0.67	0.1124	0.0014	0.22500
05LP024-1L21	1762.8	15.89	1748.7	17.06	1839.2	23.81	1839.2	23.8	1.3	4.5	4.6754	0.0888	0.3116	0.0035	0.59	0.1124	0.0015	0.10439
05LP024-1L22	1799.1	25.96	1766.9	19.73	1810.9	31.05	1810.9	31.1	1.7	1.5	4.8815	0.1504	0.3153	0.0040	0.41	0.1107	0.0019	0.11191
05LP024-1L23	1762.1	13.18	1722.4	16.3	1842.8	22.05	1842.8	22.1	1.2	5.5	4.6714	0.0736	0.3063	0.0033	0.68	0.1127	0.0014	0.13119
05LP024-1L24	1782.2	14.98	1738.7	16.78	1841.3	23.12	1841.3	23.1	1.3	4.4	4.7845	0.0854	0.3096	0.0034	0.62	0.1126	0.0015	0.21437
05LP024-1L25	1744.9	13.47	1695.9	16.17	1787	22.47	1787.0	22.5	1.3	3.7	4.5758	0.0739	0.3009	0.0033	0.67	0.1093	0.0014	0.01475
05LP024-1L26	1778.9	14.96	1753.7	16.95	1825.6	23.2	1825.6	23.2	1.3	3.2	4.7658	0.0850	0.3127	0.0035	0.62	0.1116	0.0014	0.21980

Analyses in italics/shaded are excluded due to >10% error in critical age, >10% discordance, or >5% reverse discordance.

All errors are at the 1-sigma level, and include only random uncertainties.

Best age = $^{206}Pb/^{238}U$ ages for analyses younger than 1.0 Ga and $^{206}Pb/^{207}Pb$ ages for analyses older than 1.0 Ga.

Isotope ratios are corrected for Pb/U fractionation by comparison with standard zircons Plesovice and FC1.

Table I-2b. *(continued) Detrital Zircon U-Pb geochronologic analyses – Pacific Centre for Isotopic and Geochemical Research – Sample 05LP024-1 in Unit* ***Ps****.*

Analysis No.	Age estimates with 1 sigma uncertainty (Ma)										Isotopic Ratios with absolute errors							
	$^{207}Pb/^{235}U$ Ma	$^{207}Pb/^{235}U$ ± 1σ Error	$^{206}Pb/^{238}U$ Ma	$^{206}Pb/^{238}U$ ± 1σ Error	$^{207}Pb/^{206}Pb$ Ma	$^{207}Pb/^{206}Pb$ ± 1σ Error	Preferred Age Ma	± 1σ Error	Error %	Discordancy %	$^{207}Pb/^{235}U$ Ratio	$^{207}Pb/^{235}U$ 1σ Error	$^{206}Pb/^{238}U$ Ratio	$^{206}Pb/^{238}U$ 1σ Error	Rho	$^{207}Pb/^{206}Pb$ Ratio	$^{207}Pb/^{206}Pb$ 1σ Error	Th/U Ratio
05LP024-1L27	1800.9	13.34	1720.4	16.36	1866.7	22.04	1866.7	22.0	1.2	5.7	4.8921	0.0774	0.3059	0.0033	0.68	0.1142	0.0014	0.26506
05LP024-1L28	1803.9	13.7	1747.9	16.66	1861.8	22.27	1861.8	22.3	1.2	4.6	4.9097	0.0798	0.3115	0.0034	0.67	0.1139	0.0014	0.20247
05LP024-1L29	1818.3	13.39	1756.8	16.68	1874.2	22.03	1874.2	22.0	1.2	4.6	4.9937	0.0790	0.3133	0.0034	0.69	0.1146	0.0014	0.12387
05LP024-1L30	2643.3	16.81	2583.2	23.41	2696.2	20.29	2696.2	20.3	0.8	3.1	12.5081	0.2236	0.4929	0.0054	0.62	0.1848	0.0023	0.34325
																	58 zircons	

Analyses in italics/shaded are excluded due to >10% error in critical age, >10% discordance, or >5% reverse discordance.

All errors are at the 1-sigma level, and include only random uncertainties.

Best age = $^{206}Pb/^{238}U$ ages for analyses younger than 1.0 Ga and $^{206}Pb/^{207}Pb$ ages for analyses older than 1.0 Ga.

Isotope ratios are corrected for Pb/U fractionation by comparison with standard zircons Plesovice and FC1.

Table I-2c. *Detrital zircon U-Pb geochronologic analyses – Pacific Centre for Isotopic and Geochemical Research – Sample 05LP024-2 in Unit* ***Ps****.*

Analysis No.	Age estimates with 1 sigma uncertainty (Ma)										Isotopic Ratios with absolute errors							
	$^{207}Pb/^{235}U$ Ma	$^{207}Pb/^{235}U$ ± 1σ Error	$^{206}Pb/^{238}U$ Ma	$^{206}Pb/^{238}U$ ± 1σ Error	$^{207}Pb/^{206}Pb$ Ma	$^{207}Pb/^{206}Pb$ ± 1σ Error	Preferred Age Ma	± 1σ Error	Error %	Discordancy %	$^{207}Pb/^{235}U$ Ratio	$^{207}Pb/^{235}U$ 1σ Error	$^{206}Pb/^{238}U$ Ratio	$^{206}Pb/^{238}U$ 1σ Error	Rho	$^{207}Pb/^{206}Pb$ Ratio	$^{207}Pb/^{206}Pb$ 1σ Error	Th/U Ratio
lP24-2a	2550.7	32.4	2480.3	29.04	2669.5	27.36	2669.5	27.4	1.0	7.1	11.3302	0.3935	0.4693	0.0066	0.41	0.1818	0.0030	0.2445
lp24-2b	1671.7	32.26	1732.9	23.12	1709.6	45.48	1709.6	45.5	2.7	-1.4	4.1879	0.1648	0.3084	0.0047	0.39	0.1047	0.0026	0.2446
lp24-2c	1840.3	25.2	1850.5	21.6	1815.6	31.75	1815.6	31.8	1.7	-1.9	5.1250	0.1520	0.3325	0.0045	0.45	0.1110	0.0020	0.5258
lp24-2d	2373.5	23.7	2299.8	24.75	2435	23.68	2435.0	23.7	1.0	5.6	9.3559	0.2417	0.4287	0.0055	0.50	0.1581	0.0022	0.2765
lp24-2e	2407.3	29.31	2429.7	27.74	2449.6	26.42	2449.6	26.4	1.1	0.8	9.7058	0.3090	0.4578	0.0063	0.43	0.1594	0.0025	0.4000
LP24-2F	1776.3	53.28	1697.5	29.56	1880.4	68.53	1880.4	68.5	3.6	9.7	4.7511	0.3018	0.3012	0.0060	0.31	0.1150	0.0045	0.0823
lP24-2G	*1767.2*	*44.53*	*1544*	*24.73*	*1928.7*	*55.88*	1928.7	55.9	*2.9*	*19.9*	*4.6999*	*0.2500*	*0.2706*	*0.0049*	*0.34*	*0.1182*	*0.0038*	*0.1948*
lP24-2H	2771.5	37.39	2690.2	31.82	2772.8	26.71	2772.8	26.7	1.0	3.0	14.3248	0.5644	0.5179	0.0075	0.37	0.1936	0.0032	0.3703
lP24-2I	1719.7	34.54	1749.9	24.39	1772.6	45.09	1772.6	45.1	2.5	1.3	4.4393	0.1850	0.3119	0.0050	0.38	0.1084	0.0027	0.1706
lP24-2J	1745.2	28.15	1669.1	21.06	1845.6	36.75	1845.6	36.8	2.0	9.6	4.5777	0.1546	0.2955	0.0042	0.42	0.1128	0.0023	0.1256
LP24-2K	*1712.5*	*39.79*	*1649.4*	*25.06*	*1852.5*	*54.31*	1852.5	54.3	*2.9*	*11.0*	*4.4008*	*0.2116*	*0.2916*	*0.0050*	*0.36*	*0.1133*	*0.0035*	*0.1960*
lP24-2L	1795	32.94	1706.2	22.54	1811.5	40.44	1811.5	40.4	2.2	5.8	4.8578	0.1900	0.3030	0.0046	0.38	0.1107	0.0025	0.2021
lP24-2M	1714.3	23.91	1708.5	20.15	1739.9	31.98	1739.9	32.0	1.8	1.8	4.4102	0.1274	0.3035	0.0041	0.47	0.1065	0.0019	0.4001
lP24-2N	1774.1	22.06	1748.9	19.84	1790.2	29.17	1790.2	29.2	1.6	2.3	4.7387	0.1247	0.3117	0.0040	0.49	0.1095	0.0018	0.1390
lP24-2O	1839.7	17.12	1790.5	18.93	1867.6	23.85	1867.6	23.9	1.3	4.1	5.1218	0.1032	0.3202	0.0039	0.60	0.1142	0.0015	0.2478
LP24-2P	1742.6	18.99	1706.5	18.72	1777.4	26.69	1777.4	26.7	1.5	4.0	4.5631	0.1040	0.3031	0.0038	0.55	0.1087	0.0016	0.3493
LP24-2Q	1778.4	24.23	1712.5	20.02	1780.5	31.44	1780.5	31.4	1.8	3.8	4.7631	0.1375	0.3043	0.0041	0.46	0.1089	0.0019	0.1704
lP24-2R	1799.7	31.7	1697.6	21.97	1749	40.72	1749.0	40.7	2.3	2.9	4.8852	0.1837	0.3013	0.0044	0.39	0.1070	0.0024	0.2880
LP24-2S	1754.1	22.32	1656.1	19.1	1846.8	29.32	1846.8	29.3	1.6	10.3	4.6267	0.1237	0.2929	0.0038	0.49	0.1129	0.0019	0.2636
lP24-2T	*2332.6*	*20.52*	*2387.9*	*24.16*	*2229.6*	*25.44*	2229.6	25.4	*1.1*	*-7.1*	*8.9470*	*0.2010*	*0.4484*	*0.0054*	*0.54*	*0.1402*	*0.0021*	*0.3485*
LP24-2U	1757.5	26.54	1628.7	20.08	1822.8	33.6	1822.8	33.6	1.8	10.6	4.6457	0.1476	0.2874	0.0040	0.44	0.1114	0.0021	0.1795
lP24-2V	2418.2	46.46	2376.4	34.54	2648.3	37.71	2648.3	37.7	1.4	10.3	9.8220	0.4952	0.4458	0.0078	0.34	0.1795	0.0041	0.4662
lP24-2W	1757.4	18.76	1733.2	18.87	1769.3	26.26	1769.3	26.3	1.5	2.0	4.6448	0.1043	0.3085	0.0038	0.55	0.1082	0.0016	0.1015
lP24-2X	1829.7	19.58	1808.8	19.78	1898	26.02	1898.0	26.0	1.4	4.7	5.0615	0.1169	0.3239	0.0041	0.54	0.1162	0.0017	0.2894
lP24-2Y	1690.7	21.92	1709.2	19.71	1782.6	30.49	1782.6	30.5	1.7	4.1	4.2860	0.1141	0.3036	0.0040	0.49	0.1090	0.0018	0.1276
lP24-2Z	1789.3	20.02	1727.2	19.08	1792.6	27.18	1792.6	27.2	1.5	3.6	4.8253	0.1149	0.3073	0.0039	0.53	0.1096	0.0017	0.3015
lP24-2AA	1747.2	25.36	1666.5	19.89	1767.6	32.72	1767.6	32.7	1.9	5.7	4.5884	0.1396	0.2950	0.0040	0.45	0.1081	0.0020	0.1883
lP24-2BB	*1692*	*14.05*	*1473.4*	*15.48*	*1894*	*22.27*	1894.0	22.3	*1.2*	*22.2*	*4.2930*	*0.0733*	*0.2568*	*0.0030*	*0.69*	*0.1159*	*0.0015*	*0.0271*
lP24-2CC	1756.3	21.61	1661.6	18.86	1784.7	28.95	1784.7	29.0	1.6	6.9	4.6390	0.1200	0.2940	0.0038	0.50	0.1091	0.0018	0.2404
lP24-2DD	*1731.3*	*28.35*	*1547.4*	*19.85*	*1873.1*	*35.85*	1873.1	35.9	*1.9*	*17.4*	*4.5017*	*0.1536*	*0.2713*	*0.0039*	*0.42*	*0.1146*	*0.0023*	*0.1056*
lP24-2EE	*1738.8*	*25.43*	*1629.2*	*19.8*	*1837.1*	*33.05*	1837.1	33.1	*1.8*	*11.3*	*4.5425*	*0.1388*	*0.2875*	*0.0040*	*0.45*	*0.1123*	*0.0021*	*0.2317*
lP24-2FF	1771.5	26.98	1663.3	20.31	1812.5	34.08	1812.5	34.1	1.9	8.2	4.7238	0.1521	0.2944	0.0041	0.43	0.1108	0.0021	0.2508

Analyses in italics/shaded are excluded due to >10% error in critical age, >10% discordance, or >5% reverse discordance.

All errors are at the 1-sigma level, and include only random uncertainties.

Preferred age = $^{206}Pb/^{238}U$ ages for analyses younger than 1.0 Ga and $^{206}Pb/^{207}Pb$ ages for analyses older than 1.0 Ga.

Isotope ratios are corrected for Pb/U fractionation by comparison with standard zircons Plesovice and FC1.

***Table I-2.**c (continued) Detrital zircon U-Pb geochronologic analyses – Pacific Centre for Isotopic and Geochemical Research – Sample 05LP024-2 in Unit **Ps**.*

Analysis No.	Age estimates with 1 sigma uncertainty (Ma)										Isotopic Ratios with absolute errors							
	$^{207}Pb/^{235}U$ Ma	$^{207}Pb/^{235}U$ ± 1σ Error	$^{206}Pb/^{238}U$ Ma	$^{206}Pb/^{238}U$ ± 1σ Error	$^{207}Pb/^{206}Pb$ Ma	$^{207}Pb/^{206}Pb$ ± 1σ Error	Preferred Age Ma	± 1σ Error	Error %	Discordancy %	$^{207}Pb/^{235}U$ Ratio	$^{207}Pb/^{235}U$ 1σ Error	$^{206}Pb/^{238}U$ Ratio	$^{206}Pb/^{238}U$ 1σ Error	Rho	$^{207}Pb/^{206}Pb$ Ratio	$^{207}Pb/^{206}Pb$ 1σ Error	Th/U Ratio
lP24-2GG	1681.9	26.24	1627.4	20.23	1810.6	34.94	1810.6	34.9	1.9	10.1	4.2403	0.1354	0.2872	0.0040	0.44	0.1107	0.0022	0.3964
lP24-2HH	3016.9	58.05	2953.6	42.76	3069.2	33.35	3069.2	33.4	1.1	3.8	18.5154	1.1157	0.5812	0.0105	0.30	0.2325	0.0049	0.4728
lP24-2II	2950.7	80.27	2869.4	55.53	3154.4	45.27	3154.4	45.3	1.4	9.0	17.2842	1.4454	0.5607	0.0134	0.29	0.2453	0.0071	0.2011
lP24-2jj	1700.6	21.64	1677.3	19.23	1795.4	29.94	1795.4	29.9	1.7	6.6	4.3382	0.1138	0.2972	0.0039	0.50	0.1098	0.0018	0.1154
lp24-2kk	1741.3	30.5	1622.5	21.1	1787	38.43	1787.0	38.4	2.2	9.2	4.5561	0.1669	0.2862	0.0042	0.40	0.1093	0.0023	0.2295
lp24-2ll	2536.6	42.44	2407.2	32.26	2641.6	32.56	2641.6	32.6	1.2	8.9	11.1601	0.5082	0.4527	0.0073	0.35	0.1788	0.0036	0.2695
lp24-2mm	*1695.6*	*21.1*	*1552.6*	*17.84*	*1834.6*	*29.07*	1834.6	29.1	*1.6*	*15.4*	*4.3116*	*0.1104*	*0.2723*	*0.0035*	*0.50*	*0.1122*	*0.0018*	*0.2687*
lp24-2nn	2564.6	39.88	2465.6	31.85	2692.7	30.85	2692.7	30.9	1.1	8.4	11.4997	0.4909	0.4659	0.0072	0.36	0.1844	0.0035	0.1532
lp24-2oo	1688.8	19.53	1570.9	17.55	1759.9	27.97	1759.9	28.0	1.6	10.7	4.2764	0.1015	0.2760	0.0035	0.53	0.1077	0.0017	0.1598
lp24-2pp	1755.6	32.25	1632.8	21.7	1798.4	40.63	1798.4	40.6	2.3	9.2	4.6349	0.1790	0.2883	0.0043	0.39	0.1099	0.0025	0.2365
lp24-2qq	2438.8	26.93	2362.6	26.04	2508.4	25.41	2508.4	25.4	1.0	5.8	10.0432	0.2929	0.4427	0.0058	0.45	0.1651	0.0025	0.2147
lp24-2rr	2419.3	26.43	2306.7	25.37	2474.1	25.52	2474.1	25.5	1.0	6.8	9.8336	0.2819	0.4302	0.0056	0.46	0.1618	0.0025	0.1907
lp24-2ss	*1755.5*	*24.94*	*1627.6*	*19.63*	*1909.8*	*32.08*	1909.8	32.1	*1.7*	*14.8*	*4.6343*	*0.1384*	*0.2872*	*0.0039*	*0.46*	*0.1169*	*0.0021*	*0.2434*
lp24-2tt	*1720*	*32.17*	*1611.4*	*21.88*	*1837.8*	*40.28*	1837.8	40.3	*2.2*	*12.3*	*4.4406*	*0.1724*	*0.2840*	*0.0044*	*0.40*	*0.1124*	*0.0025*	*0.3201*
lp24-2uu	2566.1	21.7	2453.5	25.24	2732.7	22.18	2732.7	22.2	0.8	10.2	11.5183	0.2676	0.4632	0.0057	0.53	0.1889	0.0026	0.3028
lp24-2vv	1732.9	21.87	1679.9	19.07	1757.3	29.85	1757.3	29.9	1.7	4.4	4.5107	0.1187	0.2977	0.0038	0.49	0.1075	0.0018	0.2640
lp24-2ww	1730.5	19.72	1654	18.37	1832.5	27.67	1832.5	27.7	1.5	9.7	4.4974	0.1068	0.2925	0.0037	0.53	0.1120	0.0017	0.3811
lp24-2xx	1896.6	39.94	1789.2	26.38	1991.9	43.09	1991.9	43.1	2.2	10.2	5.4744	0.2546	0.3199	0.0054	0.36	0.1224	0.0030	0.0046
lp24-2yy	2622.2	32.89	2441	28.33	2686.9	27.04	2686.9	27.0	1.0	9.2	12.2296	0.4285	0.4603	0.0064	0.40	0.1837	0.0030	0.5002
lp24-2zz	2610	39.38	2511.6	32.07	2755.8	30.5	2755.8	30.5	1.1	8.9	12.0721	0.5070	0.4764	0.0074	0.37	0.1916	0.0036	0.1822
lp24-2b1	*1750.7*	*35.24*	*1557.1*	*22.29*	*1928.2*	*43.67*	1928.2	43.7	*2.3*	*19.2*	*4.6081*	*0.1946*	*0.2732*	*0.0044*	*0.38*	*0.1181*	*0.0029*	*0.2527*
lp24-2b2	2527.6	32.21	2438	28.01	2527	27.63	2527.0	27.6	1.1	3.5	11.0527	0.3823	0.4597	0.0063	0.40	0.1669	0.0028	0.3961
lp24-2b3	1725.3	20.59	1673.2	18.73	1772.4	28.85	1772.4	28.9	1.6	5.6	4.4691	0.1109	0.2964	0.0038	0.51	0.1084	0.0017	0.2101
lp24-2b4	*2416.3*	*82.48*	*2335*	*54.21*	*2753.4*	*61.43*	2753.4	61.4	*2.2*	*15.2*	*9.8021*	*0.8775*	*0.4365*	*0.0121*	*0.31*	*0.1913*	*0.0073*	*0.6602*
lp24-2b5	1673.9	29.17	1589.4	20.47	1756.4	38.84	1756.4	38.8	2.2	9.5	4.1996	0.1494	0.2796	0.0041	0.41	0.1074	0.0023	0.1412
lp24-2b6	*1769.8*	*26.99*	*1615.5*	*20*	*1891.3*	*34.63*	1891.3	34.6	*1.8*	*14.6*	*4.7141*	*0.1519*	*0.2848*	*0.0040*	*0.43*	*0.1157*	*0.0023*	*0.2796*
lp24-2b7	1700.7	26.92	1614.4	20.19	1805.1	35.24	1805.1	35.2	2.0	10.6	4.3384	0.1416	0.2846	0.0040	0.43	0.1104	0.0022	0.1842
lp24-2b8	1662.7	20.67	1589.8	18.12	1776.3	29.66	1776.3	29.7	1.7	10.5	4.1424	0.1047	0.2797	0.0036	0.51	0.1086	0.0018	0.2349
05LP-024-2L1	1833.3	5.4	1821.8	3.6	1853.8	7.06	1853.8	7.1	0.4	1.7	5.0829	0.0323	0.3266	0.0007	0.36	0.1134	0.0004	0.1595
05LP-024-2L2	1867.8	8.97	1862.2	5.12	1876.7	9.6	1876.7	9.6	0.5	0.8	5.2935	0.0556	0.3349	0.0011	0.30	0.1148	0.0006	0.0517
05LP-024-2L3	1825.7	6	1814	3.82	1827	7.53	1827.0	7.5	0.4	0.7	5.0381	0.0357	0.3250	0.0008	0.34	0.1117	0.0005	0.1534
05LP-024-2L4	2647.1	8.85	2654.4	6.03	2677	6.88	2677.0	6.9	0.3	0.8	12.5577	0.1181	0.5095	0.0014	0.29	0.1826	0.0008	0.4125

Analyses in italics/shaded are excluded due to >10% error in critical age, >10% discordance, or >5% reverse discordance.
All errors are at the 1-sigma level, and include only random uncertainties.
Preferred age = $^{206}Pb/^{238}U$ ages for analyses younger than 1.0 Ga and $^{206}Pb/^{207}Pb$ ages for analyses older than 1.0 Ga.
Isotope ratios are corrected for Pb/U fractionation by comparison with standard zircons Plesovice and FC1.

Table I-2c. *(continued) Detrital zircon U-Pb geochronologic analyses – Pacific Centre for Isotopic and Geochemical Research – Sample 05LP024-2 in Unit* ***Ps****.*

Analysis No.	Age estimates with 1 sigma uncertainty (Ma)										Isotopic Ratios with absolute errors							
	$^{207}Pb/^{235}U$ Ma	$^{207}Pb/^{235}U$ ± 1σ Error	$^{206}Pb/^{238}U$ Ma	$^{206}Pb/^{238}U$ ± 1σ Error	$^{207}Pb/^{206}Pb$ Ma	$^{207}Pb/^{206}Pb$ ± 1σ Error	Preferred Age Ma	± 1σ Error	Error %	Discordancy %	$^{207}Pb/^{235}U$ Ratio	$^{207}Pb/^{235}U$ 1σ Error	$^{206}Pb/^{238}U$ Ratio	$^{206}Pb/^{238}U$ 1σ Error	Rho	$^{207}Pb/^{206}Pb$ Ratio	$^{207}Pb/^{206}Pb$ 1σ Error	Th/U Ratio
05LP-024-2L5	1858.9	5.37	1871	3.68	1868.8	7.05	1868.8	7.1	0.4	-0.1	5.2387	0.0330	0.3368	0.0008	0.36	0.1143	0.0005	0.2483
05LP-024-2L6	1917.3	5.49	1885.2	3.72	1960	6.97	1960.0	7.0	0.4	3.8	5.6078	0.0357	0.3397	0.0008	0.36	0.1203	0.0005	0.4532
05LP-024-2L7	1782.7	6.33	1758.6	3.91	1817.5	7.97	1817.5	8.0	0.4	3.2	4.7877	0.0361	0.3136	0.0008	0.34	0.1111	0.0005	0.2252
05LP-024-2L8	1837.2	8.16	1829.7	4.75	1851.6	9.2	1851.6	9.2	0.5	1.2	5.1065	0.0491	0.3282	0.0010	0.31	0.1132	0.0006	0.0722
05LP-024-2L9	2628.2	6.65	2610.5	5.03	2659.3	6.24	2659.3	6.2	0.2	1.8	12.3077	0.0871	0.4992	0.0012	0.33	0.1807	0.0007	0.1937
05LP-024-2L10	2802.4	6.63	2787.5	5.23	2839.3	6.03	2839.3	6.0	0.2	1.8	14.7985	0.1032	0.5410	0.0013	0.33	0.2016	0.0008	0.1065
05LP-024-2L11	1733.1	4.8	1675.7	3.24	1784.3	7.11	1784.3	7.1	0.4	6.1	4.5113	0.0260	0.2969	0.0007	0.38	0.1091	0.0004	0.1832
05LP-024-2L12	1845.3	5.84	1832.5	3.83	1863.7	7.54	1863.7	7.5	0.4	1.7	5.1558	0.0354	0.3288	0.0008	0.35	0.1140	0.0005	0.3852
05LP-024-2L13	1850.2	7.27	1843.4	4.43	1866.8	8.59	1866.8	8.6	0.5	1.3	5.1855	0.0443	0.3310	0.0009	0.32	0.1142	0.0005	0.1469
05LP-024-2L14	1824.7	8.56	1816.6	4.93	1827.7	9.73	1827.7	9.7	0.5	0.6	5.0319	0.0509	0.3255	0.0010	0.31	0.1117	0.0006	0.1769
05LP-024-2L15	1803.6	7.73	1785.2	4.53	1815.5	9.16	1815.5	9.2	0.5	1.7	4.9080	0.0450	0.3191	0.0009	0.32	0.1110	0.0006	0.1387
05LP-024-2L16	1879.4	5.94	1869	3.93	1881.9	7.63	1881.9	7.6	0.4	0.7	5.3655	0.0372	0.3363	0.0008	0.35	0.1151	0.0005	0.2124
05LP-024-2L17	2622.6	7.79	2615.9	5.62	2683.6	6.87	2683.6	6.9	0.3	2.5	12.2356	0.1015	0.5005	0.0013	0.32	0.1834	0.0008	0.1053
05LP-024-2L18	1814.3	6.53	1789.6	4.08	1848.7	8.28	1848.7	8.3	0.4	3.2	4.9702	0.0384	0.3200	0.0008	0.34	0.1130	0.0005	0.2548
05LP-024-2L19	1801.6	6.45	1791.3	4.06	1813.5	8.31	1813.5	8.3	0.5	1.2	4.8962	0.0375	0.3203	0.0008	0.34	0.1109	0.0005	0.0713
05LP-024-2L20	1934.4	6.04	1919.4	4.07	1994.6	7.62	1994.6	7.6	0.4	3.8	5.7201	0.0400	0.3468	0.0009	0.35	0.1226	0.0005	0.2026
																	68 zircons	

Analyses in italics/shaded are excluded due to >10% error in critical age, >10% discordance, or >5% reverse discordance.

All errors are at the 1-sigma level, and include only random uncertainties.

Preferred age = $^{206}Pb/^{238}U$ ages for analyses younger than 1.0 Ga and $^{206}Pb/^{207}Pb$ ages for analyses older than 1.0 Ga.

Isotope ratios are corrected for Pb/U fractionation by comparison with standard zircons Plesovice and FC1.

Table I-3a. *Detrital Zircon U-Pb geochronologic analyses – Pacific Centre for Isotopic and Geochemical Research – Sample 05LP025 in Unit* **Pa**.

Analysis No.	Age estimates with 1 sigma uncertainty (Ma)										Isotopic Ratios with absolute errors							
	$^{207}Pb/^{235}U$ Ma	$^{207}Pb/^{235}U$ ± 1σ Error	$^{206}Pb/^{238}U$ Ma	$^{206}Pb/^{238}U$ ± 1σ Error	$^{207}Pb/^{206}Pb$ Ma	$^{207}Pb/^{206}Pb$ ± 1σ Error	Preferred Age Ma*	± 1σ Error	Error %	Discordancy %	$^{207}Pb/^{235}U$ Ratio	$^{207}Pb/^{235}U$ 1σ Error	$^{206}Pb/^{238}U$ Ratio	$^{206}Pb/^{238}U$ 1σ Error	Rho	$^{207}Pb/^{206}Pb$ Ratio	$^{207}Pb/^{206}Pb$ 1σ Error	Th/U Ratio
251a	*1162.3*	*10.96*	*1045.3*	*4.94*	*1298*	*19.31*	*1298.0*	*19.3*	*1.5*	*19.5*	*2.1415*	*0.0339*	*0.1760*	*0.0009*	*0.32*	*0.0842*	*0.0008*	*0.13502*
251b	962.2	40.22	831.3	11.98	904.2	90.41	831.3	12.0	1.4	8.1	1.5795	0.1022	0.1376	0.0021	0.24	0.0692	0.0031	0.76006
251c	1429.5	31.66	1342.9	13.91	1373.8	42.52	1373.8	42.5	3.1	2.2	3.0872	0.1274	0.2316	0.0027	0.28	0.0876	0.0020	0.34439
251d	*1726.2*	*40.88*	*1505.8*	*17.94*	*1709.5*	*43.1*	*1709.5*	*43.1*	*2.5*	*11.9*	*4.4741*	*0.2204*	*0.2631*	*0.0035*	*0.27*	*0.1047*	*0.0025*	*0.11786*
251e	1818	46.54	1633.5	18.03	1661.1	41.82	1661.1	41.8	2.5	1.7	4.9923	0.2746	0.2884	0.0036	0.23	0.1020	0.0023	0.24909
251g	1883.6	48.88	1808.4	21.22	1807.2	42.13	1807.2	42.1	2.3	-0.1	5.3924	0.3077	0.3238	0.0044	0.24	0.1105	0.0026	0.14130
251h	1310.1	76.91	1340.4	30.6	1387.1	122.02	1387.1	122.0	8.8	3.4	2.6338	0.2753	0.2311	0.0058	0.24	0.0882	0.0058	0.63201
251i	*810.9*	*124.42*	*769.4*	*32.88*	*695.6*	*336.9*	*769.4*	*32.9*	*4.3*	*-11*	*1.2225*	*0.2724*	*0.1268*	*0.0058*	*0.20*	*0.0626*	*0.0110*	*0.29047*
251j	*1460.1*	*1938.82*	*1500*	*405.8*	*2577.6*	*1009*	*2577.6*	*1009.0*	*39.1*	*42*	*3.2121*	*8.0428*	*0.2620*	*0.0794*	*0.12*	*0.1720*	*0.1515*	*0.87240*
251k	1786.3	59.06	1640.7	24.54	1822.3	56.66	1822.3	56.7	3.1	10	4.8079	0.3378	0.2898	0.0049	0.24	0.1114	0.0036	0.46035
251l	1831	33.32	1746.8	15.4	1755.2	31.7	1755.2	31.7	1.8	0	5.0695	0.1992	0.3112	0.0031	0.26	0.1074	0.0019	0.47915
251m	1654.9	50.21	1361.5	18.9	1452.8	56.06	1452.8	56.1	3.9	6	4.1030	0.2523	0.2352	0.0036	0.25	0.0913	0.0027	0.40246
251n	*1036.3*	*72.94*	*844.8*	*25.29*	*1274.5*	*136.71*	*1274.5*	*136.7*	*10.7*	*34*	*1.7748*	*0.1993*	*0.1400*	*0.0045*	*0.28*	*0.0832*	*0.0061*	*0.24844*
251o	*1306.5*	*32.49*	*1108.2*	*11.35*	*1250.1*	*50.99*	*1250.1*	*51.0*	*4.1*	*11*	*2.6207*	*0.1159*	*0.1876*	*0.0021*	*0.25*	*0.0822*	*0.0022*	*0.15482*
251q	*1073.8*	*45.1*	*827.8*	*13.66*	*1144.4*	*85.5*	*827.8*	*13.7*	*1.7*	*28*	*1.8793*	*0.1279*	*0.1370*	*0.0024*	*0.26*	*0.0779*	*0.0035*	*0.43181*
251r	*1126.4*	*274.72*	*943.1*	*96*	*2297.9*	*386.37*	*943.1*	*96.0*	*10.2*	*59*	*2.0323*	*0.8204*	*0.1576*	*0.0172*	*0.27*	*0.1459*	*0.0376*	*0.41325*
252a	*1352.8*	*38.71*	*1163.3*	*14.79*	*1583*	*52.55*	*1583.0*	*52.6*	*3.3*	*27*	*2.7898*	*0.1445*	*0.1978*	*0.0028*	*0.27*	*0.0978*	*0.0028*	*0.18659*
252e	1099.2	7.4	1042.7	3.58	1111.1	14.32	1111.1	14.3	1.3	6	1.9521	0.0215	0.1756	0.0007	0.34	0.0766	0.0006	0.30228
252f	2666.2	20.21	2411.1	10.57	2631	12.07	2631.0	12.1	0.5	8	12.8156	0.2751	0.4536	0.0024	0.24	0.1776	0.0013	0.51121
252i	1677.4	89.94	1587.2	29.04	1628.4	79.4	1628.4	79.4	4.9	3	4.2172	0.4621	0.2792	0.0058	0.19	0.1002	0.0044	0.58438
252l	1780.2	54.22	1660.4	17.55	1670.9	45.57	1670.9	45.6	2.7	1	4.7733	0.3083	0.2938	0.0035	0.19	0.1026	0.0026	0.24257
252m	617.1	194.67	722.2	41.06	701.6	662.06	722.2	41.1	5.7	-3	0.8362	0.3521	0.1186	0.0071	0.14	0.0628	0.0243	0.45520
252n	1191.8	128.55	983.2	26.18	1054.8	227.66	983.2	26.2	2.7	7	2.2342	0.4095	0.1648	0.0047	0.16	0.0745	0.0091	0.24528
252o	*2335.3*	*566.95*	*1257.6*	*52.98*	*1814.1*	*171.44*	*1814.1*	*171.4*	*9.5*	*31*	*8.9737*	*5.5690*	*0.2154*	*0.0100*	*0.07*	*0.1109*	*0.0111*	*0.60673*
252q	*891.6*	*281.16*	*703.1*	*58.56*	*1285.4*	*588.68*	*703.1*	*58.6*	*8.3*	*45*	*1.4062*	*0.6663*	*0.1152*	*0.0101*	*0.19*	*0.0837*	*0.0309*	*0.30510*
252r	1128.7	14.57	1010.4	6.03	1109.9	27.1	1109.9	27.1	2.4	9	2.0391	0.0436	0.1697	0.0011	0.30	0.0766	0.0011	0.15625
252s	*1184.1*	*11.05*	*952.3*	*4.75*	*1550.4*	*18.79*	*952.3*	*4.8*	*0.5*	*39*	*2.2096*	*0.0349*	*0.1592*	*0.0009*	*0.34*	*0.0961*	*0.0010*	*0.50165*
25a	*1101.9*	*43.59*	*887.8*	*15.08*	*1100*	*82.37*	*887.8*	*15.1*	*1.7*	*19*	*1.9600*	*0.1271*	*0.1477*	*0.0027*	*0.28*	*0.0762*	*0.0032*	*0.18992*
25b	*1231.1*	*54.2*	*1067*	*19.84*	*1438.9*	*90.45*	*1438.9*	*90.5*	*6.3*	*26*	*2.3617*	*0.1795*	*0.1800*	*0.0036*	*0.27*	*0.0906*	*0.0044*	*0.22579*
25c	*1378*	*117.66*	*981.4*	*25.84*	*1215.5*	*148.36*	*981.4*	*25.8*	*2.6*	*19*	*2.8849*	*0.4502*	*0.1644*	*0.0047*	*0.18*	*0.0808*	*0.0064*	*0.24268*
25d	*898.7*	*10.65*	*796.2*	*4.4*	*1047*	*25.3*	*796.2*	*4.4*	*0.6*	*24*	*1.4232*	*0.0254*	*0.1315*	*0.0008*	*0.33*	*0.0742*	*0.0009*	*0.02803*

Analyses in italics/shaded are excluded due to >10% error in critical age, >10% discordance, or >5% reverse discordance.
All errors are at the 1-sigma level, and include only random uncertainties.
Best age = $^{206}Pb/^{238}U$ ages for analyses younger than 1.0 Ga and $^{206}Pb/^{207}Pb$ ages for analyses older than 1.0 Ga.
Isotope ratios are corrected for Pb/U fractionation by comparison with standard zircons Plesovice and FC1.

Table I-3a. *(continued) Detrital Zircon U-Pb geochronologic analyses – Pacific Centre for Isotopic and Geochemical Research – Sample 05LP025 in Unit* ***Pa****.*

Analysis No.	Age estimates with 1 sigma uncertainty (Ma)										Isotopic Ratios with absolute errors							
	$^{207}Pb/^{235}U$ Ma	$^{207}Pb/^{235}U$ ± 1σ Error	$^{206}Pb/^{238}U$ Ma	$^{206}Pb/^{238}U$ ± 1σ Error	$^{207}Pb/^{206}Pb$ Ma	$^{207}Pb/^{206}Pb$ ± 1σ Error	Preferred Age Ma*	± 1σ Error	Error %	Discordancy %	$^{207}Pb/^{235}U$ Ratio	$^{207}Pb/^{235}U$ 1σ Error	$^{206}Pb/^{238}U$ Ratio	$^{206}Pb/^{238}U$ 1σ Error	Rho	$^{207}Pb/^{206}Pb$ Ratio	$^{207}Pb/^{206}Pb$ 1σ Error	Th/U Ratio
25e	1725.3	22.45	1607	9.69	1631	23.77	1631.0	23.8	1.5	1	4.4696	0.1209	0.2831	0.0019	0.25	0.1004	0.0013	0.30595
25f	2524.3	120.81	2314.9	37.08	2422.4	52.45	2422.4	52.5	2.2	4	11.0143	1.4295	0.4320	0.0082	0.15	0.1569	0.0049	0.25912
25g	1102.3	11.7	1044.9	5.24	1056.1	22.77	1056.1	22.8	2.2	1	1.9614	0.0341	0.1760	0.0010	0.31	0.0746	0.0008	0.53836
25h	*1129.2*	*159.89*	*1295.3*	*47.94*	*1117.5*	*277.84*	*1117.5*	*277.8*	*24.9*	*-16*	*2.0406*	*0.4788*	*0.2225*	*0.0091*	*0.17*	*0.0769*	*0.0117*	*0.47465*
25i	*1497.6*	*88.3*	*1297.5*	*31.45*	*1924.4*	*100.52*	*1924.4*	*100.5*	*5.2*	*33*	*3.3708*	*0.3801*	*0.2230*	*0.0060*	*0.24*	*0.1179*	*0.0068*	*0.40043*
25j	*1249.7*	*127.93*	*1088.3*	*39.83*	*939.8*	*192.08*	*939.8*	*192.1*	*20.4*	*-16*	*2.4239*	*0.4314*	*0.1839*	*0.0073*	*0.22*	*0.0704*	*0.0070*	*0.38358*
25k	1705.1	76.87	1667.5	30.55	1751.3	72.08	1751.3	72.1	4.1	5	4.3616	0.4059	0.2952	0.0061	0.22	0.1071	0.0043	0.24198
25l	*1590.4*	*135.75*	*1312.6*	*29.78*	*1486.3*	*125.46*	*1486.3*	*125.5*	*8.4*	*12*	*3.7889*	*0.6402*	*0.2258*	*0.0057*	*0.15*	*0.0929*	*0.0064*	*0.19475*
25m	*898.7*	*362.97*	*1059.3*	*121.4*	*946.7*	*779.45*	*946.7*	*779.5*	*82.3*	*-12*	*1.4233*	*0.8663*	*0.1786*	*0.0222*	*0.20*	*0.0706*	*0.0351*	*0.31138*
25n	*1285.5*	*249.36*	*1153*	*58.07*	*1034.9*	*336.77*	*1034.9*	*336.8*	*32.5*	*-11*	*2.5467*	*0.8710*	*0.1959*	*0.0108*	*0.16*	*0.0738*	*0.0138*	*0.47508*
25o	*1514.7*	*109.84*	*1188.5*	*40.46*	*1724.9*	*128.49*	*1724.9*	*128.5*	*7.4*	*31*	*3.4450*	*0.4809*	*0.2025*	*0.0076*	*0.27*	*0.1056*	*0.0077*	*0.67377*
25p	*1423.3*	*182.88*	*916.2*	*45.38*	*1608.7*	*208.89*	*916.2*	*45.4*	*5.0*	*43*	*3.0623*	*0.7317*	*0.1527*	*0.0081*	*0.22*	*0.0992*	*0.0119*	*0.49318*
25q	*1306.3*	*102.51*	*1193*	*27.75*	*1192.5*	*147.18*	*1192.5*	*147.2*	*12.3*	*0*	*2.6202*	*0.3655*	*0.2033*	*0.0052*	*0.18*	*0.0798*	*0.0063*	*0.88569*
25r	*995.8*	*21.61*	*955.4*	*8.86*	*1129.5*	*45.66*	*955.4*	*8.9*	*0.9*	*15*	*1.6664*	*0.0568*	*0.1598*	*0.0016*	*0.29*	*0.0773*	*0.0018*	*0.13797*
25s	*2484.8*	*523.61*	*1692.1*	*45.61*	*1584.5*	*147.32*	*1584.5*	*147.3*	*9.3*	*-7*	*10.5559*	*5.9591*	*0.3002*	*0.0092*	*0.05*	*0.0979*	*0.0081*	*0.40028*
25t	*1677.4*	*263.06*	*1037*	*48.58*	*1060.1*	*247.17*	*1060.1*	*247.2*	*23.3*	*2*	*4.2173*	*1.3517*	*0.1745*	*0.0089*	*0.16*	*0.0747*	*0.0100*	*0.43320*
25u	1329.6	31.47	1190.4	11.57	1264.7	45.85	1264.7	45.9	3.6	6	2.7040	0.1148	0.2028	0.0022	0.25	0.0828	0.0020	0.52391
25v	*1678.6*	*511.78*	*1216.3*	*61.81*	*996*	*412.69*	*996.0*	*412.7*	*41.4*	*-22*	*4.2236*	*2.6328*	*0.2077*	*0.0116*	*0.09*	*0.0724*	*0.0169*	*0.23602*
25w	*1248.8*	*260.6*	*1168.2*	*74.57*	*1134.6*	*406.5*	*1134.6*	*406.5*	*35.8*	*-3*	*2.4208*	*0.8780*	*0.1987*	*0.0139*	*0.19*	*0.0775*	*0.0181*	*0.38667*
25x	1076.5	21.01	1027.6	8.99	1014.3	40.89	1014.3	40.9	4.0	-1	1.8870	0.0597	0.1728	0.0016	0.30	0.0730	0.0015	0.17469
25y	*1770.5*	*22.28*	*1741.9*	*11.04*	*1627*	*23.63*	*1627.0*	*23.6*	*1.5*	*-7*	*4.7181*	*0.1255*	*0.3103*	*0.0022*	*0.27*	*0.1002*	*0.0013*	*0.22520*
25z	*1508.8*	*183.35*	*1219.8*	*42.34*	*1526.8*	*171.48*	*1526.8*	*171.5*	*11.2*	*20*	*3.4191*	*0.7980*	*0.2083*	*0.0079*	*0.16*	*0.0949*	*0.0092*	*0.32911*
25aa	*1192.2*	*79.23*	*859.2*	*17.85*	*1198.2*	*119.35*	*859.2*	*17.9*	*2.1*	*28*	*2.2354*	*0.2525*	*0.1426*	*0.0032*	*0.20*	*0.0801*	*0.0050*	*0.25199*
05LP025L1	1926.8	5.65	1961.4	3.74	1880.7	6.95	1880.7	7.0	0.4	-4.3	5.6698	0.0371	0.3556	0.0008	0.34	0.1151	0.0004	0.39826
05LP025L2	1399.5	4.8	1392.3	2.82	1412.7	8.06	1412.7	8.1	0.6	1.4	2.9682	0.0188	0.2411	0.0005	0.35	0.0894	0.0004	0.07482
05LP025L3	1093.4	3.39	1102.2	2.03	1066	7.84	1066.0	7.8	0.7	-3.4	1.9354	0.0098	0.1865	0.0004	0.39	0.0749	0.0003	0.00056
05LP025L4	1035.2	3.81	1053.7	2.14	1018.3	8.86	1018.3	8.9	0.9	-3.5	1.7719	0.0104	0.1776	0.0004	0.37	0.0732	0.0003	0.12798
05LP025L5	1496.6	5.9	1498.3	3.38	1488.4	8.82	1488.4	8.8	0.6	-0.7	3.3663	0.0254	0.2617	0.0007	0.33	0.0930	0.0004	0.16737
05LP025L6	1302.5	5.6	1322.1	3.12	1317.5	9.65	1317.5	9.7	0.7	-0.3	2.6067	0.0199	0.2276	0.0006	0.35	0.0851	0.0004	0.10351
05LP025L7	1202.8	4.53	1175.3	2.5	1233.7	8.82	1233.7	8.8	0.7	4.7	2.2694	0.0146	0.2000	0.0005	0.37	0.0815	0.0004	0.34766
05LP025L8	1568.9	4.35	1569.6	2.86	1599.1	7.01	1599.1	7.0	0.4	1.8	3.6885	0.0201	0.2757	0.0006	0.38	0.0987	0.0004	0.22937
05LP025L9	1894.2	6.1	1924	3.96	1908.3	7.37	1908.3	7.4	0.4	-0.8	5.4591	0.0388	0.3478	0.0008	0.34	0.1168	0.0005	0.13351

Analyses in italics/shaded are excluded due to >10% error in critical age, >10% discordance, or >5% reverse discordance.

All errors are at the 1-sigma level, and include only random uncertainties.

Best age = $^{206}Pb/^{238}U$ ages for analyses younger than 1.0 Ga and $^{206}Pb/^{207}Pb$ ages for analyses older than 1.0 Ga.

Isotope ratios are corrected for Pb/U fractionation by comparison with standard zircons Plesovice and FC1.

Table I-3a. *(continued) Detrital Zircon U-Pb geochronologic analyses – Pacific Centre for Isotopic and Geochemical Research – Sample 05LP025 in Unit* ***Pa****.*

Analysis No.	Age estimates with 1 sigma uncertainty (Ma)										Isotopic Ratios with absolute errors							
	$^{207}Pb/^{235}U$ Ma	$^{207}Pb/^{235}U$ ± 1σ Error	$^{206}Pb/^{238}U$ Ma	$^{206}Pb/^{238}U$ ± 1σ Error	$^{207}Pb/^{206}Pb$ Ma	$^{207}Pb/^{206}Pb$ ± 1σ Error	Preferred Age Ma*	± 1σ Error	Error %	Discordancy %	$^{207}Pb/^{235}U$ Ratio	$^{207}Pb/^{235}U$ 1σ Error	$^{206}Pb/^{238}U$ Ratio	$^{206}Pb/^{238}U$ 1σ Error	Rho	$^{207}Pb/^{206}Pb$ Ratio	$^{207}Pb/^{206}Pb$ 1σ Error	Th/U Ratio
05LP025L10	1392.7	7.37	1393.7	3.92	1393.7	11.22	1393.7	11.2	0.8	0.0	2.9417	0.0286	0.2414	0.0008	0.32	0.0885	0.0005	0.23876
05LP025L12	1841.2	14.33	1831.2	7.73	1861.1	14.43	1861.1	14.4	0.8	1.6	5.1309	0.0866	0.3285	0.0016	0.29	0.1138	0.0009	0.26987
05LP025L13	1142.4	5.8	1139.7	3	1131.7	11.36	1131.7	11.4	1.0	-0.7	2.0805	0.0176	0.1934	0.0006	0.34	0.0774	0.0004	0.16009
05LP025L14	1500	6.53	1511.4	3.69	1466.9	9.57	1466.9	9.6	0.7	-3.0	3.3809	0.0282	0.2642	0.0007	0.33	0.0920	0.0005	0.25893
05LP025L15	1463.8	5.46	1507.7	3.28	1438	8.61	1438.0	8.6	0.6	-4.8	3.2276	0.0227	0.2635	0.0006	0.35	0.0906	0.0004	0.19654
05LP025L16	1171.4	5.67	1165.5	2.98	1168.7	10.89	1168.7	10.9	0.9	0.3	2.1699	0.0177	0.1982	0.0006	0.34	0.0789	0.0004	0.25781
05LP025L17	1400.9	6.49	1383.4	3.53	1402.7	10.16	1402.7	10.2	0.7	1.4	2.9736	0.0254	0.2394	0.0007	0.33	0.0889	0.0005	0.18640
05LP025L18	1311.1	4.92	1321	2.86	1306.5	8.85	1306.5	8.9	0.7	-1.1	2.6373	0.0176	0.2274	0.0006	0.36	0.0846	0.0004	0.20412
05LP025L19	1081.6	4.75	1081.3	2.55	1091.1	10.2	1091.1	10.2	0.9	0.9	1.9013	0.0136	0.1826	0.0005	0.36	0.0759	0.0004	0.45991
05LP025L20	1809.5	4.98	1810.4	3.41	1827.8	7.01	1827.8	7.0	0.4	1.0	4.9421	0.0291	0.3242	0.0007	0.37	0.1117	0.0004	0.17004
05LP025L21	1823.1	11.41	1825	6.41	1848.1	12.29	1848.1	12.3	0.7	1.2	5.0226	0.0677	0.3272	0.0013	0.30	0.1130	0.0008	0.33928
05LP025L22	1361	4.36	1359.4	2.7	1379.9	7.97	1379.9	8.0	0.6	1.5	2.8207	0.0164	0.2348	0.0005	0.38	0.0879	0.0004	0.11260
05LP025L23	1127.3	4.51	1125.9	2.5	1123.7	9.51	1123.7	9.5	0.8	-0.2	2.0349	0.0135	0.1908	0.0005	0.36	0.0771	0.0004	0.11991
																	43 zircons	

Analyses in italics/shaded are excluded due to >10% error in critical age, >10% discordance, or >5% reverse discordance.
All errors are at the 1-sigma level, and include only random uncertainties.
Best age = $^{206}Pb/^{238}U$ ages for analyses younger than 1.0 Ga and $^{206}Pb/^{207}Pb$ ages for analyses older than 1.0 Ga.
Isotope ratios are corrected for Pb/U fractionation by comparison with standard zircons Plesovice and FC1.

Table I-3b. *Detrital Zircon U-Pb geochronologic analyses – Pacific Centre for Isotopic and Geochemical Research – Sample 05LP026 in Unit* ***Pa****.*

Analysis No.	Age estimates with 1 sigma uncertainty (Ma)										Isotopic Ratios with absolute errors							
	$^{207}Pb/^{235}U$ Ma	$^{207}Pb/^{235}U$ ± 1σ Error	$^{206}Pb/^{238}U$ Ma	$^{206}Pb/^{238}U$ ± 1σ Error	$^{207}Pb/^{206}Pb$ Ma	$^{207}Pb/^{206}Pb$ ± 1σ Error	Preferred Age Ma*	± 1σ Error	Error %	Discordancy %	$^{207}Pb/^{235}U$ Ratio	$^{207}Pb/^{235}U$ 1σ Error	$^{206}Pb/^{238}U$ Ratio	$^{206}Pb/^{238}U$ 1σ Error	Rho	$^{207}Pb/^{206}Pb$ Ratio	$^{207}Pb/^{206}Pb$ 1σ Error	Th/U Ratio
05LP026 1	1752.9	16.56	1756.7	15.61	1806.4	23.78	1806.4	23.8	1.3	2.8	4.6200	0.0917	0.3133	0.0032	0.51	0.1104	0.0015	0.14976
05LP026 2	1722	17.25	1716.1	15.59	1847.8	24.38	1847.8	24.4	1.3	7.1	4.4515	0.0926	0.3050	0.0032	0.50	0.1130	0.0015	0.17297
05LP026 3	1287.3	12.55	1275.3	11.5	1376.1	25.23	1376.1	25.2	1.8	7.3	2.5531	0.0439	0.2188	0.0022	0.58	0.0877	0.0012	0.27034
05LP026 4	1819.7	20.66	1792.3	16.86	1877.7	25.9	1877.7	25.9	1.4	4.5	5.0024	0.1222	0.3205	0.0035	0.44	0.1149	0.0017	0.41565
05LP026 5	1746.2	15.29	1750.5	15.3	1824.4	22.9	1824.4	22.9	1.3	4.1	4.5829	0.0841	0.3120	0.0031	0.54	0.1115	0.0014	0.25996
05LP026 6	1422.1	25.47	1401.4	15.84	1475.2	37.37	1475.2	37.4	2.5	5.0	3.0576	0.1018	0.2428	0.0031	0.38	0.0924	0.0018	0.19517
05LP026 7	1074.6	9.84	1080.4	9.61	1099.9	25	1099.9	25.0	2.3	1.8	1.8816	0.0279	0.1825	0.0018	0.65	0.0762	0.0010	0.03780
05LP026 8	1326.9	32.18	1257.4	17.03	1317.2	49.85	1317.2	49.9	3.8	4.5	2.6942	0.1171	0.2154	0.0032	0.34	0.0851	0.0022	0.16994
05LP026 9	1130.8	28.59	1114.3	15.37	1163.6	52.98	1163.6	53.0	4.6	4.2	2.0456	0.0858	0.1887	0.0028	0.36	0.0787	0.0021	0.17604
05LP026 11	*1083.4*	*26.85*	*1017.6*	*14.01*	*1210*	*51.94*	*1210.0*	*51.9*	*4.3*	*15.9*	*1.9066*	*0.0769*	*0.1710*	*0.0025*	*0.37*	*0.0805*	*0.0022*	*0.18601*
05LP026 12	1291.2	11.39	1278.9	11.3	1325.8	24.15	1325.8	24.2	1.8	3.5	2.5667	0.0400	0.2194	0.0021	0.63	0.0855	0.0011	0.14923
05LP026 13	2432.1	20.1	2490.1	21.28	2528.6	20.79	2528.6	20.8	0.8	1.5	9.9707	0.2172	0.4715	0.0049	0.47	0.1671	0.0021	0.25808
05LP026 14	1110.9	17.48	1089.9	11.47	1146.9	35.68	1146.9	35.7	3.1	5.0	1.9863	0.0514	0.1842	0.0021	0.44	0.0780	0.0014	0.43110
05LP026 15	3278.9	21.67	3210.8	25.73	3375.4	18.05	3375.4	18.1	0.5	4.9	24.2588	0.5390	0.6456	0.0066	0.46	0.2822	0.0033	0.31858
05LP026 16	1689.4	17.38	1676.9	15.39	1757.5	24.92	1757.5	24.9	1.4	4.6	4.2795	0.0904	0.2971	0.0031	0.49	0.1075	0.0015	0.24544
05LP026 17	1077.7	19.96	1122.4	12.73	1150.1	40.63	1150.1	40.6	3.5	2.4	1.8904	0.0568	0.1902	0.0024	0.41	0.0781	0.0016	0.41354
05LP026 18	1351.4	15.03	1362	12.82	1456.9	27.06	1456.9	27.1	1.9	6.5	2.7844	0.0560	0.2353	0.0025	0.52	0.0915	0.0013	0.24891
05LP026 19	*1238.7*	*41.62*	*1222.6*	*21.48*	*1388.4*	*66.39*	*1388.4*	*66.4*	*4.8*	*11.9*	*2.3868*	*0.1388*	*0.2088*	*0.0040*	*0.33*	*0.0883*	*0.0031*	*0.01196*
05LP026 20	1800.3	20.16	1808.3	16.96	1847.3	25.69	1847.3	25.7	1.4	2.1	4.8885	0.1169	0.3238	0.0035	0.45	0.1130	0.0016	0.19096
05LP026 21	1561.5	18.37	1561.6	14.99	1615.4	27.5	1615.4	27.5	1.7	3.3	3.6548	0.0842	0.2741	0.0030	0.47	0.0995	0.0015	0.43829
05LP026 22	2637.5	24.6	2645.5	23.53	2670.5	21.55	2670.5	21.6	0.8	0.9	12.4301	0.3254	0.5074	0.0055	0.41	0.1819	0.0024	0.28001
05LP026 23	1219.1	14.08	1198.1	11.43	1332.9	28.1	1332.9	28.1	2.1	10.1	2.3224	0.0461	0.2043	0.0021	0.53	0.0858	0.0013	0.17509
05LP026 24	993.7	11.78	1027.9	9.82	1046.2	29.33	1046.2	29.3	2.8	1.7	1.6609	0.0309	0.1729	0.0018	0.56	0.0742	0.0011	0.01501
05LP026 25	1187.6	14.94	1173.3	11.48	1230.7	30.25	1230.7	30.3	2.5	4.7	2.2206	0.0474	0.1996	0.0021	0.50	0.0814	0.0013	0.21519
05LP026 26	1394.9	24.6	1411.1	16.19	1533	36.96	1533.0	37.0	2.4	8.0	2.9501	0.0957	0.2447	0.0031	0.39	0.0953	0.0019	0.36617
05LP026 27	1789.8	27.67	1780.8	19.37	1890.4	31.81	1890.4	31.8	1.7	5.8	4.8280	0.1588	0.3182	0.0040	0.38	0.1157	0.0021	0.34130
05LP026 28	1678.5	102.98	1848	53.24	1960.4	96.6	1960.4	96.6	4.9	5.7	4.2231	0.5298	0.3320	0.0110	0.26	0.1203	0.0067	0.21853
05LP026 29	1297.8	41.05	1305.5	21.49	1397.8	61.41	1397.8	61.4	4.4	6.6	2.5898	0.1451	0.2245	0.0041	0.32	0.0887	0.0029	0.20301
05LP026 30	2724.4	33.05	2709.3	26.37	2667.4	24.13	2667.4	24.1	0.9	-1.6	13.6303	0.4762	0.5224	0.0062	0.34	0.1816	0.0027	0.70636
05LP026 31	2494.2	34.01	2439.2	25.57	2631.8	26.25	2631.8	26.3	1.0	7.3	10.6632	0.3906	0.4599	0.0058	0.34	0.1777	0.0028	0.01674
05LP026 32	1240.7	28.22	1302.1	16.62	1235.8	47.05	1235.8	47.1	3.8	-5.4	2.3937	0.0943	0.2238	0.0032	0.36	0.0816	0.0020	0.33003
05LP026 33	1214.4	47.35	1200	23.08	1246.4	77.12	1246.4	77.1	6.2	3.7	2.3069	0.1542	0.2046	0.0043	0.32	0.0820	0.0033	0.18773

Analyses in italics/shaded are excluded due to >10% error in critical age, >10% discordance, or >5% reverse discordance.

All errors are at the 1-sigma level, and include only random uncertainties.

Best age = $^{206}Pb/^{238}U$ ages for analyses younger than 1.0 Ga and $^{206}Pb/^{207}Pb$ ages for analyses older than 1.0 Ga.

Isotope ratios are corrected for Pb/U fractionation by comparison with standard zircons Plesovice and FC1.

Table I-3b. *(continued) Detrital Zircon U-Pb geochronologic analyses – Pacific Centre for Isotopic and Geochemical Research – Sample 05LP026 in Unit* ***Pa****.*

Analysis No.	Age estimates with 1 sigma uncertainty (Ma)										Isotopic Ratios with absolute errors							
	$^{207}Pb/^{235}U$ Ma	$^{207}Pb/^{235}U$ ± 1σ Error	$^{206}Pb/^{238}U$ Ma	$^{206}Pb/^{238}U$ ± 1σ Error	$^{207}Pb/^{206}Pb$ Ma	$^{207}Pb/^{206}Pb$ ± 1σ Error	Preferred Age Ma*	± 1σ Error	Error %	Discordancy %	$^{207}Pb/^{235}U$ Ratio	$^{207}Pb/^{235}U$ 1σ Error	$^{206}Pb/^{238}U$ Ratio	$^{206}Pb/^{238}U$ 1σ Error	Rho	$^{207}Pb/^{206}Pb$ Ratio	$^{207}Pb/^{206}Pb$ 1σ Error	Th/U Ratio
05LP026 34	1376.3	48.62	1398.5	24.84	1410	68.74	1410.0	68.7	4.9	0.8	2.8786	0.1857	0.2423	0.0048	0.31	0.0893	0.0033	0.33258
05LP026 35	1448.6	70.46	1474.8	34.61	1487.1	89.65	1487.1	89.7	6.0	0.8	3.1647	0.2890	0.2571	0.0068	0.29	0.0930	0.0045	0.36406
05LP026 36	1409.6	85.8	1364.7	38.71	1388.2	113.62	1388.2	113.6	8.2	1.7	3.0077	0.3386	0.2358	0.0074	0.28	0.0883	0.0054	0.85064
05LP026 37	1456.7	58.27	1477.6	27.89	1412.1	75.21	1412.1	75.2	5.3	-4.6	3.1982	0.2409	0.2576	0.0054	0.28	0.0894	0.0036	0.37687
05LP026 38	986.6	21.5	945.7	11.75	990.9	48.03	945.7	11.8	1.2	4.6	1.6423	0.0559	0.1580	0.0021	0.39	0.0722	0.0017	0.15460
05LP026 39	*821.8*	*34.18*	*810.9*	*15.33*	*714.3*	*90.91*	*810.9*	*15.3*	*1.9*	*-13.5*	*1.2464*	*0.0756*	*0.1340*	*0.0027*	*0.33*	*0.0632*	*0.0028*	*0.35465*
05LP026 40	*1008.8*	*55.41*	*1107*	*26.93*	*1044.8*	*111.45*	*1044.8*	*111.5*	*10.7*	*-6.0*	*1.7008*	*0.1474*	*0.1873*	*0.0050*	*0.31*	*0.0741*	*0.0043*	*0.35417*
05LP026 41	*520.8*	*203.9*	*895.6*	*102.29*	*918.2*	*761.89*	*895.6*	*102.3*	*11.4*	*2.5*	*0.6701*	*0.3354*	*0.1490*	*0.0182*	*0.24*	*0.0697*	*0.0334*	*0.61079*
05LP026 42	*1310.5*	*176.47*	*1264.9*	*66.34*	*1266.2*	*249.15*	*1266.2*	*249.2*	*19.7*	*0.1*	*2.6353*	*0.6318*	*0.2168*	*0.0125*	*0.24*	*0.0829*	*0.0115*	*0.27128*
05LP026 43	*1304.3*	*213.53*	*1160.1*	*65.57*	*652.3*	*304.81*	*652.3*	*304.8*	*46.7*	*-77.8*	*2.6130*	*0.7598*	*0.1972*	*0.0122*	*0.21*	*0.0614*	*0.0096*	*0.18029*
05LP026 44	1710.4	71.12	1646.7	33.22	1682.4	72.63	1682.4	72.6	4.3	2.1	4.3899	0.3775	0.2910	0.0067	0.27	0.1032	0.0042	0.47531
05LP026 45	888.2	42.9	907.7	20.31	912.4	101.53	907.7	20.3	2.2	0.5	1.3983	0.1013	0.1512	0.0036	0.33	0.0695	0.0035	0.11813
05LP026 46	*1140*	*167.62*	*1140.7*	*61.06*	*1377.8*	*285.47*	*1377.8*	*285.5*	*20.7*	*17.2*	*2.0731*	*0.5073*	*0.1936*	*0.0113*	*0.24*	*0.0878*	*0.0144*	*1.21273*
05LP026 47	1229.9	69.58	1251.6	34.26	1351.1	109.23	1351.1	109.2	8.1	7.4	2.3577	0.2301	0.2143	0.0065	0.31	0.0866	0.0051	0.74026
05LP026 48	*1083.1*	*52.95*	*1035.8*	*24.1*	*1459.7*	*93.25*	*1035.8*	*24.1*	*2.3*	*29.0*	*1.9057*	*0.1515*	*0.1743*	*0.0044*	*0.32*	*0.0916*	*0.0046*	*0.83863*
05LP026 49	*1247.9*	*95.74*	*1081.6*	*34.32*	*1151.6*	*138.06*	*1151.6*	*138.1*	*12.0*	*6.1*	*2.4178*	*0.3223*	*0.1827*	*0.0063*	*0.26*	*0.0782*	*0.0057*	*0.35340*
05LP026 50	1328.9	56.82	1369.8	26.87	1315.7	80.14	1315.7	80.1	6.1	-4.1	2.7018	0.2072	0.2368	0.0052	0.28	0.0850	0.0036	0.17465
05LP026 51	2458.1	41.69	2397.1	27.78	2380.9	31.37	2380.9	31.4	1.3	-0.7	10.2550	0.4621	0.4504	0.0063	0.31	0.1531	0.0029	0.34177
05LP026 52	1833.2	59.03	1864.5	32.26	1898.2	58.22	1898.2	58.2	3.1	1.8	5.0828	0.3536	0.3354	0.0067	0.29	0.1162	0.0038	0.31647
05LP026 53	794.2	75.23	654	25.53	676.4	199.26	654.0	25.5	3.9	3.3	1.1863	0.1620	0.1068	0.0044	0.30	0.0621	0.0062	0.50091
05LP026 54	*1303.1*	*85.34*	*1016.2*	*27.91*	*1267.9*	*115.39*	*1016.2*	*27.9*	*2.7*	*19.9*	*2.6086*	*0.3033*	*0.1707*	*0.0051*	*0.26*	*0.0830*	*0.0051*	*0.14419*
05LP026 55	1720.9	28.77	1742.8	19.59	1684.1	34.82	1684.1	34.8	2.1	-3.5	4.4459	0.1543	0.3104	0.0040	0.37	0.1033	0.0020	0.23642
05LP026 56	*1405.3*	*149.56*	*1359.9*	*65.51*	*1438.9*	*194.5*	*1438.9*	*194.5*	*13.5*	*5.5*	*2.9909*	*0.5878*	*0.2349*	*0.0126*	*0.27*	*0.0906*	*0.0099*	*0.17387*
05LP026 57	*1078.7*	*182.83*	*1155.3*	*73.39*	*993.3*	*334.68*	*993.3*	*334.7*	*33.7*	*-16.3*	*1.8932*	*0.5210*	*0.1963*	*0.0136*	*0.25*	*0.0723*	*0.0133*	*0.16638*
05LP026 58	*1868.1*	*122.47*	*1875*	*55.31*	*1741*	*106.52*	*1741.0*	*106.5*	*6.1*	*-7.7*	*5.2952*	*0.7593*	*0.3376*	*0.0115*	*0.24*	*0.1065*	*0.0064*	*0.62887*
05LP026 59	2722.3	124.64	2749	59.56	2640.3	58.63	2640.3	58.6	2.2	-4.1	13.6006	1.7923	0.5318	0.0142	0.20	0.1786	0.0064	0.36509
05LP026 60	1590.7	77.81	1508.7	33.89	1557.6	86.71	1557.6	86.7	5.6	3.1	3.7903	0.3671	0.2637	0.0066	0.26	0.0965	0.0046	0.72675
2605LP026	1120.6	230.61	993.8	69.39	992	389.69	993.8	69.4	7.0	-0.2	2.0150	0.6848	0.1667	0.0126	0.22	0.0722	0.0158	0.25581
05LP026 62	*1071.6*	*65.8*	*1099*	*29.5*	*1086.2*	*128.34*	*1086.2*	*128.3*	*11.8*	*-1.2*	*1.8731*	*0.1862*	*0.1859*	*0.0054*	*0.29*	*0.0757*	*0.0051*	*0.27310*
05LP026 63	*1121.3*	*132.35*	*1086.2*	*40.35*	*1022.7*	*235.88*	*1022.7*	*235.9*	*23.1*	*-6.2*	*2.0171*	*0.3933*	*0.1835*	*0.0074*	*0.21*	*0.0733*	*0.0092*	*0.42735*
05LP026 64	*1509.8*	*169.56*	*1223.5*	*51.01*	*1297.9*	*187.24*	*1297.9*	*187.2*	*14.4*	*5.7*	*3.4234*	*0.7387*	*0.2090*	*0.0096*	*0.21*	*0.0842*	*0.0086*	*0.34980*

Analyses in italics/shaded are excluded due to >10% error in critical age, >10% discordance, or >5% reverse discordance.

All errors are at the 1-sigma level, and include only random uncertainties.

Best age = $^{206}Pb/^{238}U$ ages for analyses younger than 1.0 Ga and $^{206}Pb/^{207}Pb$ ages for analyses older than 1.0 Ga.

Isotope ratios are corrected for Pb/U fractionation by comparison with standard zircons Plesovice and FC1.

Table I-3b. *(continued) Detrital Zircon U-Pb geochronologic analyses – Pacific Centre for Isotopic and Geochemical Research – Sample 05LP026 in Unit* ***Pa****.*

Analysis No.	Age estimates with 1 sigma uncertainty (Ma)										Isotopic Ratios with absolute errors							
	$^{207}Pb/^{235}U$ Ma	$^{207}Pb/^{235}U$ ± 1σ Error	$^{206}Pb/^{238}U$ Ma	$^{206}Pb/^{238}U$ ± 1σ Error	$^{207}Pb/^{206}Pb$ Ma	$^{207}Pb/^{206}Pb$ ± 1σ Error	Preferred Age Ma*	± 1σ Error	Error %	Discordancy %	$^{207}Pb/^{235}U$ Ratio	$^{207}Pb/^{235}U$ 1σ Error	$^{206}Pb/^{238}U$ Ratio	$^{206}Pb/^{238}U$ 1σ Error	Rho	$^{207}Pb/^{206}Pb$ Ratio	$^{207}Pb/^{206}Pb$ 1σ Error	Th/U Ratio
05LP026 65	1959.3	143.9	2018.5	64.53	1952.4	113.31	1952.4	113.3	5.8	-3.4	5.8868	0.9760	0.3677	0.0137	0.22	0.1197	0.0079	0.83391
05LP-026L5	1290	4.66	1300	2.87	1314.4	9.04	1314.4	9.0	0.7	1.1	2.5626	0.0164	0.2234	0.0005	0.38	0.0850	0.0004	0.11502
05LP-026L6	2520.2	5.89	2465.5	4.75	2589.5	6.82	2589.5	6.8	0.3	4.8	10.9657	0.0694	0.4659	0.0011	0.37	0.1733	0.0007	0.32325
05LP-026L8	1933	7.78	1946.6	4.92	1975.1	9.09	1975.1	9.1	0.5	1.4	5.7108	0.0515	0.3525	0.0010	0.32	0.1213	0.0006	0.12068
05LP-026L9	1567.5	5.83	1565.5	3.63	1586.1	9.11	1586.1	9.1	0.6	1.3	3.6820	0.0269	0.2749	0.0007	0.36	0.0980	0.0005	0.38918
05LP-026L10	1060.2	4.45	1062	2.51	1058.5	10.58	1058.5	10.6	1.0	-0.3	1.8410	0.0124	0.1791	0.0005	0.38	0.0746	0.0004	0.54284
05LP-026L11	1433.5	8.78	1410.4	4.6	1447.2	13.14	1447.2	13.1	0.9	2.5	3.1031	0.0355	0.2446	0.0009	0.32	0.0910	0.0006	0.21821
05LP-026L12	1436.4	5.46	1454.2	3.37	1419.9	9.42	1419.9	9.4	0.7	-2.4	3.1151	0.0221	0.2531	0.0007	0.37	0.0897	0.0004	0.17382
05LP-026L13	1119.2	4.78	1117.1	2.71	1138.6	10.4	1138.6	10.4	0.9	1.9	2.0109	0.0142	0.1892	0.0005	0.37	0.0777	0.0004	0.09758
05LP-026L14	1809.8	6.51	1814.1	4.24	1821.7	8.94	1821.7	8.9	0.5	0.4	4.9438	0.0381	0.3250	0.0009	0.35	0.1114	0.0006	0.15544
05LP-026L15	1785.4	7.66	1807.2	4.72	1791.7	9.91	1791.7	9.9	0.6	-0.9	4.8026	0.0438	0.3236	0.0010	0.33	0.1095	0.0006	0.17090
05LP-026L16	1102.8	4.7	1130.1	2.73	1096.3	10.49	1096.3	10.5	1.0	-3.1	1.9626	0.0137	0.1916	0.0005	0.37	0.0761	0.0004	0.07720
05LP-026L17	*1160.6*	*13.24*	*1201.8*	*6.38*	*1097.5*	*24.17*	*1097.5*	*24.2*	*2.2*	*-9.5*	*2.1363*	*0.0409*	*0.2049*	*0.0012*	*0.30*	*0.0761*	*0.0009*	*0.14180*
05LP-026L18	1094.4	10.81	1077.8	5.02	1094.6	21.27	1094.6	21.3	1.9	1.5	1.9384	0.0313	0.1820	0.0009	0.31	0.0760	0.0008	0.16582
																	59 zircons	

Analyses in italics/shaded are excluded due to >10% error in critical age, >10% discordance, or >5% reverse discordance.

All errors are at the 1-sigma level, and include only random uncertainties.

Best age = $^{206}Pb/^{238}U$ ages for analyses younger than 1.0 Ga and $^{206}Pb/^{207}Pb$ ages for analyses older than 1.0 Ga.

Isotope ratios are corrected for Pb/U fractionation by comparison with standard zircons Plesovice and FC1.

Table I-4. *Detrital Zircon U-Pb geochronologic analyses – Pacific Centre for Isotopic and Geochemical Research – Sample 03LP010 in Toobally Formation.*

Analysis No.	Age estimates with 1 sigma uncertainty (Ma)										Isotopic Ratios with absolute errors							
	$^{207}Pb/^{235}U$ Ma	$^{207}Pb/^{235}U$ ± 1σ Error	$^{206}Pb/^{238}U$ Ma	$^{206}Pb/^{238}U$ ± 1σ Error	$^{207}Pb/^{206}Pb$ Ma	$^{207}Pb/^{206}Pb$ ± 1σ Error	Preferred Age Ma*	± 1σ Error	Error %	Discordancy %	$^{207}Pb/^{235}U$ Ratio	$^{207}Pb/^{235}U$ 1σ Error	$^{206}Pb/^{238}U$ Ratio	$^{206}Pb/^{238}U$ 1σ Error	Rho	$^{207}Pb/^{206}Pb$ Ratio	$^{207}Pb/^{206}Pb$ 1σ Error	Th/U Ratio
03LP010L1	1079.8	10.13	1027.9	4.1	1138.5	23.63	1138.5	23.6	2.1	9.7	1.8962	0.0289	0.1729	0.0008	0.28	0.0777	0.0009	0.15
03LP010L2	1643.8	17.64	1604.1	8.85	1712.3	21.2	1712.3	21.2	1.2	6.3	4.0476	0.0877	0.2825	0.0018	0.29	0.1049	0.0012	0.11
03LP010L3	*1232.6*	*18.5*	*1189.9*	*7.4*	*1348.6*	*39.29*	*1348.6*	*39.3*	*2.9*	*11.8*	*2.3667*	*0.0613*	*0.2027*	*0.0014*	*0.26*	*0.0865*	*0.0018*	*0.14*
03LP010L4	975.6	9.15	960.7	3.72	973	23.58	960.7	3.7	0.4	1.3	1.6140	0.0236	0.1607	0.0007	0.29	0.0715	0.0008	0.22
03LP010L5	2652.5	12.09	2582.7	7.7	2713.6	10.36	2713.6	10.4	0.4	4.8	12.6301	0.1623	0.4928	0.0018	0.28	0.1867	0.0012	0.29
03LP010L6	1431.7	19.09	1414.2	8.6	1485.9	32.79	1485.9	32.8	2.2	4.8	3.0962	0.0770	0.2453	0.0017	0.27	0.0929	0.0016	0.22
03LP010L7	1724.1	16.43	1723.6	8.39	1761.5	22.47	1761.5	22.5	1.3	2.2	4.4627	0.0884	0.3065	0.0017	0.28	0.1077	0.0013	0.11
03LP010L8	986.2	18.18	968.4	6.78	1026	48.21	1026.0	48.2	4.7	5.6	1.6412	0.0473	0.1621	0.0012	0.26	0.0734	0.0018	0.07
03LP010L9	1464.5	15.96	1477	7.62	1437.5	25.5	1437.5	25.5	1.8	-2.7	3.2304	0.0665	0.2575	0.0015	0.28	0.0906	0.0012	0.09
03LP010L10	1524.7	14.46	1485	7.01	1602.2	21.81	1602.2	21.8	1.4	7.3	3.4888	0.0639	0.2591	0.0014	0.29	0.0988	0.0012	0.26
03LP010L11	1749.4	14.1	1768.6	7.51	1753.7	17.8	1753.7	17.8	1.0	-0.8	4.6008	0.0778	0.3157	0.0015	0.29	0.1073	0.0011	0.15
03LP010L12	1319.5	8.49	1299.4	4.23	1333.8	15.49	1333.8	15.5	1.2	2.6	2.6675	0.0307	0.2233	0.0008	0.31	0.0858	0.0007	0.12
03LP010L13	*1101.8*	*13.01*	*1049.9*	*5.82*	*1217.3*	*25.84*	*1217.3*	*25.8*	*2.1*	*13.8*	*1.9597*	*0.0379*	*0.1769*	*0.0011*	*0.31*	*0.0808*	*0.0011*	*0.12*
03LP010L14	1125.7	20.66	1154.5	8.21	1101.3	47.55	1101.3	47.6	4.3	-4.8	2.0303	0.0617	0.1961	0.0015	0.26	0.0762	0.0018	0.12
03LP010L15	760.2	11.22	758.2	4.01	760.4	37.73	758.2	4.0	0.5	0.3	1.1142	0.0234	0.1248	0.0007	0.27	0.0646	0.0012	0.14
03LP010L16	1244.5	10.63	1201.5	4.9	1324.6	20.38	1324.6	20.4	1.5	9.3	2.4064	0.0357	0.2049	0.0009	0.30	0.0854	0.0009	0.02
03LP010L17	1143.7	37.5	1143.2	14.76	1170.9	82.91	1170.9	82.9	7.1	2.4	2.0845	0.1139	0.1940	0.0027	0.26	0.0790	0.0034	0.11
03LP010L18	1817.8	25.94	1781.8	12.81	1866.3	33.56	1866.3	33.6	1.8	4.5	4.9908	0.1531	0.3184	0.0026	0.27	0.1141	0.0022	0.17
03LP010L19	2853.9	32.96	2838.2	20.58	2889.2	20.3	2889.2	20.3	0.7	1.8	15.6206	0.5396	0.5531	0.0050	0.26	0.2079	0.0026	0.13
03LP010L20	1320.4	16.8	1342.5	8.06	1378.4	28.96	1378.4	29.0	2.1	2.6	2.6707	0.0607	0.2315	0.0015	0.29	0.0878	0.0013	0.18
03LP010L21	1809.4	17.83	1800	9.56	1855.5	21.54	1855.5	21.5	1.2	3.0	4.9418	0.1044	0.3221	0.0020	0.29	0.1135	0.0014	0.16
03LP010L22	1709.1	30.67	1782.5	16.23	1726.3	37.15	1726.3	37.2	2.2	-3.3	4.3825	0.1626	0.3185	0.0033	0.28	0.1057	0.0022	0.11
03LP010L23	1047.2	26.37	1048.6	11.72	1102.8	56.06	1102.8	56.1	5.1	4.9	1.8048	0.0728	0.1767	0.0021	0.30	0.0763	0.0022	0.04
03LP010L24	1476.2	20.42	1514	10.17	1529.6	31.31	1529.6	31.3	2.0	1.0	3.2796	0.0861	0.2647	0.0020	0.29	0.0951	0.0016	0.11
03LP010L25	1089.7	11.04	1104.7	5.19	1160.9	24.13	1160.9	24.1	2.1	4.8	1.9247	0.0318	0.1869	0.0010	0.31	0.0786	0.0010	0.09
03LP010L26	1522.8	18.16	1472.8	8.86	1564.1	26.25	1564.1	26.3	1.7	5.8	3.4806	0.0802	0.2567	0.0017	0.29	0.0968	0.0014	0.13
03LP010L27	1490.7	13.24	1451	6.69	1559.1	20.51	1559.1	20.5	1.3	6.9	3.3411	0.0566	0.2524	0.0013	0.30	0.0966	0.0011	0.12
03LP010L28	721.7	9.62	728.5	3.89	725	32.68	728.5	3.9	0.5	-0.5	1.0356	0.0193	0.1196	0.0007	0.31	0.0635	0.0010	0.19
03LP010L29	1176.8	26.03	1223.2	12.41	1235.5	48.71	1235.5	48.7	3.9	1.0	2.1867	0.0817	0.2090	0.0023	0.30	0.0816	0.0021	0.12

Analyses in italics/shaded are excluded due to >10% error in critical age, >10% discordance, or >5% reverse discordance.

All errors are at the 1-sigma level, and include only random uncertainties.

Best age = $^{206}Pb/^{238}U$ ages for analyses younger than 1.0 Ga and $^{206}Pb/^{207}Pb$ ages for analyses older than 1.0 Ga.

Isotope ratios are corrected for Pb/U fractionation by comparison with standard zircons Plesovice and FC1.

Table I-4. *(continued) Detrital Zircon U-Pb geochronologic analyses – Pacific Centre for Isotopic and Geochemical Research – Sample 03LP010 in Toobally Formation.*

Analysis No.	Age estimates with 1 sigma uncertainty (Ma)										Isotopic Ratios with absolute errors							
	$^{207}Pb/^{235}U$ Ma	$^{207}Pb/^{235}U$ ± 1σ Error	$^{206}Pb/^{238}U$ Ma	$^{206}Pb/^{238}U$ ± 1σ Error	$^{207}Pb/^{206}Pb$ Ma	$^{207}Pb/^{206}Pb$ ± 1σ Error	Preferred Age Ma*	± 1σ Error	Error %	Discordancy %	$^{207}Pb/^{235}U$ Ratio	$^{207}Pb/^{235}U$ 1σ Error	$^{206}Pb/^{238}U$ Ratio	$^{206}Pb/^{238}U$ 1σ Error	Rho	$^{207}Pb/^{206}Pb$ Ratio	$^{207}Pb/^{206}Pb$ 1σ Error	Th/U Ratio
03LP010L30	1502.5	18.34	1494	9.08	1520.7	27.81	1520.7	27.8	1.8	1.8	3.3918	0.0793	0.2608	0.0018	0.29	0.0946	0.0014	0.16
03LP010L31	1719.6	36.63	1773.1	19.15	1687.7	42.12	1687.7	42.1	2.5	-5.1	4.4386	0.1962	0.3166	0.0039	0.28	0.1035	0.0024	0.09
03LP010L32	780.3	9.91	776.5	4.15	860.8	30.71	860.8	30.7	3.6	9.8	1.1566	0.0210	0.1280	0.0007	0.31	0.0678	0.0010	0.15
03LP010L34	1441.1	14.9	1456.4	7.55	1455.5	24.44	1455.5	24.4	1.7	-0.1	3.1340	0.0607	0.2535	0.0015	0.30	0.0914	0.0012	0.12
03LP010L35	1628.4	16.88	1616.5	8.73	1668	24.13	1668.0	24.1	1.4	3.1	3.9717	0.0827	0.2850	0.0017	0.29	0.1024	0.0014	0.29
03LP010L36	2647.7	23.47	2637.3	14.58	2716.4	18.49	2716.4	18.5	0.7	2.9	12.5667	0.3136	0.5055	0.0034	0.27	0.1871	0.0021	0.34
03LP010L37	1489	19.61	1495.8	9.84	1472.8	29.24	1472.8	29.2	2.0	-1.6	3.3338	0.0837	0.2612	0.0019	0.29	0.0923	0.0014	0.21
03LP010L38	646.9	6.7	653.1	2.86	658.5	25.2	653.1	2.9	0.4	0.8	0.8910	0.0125	0.1066	0.0005	0.33	0.0616	0.0007	0.10
03LP010L39	652.6	6.79	649	2.87	687.8	25.3	649.0	2.9	0.4	5.6	0.9016	0.0127	0.1059	0.0005	0.33	0.0624	0.0008	0.10
03LP010L40	2672.5	33.03	2691.3	20.69	2782.3	23.13	2782.3	23.1	0.8	3.3	12.9014	0.4522	0.5182	0.0049	0.27	0.1947	0.0028	0.12
03LP010L41	1124.9	17.22	1165.1	8.1	1213.2	36.22	1213.2	36.2	3.0	4.0	2.0278	0.0513	0.1981	0.0015	0.30	0.0807	0.0015	0.11
03LP010L42	1103.3	10.63	1084.8	5.01	1134.5	24.03	1134.5	24.0	2.1	4.4	1.9640	0.0310	0.1833	0.0009	0.32	0.0775	0.0009	0.23
03LP010L43	1303.8	14.33	1323.4	7.13	1293.9	26.57	1293.9	26.6	2.1	-2.3	2.6111	0.0510	0.2279	0.0014	0.31	0.0841	0.0012	0.29
03LP010L1	1184.3	19.67	1153	12.72	1179.7	38.21	1179.7	38.2	3.2	0.9	2.2103	0.0622	0.1959	0.0024	0.43	0.0793	0.0016	0.27
03LP010L2	1364.4	10.59	1345.5	12.33	1423.6	22.55	1423.6	22.6	1.6	4.8	2.8333	0.0400	0.2321	0.0024	0.72	0.0899	0.0011	0.20
03LP010L3	1238.7	11.48	1211	11.48	1292.6	24.7	1292.6	24.7	1.9	5.2	2.3869	0.0383	0.2067	0.0022	0.65	0.0840	0.0011	0.13
03LP010L4	*119.7*	*4.45*	*88.8*	*1.34*	*798.3*	*81.67*	*88.8*	*1.3*	*1.5*	*86.9*	*0.1251*	*0.0049*	*0.0139*	*0.0002*	*0.38*	*0.0658*	*0.0026*	*0.15*
03LP010L5	*2151.6*	*138.85*	*1128.1*	*111.84*	*4589.7*	*164.19*	*4589.7*	*164.2*	*3.6*	*64.3*	*7.3225*	*1.1381*	*0.1913*	*0.0207*	*0.70*	*0.6348*	*0.0766*	*0.78*
03LP010L6	1582.9	12.25	1572.8	14.35	1610.3	22.28	1610.3	22.3	1.4	2.0	3.7538	0.0573	0.2763	0.0028	0.67	0.0993	0.0012	0.16
03LP010L7	*1576*	*77*	*1220.1*	*52.68*	*3240.3*	*103.04*	*3240.3*	*103.0*	*3.2*	*56.9*	*3.7215*	*0.3581*	*0.2084*	*0.0099*	*0.49*	*0.2590*	*0.0176*	*0.48*
03LP010L8	2045.3	12.92	2050	17.89	2059.8	20.17	2059.8	20.2	1.0	0.6	6.4958	0.0954	0.3744	0.0038	0.69	0.1272	0.0015	0.13
03LP010L9	1153.1	23.36	1149.8	13.95	1198	44.57	1198.0	44.6	3.7	3.9	2.1132	0.0716	0.1953	0.0026	0.39	0.0800	0.0018	0.13
03LP010L10	2484	18.7	2436.2	21.6	2478	20.42	2478.0	20.4	0.8	0.7	10.5466	0.2126	0.4593	0.0049	0.53	0.1621	0.0020	0.22
03LP010L11	1751.9	12.45	1730.1	15.6	1774	21.42	1774.0	21.4	1.2	1.9	4.6145	0.0688	0.3079	0.0032	0.69	0.1085	0.0013	0.30
03LP010L12	1780.4	13.06	1700.4	15.49	1876.3	21.4	1876.3	21.4	1.1	7.2	4.7744	0.0743	0.3018	0.0031	0.67	0.1148	0.0014	0.21
03LP010L13	1235.4	12.88	1234.5	12.07	1269.7	26.44	1269.7	26.4	2.1	2.7	2.3761	0.0428	0.2111	0.0023	0.60	0.0830	0.0011	0.23
03LP010L14	1697.7	16.51	1593.5	15.39	1783.4	24.28	1783.4	24.3	1.4	7.7	4.3225	0.0866	0.2804	0.0031	0.54	0.1090	0.0015	0.09
03LP010L15	1054.9	14.01	1056.1	10.98	1056.8	32.25	1056.8	32.3	3.1	0.1	1.8263	0.0390	0.1780	0.0020	0.53	0.0746	0.0012	0.22
03LP010L16	1061.3	13.5	1037.6	10.67	1047.1	31.19	1047.1	31.2	3.0	-0.2	1.8440	0.0378	0.1746	0.0019	0.54	0.0742	0.0012	0.28
03LP010L17	1546.2	13.55	1472.2	13.97	1646.8	23.39	1646.8	23.4	1.4	8.4	3.5848	0.0612	0.2566	0.0027	0.62	0.1012	0.0013	0.40
03LP010L18	1248.2	12.57	1222.8	11.94	1286.4	26	1286.4	26.0	2.0	4.0	2.4187	0.0423	0.2089	0.0022	0.61	0.0837	0.0011	0.16

Analyses in italics/shaded are excluded due to >10% error in critical age, >10% discordance, or >5% reverse discordance.

All errors are at the 1-sigma level, and include only random uncertainties.

Best age = $^{206}Pb/^{238}U$ ages for analyses younger than 1.0 Ga and $^{206}Pb/^{207}Pb$ ages for analyses older than 1.0 Ga.

Isotope ratios are corrected for Pb/U fractionation by comparison with standard zircons Plesovice and FC1.

Table I-4. *(continued) Detrital Zircon U-Pb geochronologic analyses – Pacific Centre for Isotopic and Geochemical Research – Sample 03LP010 in Toobally Formation.*

Analysis No.	Age estimates with 1 sigma uncertainty (Ma)										Isotopic Ratios with absolute errors							
	$^{207}Pb/^{235}U$ Ma	$^{207}Pb/^{235}U$ ± 1σ Error	$^{206}Pb/^{238}U$ Ma	$^{206}Pb/^{238}U$ ± 1σ Error	$^{207}Pb/^{206}Pb$ Ma	$^{207}Pb/^{206}Pb$ ± 1σ Error	Preferred Age Ma*	± 1σ Error	Error %	Discordancy %	$^{207}Pb/^{235}U$ Ratio	$^{207}Pb/^{235}U$ 1σ Error	$^{206}Pb/^{238}U$ Ratio	$^{206}Pb/^{238}U$ 1σ Error	Rho	$^{207}Pb/^{206}Pb$ Ratio	$^{207}Pb/^{206}Pb$ 1σ Error	Th/U Ratio
03LP010L19	1536.7	10.83	1512.8	13.83	1573.1	21.64	1573.1	21.6	1.4	3.1	3.5421	0.0485	0.2645	0.0027	0.75	0.0973	0.0011	0.26
03LP010L20	1769.1	13.31	1711.6	15.74	1845.7	21.75	1845.7	21.8	1.2	5.7	4.7103	0.0748	0.3041	0.0032	0.66	0.1128	0.0014	0.22
03LP010L21	1099.4	16.83	1075.3	11.85	1146.1	34.97	1146.1	35.0	3.1	5.1	1.9527	0.0489	0.1815	0.0022	0.48	0.0780	0.0014	0.20
03LP010L22	2575.5	24.71	2345.7	22.76	2738.9	22.07	2738.9	22.1	0.8	10.2	11.6356	0.3075	0.4389	0.0051	0.44	0.1896	0.0026	0.40
03LP010L23	1179.3	12.05	1178.7	11.58	1174.3	26.37	1174.3	26.4	2.2	-0.4	2.1944	0.0379	0.2006	0.0022	0.62	0.0791	0.0011	0.07
03LP010L24	1171.1	16.11	1164.3	12.38	1209.3	32.14	1209.3	32.1	2.7	3.4	2.1689	0.0503	0.1979	0.0023	0.50	0.0805	0.0013	0.37
03LP010L25	1282	12.6	1222.9	12	1381.9	25.24	1381.9	25.2	1.8	9.4	2.5344	0.0439	0.2089	0.0023	0.62	0.0880	0.0012	0.06
																	62 zircons	

Analyses in italics/shaded are excluded due to >10% error in critical age, >10% discordance, or >5% reverse discordance.
All errors are at the 1-sigma level, and include only random uncertainties.
Best age = $^{206}Pb/^{238}U$ ages for analyses younger than 1.0 Ga and $^{206}Pb/^{207}Pb$ ages for analyses older than 1.0 Ga.
Isotope ratios are corrected for Pb/U fractionation by comparison with standard zircons Plesovice and FC1.

Table I-5a. *Detrital Zircon U-Pb geochronologic analyses – Arizona Laserchron Center – Sample 02LP120 in Crow Formation.*

Isotopic ratios									Apparent ages (Ma)									
Sample	U (ppm)	$^{206}Pb/^{204}Pb$	U/Th	$^{207}Pb/^{235}U$	± (%) (1 sigma)	$^{206}Pb/^{238}U$	± (%) (1 sigma)	error corr.	$^{206}Pb/^{238}U$	± (Ma) (1 sigma)	$^{207}Pb/^{235}U$	± (Ma) (1 sigma)	$^{206}Pb/^{207}Pb$	± (Ma) (1 sigma)	BEST AGE	± (Ma) (1 sigma)	Error %	Discordance %
02LCP120-85	204	12099	1.3	0.60249	6.1	0.07569	1.9	0.31	470.3	8.6	479	23	520	127	470	9	1.8	9.6
02LCP120-87	*1543*	*9849*	*3.6*	*0.61433*	*1.7*	*0.07570*	*1.1*	*0.61*	*470.4*	*4.8*	*486*	*7*	*562*	*30*	*470*	*5*	*1.0*	*16.3*
02LCP120-32	*166*	*11370*	*1.5*	*0.57785*	*3.8*	*0.07610*	*1.0*	*0.26*	*472.8*	*4.6*	*463*	*14*	*415*	*82*	*473*	*5*	*1.0*	*-13.9*
02LCP120-57	137	5461	1.3	0.59775	9.5	0.07611	3.0	0.32	472.8	13.9	476	36	490	199	473	14	2.9	3.5
02LCP120-81	323	30761	0.7	0.62237	3.2	0.07808	1.0	0.31	484.7	4.7	491	12	522	66	485	5	1.0	7.1
02LCP120-27	329	6080	2.0	0.61362	3.4	0.07812	1.2	0.34	484.9	5.4	486	13	490	70	485	5	1.1	1.0
02LCP120-86	*239*	*27184*	*1.2*	*0.59523*	*3.6*	*0.07819*	*1.0*	*0.29*	*485.3*	*4.9*	*474*	*14*	*421*	*77*	*485*	*5*	*1.0*	*-15.3*
02LCP120-48	*240*	*33635*	*1.0*	*0.63334*	*3.6*	*0.07853*	*1.0*	*0.28*	*487.3*	*4.7*	*498*	*14*	*548*	*75*	*487*	*5*	*1.0*	*11.1*
02LCP120-94	183	37937	1.3	1.02541	3.2	0.11878	1.1	0.35	723.5	7.7	717	16	695	63	724	8	1.1	-4.1
02LCP120-79	207	19876	2.4	2.22352	1.7	0.20101	1.0	0.61	1180.7	10.8	1189	12	1203	26	1203	26	2.2	1.9
02LCP120-63	291	42757	1.8	4.38191	1.2	0.29474	1.0	0.82	1665.2	14.7	1709	10	1763	13	1763	13	0.7	5.5
02LCP120-96	73	5890	7.0	5.01709	2.7	0.33018	1.0	0.38	1839.3	16.4	1822	23	1803	45	1803	45	2.5	-2.0
02LCP120-44	140	32433	2.1	4.87570	1.6	0.31680	1.0	0.63	1774.1	15.5	1798	14	1826	23	1826	23	1.3	2.8
02LCP120-17	193	2348	2.5	4.60373	2.8	0.29904	1.2	0.43	1686.5	17.5	1750	23	1827	45	1827	45	2.5	7.7
02LCP120-33	52	15523	1.5	4.97785	2.6	0.32249	1.0	0.39	1801.9	15.7	1816	22	1831	43	1831	43	2.3	1.6
02LCP120-4	69	11990	1.5	4.85183	2.4	0.31361	1.0	0.41	1758.4	15.4	1794	21	1835	40	1835	40	2.2	4.2
02LCP120-8	148	16381	1.8	4.83926	1.7	0.31275	1.5	0.87	1754.2	22.9	1792	14	1836	15	1836	15	0.8	4.5
02LCP120-19	*406*	*22481*	*1.7*	*4.08079*	*3.4*	*0.26305*	*3.3*	*0.98*	*1505.4*	*43.9*	*1651*	*27*	*1840*	*13*	*1840*	*13*	*0.7*	*18.2*
02LCP120-15	*141*	*10461*	*2.4*	*4.39411*	*3.6*	*0.28275*	*3.5*	*0.98*	*1605.2*	*49.6*	*1711*	*30*	*1844*	*14*	*1844*	*14*	*0.8*	*13.0*
02LCP120-34	109	22204	1.6	4.96934	1.2	0.31857	1.0	0.82	1782.7	15.6	1814	10	1850	13	1850	13	0.7	3.6
02LCP120-82	76	17566	1.9	5.28086	3.3	0.33788	2.9	0.90	1876.5	47.7	1866	28	1854	26	1854	26	1.4	-1.2
02LCP120-98	56	18052	2.6	5.33485	2.5	0.34083	1.0	0.40	1890.7	16.4	1875	21	1857	41	1857	41	2.2	-1.8
02LCP120-36	251	14010	3.2	4.64415	2.8	0.29580	2.7	0.94	1670.5	39.0	1757	24	1862	18	1862	18	1.0	10.3
02LCP120-1	132	17659	2.8	5.08626	1.2	0.32342	1.0	0.82	1806.4	15.8	1834	10	1865	13	1865	13	0.7	3.1
02LCP120-50	156	61267	2.1	4.96689	1.5	0.31563	1.0	0.69	1768.3	15.5	1814	12	1866	19	1866	19	1.0	5.2
02LCP120-24	111	47124	1.9	5.36939	1.4	0.34105	1.0	0.73	1891.7	16.4	1880	12	1867	17	1867	17	0.9	-1.3
02LCP120-58	258	27360	1.4	4.84238	2.7	0.30750	2.4	0.88	1728.4	35.6	1792	22	1867	22	1867	22	1.2	7.4
02LCP120-30	62	18835	2.1	5.28376	2.2	0.33552	1.0	0.45	1865.1	16.2	1866	19	1868	36	1868	36	1.9	0.2
02LCP120-37	236	81365	9.7	4.97269	1.2	0.31576	1.0	0.82	1769.0	15.5	1815	10	1868	13	1868	13	0.7	5.3
02LCP120-74	109	8775	1.2	5.13989	2.4	0.32633	1.4	0.57	1820.6	21.9	1843	21	1868	36	1868	36	1.9	2.5
02LCP120-73	54	10904	1.2	5.22378	2.0	0.33099	1.3	0.63	1843.2	20.3	1857	17	1871	28	1871	28	1.5	1.5
02LCP120-97	94	78114	2.3	5.30917	1.6	0.33646	1.0	0.65	1869.6	16.2	1870	13	1871	21	1871	21	1.1	0.1
02LCP120-56	116	15449	3.6	5.32916	1.6	0.33737	1.3	0.81	1874.0	20.4	1874	13	1873	17	1873	17	0.9	-0.1
02LCP120-18	115	34698	1.4	5.10573	1.4	0.32287	1.0	0.70	1803.7	15.7	1837	12	1875	18	1875	18	1.0	3.8

$^{206}Pb/^{204}Pb$ is measured ratio.

Analyses in italics/shaded are excluded due to >10% error in critical age, >10% discordance, or >5% reverse discordance.

All errors are at the 1-sigma level, and include only random uncertainties.

Best age = $^{206}Pb/^{238}U$ ages for analyses younger than 1.0 Ga and $^{206}Pb/^{207}Pb$ ages for analyses older than 1.0 Ga.

U concentration and U/Th are calibrated by comparison with NBS SRM 610 and have uncertainty of ~25%.

Decay constants: $^{235}U=9.8485x10^{-10}$, $^{238}U=1.55125x10^{-10}$, $^{238}U/235U=137.88$.

Isotope ratios are corrected for Pb/U fractionation by comparison with standard zircon with an age of 564 ± 4 Ma (2-sigma).

Initial Pb composition interpreted from Stacey and Kramers (1975), with uncertainties of 1.0 for $^{206}Pb/^{204}Pb$ and 0.3 for $^{207}Pb/^{204}Pb$.

Table I-5a. *(continued) Detrital Zircon U-Pb geochronologic analyses – Arizona Laserchron Center – Sample 02LP120 in Crow Formation.*

Isotopic ratios									Apparent ages (Ma)									
Sample	U (ppm)	$^{206}Pb/^{204}Pb$	U/Th	$^{207}Pb/^{235}U$	± (%) (1 sigma)	$^{206}Pb/^{238}U$	± (%) (1 sigma)	error corr.	$^{206}Pb/^{238}U$	± (Ma) (1 sigma)	$^{207}Pb/^{235}U$	± (Ma) (1 sigma)	$^{206}Pb/^{207}Pb$	± (Ma) (1 sigma)	BEST AGE	± (Ma) (1 sigma)	Error %	Discordance %
02LCP120-100	*111*	*38139*	*1.8*	*4.66311*	*2.2*	*0.29453*	*1.9*	*0.89*	*1664.2*	*28.0*	*1761*	*18*	*1877*	*18*	*1877*	*18*	*1.0*	*11.3*
02LCP120-10	268	67180	4.8	5.10990	1.3	0.32233	1.0	0.77	1801.1	15.7	1838	11	1879	15	1879	15	0.8	4.1
02LCP120-41	94	9425	1.1	5.15719	1.9	0.32533	1.2	0.64	1815.7	19.6	1846	17	1879	27	1879	27	1.4	3.4
02LCP120-43	126	47674	1.7	5.26006	2.0	0.33180	1.8	0.89	1847.1	29.1	1862	17	1879	16	1879	16	0.9	1.7
02LCP120-68	177	18118	1.4	5.16557	1.2	0.32594	1.0	0.81	1818.7	15.9	1847	11	1879	13	1879	13	0.7	3.2
02LCP120-26	85	29552	2.2	5.20180	1.8	0.32782	1.0	0.55	1827.8	15.9	1853	15	1881	27	1881	27	1.4	2.8
02LCP120-54	117	53222	3.1	5.31290	2.0	0.33471	1.7	0.84	1861.1	27.3	1871	17	1882	20	1882	20	1.1	1.1
02LCP120-13	199	60039	1.8	5.26727	1.2	0.33165	1.0	0.82	1846.4	16.1	1864	10	1883	13	1883	13	0.7	1.9
02LCP120-76	156	58462	1.6	5.26729	1.3	0.33122	1.0	0.78	1844.3	16.7	1864	11	1885	15	1885	15	0.8	2.2
02LCP120-2	178	27190	3.6	5.25036	1.2	0.32977	1.0	0.82	1837.3	16.0	1861	10	1887	13	1887	13	0.7	2.6
02LCP120-23	200	54461	2.0	5.30797	1.2	0.33308	1.0	0.82	1853.3	16.1	1870	11	1889	13	1889	13	0.7	1.9
02LCP120-47	155	36118	2.1	5.40971	1.4	0.33917	1.0	0.73	1882.7	16.3	1886	12	1890	17	1890	17	0.9	0.4
02LCP120-25	146	48453	1.4	5.36706	1.4	0.33621	1.0	0.74	1868.4	16.2	1880	12	1892	16	1892	16	0.8	1.2
02LCP120-53	220	48262	2.4	5.24105	2.2	0.32829	2.1	0.95	1830.1	33.6	1859	19	1892	13	1892	13	0.7	3.3
02LCP120-92	139	48000	2.5	5.35615	1.4	0.33509	1.0	0.74	1863.0	16.2	1878	12	1894	16	1894	16	0.8	1.6
02LCP120-60	157	47788	1.7	5.33192	1.2	0.33305	1.0	0.82	1853.1	16.1	1874	11	1897	13	1897	13	0.7	2.3
02LCP120-28	190	34937	1.8	5.13750	1.2	0.32039	1.0	0.82	1791.6	15.6	1842	10	1900	13	1900	13	0.7	5.7
02LCP120-72	86	31870	1.5	5.44136	2.1	0.33883	1.7	0.79	1881.0	26.9	1891	18	1903	23	1903	23	1.2	1.2
02LCP120-45	282	38818	2.3	4.85406	1.4	0.30194	1.2	0.86	1700.9	18.1	1794	12	1905	13	1905	13	0.7	10.7
02LCP120-69	204	43387	6.0	5.37046	1.2	0.33336	1.0	0.82	1854.7	16.1	1880	11	1908	13	1908	13	0.7	2.8
02LCP120-40	138	51825	4.6	5.29653	1.3	0.32863	1.0	0.78	1831.7	15.9	1868	11	1909	15	1909	15	0.8	4.0
02LCP120-99	158	55318	1.8	5.46627	1.2	0.33907	1.0	0.82	1882.2	16.3	1895	11	1910	13	1910	13	0.7	1.5
02LCP120-71	177	81846	2.3	5.58694	1.2	0.34632	1.0	0.82	1917.0	16.6	1914	11	1911	13	1911	13	0.7	-0.3
02LCP120-64	144	59102	2.5	5.43316	1.7	0.33504	1.6	0.90	1862.8	25.2	1890	15	1920	13	1920	13	0.7	3.0
02LCP120-70	131	23495	2.2	5.48253	1.8	0.33806	1.0	0.57	1877.3	16.3	1898	15	1920	26	1920	26	1.4	2.2
02LCP120-90	124	33763	4.8	5.71001	1.2	0.34975	1.0	0.81	1933.4	16.7	1933	11	1932	13	1932	13	0.7	-0.1
02LCP120-49	259	41172	2.1	5.42490	1.2	0.33154	1.0	0.82	1845.8	16.1	1889	11	1936	13	1936	13	0.7	4.7
02LCP120-29	191	19907	1.6	5.25246	3.3	0.31989	3.1	0.96	1789.2	48.7	1861	28	1943	16	1943	16	0.8	7.9
02LCP120-75	108	62679	1.3	5.56546	1.7	0.33760	1.3	0.78	1875.1	21.8	1911	15	1950	19	1950	19	1.0	3.8
02LCP120-6	183	38200	1.8	5.77266	1.6	0.34754	1.4	0.89	1922.8	23.1	1942	14	1963	13	1963	13	0.7	2.0
02LCP120-91	44	25421	1.3	6.03308	2.4	0.35983	1.0	0.41	1981.4	17.1	1981	21	1980	39	1980	39	2.0	-0.1
02LCP120-46	105	30694	4.2	6.28297	1.3	0.36577	1.0	0.77	2009.5	17.3	2016	11	2023	15	2023	15	0.7	0.7
02LCP120-88	205	44175	1.9	6.34301	1.2	0.36214	1.0	0.82	1992.3	17.1	2024	11	2057	12	2057	12	0.6	3.1
02LCP120-31	*943*	*9349*	*1.8*	*4.28447*	*2.3*	*0.23835*	*2.2*	*0.95*	*1378.1*	*27.4*	*1690*	*19*	*2103*	*13*	*2103*	*13*	*0.6*	*34.5*

$^{206}Pb/^{204}Pb$ is measured ratio.

Analyses in italics/shaded are excluded due to >10% error in critical age, >10% discordance, or >5% reverse discordance.

All errors are at the 1-sigma level, and include only random uncertainties.

Best age = $^{206}Pb/^{238}U$ ages for analyses younger than 1.0 Ga and $^{206}Pb/^{207}Pb$ ages for analyses older than 1.0 Ga.

U concentration and U/Th are calibrated by comparison with NBS SRM 610 and have uncertainty of ~25%.

Decay constants: $^{235}U=9.8485x10^{-10}$, $^{238}U=1.55125x10^{-10}$, $^{238}U/235U=137.88$.

Isotope ratios are corrected for Pb/U fractionation by comparison with standard zircon with an age of 564 ± 4 Ma (2-sigma).

Initial Pb composition interpreted from Stacey and Kramers (1975), with uncertainties of 1.0 for $^{206}Pb/^{204}Pb$ and 0.3 for $^{207}Pb/^{204}Pb$.

Table I-5a. *(continued) Detrital Zircon U-Pb geochronologic analyses – Arizona Laserchron Center – Sample 02LP120 in Crow Formation.*

Isotopic ratios									Apparent ages (Ma)									
Sample	U (ppm)	$^{206}Pb/^{204}Pb$	U/Th	$^{207}Pb/^{235}U$	± (%) (1 sigma)	$^{206}Pb/^{238}U$	± (%) (1 sigma)	error corr.	$^{206}Pb/^{238}U$	± (Ma) (1 sigma)	$^{207}Pb/^{235}U$	± (Ma) (1 sigma)	$^{206}Pb/^{207}Pb$	± (Ma) (1 sigma)	BEST AGE	± (Ma) (1 sigma)	Error %	Discordance %
02LCP120-61	77	26093	1.1	10.03390	1.2	0.45351	1.0	0.81	2410.8	20.1	2438	11	2461	12	2461	12	0.5	2.0
02LCP120-51	379	28252	1.8	9.98427	1.4	0.44014	1.2	0.86	2351.3	23.2	2433	13	2503	12	2503	12	0.5	6.1
02LCP120-42	*112*	*20149*	*1.4*	*8.89051*	*3.9*	*0.38788*	*3.8*	*0.96*	*2113.0*	*67.6*	*2327*	*36*	*2520*	*17*	*2520*	*17*	*0.7*	*16.2*
02LCP120-52	24	17576	1.3	10.85024	3.1	0.46169	1.7	0.56	2447.0	35.2	2510	29	2562	43	2562	43	1.7	4.5
02LCP120-21	31	13015	1.0	11.12548	2.0	0.46555	1.0	0.50	2464.0	20.5	2534	19	2590	29	2590	29	1.1	4.9
02LCP120-93	170	153632	1.6	12.03940	2.7	0.49788	2.6	0.96	2604.7	55.5	2608	25	2610	12	2610	12	0.5	0.2
02LCP120-35	*212*	*38404*	*1.8*	*10.77681*	*1.2*	*0.43878*	*1.0*	*0.82*	*2345.2*	*19.7*	*2504*	*11*	*2636*	*12*	*2636*	*12*	*0.5*	*11.0*
02LCP120-3	97	18856	2.2	12.04119	1.4	0.47721	1.2	0.86	2515.1	25.2	2608	13	2680	12	2680	12	0.4	6.2
02LCP120-12	110	37675	1.8	12.68572	1.5	0.49677	1.2	0.85	2599.9	26.3	2657	14	2700	13	2700	13	0.5	3.7
02LCP120-22	59	28357	0.6	13.28268	1.2	0.51823	1.0	0.82	2691.7	22.0	2700	12	2706	12	2706	12	0.4	0.5
02LCP120-67	178	79546	1.9	12.88428	1.3	0.50263	1.0	0.83	2625.1	22.2	2671	12	2706	12	2706	12	0.4	3.0
02LCP120-16	34	15748	1.8	13.40846	1.3	0.52102	1.0	0.75	2703.5	22.1	2709	13	2713	15	2713	15	0.6	0.4
02LCP120-7	125	35555	1.1	13.18375	1.5	0.50927	1.3	0.89	2653.5	29.1	2693	14	2723	12	2723	12	0.4	2.6
02LCP120-84	48	27698	1.0	13.34841	1.4	0.51279	1.0	0.73	2668.5	21.9	2705	13	2732	16	2732	16	0.6	2.3
02LCP120-80	238	109241	1.7	13.52643	1.2	0.51890	1.0	0.82	2694.5	22.0	2717	12	2734	12	2734	12	0.4	1.4
02LCP120-65	84	72509	0.8	13.39909	2.7	0.51381	2.6	0.97	2672.9	56.9	2708	26	2735	12	2735	12	0.4	2.3
02LCP120-55	192	55390	1.0	13.21892	1.2	0.50571	1.0	0.82	2638.3	21.7	2695	12	2739	12	2739	12	0.4	3.7
02LCP120-38	88	54413	1.6	13.31799	1.2	0.50858	1.0	0.82	2650.6	21.7	2703	12	2741	12	2741	12	0.4	3.3
02LCP120-95	89	33024	1.2	14.00304	1.6	0.53341	1.5	0.90	2755.8	33.2	2750	16	2746	12	2746	12	0.4	-0.4
02LCP120-5	50	14593	1.9	13.60061	1.4	0.51043	1.0	0.70	2658.5	21.8	2722	14	2770	17	2770	17	0.6	4.0
02LCP120-62	*130*	*12175*	*1.1*	*11.11306*	*5.0*	*0.41418*	*4.9*	*0.99*	*2234.0*	*92.7*	*2533*	*46*	*2781*	*12*	*2781*	*12*	*0.4*	*19.7*
02LCP120-66	119	53582	0.7	14.49435	1.2	0.52390	1.0	0.82	2715.7	22.2	2783	12	2832	11	2832	11	0.4	4.1
02LCP120-14	94	39869	2.9	15.39655	2.5	0.54936	2.4	0.95	2822.5	54.6	2840	24	2853	12	2853	12	0.4	1.1
02LCP120-83	58	41382	1.3	16.35518	1.4	0.56081	1.2	0.86	2870.0	28.5	2898	14	2917	12	2917	12	0.4	1.6
02LCP120-11	50	23859	2.2	18.29602	1.5	0.58442	1.2	0.79	2966.8	28.3	3005	14	3031	15	3031	15	0.5	2.1
02LCP120-39	*529*	*7459*	*1.2*	*11.00357*	*3.0*	*0.34603*	*2.9*	*0.97*	*1915.6*	*47.9*	*2523*	*28*	*3056*	*11*	*3056*	*11*	*0.4*	*37.3*
02LCP120-9	89	51456	2.1	18.51593	1.2	0.58061	1.0	0.82	2951.2	23.7	3017	12	3061	11	3061	11	0.4	3.6
02LCP120-20	132	52962	0.9	22.64464	1.2	0.63417	1.0	0.82	3166.1	25.0	3212	12	3240	11	3240	11	0.3	2.3
02LCP120-78	141	106027	1.6	23.17156	1.2	0.63529	1.0	0.82	3170.5	25.0	3234	12	3274	11	3274	11	0.3	3.2
																	85 zircons	

$^{206}Pb/^{204}Pb$ is measured ratio.

Analyses in italics/shaded are excluded due to >10% error in critical age, >10% discordance, or >5% reverse discordance.

All errors are at the 1-sigma level, and include only random uncertainties.

Best age = $^{206}Pb/^{238}U$ ages for analyses younger than 1.0 Ga and $^{206}Pb/^{207}Pb$ ages for analyses older than 1.0 Ga.

U concentration and U/Th are calibrated by comparison with NBS SRM 610 and have uncertainty of ~25%.

Decay constants: $^{235}U=9.8485x10^{-10}$, $^{238}U=1.55125x10^{-10}$, $^{238}U/235U=137.88$.

Isotope ratios are corrected for Pb/U fractionation by comparison with standard zircon with an age of 564 ± 4 Ma (2-sigma).

Initial Pb composition interpreted from Stacey and Kramers (1975), with uncertainties of 1.0 for $^{206}Pb/^{204}Pb$ and 0.3 for $^{207}Pb/^{204}Pb$.

Table I-5b. *Detrital Zircon U-Pb geochronologic analyses – Arizona Laserchron Center – Sample 02LP121 in Crow Formation.*

Isotopic ratios									Apparent ages (Ma)									
Sample	U (ppm)	$^{206}Pb/^{204}Pb$	U/Th	$^{207}Pb/^{235}U$	± (%) (1 sigma)	$^{206}Pb/^{238}U$	± (%) (1 sigma)	error corr.	$^{206}Pb/^{238}U$	± (Ma) (1 sigma)	$^{207}Pb/^{235}U$	± (Ma) (1 sigma)	$^{206}Pb/^{207}Pb$	± (Ma) (1 sigma)	BEST AGE	± (Ma) (1 sigma)	Error %	Discordance %
02LP121-86	*103*	*18201*	*0.4*	*3.95100*	*1.6*	*0.25885*	*1.0*	*0.61*	*1483.9*	*13.3*	*1624*	*13*	*1811*	*23*	*1811*	*23*	*1.3*	*18.1*
02LP121-57	*439*	*3413*	*1.4*	*4.19917*	*1.4*	*0.27377*	*1.0*	*0.71*	*1559.9*	*13.9*	*1674*	*12*	*1820*	*18*	*1820*	*18*	*1.0*	*14.3*
02LP121-62	235	46868	1.5	4.94760	1.2	0.32245	1.0	0.82	1801.7	16.0	1810	11	1820	13	1820	13	0.7	1.0
02LP121-19	272	39017	1.9	4.87565	1.5	0.31723	1.3	0.88	1776.2	20.6	1798	13	1823	13	1823	13	0.7	2.6
02LP121-8	*375*	*2769*	*1.1*	*3.51012*	*2.7*	*0.22782*	*2.6*	*0.95*	*1323.1*	*30.9*	*1530*	*21*	*1828*	*15*	*1828*	*15*	*0.8*	*27.6*
02LP121-14	64	18567	0.9	5.04142	2.3	0.32699	1.3	0.56	1823.8	21.0	1826	20	1829	35	1829	35	1.9	0.3
02LP121-97	27	9933	0.6	5.13480	4.6	0.33264	1.0	0.22	1851.2	16.1	1842	39	1831	81	1831	81	4.4	-1.1
02LP121-12	173	24162	2.0	4.82620	1.2	0.31246	1.0	0.82	1752.8	15.3	1790	10	1832	13	1832	13	0.7	4.3
02LP121-93	310	46734	0.8	4.72193	1.4	0.30463	1.2	0.86	1714.2	17.5	1771	11	1839	13	1839	13	0.7	6.8
02LP121-77	516	4626	5.5	4.68661	2.8	0.30194	2.7	0.96	1700.9	40.8	1765	24	1841	14	1841	14	0.8	7.6
02LP121-21	78	18767	0.7	5.03840	3.6	0.32457	3.3	0.90	1812.0	51.7	1826	31	1842	28	1842	28	1.5	1.6
02LP121-87	196	44649	1.2	5.10883	1.3	0.32727	1.0	0.78	1825.1	15.9	1838	11	1852	15	1852	15	0.8	1.5
02LP121-88	41	7772	0.5	5.10706	2.7	0.32673	1.0	0.37	1822.5	15.9	1837	23	1854	45	1854	45	2.4	1.7
02LP121-56	106	28544	2.2	5.11331	1.6	0.32609	1.1	0.68	1819.4	17.6	1838	14	1860	22	1860	22	1.2	2.2
02LP121-15	156	30378	1.1	5.32712	1.2	0.33957	1.0	0.82	1884.6	16.3	1873	11	1861	13	1861	13	0.7	-1.3
02LP121-41	75	29672	1.0	5.25253	2.0	0.33468	1.3	0.63	1861.0	20.2	1861	17	1861	28	1861	28	1.5	0.0
02LP121-53	120	41350	1.5	5.28130	1.8	0.33653	1.6	0.85	1870.0	25.2	1866	16	1861	17	1861	17	0.9	-0.5
02LP121-44	133	26588	0.6	5.28422	2.4	0.33566	2.1	0.88	1865.8	33.4	1866	20	1867	20	1867	20	1.1	0.1
02LP121-51	107	15820	2.4	5.31548	1.5	0.33698	1.1	0.75	1872.1	18.4	1871	13	1870	18	1870	18	1.0	-0.1
02LP121-90	392	98476	1.9	5.12885	1.2	0.32512	1.0	0.82	1814.7	15.8	1841	10	1871	13	1871	13	0.7	3.0
02LP121-23	128	24554	1.3	5.28905	1.2	0.33471	1.0	0.82	1861.2	16.2	1867	10	1874	13	1874	13	0.7	0.7
02LP121-59	96	16477	2.6	5.28678	1.8	0.33451	1.1	0.60	1860.2	17.8	1867	16	1874	26	1874	26	1.4	0.7
02LP121-5	267	41727	1.4	5.09896	1.2	0.32211	1.0	0.82	1800.0	15.7	1836	10	1877	13	1877	13	0.7	4.1
02LP121-92	159	52322	1.2	5.25627	1.6	0.33199	1.4	0.89	1848.0	22.2	1862	13	1877	13	1877	13	0.7	1.5
02LP121-13	237	39091	3.6	5.17901	1.2	0.32684	1.0	0.82	1823.1	15.9	1849	10	1879	13	1879	13	0.7	3.0
02LP121-54	137	44489	1.1	5.27285	1.3	0.33247	1.0	0.75	1850.3	16.1	1865	11	1880	16	1880	16	0.9	1.6
02LP121-4	163	28940	0.7	5.19369	2.4	0.32732	2.3	0.96	1825.4	36.9	1852	21	1881	13	1881	13	0.7	3.0
02LP121-32	201	50147	1.1	5.39369	1.2	0.33987	1.0	0.82	1886.0	16.4	1884	11	1881	13	1881	13	0.7	-0.3
02LP121-55	273	63188	1.3	5.37552	1.2	0.33861	1.0	0.82	1880.0	16.3	1881	11	1882	13	1882	13	0.7	0.1
02LP121-63	212	31479	3.3	5.31647	1.3	0.33489	1.0	0.80	1862.1	16.2	1872	11	1882	13	1882	13	0.7	1.1
02LP121-69	361	84886	0.4	5.16956	1.4	0.32563	1.2	0.87	1817.2	19.6	1848	12	1882	13	1882	13	0.7	3.4
02LP121-16	193	37976	0.9	5.21128	1.3	0.32801	1.1	0.84	1828.7	17.0	1855	11	1883	13	1883	13	0.7	2.9
02LP121-39	132	43564	1.8	5.34033	1.6	0.33596	1.4	0.88	1867.2	23.0	1875	14	1884	14	1884	14	0.7	0.9
02LP121-46	289	52158	1.3	5.31052	2.4	0.33410	2.3	0.96	1858.2	37.1	1871	21	1884	13	1884	13	0.7	1.4
02LP121-58	345	26465	1.3	5.01329	3.4	0.31544	3.4	0.98	1767.4	51.8	1822	29	1884	13	1884	13	0.7	6.2

$^{206}Pb/^{204}Pb$ is measured ratio.

Analyses in italics/shaded are excluded due to >10% error in critical age, >10% discordance, or >5% reverse discordance.

All errors are at the 1-sigma level, and include only random uncertainties.

Best age = $^{206}Pb/^{238}U$ ages for analyses younger than 1.0 Ga and $^{206}Pb/^{207}Pb$ ages for analyses older than 1.0 Ga.

U concentration and U/Th are calibrated by comparison with NBS SRM 610 and have uncertainty of ~25%.

Decay constants: $^{235}U=9.8485x10^{-10}$, $^{238}U=1.55125x10^{-10}$, $^{238}U/235U=137.88$.

Isotope ratios are corrected for Pb/U fractionation by comparison with standard zircon with an age of 564 ± 4 Ma (2-sigma).

Initial Pb composition interpreted from Stacey and Kramers (1975), with uncertainties of 1.0 for $^{206}Pb/^{204}Pb$ and 0.3 for $^{207}Pb/^{204}Pb$.

Table I-5b. *(continued) Detrital Zircon U-Pb geochronologic analyses – Arizona Laserchron Center – Sample 02LP121 in Crow Formation.*

Isotopic ratios									Apparent ages (Ma)									
Sample	U (ppm)	$^{206}Pb/^{204}Pb$	U/Th	$^{207}Pb/^{235}U$	± (%) (1 sigma)	$^{206}Pb/^{238}U$	± (%) (1 sigma)	error corr.	$^{206}Pb/^{238}U$	± (Ma) (1 sigma)	$^{207}Pb/^{235}U$	± (Ma) (1 sigma)	$^{206}Pb/^{207}Pb$	± (Ma) (1 sigma)	BEST AGE	± (Ma) (1 sigma)	Error %	Discordance %
02LP121-11	139	28050	1.1	5.28505	1.8	0.33192	1.6	0.92	1847.7	26.2	1867	15	1887	13	1887	13	0.7	2.1
02LP121-35	*213*	*11151*	*1.2*	*4.64838*	*3.3*	*0.29176*	*3.2*	*0.96*	*1650.3*	*46.0*	*1758*	*28*	*1888*	*17*	*1888*	*17*	*0.9*	*12.6*
02LP121-99	83	3488	0.7	5.32657	2.8	0.33434	1.7	0.60	1859.4	27.3	1873	24	1888	41	1888	41	2.2	1.5
02LP121-33	199	30338	1.5	5.30972	1.7	0.33267	1.5	0.89	1851.3	24.1	1870	14	1892	14	1892	14	0.7	2.2
02LP121-84	229	4296	1.9	5.31184	2.8	0.33278	1.1	0.37	1851.8	17.0	1871	24	1892	48	1892	48	2.5	2.1
02LP121-2	118	24885	1.0	5.16862	1.5	0.32353	1.1	0.77	1807.0	17.7	1848	12	1893	17	1893	17	0.9	4.5
02LP121-20	112	16012	1.1	5.20626	3.4	0.32598	3.1	0.93	1818.9	49.8	1854	29	1893	22	1893	22	1.2	3.9
02LP121-30	125	23284	0.7	5.33339	1.9	0.33317	1.1	0.60	1853.7	17.9	1874	16	1897	27	1897	27	1.4	2.3
02LP121-36	179	15021	0.6	4.96704	3.0	0.31033	2.9	0.95	1742.3	44.0	1814	26	1897	16	1897	16	0.8	8.2
02LP121-9	151	17759	0.7	5.17970	1.6	0.32339	1.4	0.89	1806.3	22.4	1849	14	1898	13	1898	13	0.7	4.8
02LP121-7	191	44527	1.4	5.21807	1.2	0.32560	1.0	0.82	1817.0	15.8	1856	10	1899	13	1899	13	0.7	4.3
02LP121-10	134	31658	1.6	5.40905	2.0	0.33698	1.8	0.90	1872.1	28.6	1886	17	1902	15	1902	15	0.8	1.6
02LP121-70	138	27821	1.6	5.41568	1.6	0.33640	1.0	0.62	1869.3	16.2	1887	14	1907	23	1907	23	1.2	2.0
02LP121-91	95	25301	1.0	5.50972	2.0	0.34184	1.1	0.56	1895.5	17.9	1902	17	1909	29	1909	29	1.5	0.7
02LP121-67	130	36520	2.9	5.21247	1.5	0.32259	1.0	0.68	1802.3	16.4	1855	13	1914	20	1914	20	1.0	5.8
02LP121-40	171	28853	1.2	5.56390	1.9	0.34413	1.7	0.90	1906.5	28.7	1911	17	1915	15	1915	15	0.8	0.4
02LP121-100	259	40341	1.5	5.59742	2.4	0.34616	2.3	0.95	1916.3	37.3	1916	20	1915	13	1915	13	0.7	-0.1
02LP121-65	246	17415	1.8	5.12593	1.9	0.31680	1.8	0.92	1774.1	27.3	1840	16	1916	14	1916	14	0.7	7.4
02LP121-76	140	84407	1.8	5.54893	1.4	0.34246	1.0	0.69	1898.5	16.4	1908	12	1919	19	1919	19	1.0	1.1
02LP121-66	*85*	*4894*	*1.0*	*4.07924*	*2.2*	*0.25101*	*1.7*	*0.79*	*1443.7*	*22.5*	*1650*	*18*	*1924*	*24*	*1924*	*24*	*1.2*	*25.0*
02LP121-79	61	37819	0.4	5.77782	2.3	0.35303	1.7	0.75	1949.1	28.6	1943	20	1937	27	1937	27	1.4	-0.6
02LP121-50	256	66994	1.2	5.85383	1.6	0.35507	1.5	0.90	1958.8	24.5	1954	14	1950	13	1950	13	0.7	-0.5
02LP121-71	211	82219	1.2	5.76157	1.2	0.34915	1.0	0.82	1930.5	16.7	1941	11	1951	13	1951	13	0.7	1.1
02LP121-89	242	66783	1.9	5.74238	1.2	0.34646	1.0	0.82	1917.7	16.6	1938	11	1959	13	1959	13	0.7	2.1
02LP121-25	218	50804	1.3	5.90206	1.2	0.35330	1.0	0.82	1950.3	16.8	1962	11	1973	12	1973	12	0.6	1.2
02LP121-34	165	51264	0.9	6.01043	2.6	0.35921	2.4	0.92	1978.4	40.5	1977	23	1976	18	1976	18	0.9	-0.1
02LP121-26	124	39686	0.9	5.95130	2.4	0.35536	2.1	0.86	1960.1	34.6	1969	21	1978	21	1978	21	1.1	0.9
02LP121-18	159	23232	0.2	6.06001	1.4	0.35257	1.0	0.71	1946.9	16.8	1985	12	2024	18	2024	18	0.9	3.8
02LP121-28	136	49871	1.1	7.09947	1.3	0.39069	1.1	0.84	2126.0	19.4	2124	11	2122	12	2122	12	0.6	-0.2
02LP121-52	451	20844	3.1	8.74088	1.2	0.42433	1.0	0.82	2280.1	19.2	2311	11	2339	12	2339	12	0.5	2.5
02LP121-17	139	38421	0.6	9.08652	1.3	0.43275	1.0	0.79	2318.1	19.5	2347	12	2372	13	2372	13	0.5	2.3
02LP121-81	255	44332	1.4	9.41549	1.2	0.44428	1.0	0.81	2369.8	19.8	2379	11	2388	12	2388	12	0.5	0.8
02LP121-38	92	32745	0.6	9.86437	1.4	0.45377	1.1	0.82	2412.0	22.7	2422	13	2431	13	2431	13	0.5	0.8
02LP121-78	160	27104	0.6	10.16463	1.5	0.44926	1.4	0.89	2392.0	27.4	2450	14	2498	12	2498	12	0.5	4.2
02LP121-73	390	41430	1.1	12.07684	1.3	0.48885	1.1	0.85	2565.7	23.7	2610	12	2645	12	2645	12	0.5	3.0

$^{206}Pb/^{204}Pb$ is measured ratio.

Analyses in italics/shaded are excluded due to >10% error in critical age, >10% discordance, or >5% reverse discordance.

All errors are at the 1-sigma level, and include only random uncertainties.

Best age = $^{206}Pb/^{238}U$ ages for analyses younger than 1.0 Ga and $^{206}Pb/^{207}Pb$ ages for analyses older than 1.0 Ga.

U concentration and U/Th are calibrated by comparison with NBS SRM 610 and have uncertainty of ~25%.

Decay constants: $^{235}U=9.8485x10^{-10}$, $^{238}U=1.55125x10^{-10}$, $^{238}U/235U=137.88$.

Isotope ratios are corrected for Pb/U fractionation by comparison with standard zircon with an age of 564 ± 4 Ma (2-sigma).

Initial Pb composition interpreted from Stacey and Kramers (1975), with uncertainties of 1.0 for $^{206}Pb/^{204}Pb$ and 0.3 for $^{207}Pb/^{204}Pb$.

Table I-5b. *(continued) Detrital Zircon U-Pb geochronologic analyses – Arizona Laserchron Center – Sample 02LP121 in Crow Formation.*

Isotopic ratios									Apparent ages (Ma)									
Sample	U (ppm)	$^{206}Pb/^{204}Pb$	U/Th	$^{207}Pb/^{235}U$	± (%) (1 sigma)	$^{206}Pb/^{238}U$	± (%) (1 sigma)	error corr.	$^{206}Pb/^{238}U$	± (Ma) (1 sigma)	$^{207}Pb/^{235}U$	± (Ma) (1 sigma)	$^{206}Pb/^{207}Pb$	± (Ma) (1 sigma)	BEST AGE	± (Ma) (1 sigma)	Error %	Discordance %
02LP121-85	401	130952	3.5	12.55272	1.2	0.50181	1.0	0.82	2621.6	21.5	2647	12	2666	12	2666	12	0.5	1.7
02LP121-48	86	11163	1.3	12.83257	1.7	0.50789	1.0	0.58	2647.6	21.8	2667	16	2682	23	2682	23	0.9	1.3
02LP121-47	90	47087	1.1	12.46052	1.2	0.49275	1.0	0.82	2582.6	21.3	2640	12	2684	12	2684	12	0.4	3.8
02LP121-64	56	21901	0.7	12.59043	1.5	0.49729	1.0	0.65	2602.1	21.4	2650	14	2686	19	2686	19	0.7	3.1
02LP121-96	150	36454	0.4	12.35701	1.5	0.48686	1.3	0.88	2557.1	27.4	2632	14	2690	12	2690	12	0.4	4.9
02LP121-37	84	23340	0.7	13.29521	1.4	0.52186	1.0	0.72	2707.1	22.1	2701	13	2696	16	2696	16	0.6	-0.4
02LP121-80	63	22748	0.4	13.17819	1.2	0.51650	1.0	0.82	2684.3	22.0	2693	12	2699	12	2699	12	0.4	0.5
02LP121-94	63	35260	0.5	13.27781	1.4	0.51946	1.2	0.81	2696.9	25.3	2700	13	2702	14	2702	14	0.5	0.2
02LP121-83	280	72091	0.9	13.16539	2.0	0.51199	1.8	0.93	2665.1	39.7	2692	18	2712	12	2712	12	0.4	1.7
02LP121-49	112	68563	0.8	13.24533	1.7	0.51373	1.6	0.91	2672.5	34.3	2697	16	2716	12	2716	12	0.4	1.6
02LP121-29	42	13512	0.5	13.30175	1.9	0.51462	1.3	0.67	2676.3	28.5	2701	18	2720	23	2720	23	0.8	1.6
02LP121-68	163	77063	1.3	13.09692	1.2	0.50656	1.0	0.82	2641.9	21.7	2687	12	2720	12	2720	12	0.4	2.9
02LP121-24	*61*	*5403*	*0.5*	*11.85073*	*2.1*	*0.45696*	*1.8*	*0.87*	*2426.1*	*37.0*	*2593*	*20*	*2726*	*17*	*2726*	*17*	*0.6*	*11.0*
02LP121-95	250	88313	0.8	13.77328	1.2	0.52778	1.0	0.82	2732.1	22.3	2734	12	2736	12	2736	12	0.4	0.1
02LP121-60	83	62791	0.6	14.00879	1.5	0.53521	1.3	0.88	2763.3	29.9	2750	14	2741	12	2741	12	0.4	-0.8
02LP121-27	131	24181	0.4	13.96571	1.2	0.53280	1.0	0.82	2753.2	22.4	2747	12	2743	12	2743	12	0.4	-0.4
02LP121-1	220	41660	0.7	13.26535	2.0	0.50118	1.8	0.93	2618.8	39.2	2699	18	2759	11	2759	11	0.4	5.1
02LP121-61	118	34650	0.6	14.44687	1.7	0.54142	1.6	0.91	2789.4	35.5	2780	16	2772	11	2772	11	0.4	-0.6
02LP121-74	188	74520	1.0	14.18687	1.2	0.52896	1.0	0.82	2737.1	22.3	2762	12	2781	11	2781	11	0.4	1.6
02LP121-45	374	55813	2.2	13.07067	2.2	0.48407	2.1	0.95	2545.0	43.7	2685	21	2792	11	2792	11	0.4	8.8
02LP121-42	106	70625	1.0	14.41612	1.8	0.53161	1.7	0.92	2748.2	37.1	2778	17	2799	11	2799	11	0.4	1.8
02LP121-98	72	45559	0.3	14.73587	1.5	0.54259	1.3	0.88	2794.3	30.2	2798	14	2801	12	2801	12	0.4	0.2
02LP121-82	54	29832	1.6	15.62045	1.4	0.54718	1.0	0.72	2813.4	22.8	2854	13	2883	16	2883	16	0.6	2.4
02LP121-31	165	70543	1.0	17.50581	1.6	0.58414	1.4	0.90	2965.6	34.2	2963	15	2961	11	2961	11	0.4	-0.2
02LP121-3	248	70302	1.3	19.82640	1.7	0.59192	1.5	0.91	2997.2	36.4	3083	16	3139	11	3139	11	0.4	4.5
02LP121-72	278	25174	0.7	21.03041	1.2	0.59789	1.0	0.82	3021.3	24.1	3140	12	3217	11	3217	11	0.3	6.1
																	90 zircons	

$^{206}Pb/^{204}Pb$ is measured ratio.

Analyses in italics/shaded are excluded due to >10% error in critical age, >10% discordance, or >5% reverse discordance.

All errors are at the 1-sigma level, and include only random uncertainties.

Best age = $^{206}Pb/^{238}U$ ages for analyses younger than 1.0 Ga and $^{206}Pb/^{207}Pb$ ages for analyses older than 1.0 Ga.

U concentration and U/Th are calibrated by comparison with NBS SRM 610 and have uncertainty of ~25%.

Decay constants: $^{235}U=9.8485x10^{-10}$, $^{238}U=1.55125x10^{-10}$, $^{238}U/235U=137.88$.

Isotope ratios are corrected for Pb/U fractionation by comparison with standard zircon with an age of 564 ± 4 Ma (2-sigma).

Initial Pb composition interpreted from Stacey and Kramers (1975), with uncertainties of 1.0 for $^{206}Pb/^{204}Pb$ and 0.3 for $^{207}Pb/^{204}Pb$.

Table I-5c. *Detrital Zircon U-Pb geochronologic analyses – Arizona Laserchron Center – Sample 004LP028 in Crow Formation.*

Isotopic ratios									Apparent ages (Ma)									
Sample	U (ppm)	$^{206}Pb/^{204}Pb$	U/Th	$^{207}Pb/^{235}U$	± (%) (1 sigma)	$^{206}Pb/^{238}U$	± (%) (1 sigma)	error corr.	$^{206}Pb/^{238}U$	± (Ma) (1 sigma)	$^{207}Pb/^{235}U$	± (Ma) (1 sigma)	$^{206}Pb/^{207}Pb$	± (Ma) (1 sigma)	BEST AGE	± (Ma) (1 sigma)	Error %	Discordance %
04LP028-75	*645*	*1778*	*0.5*	*0.99246*	*4.8*	*0.07473*	*4.4*	*0.92*	*464.6*	*19.7*	*700*	*24*	*1554*	*35*	*1554*	*35*	*2.3*	*70.1*
04LP028-63	*68*	*3812*	*0.8*	*2.76726*	*4.5*	*0.19140*	*3.3*	*0.72*	*1128.9*	*33.7*	*1347*	*34*	*1712*	*58*	*1712*	*58*	*3.4*	*34.1*
04LP028-16	*775*	*4376*	*2.8*	*2.57392*	*2.6*	*0.17582*	*2.4*	*0.91*	*1044.1*	*22.9*	*1293*	*19*	*1735*	*20*	*1735*	*20*	*1.2*	*39.8*
04LP028-10	*991*	*2699*	*0.6*	*1.76046*	*2.7*	*0.11610*	*2.3*	*0.88*	*708.1*	*15.6*	*1031*	*17*	*1799*	*23*	*1799*	*23*	*1.3*	*60.6*
04LP028-20	75	14175	0.7	4.86925	2.1	0.32039	1.2	0.56	1791.6	18.6	1797	18	1803	32	1803	32	1.8	0.6
04LP028-73	119	21767	3.0	4.87454	1.5	0.31774	1.1	0.74	1778.7	17.3	1798	13	1820	18	1820	18	1.0	2.3
04LP028-93	58	14938	1.0	4.93117	3.2	0.32150	1.9	0.59	1797.0	29.3	1808	27	1820	46	1820	46	2.5	1.3
04LP028-34	78	21974	0.7	4.99987	2.2	0.32516	1.0	0.45	1814.9	15.8	1819	19	1824	36	1824	36	2.0	0.5
04LP028-5	*364*	*12992*	*1.1*	*2.85560*	*3.6*	*0.18555*	*3.3*	*0.92*	*1097.2*	*33.1*	*1370*	*27*	*1826*	*24*	*1826*	*24*	*1.3*	*39.9*
04LP028-52	410	9499	1.4	4.47320	4.6	0.29061	4.5	0.97	1644.6	64.6	1726	38	1826	20	1826	20	1.1	9.9
04LP028-67	37	11094	1.5	4.78662	3.5	0.31107	2.2	0.63	1746.0	34.1	1783	30	1826	50	1826	50	2.7	4.4
04LP028-58	628	18219	3.9	4.70231	2.5	0.30465	2.3	0.91	1714.3	33.9	1768	21	1831	18	1831	18	1.0	6.4
04LP028-85	43	7608	0.7	5.11813	3.3	0.33112	1.8	0.53	1843.8	28.1	1839	28	1834	50	1834	50	2.7	-0.5
04LP028-14	*191*	*15253*	*1.2*	*3.86281*	*1.8*	*0.24942*	*1.5*	*0.82*	*1435.5*	*18.8*	*1606*	*14*	*1837*	*18*	*1837*	*18*	*1.0*	*21.9*
04LP028-38	*464*	*13685*	*0.9*	*3.22540*	*1.7*	*0.20823*	*1.4*	*0.81*	*1219.4*	*15.3*	*1463*	*13*	*1838*	*18*	*1838*	*18*	*1.0*	*33.7*
04LP028-59	146	24112	1.0	4.56930	2.1	0.29488	1.3	0.64	1665.9	19.7	1744	17	1838	29	1838	29	1.6	9.4
04LP028-55	65	21351	0.7	5.14641	2.1	0.33130	1.0	0.49	1844.7	16.7	1844	18	1843	33	1843	33	1.8	-0.1
04LP028-25	91	30788	1.1	4.80249	1.8	0.30874	1.0	0.56	1734.5	15.2	1785	15	1845	27	1845	27	1.5	6.0
04LP028-69	282	54529	4.8	4.96004	1.4	0.31862	1.0	0.71	1783.0	15.6	1813	12	1847	18	1847	18	1.0	3.5
04LP028-77	75	19165	0.8	5.16092	2.0	0.33149	1.0	0.51	1845.6	16.1	1846	17	1847	30	1847	30	1.6	0.1
04LP028-22	239	55017	1.8	4.76797	2.1	0.30602	1.9	0.88	1721.1	28.1	1779	18	1848	18	1848	18	1.0	6.9
04LP028-70	116	41737	0.9	4.99505	1.8	0.32065	1.4	0.77	1792.9	22.1	1819	16	1848	21	1848	21	1.1	3.0
04LP028-100	*375*	*39928*	*1.3*	*4.34972*	*3.1*	*0.27903*	*2.9*	*0.94*	*1586.5*	*40.6*	*1703*	*25*	*1849*	*18*	*1849*	*18*	*1.0*	*14.2*
04LP028-26	382	16900	2.6	4.70138	2.1	0.30124	1.8	0.88	1697.4	27.5	1768	18	1851	18	1851	18	1.0	8.3
04LP028-11	*227*	*17679*	*1.1*	*4.06676*	*3.8*	*0.26045*	*3.7*	*0.96*	*1492.1*	*49.2*	*1648*	*31*	*1852*	*18*	*1852*	*18*	*1.0*	*19.4*
04LP028-29	217	37540	7.0	4.75608	1.5	0.30434	1.0	0.67	1712.8	15.0	1777	13	1854	20	1854	20	1.1	7.6
04LP028-27	310	61736	8.7	5.14310	1.5	0.32809	1.2	0.76	1829.1	18.5	1843	13	1859	18	1859	18	1.0	1.6
04LP028-33	126	32364	1.4	5.13238	1.4	0.32737	1.0	0.71	1825.6	15.9	1842	12	1859	18	1859	18	1.0	1.8
04LP028-36	*275*	*18117*	*1.4*	*4.54110*	*1.5*	*0.28933*	*1.0*	*0.67*	*1638.2*	*14.5*	*1739*	*12*	*1861*	*20*	*1861*	*20*	*1.1*	*12.0*
04LP028-47	*417*	*9027*	*0.8*	*3.46298*	*2.9*	*0.22063*	*2.7*	*0.93*	*1285.2*	*31.3*	*1519*	*23*	*1862*	*19*	*1862*	*19*	*1.0*	*31.0*
04LP028-40	254	53692	4.4	5.03828	1.4	0.32063	1.0	0.71	1792.8	15.7	1826	12	1864	18	1864	18	1.0	3.8
04LP028-46	234	38095	2.2	5.11748	1.9	0.32506	1.6	0.84	1814.4	25.0	1839	16	1867	18	1867	18	1.0	2.8
04LP028-96	29	7177	7.2	5.26636	3.2	0.33441	2.4	0.76	1859.7	39.4	1863	27	1868	38	1868	38	2.0	0.4
04LP028-80	104	16235	1.6	5.23753	1.9	0.33232	1.7	0.86	1849.6	26.7	1859	17	1869	18	1869	18	1.0	1.0
04LP028-97	356	96430	2.1	5.05832	1.4	0.32094	1.0	0.71	1794.3	15.7	1829	12	1869	18	1869	18	1.0	4.0

$^{206}Pb/^{204}Pb$ is measured ratio.

Analyses in italics/shaded are excluded due to >10% error in critical age, >10% discordance, or >5% reverse discordance.

All errors are at the 1-sigma level, and include only random uncertainties.

Best age = $^{206}Pb/^{238}U$ ages for analyses younger than 1.0 Ga and $^{206}Pb/^{207}Pb$ ages for analyses older than 1.0 Ga.

U concentration and U/Th are calibrated by comparison with NBS SRM 610 and have uncertainty of ~25%.

Decay constants: $^{235}U=9.8485x10^{-10}$, $^{238}U=1.55125x10^{-10}$, $^{238}U/235U=137.88$.

Isotope ratios are corrected for Pb/U fractionation by comparison with standard zircon with an age of 564 ± 4 Ma (2-sigma).

Initial Pb composition interpreted from Stacey and Kramers (1975), with uncertainties of 1.0 for $^{206}Pb/^{204}Pb$ and 0.3 for $^{207}Pb/^{204}Pb$.

Table I-5c. *(continued) Detrital Zircon U-Pb geochronologic analyses – Arizona Laserchron Center – Sample 004LP028 in Crow Formation.*

Isotopic ratios									Apparent ages (Ma)									
Sample	U (ppm)	$^{206}Pb/^{204}Pb$	U/Th	$^{207}Pb/^{235}U$	± (%) (1 sigma)	$^{206}Pb/^{238}U$	± (%) (1 sigma)	error corr.	$^{206}Pb/^{238}U$	± (Ma) (1 sigma)	$^{207}Pb/^{235}U$	± (Ma) (1 sigma)	$^{206}Pb/^{207}Pb$	± (Ma) (1 sigma)	BEST AGE	± (Ma) (1 sigma)	Error %	Discordance %
04LP028-32	135	26373	2.2	5.21190	1.4	0.33048	1.0	0.71	1840.7	16.0	1855	12	1870	18	1870	18	1.0	1.6
04LP028-39	140	39782	0.9	5.14390	1.8	0.32612	1.3	0.70	1819.5	20.3	1843	16	1870	24	1870	24	1.3	2.7
04LP028-90	81	10019	178.9	5.21149	3.6	0.32869	3.0	0.85	1832.1	48.5	1855	30	1880	34	1880	34	1.8	2.5
04LP028-62	*60*	*22674*	*1.1*	*4.67005*	*1.5*	*0.29434*	*1.0*	*0.65*	*1663.2*	*14.7*	*1762*	*13*	*1881*	*21*	*1881*	*21*	*1.1*	*11.6*
04LP028-83	85	17385	1.6	5.23165	1.4	0.32945	1.0	0.70	1835.7	16.0	1858	12	1883	18	1883	18	1.0	2.5
04LP028-54	93	22479	1.1	5.41333	2.2	0.33881	1.0	0.46	1880.9	16.3	1887	19	1894	35	1894	35	1.8	0.7
04LP028-81	196	39907	1.4	5.02068	2.7	0.31398	2.5	0.92	1760.2	39.0	1823	23	1895	19	1895	19	1.0	7.1
04LP028-94	153	45996	1.4	5.08499	2.1	0.31668	1.8	0.85	1773.5	27.6	1834	18	1903	20	1903	20	1.1	6.8
04LP028-12	198	28160	1.5	5.39294	1.4	0.33416	1.0	0.71	1858.5	16.1	1884	12	1912	18	1912	18	0.9	2.8
04LP028-99	157	62728	1.5	5.44839	3.8	0.33678	3.7	0.96	1871.2	59.9	1893	33	1916	18	1916	18	0.9	2.3
04LP028-17	59	10979	0.6	5.36169	3.2	0.33100	1.0	0.31	1843.2	16.0	1879	28	1918	55	1918	55	2.9	3.9
04LP028-53	*236*	*4891*	*0.9*	*4.39351*	*3.5*	*0.27121*	*3.3*	*0.96*	*1547.0*	*45.5*	*1711*	*29*	*1918*	*18*	*1918*	*18*	*0.9*	*19.3*
04LP028-37	102	18485	0.6	5.66125	2.1	0.34638	1.7	0.83	1917.3	28.7	1926	18	1934	21	1934	21	1.1	0.9
04LP028-64	*255*	*20255*	*0.8*	*4.48927*	*1.7*	*0.27339*	*1.3*	*0.79*	*1558.0*	*18.1*	*1729*	*14*	*1943*	*18*	*1943*	*18*	*0.9*	*19.8*
04LP028-50	222	51065	0.4	5.65009	1.4	0.34046	1.0	0.71	1888.9	16.4	1924	12	1962	18	1962	18	0.9	3.7
04LP028-51	238	59963	0.5	5.96782	2.1	0.35797	1.8	0.87	1972.5	30.6	1971	18	1970	18	1970	18	0.9	-0.1
04LP028-87	*265*	*5855*	*1.4*	*4.81989*	*3.5*	*0.28835*	*3.4*	*0.96*	*1633.3*	*48.3*	*1788*	*30*	*1974*	*18*	*1974*	*18*	*0.9*	*17.3*
04LP028-24	*219*	*15806*	*0.7*	*4.90504*	*2.1*	*0.29274*	*1.8*	*0.87*	*1655.2*	*26.1*	*1803*	*17*	*1979*	*18*	*1979*	*18*	*0.9*	*16.4*
04LP028-71	232	67145	0.7	5.80270	1.6	0.34580	1.2	0.77	1914.5	19.9	1947	14	1981	18	1981	18	0.9	3.4
04LP028-45	*241*	*28367*	*0.6*	*4.73471*	*2.0*	*0.27782*	*1.7*	*0.86*	*1580.4*	*23.5*	*1773*	*16*	*2009*	*18*	*2009*	*18*	*0.9*	*21.3*
04LP028-43	*251*	*11167*	*0.5*	*4.38389*	*3.0*	*0.25623*	*2.8*	*0.94*	*1470.5*	*37.0*	*1709*	*25*	*2016*	*18*	*2016*	*18*	*0.9*	*27.1*
04LP028-7	*214*	*16138*	*0.8*	*5.19825*	*2.9*	*0.30212*	*2.7*	*0.94*	*1701.8*	*40.8*	*1852*	*25*	*2026*	*18*	*2026*	*18*	*0.9*	*16.0*
04LP028-41	192	48762	0.9	6.32871	1.4	0.36643	1.0	0.71	2012.6	17.3	2022	12	2033	18	2033	18	0.9	1.0
04LP028-86	133	23343	0.3	6.23917	1.5	0.36014	1.1	0.73	1982.9	18.3	2010	13	2038	18	2038	18	0.9	2.7
04LP028-1	*310*	*7105*	*1.0*	*5.19887*	*1.5*	*0.29495*	*1.0*	*0.68*	*1666.2*	*14.7*	*1852*	*13*	*2068*	*19*	*2068*	*19*	*0.9*	*19.4*
04LP028-21	*543*	*6577*	*0.7*	*5.34760*	*3.5*	*0.26964*	*3.4*	*0.96*	*1539.0*	*46.0*	*1877*	*30*	*2274*	*17*	*2274*	*17*	*0.7*	*32.3*
04LP028-2	*107*	*10600*	*0.6*	*5.73467*	*3.9*	*0.27623*	*3.7*	*0.97*	*1572.4*	*52.0*	*1937*	*33*	*2352*	*17*	*2352*	*17*	*0.7*	*33.1*
04LP028-8	75	23197	0.5	9.15130	1.5	0.43746	1.0	0.67	2339.3	19.6	2353	14	2365	19	2365	19	0.8	1.1
04LP028-35	*253*	*24959*	*1.1*	*7.02054*	*3.9*	*0.32991*	*3.7*	*0.96*	*1837.9*	*59.8*	*2114*	*35*	*2395*	*17*	*2395*	*17*	*0.7*	*23.3*
04LP028-61	574	20076	2.8	8.67904	2.0	0.40440	1.8	0.87	2189.3	32.9	2305	19	2409	17	2409	17	0.7	9.1
04LP028-79	*202*	*16213*	*0.6*	*7.05641*	*2.6*	*0.32873*	*2.4*	*0.92*	*1832.2*	*37.5*	*2119*	*23*	*2409*	*17*	*2409*	*17*	*0.7*	*23.9*
04LP028-60	234	43139	1.5	9.75188	2.4	0.45283	2.2	0.91	2407.8	43.6	2412	22	2415	17	2415	17	0.7	0.3

$^{206}Pb/^{204}Pb$ is measured ratio.

Analyses in italics/shaded are excluded due to >10% error in critical age, >10% discordance, or >5% reverse discordance.

All errors are at the 1-sigma level, and include only random uncertainties.

Best age = $^{206}Pb/^{238}U$ ages for analyses younger than 1.0 Ga and $^{206}Pb/^{207}Pb$ ages for analyses older than 1.0 Ga.

U concentration and U/Th are calibrated by comparison with NBS SRM 610 and have uncertainty of ~25%.

Decay constants: $^{235}U=9.8485x10^{-10}$, $^{238}U=1.55125x10^{-10}$, $^{238}U/235U=137.88$.

Isotope ratios are corrected for Pb/U fractionation by comparison with standard zircon with an age of 564 ± 4 Ma (2-sigma).

Initial Pb composition interpreted from Stacey and Kramers (1975), with uncertainties of 1.0 for $^{206}Pb/^{204}Pb$ and 0.3 for $^{207}Pb/^{204}Pb$.

Table I-5c. *(continued) Detrital Zircon U-Pb geochronologic analyses – Arizona Laserchron Center – Sample 004LP028 in Crow Formation.*

Isotopic ratios									Apparent ages (Ma)									
Sample	U (ppm)	$^{206}Pb/^{204}Pb$	U/Th	$^{207}Pb/^{235}U$	± (%) (1 sigma)	$^{206}Pb/^{238}U$	± (%) (1 sigma)	error corr.	$^{206}Pb/^{238}U$	± (Ma) (1 sigma)	$^{207}Pb/^{235}U$	± (Ma) (1 sigma)	$^{206}Pb/^{207}Pb$	± (Ma) (1 sigma)	BEST AGE	± (Ma) (1 sigma)	Error %	Discordance %
04LP028-28	50	18145	0.6	9.27973	4.6	0.42970	4.0	0.87	2304.3	76.7	2366	42	2420	38	2420	38	1.6	4.8
04LP028-84	68	15710	0.6	9.66227	1.6	0.43340	1.0	0.63	2321.0	19.5	2403	15	2473	21	2473	21	0.8	6.1
04LP028-30	199	34847	1.5	10.42614	3.3	0.46123	3.2	0.95	2445.0	64.5	2473	31	2497	17	2497	17	0.7	2.1
04LP028-88	*214*	*14843*	*1.3*	*8.91337*	*1.7*	*0.39358*	*1.4*	*0.81*	*2139.4*	*24.9*	*2329*	*16*	*2500*	*17*	*2500*	*17*	*0.7*	*14.4*
04LP028-44	89	30225	1.2	10.66709	1.4	0.46124	1.0	0.71	2445.0	20.3	2495	13	2535	17	2535	17	0.7	3.6
04LP028-92	*373*	*7806*	*0.6*	*3.86787*	*3.1*	*0.16175*	*2.9*	*0.95*	*966.5*	*26.4*	*1607*	*25*	*2591*	*17*	*2591*	*17*	*0.7*	*62.7*
04LP028-49	169	38143	1.2	10.95628	4.0	0.44918	3.0	0.75	2391.6	59.5	2519	37	2624	44	2624	44	1.7	8.9
04LP028-48	130	64436	0.5	11.48351	1.4	0.46636	1.0	0.71	2467.6	20.5	2563	13	2640	17	2640	17	0.6	6.5
04LP028-74	*359*	*13143*	*0.8*	*5.23019*	*3.2*	*0.21201*	*3.0*	*0.95*	*1239.5*	*33.6*	*1858*	*27*	*2643*	*17*	*2643*	*17*	*0.6*	*53.1*
04LP028-98	130	64087	0.9	12.64295	1.4	0.50133	1.0	0.71	2619.5	21.5	2653	13	2679	17	2679	17	0.6	2.2
04LP028-18	*66*	*15486*	*0.4*	*9.69523*	*3.6*	*0.38275*	*3.4*	*0.95*	*2089.1*	*61.0*	*2406*	*33*	*2687*	*19*	*2687*	*19*	*0.7*	*22.3*
04LP028-19	72	24807	0.4	12.74764	1.4	0.50207	1.0	0.71	2622.7	21.6	2661	13	2691	17	2691	17	0.6	2.5
04LP028-89	*85*	*7523*	*0.7*	*9.91182*	*2.7*	*0.38859*	*2.3*	*0.85*	*2116.3*	*41.5*	*2427*	*25*	*2698*	*24*	*2698*	*24*	*0.9*	*21.6*
04LP028-76	54	23313	0.2	13.17651	1.8	0.51198	1.0	0.55	2665.1	21.8	2692	17	2713	25	2713	25	0.9	1.8
04LP028-78	48	18756	2.0	13.20730	1.5	0.51305	1.0	0.69	2669.6	21.9	2695	14	2713	17	2713	17	0.6	1.6
04LP028-9	*259*	*8555*	*0.7*	*8.85129*	*4.3*	*0.34346*	*4.1*	*0.96*	*1903.3*	*67.6*	*2323*	*39*	*2715*	*20*	*2715*	*20*	*0.7*	*29.9*
04LP028-82	150	43395	0.6	13.06887	3.1	0.50622	2.9	0.95	2640.5	63.0	2685	29	2718	16	2718	16	0.6	2.9
04LP028-4	*279*	*30381*	*1.3*	*10.94255*	*4.3*	*0.42299*	*4.2*	*0.97*	*2274.0*	*80.3*	*2518*	*40*	*2721*	*16*	*2721*	*16*	*0.6*	*16.4*
04LP028-15	116	35770	0.9	13.30349	1.5	0.51447	1.0	0.66	2675.7	21.9	2701	14	2721	19	2721	19	0.7	1.7
04LP028-66	*171*	*55580*	*0.5*	*11.70478*	*2.3*	*0.45263*	*2.1*	*0.90*	*2406.9*	*42.6*	*2581*	*22*	*2721*	*16*	*2721*	*16*	*0.6*	*11.5*
04LP028-23	103	50119	0.9	12.87241	2.4	0.49754	2.2	0.91	2603.2	46.0	2670	22	2722	16	2722	16	0.6	4.4
04LP028-57	*227*	*25963*	*0.7*	*11.70837*	*1.7*	*0.45110*	*1.4*	*0.81*	*2400.2*	*28.1*	*2581*	*16*	*2727*	*16*	*2727*	*16*	*0.6*	*12.0*
04LP028-31	113	24485	1.2	13.55467	1.8	0.51701	1.5	0.83	2686.5	32.5	2719	17	2743	17	2743	17	0.6	2.1
04LP028-65	66	10408	0.5	13.66600	1.4	0.52047	1.0	0.70	2701.2	22.1	2727	13	2746	17	2746	17	0.6	1.6
04LP028-68	87	29299	1.1	13.34960	1.4	0.50075	1.0	0.71	2617.0	21.5	2705	13	2771	16	2771	16	0.6	5.6
04LP028-95	*96*	*19253*	*0.9*	*12.62451*	*2.4*	*0.45303*	*2.2*	*0.91*	*2408.7*	*43.8*	*2652*	*23*	*2843*	*16*	*2843*	*16*	*0.6*	*15.3*
04LP028-6	72	10846	1.2	15.39046	3.6	0.52195	3.3	0.94	2707.4	73.9	2840	34	2935	20	2935	20	0.7	7.8
																	60 zircons	

$^{206}Pb/^{204}Pb$ is measured ratio.

Analyses in italics/shaded are excluded due to >10% error in critical age, >10% discordance, or >5% reverse discordance.

All errors are at the 1-sigma level, and include only random uncertainties.

Best age = $^{206}Pb/^{238}U$ ages for analyses younger than 1.0 Ga and $^{206}Pb/^{207}Pb$ ages for analyses older than 1.0 Ga.

U concentration and U/Th are calibrated by comparison with NBS SRM 610 and have uncertainty of ~25%.

Decay constants: $^{235}U=9.8485x10^{-10}$, $^{238}U=1.55125x10^{-10}$, $^{238}U/235U=137.88$.

Isotope ratios are corrected for Pb/U fractionation by comparison with standard zircon with an age of 564 ± 4 Ma (2-sigma).

Initial Pb composition interpreted from Stacey and Kramers (1975), with uncertainties of 1.0 for $^{206}Pb/^{204}Pb$ and 0.3 for $^{207}Pb/^{204}Pb$.

Table I-5d. *Detrital Zircon U-Pb geochronologic analyses – Pacific Centre for Isotopic and Geochemical Research – Sample 05LP003-1 in Crow Formation.*

Analysis No.	Age estimates with 1 sigma uncertainty (Ma)										Isotopic Ratios with absolute errors							
	$^{207}Pb/^{235}U$ Ma	$^{207}Pb/^{235}U$ ± 1σ Error	$^{206}Pb/^{238}U$ Ma	$^{206}Pb/^{238}U$ ± 1σ Error	$^{207}Pb/^{206}Pb$ Ma	$^{207}Pb/^{206}Pb$ ± 1σ Error	Preferred Age Ma*	± 1σ Error	Error %	Discordancy %	$^{207}Pb/^{235}U$ Ratio	$^{207}Pb/^{235}U$ 1σ Error	$^{206}Pb/^{238}U$ Ratio	$^{206}Pb/^{238}U$ 1σ Error	Rho	$^{207}Pb/^{206}Pb$ Ratio	$^{207}Pb/^{206}Pb$ 1σ Error	Th/U Ratio
lp31	*2504.6*	*388.33*	*2507.7*	*200.17*	*2271.6*	*245.81*	*2271.6*	*245.8*	*10.8*	*-10.4*	*10.7833*	*4.5065*	*0.4755*	*0.0458*	*0.23*	*0.1436*	*0.0223*	*0.4599*
lp32	1822.1	78.35	1733.3	36.91	1798.9	83.14	1798.9	83.1	4.6	3.6	5.0164	0.4643	0.3085	0.0075	0.26	0.1100	0.0052	0.1674
lp33	1754	63.44	1789	31.84	1800.7	71.85	1800.7	71.9	4.0	0.6	4.6262	0.3515	0.3199	0.0065	0.27	0.1101	0.0045	0.4115
lp34	2579.4	35.5	2520.5	20.9	2608.2	31.67	2608.2	31.7	1.2	3.4	11.6835	0.4434	0.4784	0.0048	0.26	0.1752	0.0034	0.4296
lp35	1936.1	40.18	2002.4	21.73	1902.6	43.63	1902.6	43.6	2.3	-5.2	5.7311	0.2664	0.3643	0.0046	0.27	0.1165	0.0029	0.8275
lp36	2522.1	65.62	2528.9	35.82	2530.2	46.27	2530.2	46.3	1.8	0.1	10.9883	0.7748	0.4804	0.0082	0.24	0.1672	0.0047	0.2959
lp37	*1753.5*	*54.13*	*1874.6*	*29.13*	*1768.6*	*61.63*	*1768.6*	*61.6*	*3.5*	*-6.0*	*4.6231*	*0.2998*	*0.3375*	*0.0060*	*0.28*	*0.1082*	*0.0037*	*0.1286*
lp38	1767.4	41.33	1775	21.1	1852.7	47.22	1852.7	47.2	2.5	4.2	4.7009	0.2321	0.3170	0.0043	0.28	0.1133	0.0030	0.1288
lp39	2482.9	107.4	2469.9	59.71	2586.7	75.3	2586.7	75.3	2.9	4.5	10.5334	1.2199	0.4669	0.0136	0.25	0.1730	0.0080	0.2621
lp310	*1916*	*255.35*	*1928.4*	*127.04*	*1979.1*	*242.28*	*1979.1*	*242.3*	*12.2*	*2.6*	*5.5995*	*1.6596*	*0.3487*	*0.0266*	*0.26*	*0.1216*	*0.0180*	*0.6808*
lp311	1745.7	48.28	1778	24.6	1806.6	55.75	1806.6	55.8	3.1	1.6	4.5803	0.2654	0.3176	0.0050	0.27	0.1104	0.0035	0.3778
lp312	2716.6	78.08	2715.2	43.43	2708.6	50.77	2708.6	50.8	1.9	-0.2	13.5194	1.1165	0.5238	0.0103	0.24	0.1862	0.0058	0.3864
lp313	2203.2	94.4	2201	51.02	2320.8	75.8	2320.8	75.8	3.3	5.2	7.7566	0.8141	0.4070	0.0111	0.26	0.1478	0.0067	0.4339
lp314	2802.8	118.78	2779.2	64.81	2836.6	66.44	2836.6	66.4	2.3	2.0	14.8048	1.8489	0.5390	0.0155	0.23	0.2013	0.0084	0.3596
lp315	*2438*	*882.11*	*1751*	*148.66*	*1679.8*	*413.75*	*1679.8*	*413.8*	*24.6*	*-4.2*	*10.0346*	*9.5862*	*0.3121*	*0.0303*	*0.10*	*0.1031*	*0.0266*	*0.0904*
lp316	2598.8	86.21	2574.9	48.11	2662.2	58.13	2662.2	58.1	2.2	3.3	11.9281	1.0977	0.4910	0.0111	0.25	0.1810	0.0065	0.2347
lp317	2494.8	73.33	2429.6	40.82	2666.4	52.47	2666.4	52.5	2.0	8.9	10.6703	0.8428	0.4577	0.0092	0.26	0.1815	0.0059	0.3732
lp318	1793.7	59.88	1895.2	32.07	1831.8	67.16	1831.8	67.2	3.7	-3.5	4.8506	0.3450	0.3418	0.0067	0.27	0.1120	0.0042	0.2280
lp319	*3022.6*	*472.21*	*2992.5*	*184.05*	*2530.3*	*193.91*	*2530.3*	*193.9*	*7.7*	*-18.3*	*18.6254*	*9.1270*	*0.5908*	*0.0454*	*0.16*	*0.1673*	*0.0207*	*0.9433*
lp320	2589.1	88.17	2564.3	48.99	2610.4	60.54	2610.4	60.5	2.3	1.8	11.8053	1.1119	0.4885	0.0113	0.25	0.1755	0.0065	0.4104
lp321	2743.5	213.43	2665.7	99.55	2739.4	108.92	2739.4	108.9	4.0	2.7	13.9079	3.1336	0.5121	0.0234	0.20	0.1897	0.0131	0.8717
lp322	2706.7	137.4	2655.2	73.53	2672.8	81.78	2672.8	81.8	3.1	0.7	13.3780	1.9456	0.5097	0.0172	0.23	0.1822	0.0093	0.5146
lp323	*1699*	*139.9*	*1868.2*	*65.61*	*1486.4*	*174.67*	*1486.4*	*174.7*	*11.8*	*-25.7*	*4.3297*	*0.7343*	*0.3362*	*0.0136*	*0.24*	*0.0929*	*0.0091*	*0.4981*
lp324	2294	111.4	2224.2	58.67	2353	87.32	2353.0	87.3	3.7	5.5	8.5760	1.0506	0.4120	0.0129	0.25	0.1506	0.0079	0.4787
lp325	1875.3	50.94	1988.6	26.62	1862	55.72	1862.0	55.7	3.0	-6.8	5.3399	0.3181	0.3614	0.0056	0.26	0.1139	0.0036	0.5446
lp326	*2318.6*	*45.33*	*2227.4*	*25.46*	*2524.6*	*42.51*	*2524.6*	*42.5*	*1.7*	*11.8*	*8.8110*	*0.4380*	*0.4127*	*0.0056*	*0.27*	*0.1667*	*0.0043*	*0.4005*
lp327	1936.8	59.29	1958.5	30.49	1881.1	63.02	1881.1	63.0	3.4	-4.1	5.7362	0.3934	0.3550	0.0064	0.26	0.1151	0.0041	0.2357
lp328	*2993.7*	*201.23*	*2969*	*105.37*	*2796.4*	*96.68*	*2796.4*	*96.7*	*3.5*	*-6.2*	*18.0747*	*3.7803*	*0.5850*	*0.0259*	*0.21*	*0.1964*	*0.0120*	*0.3310*
lp329	2821.3	88	2785.4	50.3	2790.1	55.72	2790.1	55.7	2.0	0.2	15.0962	1.3949	0.5405	0.0120	0.24	0.1956	0.0068	0.2262
lp330	1839.6	129.79	1745	57.19	1795	136.71	1795.0	136.7	7.6	2.8	5.1208	0.7824	0.3109	0.0116	0.24	0.1097	0.0086	0.2706
lp331	2716.6	78.7	2700.3	42.92	2684.5	52.62	2684.5	52.6	2.0	-0.6	13.5183	1.1253	0.5203	0.0101	0.23	0.1835	0.0060	0.3790
lp332	2851.5	110.89	2685.2	57.34	2549.3	67.31	2549.3	67.3	2.6	-5.3	15.5812	1.8109	0.5167	0.0135	0.22	0.1692	0.0070	0.1746

Analyses in italics/shaded are excluded due to >10% error in critical age, >10% discordance, or >5% reverse discordance.

All errors are at the 1-sigma level, and include only random uncertainties.

Best age = $^{206}Pb/^{238}U$ ages for analyses younger than 1.0 Ga and $^{206}Pb/^{207}Pb$ ages for analyses older than 1.0 Ga.

Isotope ratios are corrected for Pb/U fractionation by comparison with standard zircons Plesovice and FC1.

Table I-5d. *(continued) Detrital Zircon U-Pb geochronologic analyses – Pacific Centre for Isotopic and Geochemical Research – Sample 05LP003-1 in Crow Formation.*

Analysis No.	Age estimates with 1 sigma uncertainty (Ma)										Isotopic Ratios with absolute errors							
	$^{207}Pb/^{235}U$ Ma	$^{207}Pb/^{235}U$ ± 1σ Error	$^{206}Pb/^{238}U$ Ma	$^{206}Pb/^{238}U$ ± 1σ Error	$^{207}Pb/^{206}Pb$ Ma	$^{207}Pb/^{206}Pb$ ± 1σ Error	Preferred Age Ma*	± 1σ Error	Error %	Discordancy %	$^{207}Pb/^{235}U$ Ratio	$^{207}Pb/^{235}U$ 1σ Error	$^{206}Pb/^{238}U$ Ratio	$^{206}Pb/^{238}U$ 1σ Error	Rho	$^{207}Pb/^{206}Pb$ Ratio	$^{207}Pb/^{206}Pb$ 1σ Error	Th/U Ratio
lp333	1951.2	171.95	2040.2	93.28	2197.2	160.73	2197.2	160.7	7.3	7.1	5.8323	1.1570	0.3723	0.0199	0.27	0.1376	0.0135	0.8752
lp334	1649.2	63.48	1742.3	33.36	1758.3	77.13	1758.3	77.1	4.4	0.9	4.0746	0.3173	0.3103	0.0068	0.28	0.1076	0.0047	0.2728
lp335	2795.1	232.3	2825.9	132.06	2858	124.57	2858.0	124.6	4.4	1.1	14.6854	3.5886	0.5502	0.0318	0.24	0.2040	0.0163	0.4123
lp336	1790.4	68.48	1868.5	37.23	1867.7	75.34	1867.7	75.3	4.0	0.0	4.8313	0.3933	0.3362	0.0077	0.28	0.1142	0.0049	0.3277
lp337	1748.6	68.8	1880	38.67	1878.3	79.17	1878.3	79.2	4.2	-0.1	4.5964	0.3792	0.3386	0.0080	0.29	0.1149	0.0052	0.2147
lp338	2723.6	83.49	2682.8	47.98	2716.5	58.25	2716.5	58.3	2.1	1.2	13.6195	1.2020	0.5162	0.0113	0.25	0.1871	0.0068	0.4567
lp339	2692.1	135.97	2699.9	81.19	2867	84.63	2867.0	84.6	3.0	5.8	13.1722	1.8978	0.5202	0.0192	0.26	0.2051	0.0110	0.8160
lp340	*1880.3*	*198.88*	*1820.8*	*104.55*	*2181*	*193.04*	*2181.0*	*193.0*	*8.9*	*16.5*	*5.3712*	*1.2479*	*0.3264*	*0.0215*	*0.28*	*0.1363*	*0.0162*	*0.8128*
lp341	2479.3	76.07	2417.6	44.09	2696.5	60.12	2696.5	60.1	2.2	10.3	10.4929	0.8610	0.4550	0.0100	0.27	0.1848	0.0069	0.3258
lp342	*1617.9*	*199.49*	*1701*	*102.32*	*1717.6*	*223.95*	*1717.6*	*224.0*	*13.0*	*1.0*	*3.9205*	*0.9667*	*0.3020*	*0.0207*	*0.28*	*0.1052*	*0.0138*	*0.2861*
lp343	*2169.8*	*329.51*	*2090.4*	*116.69*	*1976.1*	*244.6*	*1976.1*	*244.6*	*12.4*	*-5.8*	*7.4736*	*2.7498*	*0.3830*	*0.0250*	*0.18*	*0.1214*	*0.0181*	*0.4739*
lp344	1864.1	112.86	1960.1	62.31	2041.4	115.62	2041.4	115.6	5.7	4.0	5.2702	0.6970	0.3554	0.0131	0.28	0.1259	0.0086	0.3371
lp345	1699.7	79.65	1796.3	42.52	1829.7	92.05	1829.7	92.1	5.0	1.8	4.3331	0.4184	0.3214	0.0087	0.28	0.1119	0.0059	0.2455
lp34lp3476	1729	132.75	1821	74.17	1992.6	144.47	1992.6	144.5	7.3	8.6	4.4892	0.7177	0.3264	0.0153	0.29	0.1225	0.0105	0.4474
lp348	*2494.1*	*383.44*	*2410.7*	*210.47*	*2749.7*	*247.79*	*2749.7*	*247.8*	*9.0*	*12.3*	*10.6615*	*4.4038*	*0.4535*	*0.0475*	*0.25*	*0.1909*	*0.0314*	*0.2967*
lp349	3025.3	73.44	3004.1	44.65	2996.3	51.75	2996.3	51.8	1.7	-0.3	18.6783	1.4233	0.5936	0.0110	0.24	0.2221	0.0073	0.6045
lp350	*1937*	*64.89*	*2028.4*	*34.1*	*1895*	*69.77*	*1895.0*	*69.8*	*3.7*	*-7.0*	*5.7370*	*0.4305*	*0.3698*	*0.0073*	*0.26*	*0.1160*	*0.0046*	*0.6827*
lp351	2189.2	80.89	2263.4	46.28	2367.6	73.91	2367.6	73.9	3.1	4.4	7.6367	0.6881	0.4206	0.0102	0.27	0.1519	0.0068	0.3319
lp352	*2233.6*	*431.89*	*2179.5*	*201.83*	*2131.6*	*298.7*	*2131.6*	*298.7*	*14.0*	*-2.2*	*8.0231*	*3.8380*	*0.4023*	*0.0439*	*0.23*	*0.1325*	*0.0251*	*0.8209*
lp353	1762.9	60.72	1821.9	32.79	1944.8	72.76	1944.8	72.8	3.7	6.3	4.6759	0.3394	0.3266	0.0068	0.28	0.1192	0.0050	0.4597
lp354	*2344*	*146.71*	*2239*	*82.28*	*2616.1*	*109.37*	*2616.1*	*109.4*	*4.2*	*14.4*	*9.0591*	*1.4534*	*0.4153*	*0.0181*	*0.27*	*0.1761*	*0.0120*	*0.1694*
lp355	1748.8	102.39	1838.7	56.5	1881.9	116.98	1881.9	117.0	6.2	2.3	4.5972	0.5644	0.3301	0.0117	0.29	0.1151	0.0078	0.2590
lp356	*2275.1*	*168.21*	*2278.2*	*103.36*	*2633.6*	*129.38*	*2633.6*	*129.4*	*4.9*	*13.5*	*8.3992*	*1.5570*	*0.4239*	*0.0228*	*0.29*	*0.1779*	*0.0145*	*0.6006*
lp357	*1644.9*	*115.39*	*1695.4*	*64.51*	*1986.7*	*139.17*	*1986.7*	*139.2*	*7.0*	*14.7*	*4.0529*	*0.5742*	*0.3008*	*0.0130*	*0.31*	*0.1221*	*0.0100*	*0.3212*
lp358	*1895.5*	*222.4*	*1751.1*	*97.57*	*2310.8*	*215.05*	*2310.8*	*215.1*	*9.3*	*24.2*	*5.4676*	*1.4166*	*0.3121*	*0.0199*	*0.25*	*0.1470*	*0.0199*	*0.4762*
lp359	1819.3	74.77	1811.8	37.74	1921.9	86.84	1921.9	86.8	4.5	5.7	5.0000	0.4418	0.3245	0.0078	0.27	0.1177	0.0059	0.3416
lp360	1854.6	142.19	1784.8	65.98	1880.7	147.66	1880.7	147.7	7.9	5.1	5.2118	0.8699	0.3190	0.0135	0.25	0.1151	0.0099	0.1611
05LP003L1	1910.7	7.73	1896.7	4.74	1927.9	8.88	1927.9	8.9	0.5	1.6	5.5647	0.0500	0.3421	0.0010	0.32	0.1181	0.0006	0.2123
05LP003L2	2683.7	8.16	2725.2	5.96	2699.2	6.99	2699.2	7.0	0.3	-1.0	13.0564	0.1130	0.5262	0.0014	0.31	0.1851	0.0008	0.2323
05LP003L3	1843.2	7.28	1863.8	4.53	1843.8	8.86	1843.8	8.9	0.5	-1.1	5.1430	0.0441	0.3353	0.0009	0.33	0.1127	0.0006	0.1888
05LP003L4	2577.8	4.95	2567.6	4.32	2593.8	6.11	2593.8	6.1	0.2	1.0	11.6641	0.0617	0.4893	0.0010	0.39	0.1737	0.0006	0.1235

Analyses in italics/shaded are excluded due to >10% error in critical age, >10% discordance, or >5% reverse discordance.

All errors are at the 1-sigma level, and include only random uncertainties.

Best age = $^{206}Pb/^{238}U$ ages for analyses younger than 1.0 Ga and $^{206}Pb/^{207}Pb$ ages for analyses older than 1.0 Ga.

Isotope ratios are corrected for Pb/U fractionation by comparison with standard zircons Plesovice and FC1.

Table I-5d. *(continued) Detrital Zircon U-Pb geochronologic analyses – Pacific Centre for Isotopic and Geochemical Research – Sample 05LP003-1 in Crow Formation.*

Analysis No.	Age estimates with 1 sigma uncertainty (Ma)										Isotopic Ratios with absolute errors							
	$^{207}Pb/^{235}U$ Ma	$^{207}Pb/^{235}U$ ± 1σ Error	$^{206}Pb/^{238}U$ Ma	$^{206}Pb/^{238}U$ ± 1σ Error	$^{207}Pb/^{206}Pb$ Ma	$^{207}Pb/^{206}Pb$ ± 1σ Error	Preferred Age Ma*	± 1σ Error	Error %	Discordancy %	$^{207}Pb/^{235}U$ Ratio	$^{207}Pb/^{235}U$ 1σ Error	$^{206}Pb/^{238}U$ Ratio	$^{206}Pb/^{238}U$ 1σ Error	Rho	$^{207}Pb/^{206}Pb$ Ratio	$^{207}Pb/^{206}Pb$ 1σ Error	Th/U Ratio
05LP003L5	1897.6	5.78	1901.4	3.92	1898.5	7.68	1898.5	7.7	0.4	-0.2	5.4809	0.0369	0.3431	0.0008	0.36	0.1162	0.0005	0.3659
05LP003L6	1896.3	7.72	1888.5	4.77	1930.9	9.03	1930.9	9.0	0.5	2.2	5.4724	0.0492	0.3404	0.0010	0.32	0.1183	0.0006	0.3888
05LP003L7	1823.4	12.42	1835	7.01	1837.3	13.43	1837.3	13.4	0.7	0.1	5.0244	0.0737	0.3293	0.0015	0.30	0.1123	0.0008	0.3967
05LP003L8	1816.7	7.74	1805.9	4.68	1838.7	9.46	1838.7	9.5	0.5	1.8	4.9844	0.0456	0.3233	0.0010	0.32	0.1124	0.0006	0.1922
05LP003L9	1968.9	17.08	1934.3	9.44	2011.3	16.12	2011.3	16.1	0.8	3.8	5.9525	0.1169	0.3499	0.0020	0.29	0.1238	0.0011	0.2810
05LP003L10	3213.4	8.72	3203.5	6.86	3241.1	6.64	3241.1	6.6	0.2	1.2	22.6820	0.2033	0.6437	0.0018	0.30	0.2591	0.0011	0.1924
05LP003L11	2062.5	17.56	2053.6	9.9	2063.5	15.73	2063.5	15.7	0.8	0.5	6.6236	0.1318	0.3752	0.0021	0.28	0.1275	0.0011	0.2057
05LP003L12	2592.2	7.56	2578.5	5.55	2590.8	7.27	2590.8	7.3	0.3	0.5	11.8449	0.0957	0.4918	0.0013	0.32	0.1734	0.0008	0.2016
05LP003L13	1936.6	7.67	1920	4.84	1992.6	9.05	1992.6	9.1	0.5	3.6	5.7347	0.0509	0.3470	0.0010	0.33	0.1225	0.0006	0.2526
05LP003L14	1840.9	6.09	1835.1	4.03	1844.9	8.33	1844.9	8.3	0.5	0.5	5.1286	0.0368	0.3293	0.0008	0.35	0.1128	0.0005	0.1243
05LP003L15	1938.3	9.56	1946.9	5.73	1913.4	10.52	1913.4	10.5	0.5	-1.8	5.7458	0.0635	0.3526	0.0012	0.31	0.1172	0.0007	0.2559
05LP003L16	1850.1	6.69	1868.8	4.36	1843.1	8.8	1843.1	8.8	0.5	-1.4	5.1846	0.0408	0.3363	0.0009	0.34	0.1127	0.0006	0.0943
05LP003L17	2724.4	10.78	2766.8	7.52	2710.1	8.46	2710.1	8.5	0.3	-2.1	13.6304	0.1554	0.5360	0.0018	0.29	0.1863	0.0010	0.3263
05LP003L18	2431.7	8.65	2442.3	5.98	2415.4	8.31	2415.4	8.3	0.3	-1.1	9.9670	0.0934	0.4606	0.0014	0.31	0.1562	0.0008	0.2521
05LP003L19	1785.8	7.06	1804.2	4.48	1802.4	9.4	1802.4	9.4	0.5	-0.1	4.8053	0.0404	0.3230	0.0009	0.34	0.1102	0.0006	0.1682
05LP003L20	1831.6	6.21	1894.9	4.25	1821.4	8.64	1821.4	8.6	0.5	-4.0	5.0729	0.0371	0.3417	0.0009	0.35	0.1113	0.0005	0.1333
05LP003L21	1830.7	5.22	1857.7	3.79	1847.1	8.02	1847.1	8.0	0.4	-0.6	5.0674	0.0312	0.3340	0.0008	0.38	0.1129	0.0005	0.1658
05LP003L22	1886.6	8.33	1897	5.17	1877.1	10.08	1877.1	10.1	0.5	-1.1	5.4107	0.0526	0.3422	0.0011	0.32	0.1148	0.0006	0.0020
05LP003L23	1874.6	9.14	1853.5	5.45	1861.5	10.79	1861.5	10.8	0.6	0.4	5.3359	0.0570	0.3331	0.0011	0.32	0.1138	0.0007	0.1113
05LP003L24	1899	9.84	1922.6	5.94	1876.5	11.24	1876.5	11.2	0.6	-2.5	5.4897	0.0629	0.3475	0.0012	0.31	0.1148	0.0007	0.1365
																	65 zircons	

Analyses in italics/shaded are excluded due to >10% error in critical age, >10% discordance, or >5% reverse discordance.
All errors are at the 1-sigma level, and include only random uncertainties.
Best age = $^{206}Pb/^{238}U$ ages for analyses younger than 1.0 Ga and $^{206}Pb/^{207}Pb$ ages for analyses older than 1.0 Ga.
Isotope ratios are corrected for Pb/U fractionation by comparison with standard zircons Plesovice and FC1.

Table I-5e. *Detrital Zircon U-Pb geochronologic analyses – Pacific Centre for Isotopic and Geochemical Research – Sample 05LP011-1 in Crow Formation.*

Analysis No.	Age estimates with 1 sigma uncertainty (Ma)										Isotopic Ratios with absolute errors							
	$^{207}Pb/^{235}U$ Ma	$^{207}Pb/^{235}U$ ± 1σ Error	$^{206}Pb/^{238}U$ Ma	$^{206}Pb/^{238}U$ ± 1σ Error	$^{207}Pb/^{206}Pb$ Ma	$^{207}Pb/^{206}Pb$ ± 1σ Error	Preferred Age Ma*	± 1σ Error	Error %	Discordancy %	$^{207}Pb/^{235}U$ Ratio	$^{207}Pb/^{235}U$ 1σ Error	$^{206}Pb/^{238}U$ Ratio	$^{206}Pb/^{238}U$ 1σ Error	Rho	$^{207}Pb/^{206}Pb$ Ratio	$^{207}Pb/^{206}Pb$ 1σ Error	Th/U Ratio
111	*1518.7*	*659.51*	*1349.7*	*150.43*	*1542.3*	*809.09*	*1542.3*	*809.1*	*52.5*	*12.5*	*3.4626*	*2.8986*	*0.2329*	*0.0288*	*0.15*	*0.0957*	*0.0548*	*0.47887*
112	1851.6	81.78	1700.1	34.6	1832.1	75.72	1832.1	75.7	4.1	7.2	5.1939	0.4989	0.3018	0.0070	0.24	0.1120	0.0048	0.19248
113	*1975.3*	*265.25*	*1935.6*	*123.44*	*1705.1*	*233.16*	*1705.1*	*233.2*	*13.7*	*-13.5*	*5.9962*	*1.8276*	*0.3502*	*0.0259*	*0.24*	*0.1045*	*0.0143*	*0.51773*
114	*1591.9*	*478.26*	*1441.9*	*254.83*	*2661.7*	*436.26*	*2661.7*	*436.3*	*16.4*	*45.8*	*3.7959*	*2.2590*	*0.2507*	*0.0494*	*0.33*	*0.1810*	*0.0557*	*0.00000*
115	1820.4	46.61	1754.9	22.56	1812	48.6	1812.0	48.6	2.7	3.2	5.0063	0.2757	0.3129	0.0046	0.27	0.1108	0.0030	0.35534
111	2542.6	34.4	2489.9	19.36	2635.1	21.77	2635.1	21.8	0.8	5.5	11.2324	0.4145	0.4714	0.0044	0.25	0.1781	0.0024	0.20606
112	1861	15.15	1851.1	8.09	1827.3	15.63	1827.3	15.6	0.9	-1.3	5.2514	0.0933	0.3326	0.0017	0.28	0.1117	0.0010	0.18203
113	1786.1	37.34	1791.1	18.86	1807.1	37.64	1807.1	37.6	2.1	0.9	4.8069	0.2135	0.3203	0.0039	0.27	0.1105	0.0023	0.45905
114	1816.8	50.8	1753.1	23.15	1838.1	46.91	1838.1	46.9	2.6	4.6	4.9849	0.2994	0.3125	0.0047	0.25	0.1124	0.0030	0.00357
115	1816.2	14.82	1725.6	7.63	1854.2	15.7	1854.2	15.7	0.8	6.9	4.9815	0.0873	0.3069	0.0016	0.29	0.1134	0.0010	0.33440
116	1809.3	21.07	1813.8	10.79	1806.1	21.47	1806.1	21.5	1.2	-0.4	4.9409	0.1233	0.3249	0.0022	0.27	0.1104	0.0013	0.23571
117	1853.4	20.03	1865.3	10.47	1882.3	19.79	1882.3	19.8	1.1	0.9	5.2047	0.1224	0.3356	0.0022	0.28	0.1152	0.0013	0.32267
118	1866.7	29.9	1860.2	14.95	1862.3	28.54	1862.3	28.5	1.5	0.1	5.2865	0.1851	0.3345	0.0031	0.26	0.1139	0.0018	0.22904
119	1845.3	22.46	1879.3	11.65	1842.8	22.13	1842.8	22.1	1.2	-2.0	5.1556	0.1361	0.3385	0.0024	0.27	0.1127	0.0014	0.23402
1110	2688.9	24.21	2628.7	13.87	2736.2	14.96	2736.2	15.0	0.5	3.9	13.1277	0.3368	0.5035	0.0032	0.25	0.1893	0.0017	0.49446
1111	1969.3	30.28	1940.6	14.72	1911	26.53	1911.0	26.5	1.4	-1.5	5.9550	0.2074	0.3513	0.0031	0.25	0.1170	0.0017	0.35360
1112	1838.6	29.49	1714.7	14.08	1922.5	28.59	1922.5	28.6	1.5	10.8	5.1149	0.1776	0.3047	0.0029	0.27	0.1178	0.0019	0.41237
1113	1787	109.48	1781.7	45.27	1945.4	92.48	1945.4	92.5	4.8	8.4	4.8121	0.6267	0.3184	0.0093	0.22	0.1193	0.0064	0.54321
1114	2490.9	151.08	2371.2	56.47	2586.7	67.28	2586.7	67.3	2.6	8.3	10.6247	1.7297	0.4446	0.0127	0.17	0.1730	0.0071	0.97101
1115	2779.3	65.73	2742.3	33.32	2717.9	33.13	2717.9	33.1	1.2	-0.9	14.4443	0.9998	0.5302	0.0079	0.22	0.1872	0.0038	0.30051
1116	1928	130.45	1814.3	55.02	1826	111.61	1826.0	111.6	6.1	0.6	5.6775	0.8579	0.3250	0.0113	0.23	0.1116	0.0071	0.54929
1117	2624.6	83.8	2506.8	39.08	2537.9	44.69	2537.9	44.7	1.8	1.2	12.2605	1.0944	0.4753	0.0089	0.21	0.1680	0.0046	0.20554
1118	*2167.4*	*129.25*	*2114.3*	*56.78*	*1941.4*	*92.89*	*1941.4*	*92.9*	*4.8*	*-8.9*	*7.4531*	*1.0761*	*0.3882*	*0.0122*	*0.22*	*0.1190*	*0.0064*	*0.47542*
1119	*2777.3*	*171.47*	*2779.8*	*84.37*	*2404.2*	*87.62*	*2404.2*	*87.6*	*3.6*	*-15.6*	*14.4126*	*2.6027*	*0.5391*	*0.0201*	*0.21*	*0.1552*	*0.0083*	*0.66419*
1120	2041.2	139.85	2010.6	61.42	1940.4	104.88	1940.4	104.9	5.4	-3.6	6.4656	1.0283	0.3660	0.0130	0.22	0.1189	0.0072	0.50658
1121	2744	101.53	2720.2	50.34	2659.9	52.27	2659.9	52.3	2.0	-2.3	13.9159	1.4915	0.5250	0.0119	0.21	0.1808	0.0058	0.74130
1122	2620.2	67.93	2622.2	34.34	2711.4	35.97	2711.4	36.0	1.3	3.3	12.2042	0.8834	0.5020	0.0080	0.22	0.1865	0.0041	0.16882
1123	1653.5	47.91	1696.3	23.5	1665.3	54.83	1665.3	54.8	3.3	-1.9	4.0961	0.2404	0.3010	0.0047	0.27	0.1023	0.0031	0.56369
1124	*1863.4*	*30.7*	*1930.6*	*14.98*	*1798.7*	*28.4*	*1798.7*	*28.4*	*1.6*	*-7.3*	*5.2659*	*0.1895*	*0.3492*	*0.0031*	*0.25*	*0.1100*	*0.0017*	*0.31810*
1125	1810.7	24.71	1838.8	12.84	1845.3	25.16	1845.3	25.2	1.4	0.4	4.9493	0.1448	0.3301	0.0027	0.27	0.1128	0.0016	0.34386
1126	1815.9	19.59	1760.5	9.98	1855.3	20.42	1855.3	20.4	1.1	5.1	4.9800	0.1154	0.3140	0.0020	0.28	0.1134	0.0013	0.26960
1127	2087.4	34.04	2066.7	17.39	2090.6	27.98	2090.6	28.0	1.3	1.1	6.8125	0.2619	0.3779	0.0037	0.26	0.1295	0.0021	0.42049

Analyses in italics/shaded are excluded due to >10% error in critical age, >10% discordance, or >5% reverse discordance.
All errors are at the 1-sigma level, and include only random uncertainties.
Best age = $^{206}Pb/^{238}U$ ages for analyses younger than 1.0 Ga and $^{206}Pb/^{207}Pb$ ages for analyses older than 1.0 Ga.
Isotope ratios are corrected for Pb/U fractionation by comparison with standard zircons Plesovice and FC1.

Table I-5e. *(continued) Detrital Zircon U-Pb geochronologic analyses – Pacific Centre for Isotopic and Geochemical Research – Sample 05LP011-1 in Crow Formation.*

Analysis No.	Age estimates with 1 sigma uncertainty (Ma)										Isotopic Ratios with absolute errors							
	$^{207}Pb/^{235}U$ Ma	$^{207}Pb/^{235}U$ ± 1σ Error	$^{206}Pb/^{238}U$ Ma	$^{206}Pb/^{238}U$ ± 1σ Error	$^{207}Pb/^{206}Pb$ Ma	$^{207}Pb/^{206}Pb$ ± 1σ Error	Preferred Age Ma*	± 1σ Error	Error %	Discordancy %	$^{207}Pb/^{235}U$ Ratio	$^{207}Pb/^{235}U$ 1σ Error	$^{206}Pb/^{238}U$ Ratio	$^{206}Pb/^{238}U$ 1σ Error	Rho	$^{207}Pb/^{206}Pb$ Ratio	$^{207}Pb/^{206}Pb$ 1σ Error	Th/U Ratio
1128	1782.2	28.77	1767.1	14.41	1779.2	29.8	1779.2	29.8	1.7	0.7	4.7847	0.1639	0.3154	0.0029	0.27	0.1088	0.0018	0.29975
1129	1793.4	19.23	1713.8	9.74	1870.7	20.47	1870.7	20.5	1.1	8.4	4.8485	0.1108	0.3046	0.0020	0.28	0.1144	0.0013	0.16242
1130	1852.7	17.4	1793	9.01	1882	18.2	1882.0	18.2	1.0	4.7	5.2004	0.1063	0.3207	0.0019	0.28	0.1151	0.0012	0.27887
1131	2695.3	15.94	2659.6	10.17	2704.3	12.69	2704.3	12.7	0.5	1.7	13.2177	0.2233	0.5107	0.0024	0.28	0.1857	0.0014	0.69770
1132	2002.2	15.73	1941.6	8.6	2012.3	15.99	2012.3	16.0	0.8	3.5	6.1841	0.1113	0.3515	0.0018	0.28	0.1238	0.0011	0.25969
1133	1856.9	16.79	1869.6	9.11	1873.1	17.95	1873.1	18.0	1.0	0.2	5.2264	0.1030	0.3365	0.0019	0.29	0.1146	0.0012	0.32511
1134	1897.9	23.38	1816.3	11.4	1868.3	22.76	1868.3	22.8	1.2	2.8	5.4831	0.1493	0.3255	0.0023	0.26	0.1143	0.0015	0.20206
1135	2686.8	22.02	2662.4	13.57	2836.5	15.41	2836.5	15.4	0.5	6.1	13.0996	0.3058	0.5114	0.0032	0.27	0.2013	0.0019	0.25632
1136	2570	47.3	2561.3	26.97	2642.6	29.83	2642.6	29.8	1.1	3.1	11.5663	0.5854	0.4878	0.0062	0.25	0.1789	0.0033	0.46952
1137	1922.5	30.97	1960.6	15.73	1857.9	28.91	1857.9	28.9	1.6	-5.5	5.6420	0.2026	0.3555	0.0033	0.26	0.1136	0.0018	0.23024
1138	2646.5	44.2	2629.3	24.53	2642.6	27.11	2642.6	27.1	1.0	0.5	12.5502	0.5899	0.5036	0.0057	0.24	0.1789	0.0030	0.44932
1139	1774.3	117.02	1839.7	58.08	1821.3	112.33	1821.3	112.3	6.2	-1.0	4.7399	0.6615	0.3303	0.0120	0.26	0.1113	0.0072	0.11967
1140	1832.8	54.9	1873.2	28.6	1867.4	54.68	1867.4	54.7	2.9	-0.3	5.0804	0.3287	0.3372	0.0059	0.27	0.1142	0.0035	0.28699
1141	*724.6*	*32.58*	*672.5*	*12.42*	*866.7*	*94.12*	*672.5*	*12.4*	*1.8*	*22.4*	*1.0414*	*0.0655*	*0.1100*	*0.0021*	*0.31*	*0.0679*	*0.0032*	*0.43400*
1142	1822.9	65.75	1918.6	34.29	1885.8	62.19	1885.8	62.2	3.3	-1.7	5.0214	0.3899	0.3467	0.0072	0.27	0.1154	0.0041	0.28276
1143	*1330.4*	*77.83*	*1277.9*	*37.28*	*1650.6*	*109.38*	*1650.6*	*109.4*	*6.6*	*22.6*	*2.7070*	*0.2842*	*0.2192*	*0.0071*	*0.31*	*0.1014*	*0.0062*	*0.40971*
1144	*1203.2*	*44*	*1212*	*18.99*	*1137*	*73.72*	*1137.0*	*73.7*	*6.5*	*-6.6*	*2.2705*	*0.1417*	*0.2069*	*0.0036*	*0.27*	*0.0776*	*0.0030*	*0.18739*
1145	1870.4	45.38	1916.7	23.75	2028.5	42.5	2028.5	42.5	2.1	5.5	5.3096	0.2820	0.3463	0.0050	0.27	0.1250	0.0030	0.40945
1146	1830.6	42.02	1842.9	20.36	1802.1	40.47	1802.1	40.5	2.2	-2.3	5.0671	0.2511	0.3309	0.0042	0.26	0.1102	0.0025	0.24944
1147	*2410.3*	*75.68*	*2345.5*	*38.7*	*2680.4*	*46.09*	*2680.4*	*46.1*	*1.7*	*12.5*	*9.7375*	*0.8003*	*0.4389*	*0.0086*	*0.24*	*0.1830*	*0.0052*	*0.43814*
1148	1897.4	37.27	1905.9	18.74	1954.1	35.02	1954.1	35.0	1.8	2.5	5.4796	0.2378	0.3440	0.0039	0.26	0.1199	0.0024	0.51368
1149	1766.8	38.94	1834.7	20.51	1869.5	40.45	1869.5	40.5	2.2	1.9	4.6976	0.2185	0.3292	0.0042	0.28	0.1143	0.0026	0.27444
1150	*1821.2*	*33.83*	*1948.4*	*17.83*	*1681.2*	*34.84*	*1681.2*	*34.8*	*2.1*	*-15.9*	*5.0109*	*0.2003*	*0.3529*	*0.0037*	*0.27*	*0.1031*	*0.0020*	*0.27122*
1151	1992.1	23.29	1935.2	12.19	2033.7	22.66	2033.7	22.7	1.1	4.8	6.1131	0.1632	0.3501	0.0026	0.27	0.1254	0.0016	0.26925
1152	1968.1	23.74	1971.7	12.91	2020.2	23.6	2020.2	23.6	1.2	2.4	5.9468	0.1624	0.3578	0.0027	0.28	0.1244	0.0017	0.43799
1153	2667.4	44.75	2666.2	24.97	2737.2	27.05	2737.2	27.1	1.0	2.6	12.8323	0.6096	0.5122	0.0059	0.24	0.1894	0.0031	0.35799
1154	*2222.6*	*29.62*	*1816.8*	*14.78*	*2654.5*	*24.4*	*2654.5*	*24.4*	*0.9*	*31.6*	*7.9252*	*0.2604*	*0.3256*	*0.0030*	*0.28*	*0.1802*	*0.0027*	*0.48027*
1155	1818.8	29.49	1783.2	14.84	1859.7	30.55	1859.7	30.6	1.6	4.1	4.9967	0.1742	0.3187	0.0030	0.27	0.1137	0.0019	0.52526
1156	2771.4	22.72	2782.2	14.28	2800.2	17.35	2800.2	17.4	0.6	0.6	14.3238	0.3428	0.5397	0.0034	0.26	0.1968	0.0021	0.34986
1157	2559.4	21.74	2589.4	13.58	2621.8	18.08	2621.8	18.1	0.7	1.2	11.4366	0.2663	0.4943	0.0032	0.27	0.1767	0.0019	0.41147
1158	1878.2	34.48	1819.7	17.31	1957.6	33.7	1957.6	33.7	1.7	7.0	5.3581	0.2159	0.3262	0.0036	0.27	0.1201	0.0023	0.22839

Analyses in italics/shaded are excluded due to >10% error in critical age, >10% discordance, or >5% reverse discordance.

All errors are at the 1-sigma level, and include only random uncertainties.

Best age = $^{206}Pb/^{238}U$ ages for analyses younger than 1.0 Ga and $^{206}Pb/^{207}Pb$ ages for analyses older than 1.0 Ga.

Isotope ratios are corrected for Pb/U fractionation by comparison with standard zircons Plesovice and FC1.

Table I-5e. *(continued) Detrital Zircon U-Pb geochronologic analyses – Pacific Centre for Isotopic and Geochemical Research – Sample 05LP011-1 in Crow Formation.*

Analysis No.	Age estimates with 1 sigma uncertainty (Ma)										Isotopic Ratios with absolute errors							
	$^{207}Pb/^{235}U$ Ma	$^{207}Pb/^{235}U$ ± 1σ Error	$^{206}Pb/^{238}U$ Ma	$^{206}Pb/^{238}U$ ± 1σ Error	$^{207}Pb/^{206}Pb$ Ma	$^{207}Pb/^{206}Pb$ ± 1σ Error	Preferred Age Ma*	± 1σ Error	Error %	Discordancy %	$^{207}Pb/^{235}U$ Ratio	$^{207}Pb/^{235}U$ 1σ Error	$^{206}Pb/^{238}U$ Ratio	$^{206}Pb/^{238}U$ 1σ Error	Rho	$^{207}Pb/^{206}Pb$ Ratio	$^{207}Pb/^{206}Pb$ 1σ Error	Th/U Ratio
1159	*604.4*	*32.47*	*498.5*	*11.26*	*957.4*	*113.74*	*498.5*	*11.3*	*2.3*	*47.9*	*0.8134*	*0.0580*	*0.0804*	*0.0019*	*0.33*	*0.0710*	*0.0041*	*19.77106*
1160	2041.9	27.72	1935.2	14.27	2091.3	26.09	2091.3	26.1	1.2	7.5	6.4707	0.2040	0.3501	0.0030	0.27	0.1295	0.0019	0.30763
05LP-011L1	1882.4	7.58	1874.3	4.48	1906.8	8.26	1906.8	8.3	0.4	1.7	5.3845	0.0477	0.3374	0.0009	0.31	0.1167	0.0005	0.41487
05LP-011L2	1933.8	5.62	1942.6	3.78	1949.7	6.77	1949.7	6.8	0.3	0.4	5.7159	0.0372	0.3517	0.0008	0.35	0.1196	0.0005	0.51005
05LP-011L3	1155.7	4.59	1147.5	2.54	1180.9	9.08	1180.9	9.1	0.8	2.8	2.1210	0.0141	0.1948	0.0005	0.36	0.0794	0.0004	0.14339
05LP-011L4	1868.6	13.42	1900.5	7.25	1893.1	13.1	1893.1	13.1	0.7	-0.4	5.2982	0.0832	0.3429	0.0015	0.28	0.1159	0.0009	0.46044
05LP-011L5	1823.2	10.36	1810.2	5.63	1848.7	10.79	1848.7	10.8	0.6	2.1	5.0230	0.0614	0.3242	0.0012	0.29	0.1130	0.0007	0.32488
05LP-011L6	2337.5	8.88	2295.2	5.54	2390.9	7.49	2390.9	7.5	0.3	4.0	8.9946	0.0875	0.4277	0.0012	0.30	0.1540	0.0007	0.55247
05LP-011L7	2624.7	11.13	2601.3	6.99	2674.4	7.73	2674.4	7.7	0.3	2.7	12.2630	0.1453	0.4971	0.0016	0.27	0.1824	0.0009	0.29452
05LP-011L8	*202.5*	*2.96*	*201*	*1.09*	*234*	*35.51*	*201.0*	*1.1*	*0.5*	*14.1*	*0.2207*	*0.0036*	*0.0317*	*0.0002*	*0.35*	*0.0509*	*0.0008*	*0.13480*
05LP-011L9	2704	10.79	2666.5	6.85	2735.7	7.37	2735.7	7.4	0.3	2.5	13.3404	0.1524	0.5123	0.0016	0.28	0.1893	0.0009	0.27712
05LP-011L10	1840.4	10.52	1804.4	5.64	1861.4	10.86	1861.4	10.9	0.6	3.1	5.1258	0.0635	0.3230	0.0012	0.29	0.1138	0.0007	0.29390
05LP-011L11	1852.7	9.12	1846.1	5.12	1848.1	9.74	1848.1	9.7	0.5	0.1	5.2005	0.0557	0.3316	0.0011	0.30	0.1130	0.0006	0.09244
05LP-011L12	1814.4	10.37	1795	5.61	1828	10.95	1828.0	11.0	0.6	1.8	4.9711	0.0610	0.3211	0.0012	0.29	0.1117	0.0007	0.43186
																	63 zircons	

Analyses in italics/shaded are excluded due to >10% error in critical age, >10% discordance, or >5% reverse discordance.
All errors are at the 1-sigma level, and include only random uncertainties.
Best age = $^{206}Pb/^{238}U$ ages for analyses younger than 1.0 Ga and $^{206}Pb/^{207}Pb$ ages for analyses older than 1.0 Ga.
Isotope ratios are corrected for Pb/U fractionation by comparison with standard zircons Plesovice and FC1.

Table I-5f. *Detrital Zircon U-Pb geochronologic analyses – Pacific Centre for Isotopic and Geochemical Research – Sample 05LP034-1 in Crow Formation.*

Analysis No.	Age estimates with 1 sigma uncertainty (Ma)										Isotopic Ratios with absolute errors							
	$^{207}Pb/^{235}U$ Ma	$^{207}Pb/^{235}U$ ± 1σ Error	$^{206}Pb/^{238}U$ Ma	$^{206}Pb/^{238}U$ ± 1σ Error	$^{207}Pb/^{206}Pb$ Ma	$^{207}Pb/^{206}Pb$ ± 1σ Error	Preferred Age Ma*	± 1σ Error	Error %	Discordancy %	$^{207}Pb/^{235}U$ Ratio	$^{207}Pb/^{235}U$ 1σ Error	$^{206}Pb/^{238}U$ Ratio	$^{206}Pb/^{238}U$ 1σ Error	Rho	$^{207}Pb/^{206}Pb$ Ratio	$^{207}Pb/^{206}Pb$ 1σ Error	Th/U Ratio
05LP034L1	2692.5	11.7	2755.6	8.31	2684.3	9.1	2684.3	9.1	0.3	-2.7	13.1785	0.1634	0.5334	0.0020	0.30	0.1835	0.0010	0.167
05LP034L2	1375.9	6.75	1384.2	4.06	1386.6	11.59	1386.6	11.6	0.8	0.2	2.8768	0.0258	0.2395	0.0008	0.36	0.0882	0.0005	0.117
05LP034L3	2700.2	9.89	2747.4	7.44	2688.5	8.66	2688.5	8.7	0.3	-2.2	13.2861	0.1392	0.5314	0.0018	0.32	0.1839	0.0010	0.367
05LP034L4	1909	8.5	1917.2	5.59	1924.7	10.6	1924.7	10.6	0.6	0.4	5.5538	0.0549	0.3464	0.0012	0.34	0.1179	0.0007	0.186
05LP034L5	1076.8	7.05	1076.4	3.75	1073.7	15.42	1073.7	15.4	1.4	-0.3	1.8878	0.0200	0.1817	0.0007	0.36	0.0752	0.0006	0.150
05LP034L6	1726.7	7.19	1731.6	4.84	1738	11.08	1738.0	11.1	0.6	0.4	4.4769	0.0388	0.3081	0.0010	0.37	0.1064	0.0006	0.097
05LP034L7	1653	10.18	1692.7	6.09	1621.5	14.39	1621.5	14.4	0.9	-4.4	4.0935	0.0511	0.3003	0.0012	0.33	0.0999	0.0008	0.245
05LP034L8	2342.1	8.84	2352.8	6.63	2373.6	10.71	2373.6	10.7	0.5	0.9	9.0403	0.0874	0.4405	0.0015	0.35	0.1525	0.0010	0.333
05LP034L9	1497	7.35	1515.6	4.66	1514.1	13.13	1514.1	13.1	0.9	-0.1	3.3682	0.0316	0.2650	0.0009	0.37	0.0943	0.0007	0.120
05LP034L10	2443.8	9.44	2469.5	7.21	2463.6	11.44	2463.6	11.4	0.5	-0.2	10.0978	0.1031	0.4668	0.0016	0.34	0.1608	0.0011	0.218
05LP034L11	1445.3	6.98	1466.7	4.52	1445.5	14.02	1445.5	14.0	1.0	-1.5	3.1511	0.0285	0.2555	0.0009	0.38	0.0910	0.0007	0.138
05LP034L12	*2047.3*	*45.76*	*2310.9*	*27.16*	*1854.5*	*41.28*	*1854.5*	*41.3*	*2.2*	*-24.6*	*6.5107*	*0.3385*	*0.4312*	*0.0060*	*0.27*	*0.1134*	*0.0026*	*0.000*
05LP034L13	1820.3	13.62	1875.5	8.32	1833.1	17.98	1833.1	18.0	1.0	-2.3	5.0055	0.0806	0.3377	0.0017	0.32	0.1121	0.0011	0.313
05LP034L14	1147	9.48	1193	5.19	1150.4	20.65	1150.4	20.7	1.8	-3.7	2.0945	0.0289	0.2033	0.0010	0.35	0.0781	0.0008	0.095
05LP034L15	1435.5	8.95	1411.8	5.29	1500	17.27	1500.0	17.3	1.2	5.9	3.1115	0.0362	0.2448	0.0010	0.36	0.0936	0.0009	0.106
05LP034L16	2547.6	15.51	2474.8	10.46	2563.6	16.76	2563.6	16.8	0.7	3.5	11.2933	0.1878	0.4680	0.0024	0.31	0.1706	0.0017	0.199
05LP034L17	2683.5	18.08	2706.7	12.51	2681	17.66	2681.0	17.7	0.7	-1.0	13.0526	0.2503	0.5218	0.0030	0.29	0.1831	0.0020	0.567
05LP034L18	1865.3	11.65	1868.8	7.63	1883.4	18.72	1883.4	18.7	1.0	0.8	5.2780	0.0721	0.3363	0.0016	0.34	0.1152	0.0012	0.427
05LP034L19	1901.4	14.86	1917.9	9.26	1943.2	20.9	1943.2	20.9	1.1	1.3	5.5053	0.0952	0.3465	0.0019	0.32	0.1191	0.0014	0.211
05LP034L20	1793.3	76.18	1880.3	43.94	1951.6	78.68	1951.6	78.7	4.0	3.7	4.8479	0.4387	0.3387	0.0091	0.30	0.1197	0.0054	0.370
05LP034L21	*2642.5*	*21.29*	*2792.5*	*15.88*	*2634.4*	*24.13*	*2634.4*	*24.1*	*0.9*	*-6.0*	*12.4968*	*0.2830*	*0.5422*	*0.0038*	*0.31*	*0.1780*	*0.0026*	*0.382*
05LP069L22	1812	15.01	1811.2	9.65	1796	26.28	1796.0	26.3	1.5	-0.8	4.9566	0.0880	0.3244	0.0020	0.34	0.1098	0.0016	0.163
05LP034L23	2542.2	17.35	2626.4	13.53	2512.9	24.64	2512.9	24.6	1.0	-4.5	11.2280	0.2089	0.5029	0.0032	0.34	0.1655	0.0025	0.254
05LP034L24	1920.5	22.18	1963.9	13.79	1929.6	30.92	1929.6	30.9	1.6	-1.8	5.6287	0.1448	0.3562	0.0029	0.32	0.1182	0.0021	0.156
05LP034L25	1848.2	18.17	1896.9	11.69	1835.4	29.64	1835.4	29.6	1.6	-3.4	5.1733	0.1104	0.3421	0.0024	0.33	0.1122	0.0019	0.477
05LP034L26	*1780.6*	*18.58*	*1693.2*	*11.13*	*1921*	*31.05*	*1921.0*	*31.1*	*1.6*	*11.9*	*4.7756*	*0.1057*	*0.3004*	*0.0023*	*0.34*	*0.1177*	*0.0021*	*0.208*
05LP034L27	1018.1	14.3	1036.6	7.39	1049.4	37.47	1049.4	37.5	3.6	1.2	1.7255	0.0384	0.1745	0.0014	0.35	0.0743	0.0014	0.220
05LP034L28	*1046.4*	*15.04*	*1076.2*	*7.86*	*989.5*	*38.9*	*1076.2*	*7.9*	*0.7*	*-8.8*	*1.8026*	*0.0415*	*0.1817*	*0.0014*	*0.34*	*0.0721*	*0.0014*	*0.134*
05LP034L29	1353.2	16.33	1363.1	9.36	1375.8	35.48	1375.8	35.5	2.6	0.9	2.7913	0.0610	0.2355	0.0018	0.35	0.0877	0.0016	0.104
05LP034L30	1225	16.16	1236.7	8.9	1204.6	37.85	1204.6	37.9	3.1	-2.7	2.3415	0.0532	0.2115	0.0017	0.35	0.0803	0.0016	0.346
05LP034L31	2670.7	21.14	2630.8	17.03	2721.1	31.97	2721.1	32.0	1.2	3.3	12.8764	0.2888	0.5040	0.0040	0.35	0.1876	0.0037	0.208
05LP034L32	1996.7	25.5	2037.4	16.48	1926.5	38.45	1926.5	38.5	2.0	-5.8	6.1452	0.1795	0.3717	0.0035	0.32	0.1180	0.0026	0.254
05LP034L33	1807.3	23.71	1768.3	14.48	1828.2	39.53	1828.2	39.5	2.2	3.3	4.9292	0.1385	0.3156	0.0030	0.33	0.1118	0.0025	0.194

Analyses in italics/shaded are excluded due to >10% error in critical age, >10% discordance, or >5% reverse discordance.

All errors are at the 1-sigma level, and include only random uncertainties.

Best age = $^{206}Pb/^{238}U$ ages for analyses younger than 1.0 Ga and $^{206}Pb/^{207}Pb$ ages for analyses older than 1.0 Ga.

Isotope ratios are corrected for Pb/U fractionation by comparison with standard zircons Plesovice and FC1.

Table I-5f. *(continued) Detrital Zircon U-Pb geochronologic analyses – Pacific Centre for Isotopic and Geochemical Research – Sample 05LP034-1 in Crow Formation.*

Analysis No.	Age estimates with 1 sigma uncertainty (Ma)										Isotopic Ratios with absolute errors							
	$^{207}Pb/^{235}U$ Ma	$^{207}Pb/^{235}U$ ± 1σ Error	$^{206}Pb/^{238}U$ Ma	$^{206}Pb/^{238}U$ ± 1σ Error	$^{207}Pb/^{206}Pb$ Ma	$^{207}Pb/^{206}Pb$ ± 1σ Error	Preferred Age Ma*	± 1σ Error	Error %	Discordancy %	$^{207}Pb/^{235}U$ Ratio	$^{207}Pb/^{235}U$ 1σ Error	$^{206}Pb/^{238}U$ Ratio	$^{206}Pb/^{238}U$ 1σ Error	Rho	$^{207}Pb/^{206}Pb$ Ratio	$^{207}Pb/^{206}Pb$ 1σ Error	Th/U Ratio
05LP034L34	2865.7	24	2941.8	20.5	2821.3	34.52	2821.3	34.5	1.2	-4.3	15.8158	0.3976	0.5783	0.0050	0.35	0.1994	0.0043	0.425
05LP034L35	*1492.4*	*19.3*	*955.6*	*7.84*	*2360.4*	*37.1*	*2360.4*	*37.1*	*1.6*	*59.5*	*3.3484*	*0.0827*	*0.1598*	*0.0014*	*0.36*	*0.1513*	*0.0033*	*0.233*
05LP034L36	1990.5	27.52	2077.6	18.58	1970.1	42.96	1970.1	43.0	2.2	-5.5	6.1015	0.1925	0.3803	0.0040	0.33	0.1209	0.0030	0.382
05LP034L37	2613.9	26.21	2655.5	21.06	2610.9	39.17	2610.9	39.2	1.5	-1.7	12.1221	0.3387	0.5097	0.0049	0.35	0.1755	0.0042	0.432
05LP034L38	1025.3	18.15	1038.7	9.54	1022.4	49.54	1022.4	49.5	4.8	-1.6	1.7449	0.0491	0.1748	0.0017	0.35	0.0733	0.0018	0.153
05LP034L39	2620.4	28.74	2640.2	22.54	2598.4	41.53	2598.4	41.5	1.6	-1.6	12.2069	0.3739	0.5062	0.0053	0.34	0.1742	0.0044	0.490
05LP034L40	1833.1	28.43	1833.5	18.03	1863.1	47.76	1863.1	47.8	2.6	1.6	5.0820	0.1703	0.3290	0.0037	0.34	0.1139	0.0031	0.435
05LP034L61	1975	27.8	2020.5	19.27	1952.3	47.97	1952.3	48.0	2.5	-3.5	5.9939	0.1915	0.3681	0.0041	0.35	0.1197	0.0033	0.261
05LP034L62	1093.1	21.33	1109.1	11.49	1070.7	55.46	1070.7	55.5	5.2	-3.6	1.9345	0.0616	0.1877	0.0021	0.35	0.0751	0.0021	0.152
05LP034L63	2688.6	58.12	2758.1	39.31	2674.2	54.02	2674.2	54.0	2.0	-3.1	13.1233	0.8085	0.5340	0.0094	0.28	0.1823	0.0061	0.127
05LP034L64	1766.7	28.34	1757.5	18.28	1809.3	52.31	1809.3	52.3	2.9	2.9	4.6969	0.1590	0.3134	0.0037	0.35	0.1106	0.0032	0.391
05LP034L65	1839.7	28.91	1866.9	19.48	1792.5	53.32	1792.5	53.3	3.0	-4.2	5.1216	0.1743	0.3359	0.0040	0.35	0.1096	0.0033	0.187
05LP034L1	2610.6	14.56	2602.2	13.53	2579.3	18.16	2579.3	18.2	0.7	-0.9	12.0797	0.1876	0.4973	0.0031	0.41	0.1722	0.0019	0.144479252
05LP034L2	1827.6	16.41	1804.6	11.35	1895.5	22.44	1895.5	22.4	1.2	4.8	5.0490	0.0978	0.3231	0.0023	0.37	0.1160	0.0015	0.061105823
05LP034L3	1849.8	15.75	1786.6	10.99	1909.6	22.09	1909.6	22.1	1.2	6.4	5.1827	0.0959	0.3194	0.0023	0.38	0.1169	0.0015	0.154214733
05LP034L4	1817.9	11.2	1804.1	9.75	1850.4	20.05	1850.4	20.1	1.1	2.5	4.9915	0.0661	0.3230	0.0020	0.47	0.1131	0.0013	0.149822464
05LP034L5	1813.9	7.85	1796.6	8.92	1825.7	18.84	1825.7	18.8	1.0	1.6	4.9681	0.0461	0.3214	0.0018	0.61	0.1116	0.0012	0.146553301
05LP034L6	2728.8	11.92	2694.1	13.34	2763.8	17.35	2763.8	17.4	0.6	2.5	13.6941	0.1725	0.5188	0.0031	0.48	0.1925	0.0021	0.2731393
05LP034L7	1144.3	7.84	1134.9	6.32	1165.1	22.22	1165.1	22.2	1.9	2.6	2.0862	0.0238	0.1925	0.0012	0.53	0.0787	0.0009	0.118112142
05LP034L8	1618.4	10.87	1624.6	9.1	1644.4	21.04	1644.4	21.0	1.3	1.2	3.9229	0.0527	0.2866	0.0018	0.47	0.1011	0.0012	0.128783305
05LP034L9	1416.2	8.66	1412.7	7.7	1432	20.94	1432.0	20.9	1.5	1.3	3.0340	0.0344	0.2450	0.0015	0.54	0.0903	0.0010	0.163472353
05LP034L10	2603.6	12.3	2576.9	13.19	2659.3	17.74	2659.3	17.7	0.7	3.1	11.9893	0.1573	0.4914	0.0031	0.47	0.1807	0.0020	0.199850436
05LP034L11	2788.6	9.32	2818	13.38	2786.4	17.02	2786.4	17.0	0.6	-1.1	14.5862	0.1431	0.5483	0.0032	0.60	0.1952	0.0020	0.358237092
05LP034L12	1951.5	9.66	1950.2	10.21	1984.1	19.08	1984.1	19.1	1.0	1.7	5.8343	0.0650	0.3533	0.0021	0.54	0.1219	0.0013	0.209205547
05LP034L13	1808.5	9.4	1815.1	9.64	1818.4	19.54	1818.4	19.5	1.1	0.2	4.9364	0.0549	0.3252	0.0020	0.55	0.1112	0.0012	0.152285798
05LP034L14	1947.8	9.57	1928.2	10.16	1995.2	19.03	1995.2	19.0	1.0	3.4	5.8091	0.0642	0.3487	0.0021	0.55	0.1227	0.0013	0.217022638
05LP034L15	1710.8	9.93	1701.3	9.35	1724.9	20.21	1724.9	20.2	1.2	1.4	4.3919	0.0527	0.3020	0.0019	0.52	0.1056	0.0012	0.330970178
05LP034L16	1851.5	12	1840.3	10.51	1844.3	20.57	1844.3	20.6	1.1	0.2	5.1932	0.0732	0.3304	0.0022	0.47	0.1128	0.0013	0.135350053
05LP034L17	2544.5	15.22	2527.3	14.19	2493.1	18.98	2493.1	19.0	0.8	-1.4	11.2549	0.1837	0.4800	0.0033	0.42	0.1636	0.0019	0.150811573
05LP034L18	1812.9	9.63	1806.1	9.84	1844.6	19.71	1844.6	19.7	1.1	2.1	4.9624	0.0566	0.3234	0.0020	0.55	0.1128	0.0012	0.106625347
05LP034L20	1073.7	7.19	1088.2	6.26	1057	22.65	1057.0	22.7	2.1	-3.0	1.8790	0.0204	0.1839	0.0012	0.58	0.0746	0.0008	0.218448862
																	59 zircons	

Analyses in italics/shaded are excluded due to >10% error in critical age, >10% discordance, or >5% reverse discordance.

All errors are at the 1-sigma level, and include only random uncertainties.

Best age = $^{206}Pb/^{238}U$ ages for analyses younger than 1.0 Ga and $^{206}Pb/^{207}Pb$ ages for analyses older than 1.0 Ga.

Isotope ratios are corrected for Pb/U fractionation by comparison with standard zircons Plesovice and FC1.

Table I-5g. *Detrital Zircon U-Pb geochronologic analyses – Pacific Centre for Isotopic and Geochemical Research – Sample 05LP069-1 in Crow Formation.*

Analysis No.	Age estimates with 1 sigma uncertainty (Ma)										Isotopic Ratios with absolute errors							
	$^{207}Pb/^{235}U$ Ma	$^{207}Pb/^{235}U$ ± 1σ Error	$^{206}Pb/^{238}U$ Ma	$^{206}Pb/^{238}U$ ± 1σ Error	$^{207}Pb/^{206}Pb$ Ma	$^{207}Pb/^{206}Pb$ ± 1σ Error	Preferred Age Ma*	± 1σ Error	Error %	Discordancy %	$^{207}Pb/^{235}U$ Ratio	$^{207}Pb/^{235}U$ 1σ Error	$^{206}Pb/^{238}U$ Ratio	$^{206}Pb/^{238}U$ 1σ Error	Rho	$^{207}Pb/^{206}Pb$ Ratio	$^{207}Pb/^{206}Pb$ 1σ Error	Th/U Ratio
05LP069L1	2322.2	9.77	2333.6	6.3	2319.5	8.57	2319.5	8.6	0.4	-0.6	8.8457	0.0948	0.4362	0.0014	0.30	0.1477	0.0007	0.3563
05LP069L2	2236.3	17.12	2216.4	9.57	2220.7	13.51	2220.7	13.5	0.6	0.2	8.0470	0.1526	0.4103	0.0021	0.27	0.1395	0.0011	0.2315
05LP069L3	2681.4	13.02	2724.1	8.53	2671.6	8.97	2671.6	9.0	0.3	-2.0	13.0248	0.1798	0.5259	0.0020	0.28	0.1821	0.0010	0.1436
05LP069L4	2841.6	12.85	2840.8	8.52	2861.8	8.38	2861.8	8.4	0.3	0.7	15.4201	0.2078	0.5538	0.0021	0.27	0.2044	0.0011	0.1877
05LP069L5	1936.6	6.53	1976.9	4.48	1904.2	7.95	1904.2	8.0	0.4	-3.8	5.7347	0.0433	0.3589	0.0009	0.35	0.1166	0.0005	0.1230
05LP069L6	2684.2	27.52	2719.4	16.29	2675.8	16.18	2675.8	16.2	0.6	-1.6	13.0624	0.3811	0.5248	0.0039	0.25	0.1825	0.0018	0.4963
05LP069L7	1894.6	7.98	1882.6	4.94	1902.1	9.12	1902.1	9.1	0.5	1.0	5.4616	0.0508	0.3392	0.0010	0.33	0.1164	0.0006	0.2574
05LP069L8	565.7	8.75	569.5	3.53	581.5	36.56	569.5	3.5	0.6	2.1	0.7457	0.0151	0.0924	0.0006	0.32	0.0594	0.0010	0.6380
05LP069L9	1860.8	12.98	1826.4	7.14	1896.1	13.46	1896.1	13.5	0.7	3.7	5.2501	0.0799	0.3275	0.0015	0.29	0.1160	0.0009	0.1594
05LP069L10	2313.1	23.33	2353.7	13.79	2371.9	17.2	2371.9	17.2	0.7	0.8	8.7578	0.2242	0.4407	0.0031	0.27	0.1523	0.0016	0.1827
05LP069L11	2140.3	14.03	2133.6	8.24	2189.5	12.2	2189.5	12.2	0.6	2.6	7.2305	0.1137	0.3923	0.0018	0.29	0.1370	0.0010	0.4461
05LP069L12	1760.9	7.39	1707.7	4.49	1847.8	9.26	1847.8	9.3	0.5	7.6	4.6643	0.0412	0.3033	0.0009	0.34	0.1130	0.0006	0.2075
05LP069L13	727.5	6.34	714.5	2.86	768.1	19.88	714.5	2.9	0.4	7.0	1.0472	0.0128	0.1172	0.0005	0.35	0.0648	0.0006	0.1436
05LP069L14	1811	14.21	1845.5	7.89	1805	15.11	1805.0	15.1	0.8	-2.2	4.9512	0.0833	0.3315	0.0016	0.29	0.1103	0.0009	0.1598
05LP069L15	1841.6	11.62	1864.9	6.66	1843.4	12.53	1843.4	12.5	0.7	-1.2	5.1329	0.0702	0.3355	0.0014	0.30	0.1127	0.0008	0.1296
05LP069L16	1928.5	9.3	1867.3	5.5	1972.3	10.04	1972.3	10.0	0.5	5.3	5.6813	0.0612	0.3360	0.0011	0.32	0.1211	0.0007	0.4823
05LP069L17	1865.9	28.51	1868.7	15.19	1912.3	27.62	1912.3	27.6	1.4	2.3	5.2817	0.1764	0.3363	0.0032	0.28	0.1171	0.0018	0.4390
05LP069L18	1838.8	6.99	1837.4	4.56	1864.2	8.77	1864.2	8.8	0.5	1.4	5.1163	0.0421	0.3298	0.0009	0.35	0.1140	0.0006	0.1539
05LP069L19	1895.4	13.61	1913.7	7.71	1909.6	13.89	1909.6	13.9	0.7	-0.2	5.4666	0.0867	0.3456	0.0016	0.29	0.1169	0.0009	0.2918
05LP069L20	2660.4	6.57	2646.6	5.43	2671.5	6.7	2671.5	6.7	0.3	0.9	12.7370	0.0888	0.5077	0.0013	0.36	0.1820	0.0007	0.3580
05LP069L21	2369.5	9.06	2315.8	6.06	2377.5	8.47	2377.5	8.5	0.4	2.6	9.3151	0.0920	0.4322	0.0014	0.32	0.1528	0.0008	0.3508
05LP069L22	1848.4	10.44	1843	6.11	1878.5	11.65	1878.5	11.7	0.6	1.9	5.1746	0.0635	0.3310	0.0013	0.31	0.1149	0.0008	0.0894
05LP069L23	2614.7	19.49	2557.2	11.39	2576.9	12.86	2576.9	12.9	0.5	0.8	12.1320	0.2521	0.4869	0.0026	0.26	0.1720	0.0013	0.1524
05LP069L24	1826.2	7.1	1782.4	4.55	1872.3	9.13	1872.3	9.1	0.5	4.8	5.0406	0.0422	0.3185	0.0009	0.35	0.1145	0.0006	0.2495
05LP069L25	678.5	5.31	665.7	2.43	679.2	18.25	665.7	2.4	0.4	2.0	0.9507	0.0102	0.1088	0.0004	0.36	0.0622	0.0005	0.1855
05LP069L26	669.5	4.25	652	2.04	687.9	14.94	652.0	2.0	0.3	5.2	0.9335	0.0081	0.1064	0.0004	0.38	0.0624	0.0004	0.0992
05LP069L27	2662.6	30.82	2706.7	18.8	2697.2	18.61	2697.2	18.6	0.7	-0.4	12.7674	0.4178	0.5218	0.0044	0.26	0.1849	0.0021	0.3023
05LP069L28	1879.6	11.66	1829.7	6.52	1865.3	12.62	1865.3	12.6	0.7	1.9	5.3669	0.0731	0.3282	0.0013	0.30	0.1141	0.0008	0.2925
05LP069L29	1959.9	10.46	1963.3	6.36	1992.1	11.22	1992.1	11.2	0.6	1.4	5.8911	0.0710	0.3560	0.0013	0.31	0.1224	0.0008	0.5227
05LP069L30	1716.2	7.28	1705.6	4.59	1750	9.92	1750.0	9.9	0.6	2.5	4.4203	0.0389	0.3029	0.0009	0.35	0.1071	0.0006	0.2847
05LP069L31	1917.6	9.25	1849.4	5.54	1958.7	10.55	1958.7	10.6	0.5	5.6	5.6095	0.0602	0.3323	0.0012	0.32	0.1202	0.0007	0.2831
05LP069L32	1845.6	9.32	1859.9	5.67	1827	11.08	1827.0	11.1	0.6	-1.8	5.1573	0.0565	0.3344	0.0012	0.32	0.1117	0.0007	0.2319

Analyses in italics/shaded are excluded due to >10% error in critical age, >10% discordance, or >5% reverse discordance.
All errors are at the 1-sigma level, and include only random uncertainties.
Best age = $^{206}Pb/^{238}U$ ages for analyses younger than 1.0 Ga and $^{206}Pb/^{207}Pb$ ages for analyses older than 1.0 Ga.
Isotope ratios are corrected for Pb/U fractionation by comparison with standard zircons Plesovice and FC1.

Table I-5g. *(continued) Detrital Zircon U-Pb geochronologic analyses – Pacific Centre for Isotopic and Geochemical Research – Sample 05LP069-1 in Crow Formation.*

Analysis No.	Age estimates with 1 sigma uncertainty (Ma)										Isotopic Ratios with absolute errors							
	$^{207}Pb/^{235}U$ Ma	$^{207}Pb/^{235}U$ ± 1σ Error	$^{206}Pb/^{238}U$ Ma	$^{206}Pb/^{238}U$ ± 1σ Error	$^{207}Pb/^{206}Pb$ Ma	$^{207}Pb/^{206}Pb$ ± 1σ Error	Preferred Age Ma*	± 1σ Error	Error %	Discordancy %	$^{207}Pb/^{235}U$ Ratio	$^{207}Pb/^{235}U$ 1σ Error	$^{206}Pb/^{238}U$ Ratio	$^{206}Pb/^{238}U$ 1σ Error	Rho	$^{207}Pb/^{206}Pb$ Ratio	$^{207}Pb/^{206}Pb$ 1σ Error	Th/U Ratio
05LP069L33	1791.2	7.53	1799.3	4.83	1767.7	9.96	1767.7	10.0	0.6	-1.8	4.8363	0.0433	0.3220	0.0010	0.34	0.1081	0.0006	0.1435
05LP069L34	1851.1	13.1	1886.5	7.57	1831.9	14.33	1831.9	14.3	0.8	-3.0	5.1909	0.0799	0.3400	0.0016	0.30	0.1120	0.0009	0.1950
05LP069L35	1834.4	14.23	1921	8.31	1818.4	15.45	1818.4	15.5	0.8	-5.6	5.0900	0.0853	0.3472	0.0017	0.30	0.1112	0.0010	0.1592
05LP069L36	1781	13.36	1796.6	7.6	1817.3	15.17	1817.3	15.2	0.8	1.1	4.7775	0.0760	0.3214	0.0016	0.31	0.1111	0.0009	0.0422
05LP069L37	3146	22.28	3110.4	14.46	3200.4	11.88	3200.4	11.9	0.4	2.8	21.1602	0.4863	0.6201	0.0036	0.25	0.2525	0.0019	0.1183
05LP069L38	1873.1	10.36	1866.4	6.19	1867	11.91	1867.0	11.9	0.6	0.0	5.3267	0.0646	0.3358	0.0013	0.31	0.1142	0.0008	0.1934
05LP069L39	2317.2	18.71	2340.6	11.22	2332.2	14.82	2332.2	14.8	0.6	-0.4	8.7969	0.1805	0.4378	0.0025	0.28	0.1488	0.0013	0.1776
05LP069L40	1863.1	18.28	1884	10.06	1852.7	18.92	1852.7	18.9	1.0	-1.7	5.2646	0.1128	0.3394	0.0021	0.29	0.1133	0.0012	0.1406
05LP069L41	2651.6	15.23	2693.2	10.06	2690.4	11.14	2690.4	11.1	0.4	-0.1	12.6191	0.2043	0.5186	0.0024	0.28	0.1841	0.0013	0.2256
05LP069L42	2691.8	10.76	2718.6	7.72	2700.3	9.12	2700.3	9.1	0.3	-0.7	13.1682	0.1501	0.5246	0.0018	0.31	0.1852	0.0010	0.6138
05LP069L43	2360.6	13.44	2404.6	8.67	2370.3	11.59	2370.3	11.6	0.5	-1.4	9.2255	0.1353	0.4521	0.0020	0.29	0.1522	0.0010	0.4207
05LP069L44	1781.5	7.4	1814.9	4.93	1779.4	10.29	1779.4	10.3	0.6	-2.0	4.7806	0.0421	0.3252	0.0010	0.35	0.1088	0.0006	0.1414
05LP069L46	2530.4	12.61	2496.3	8.23	2547.3	10.57	2547.3	10.6	0.4	2.0	11.0861	0.1501	0.4729	0.0019	0.29	0.1690	0.0011	0.2906
05LP069L47	2673.4	7.1	2666.5	6.11	2696.9	8.16	2696.9	8.2	0.3	1.1	12.9142	0.0972	0.5123	0.0014	0.37	0.1849	0.0009	0.8058
05LP069L48	1838	10.63	1874.3	6.49	1847.7	12.72	1847.7	12.7	0.7	-1.4	5.1111	0.0640	0.3374	0.0014	0.32	0.1130	0.0008	0.1389
05LP069L49	1827.1	18.44	1830.4	10.04	1833.8	19.66	1833.8	19.7	1.1	0.2	5.0461	0.1098	0.3284	0.0021	0.29	0.1121	0.0012	0.1072
05LP069L50	1947.6	11.19	1933.4	6.68	1889	12.63	1889.0	12.6	0.7	-2.4	5.8080	0.0750	0.3498	0.0014	0.31	0.1156	0.0008	0.6482
05LP069L51	2684	11.85	2707.4	8.37	2671	10.02	2671.0	10.0	0.4	-1.4	13.0607	0.1640	0.5219	0.0020	0.30	0.1820	0.0011	0.1771
05LP069L52	1863.5	9.09	1900.2	5.87	1865.1	11.53	1865.1	11.5	0.6	-1.9	5.2670	0.0561	0.3428	0.0012	0.33	0.1141	0.0007	0.4411
05LP069L53	1800.1	7.93	1791.3	5.13	1769.8	11.02	1769.8	11.0	0.6	-1.2	4.8876	0.0460	0.3203	0.0011	0.35	0.1082	0.0007	0.1224
05LP069L54	1788.5	8.58	1774.6	5.4	1785.4	11.59	1785.4	11.6	0.6	0.6	4.8204	0.0492	0.3169	0.0011	0.34	0.1092	0.0007	0.1671
05LP069L55	1826.4	15.77	1857.3	9.02	1827.8	17.66	1827.8	17.7	1.0	-1.6	5.0422	0.0938	0.3339	0.0019	0.30	0.1117	0.0011	0.1935
05LP069L56	2703.5	12.07	2725.7	8.63	2721.3	10.29	2721.3	10.3	0.4	-0.2	13.3331	0.1704	0.5263	0.0020	0.30	0.1876	0.0012	0.0357
05LP069L57	2050.7	7.39	2077.5	5.47	2047	9.99	2047.0	10.0	0.5	-1.5	6.5358	0.0548	0.3803	0.0012	0.37	0.1263	0.0007	0.0913
05LP069L58	1890.7	8.79	1888.3	5.75	1921.3	11.41	1921.3	11.4	0.6	1.7	5.4369	0.0557	0.3404	0.0012	0.34	0.1177	0.0008	0.2242
05LP069L59	1813.6	12.87	1830.8	7.5	1798.7	15.26	1798.7	15.3	0.8	-1.8	4.9662	0.0756	0.3284	0.0016	0.31	0.1100	0.0009	0.1569
05LP069L60	2607.6	16.91	2653	11.25	2648	12.91	2648.0	12.9	0.5	-0.2	12.0411	0.2172	0.5092	0.0026	0.29	0.1795	0.0014	0.2639
05LP069L61	1813.3	9.08	1822.8	5.8	1816	12.16	1816.0	12.2	0.7	-0.4	4.9646	0.0534	0.3268	0.0012	0.34	0.1110	0.0008	0.0980
05LP069L62	1807.9	9.57	1827.2	6.04	1810.1	12.61	1810.1	12.6	0.7	-0.9	4.9330	0.0559	0.3277	0.0012	0.33	0.1107	0.0008	0.2929
05LP069L63	2004.4	10.46	2020.3	6.75	2001.6	12.28	2001.6	12.3	0.6	-0.9	6.1997	0.0741	0.3681	0.0014	0.32	0.1231	0.0009	0.3496
05LP069L64	1927.6	9.22	1969.3	6.16	1924.8	11.84	1924.8	11.8	0.6	-2.3	5.6753	0.0606	0.3573	0.0013	0.34	0.1179	0.0008	0.1966
05LP069L65	2638.1	12.23	2658.1	8.68	2607.6	11	2607.6	11.0	0.4	-1.9	12.4393	0.1618	0.5103	0.0020	0.31	0.1752	0.0012	0.2935
																	64 zircons	

Analyses in italics/shaded are excluded due to >10% error in critical age, >10% discordance, or >5% reverse discordance.
All errors are at the 1-sigma level, and include only random uncertainties.
Best age = $^{206}Pb/^{238}U$ ages for analyses younger than 1.0 Ga and $^{206}Pb/^{207}Pb$ ages for analyses older than 1.0 Ga.
Isotope ratios are corrected for Pb/U fractionation by comparison with standard zircons Plesovice and FC1.

APPENDIX II. IGNEOUS GEOCHRONOLOGY

INTRODUCTION

Two whole rock $^{40}Ar/^{39}Ar$ samples were analyzed for Yukon Geological Survey at the Geochronology Laboratory of the Geological Survey of Canada, Ottawa under the supervision of Dr. M. Villeneuve. One sample was a basalt clast from the conglomerate member of Unit Pa, and the second sample was from the basalt flow (Unit Pb) overlying Unit Pssc.

METHODOLOGY

The samples were loaded into aluminum foil packets which were arranged radially inside an aluminum can along with samples of Fish Canyon Tuff sanidine (FCT-SAN, assumed age of 28.03 Ma, Renne *et al.*, 1998) as flux monitors. The samples were then irradiated for 12 hours at the research reactor of MacMaster University in a fast neutron flux of approximately $3x10^{16}$ neutrons/cm^2. Neutron flux gradients throughout the sample canister were evaluated by analyzing the sanidine flux monitors included with the sample packets and interpolating a linear fit against calculated J-factor and sample position.

Laser $^{40}Ar/^{39}Ar$ step-heating analysis was carried out at the Geological Survey of Canada laboratories in Ottawa, Ontario. Upon return from the reactor, samples were split into at least two aliquots. Each aliquot for a sample was analyzed separately to verify reproducibility of the results. Each aliquot was loaded into a 1.5 mm-diameter hole in a copper planchet. The samples and planchet were then placed in a vacuum chamber containing a ZnSe window. Heating of individual sample aliquots in steps of increasing temperature was completed using a Merchantek MIR10 10W CO_2 laser equipped with a 2 x 2 mm flat-field lens. The released Ar gas was cleaned by passive equilibration of the gas with a container filled with getters consisting of SAES™ NP-10 ST707 alloy held at 400°C and SAES alloy 201 for ten minutes. The cleaned gas was then analyzed isotopically using the secondary electron multiplier system of a VG3600 gas source mass spectrometer. Details of data collection protocols are described in Villeneuve and MacIntyre (1997) and Villeneuve *et al.* (2000).

Initially, each aliquot of a sample was treated as a separate step-heated analysis. If two aliquots gave identical plateau ages (within error), the data were combined and treated as a single step-heated analysis for data reduction. Ages were referenced to a Fish Canyon Tuff Sanidine (FCT-SAN) standard with an assumed age of 28.03 Ma (Renne *et al.*, 1998). It should be noted that any refinement or change in the accepted age of FCT-SAN will affect the absolute age (i.e., the age when used in comparison to age data produced by other laboratories or methods).

The apparent $^{40}Ar/^{39}Ar$ age of each heating step is plotted against the amount of ^{39}Ar released from the sample to form a gas-release plot. Because of the use of replicate analyses (aliquots), gas release plots differ from conventional $^{40}Ar/^{39}Ar$ spectra in that data from each aliquot is displayed in adjacent, alternately shaded regions of a gas release spectra. Upon ascertaining reproducibility of individual spectra and plateau regions between aliquots, data were combined by integrating plateau portions (marked by line above steps) weighted by analytical error.

Error analysis on individual steps follows numerical error analysis routines outlined in Scaillet (2000). Error analysis on grouped data follows algebraic methods of Roddick (1988). Analytical uncertainties for individual steps are reported at the 2-sigma level. Because the error associated with the J-factor is systematic and not related to individual analyses, correction for this uncertainty is not applied until calculation of dates from isotopic correlation diagrams (Roddick, 1988). The error limit in the final age determination includes uncertainty in the J paramenter. The error on individual J-factor values is conservatively estimated at ± 0.6% (2-sigma).

Analytical results

Sample 00TLA009 (Unit Pa)

Figure II-1 shows the gas release plots of two aliquots for sample 00TLA009, consisting of a basalt clast in the basaltic conglomerate member (Pa-bc) of Unit Pa from field station 00TLA009 (UTM coordinates 345 458 E/6 694 401N, zone 10).

The concave-upwards spectra coupled with highly variable Ca/K ratios suggest sporadic degassing of multiple mineral phases. Data indicate there may be excess ^{40}Ar in some of the steps and there may be an overprint of Ar-recoil which means the loss of ^{39}Ar on irradiation. These various factors result in an irresolvable age from complex systematics (Villeneuve, pers. comm., 2004).

Sample 01LP016 (Unit Pb)

Table II-1 lists whole rock analytical results for basalt sample 01LP016 from field station 01LP016 (UTM 336 631 E/6 706 945 N, zone 10). The results are displayed in Figure II-2.

The sample shows reproducible plateaus for degassing of different minerals in the sample (i.e., for variable Ca content in Figure II-2). The low temperature steps appear to give an indication of excess ^{40}Ar, but this is really an artifact of those steps comprising mostly atmospheric argon (Villeneuve, pers. comm., 2003). The resulting age determination for 01LP016 is 56.7 Ma ± 0.7 Ma (2-sigma).

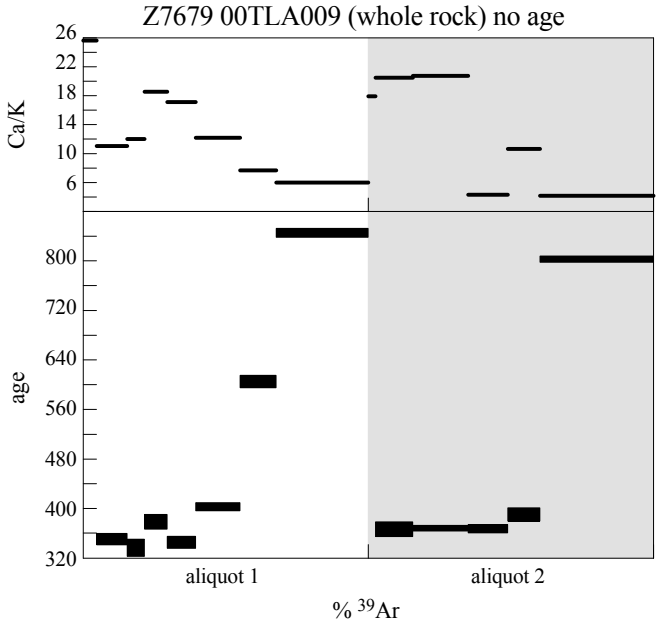


Figure II-1. *^{40}Ar/^{39}Ar age spectra for sample 00TLA009 (whole rock), basalt clast from Unit Pa-bc. Field station 00TLA009. Ca/K ratio shown at top of diagram.*

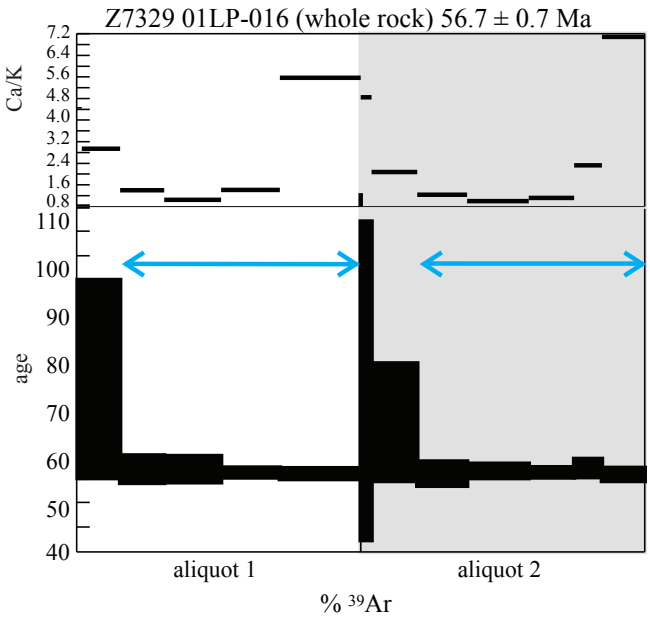


Figure II-2. *^{40}Ar/^{39}Ar age spectra for sample 01LP016 (whole rock), basalt – Unit Pb. Field station 01LP016. Ca/K ratio shown at top of diagram. Plateau segment is interpreted as the extrusion age of the volcanic rock.*

Table II-1. *Ar-Ar data for Paleocene basalt, sample 01LP016.*

01LP-016 Whole Rock; J=.00306160d Basalt (Z7329; 60.4674°N 125.9715°E) Summary Age 56.7 ± 0.7 Ma									
Power[a]	Volume ^{39}Ar x10^{-11} cc	^{36}Ar/^{39}Ar	^{37}Ar/^{39}Ar	^{38}Ar/^{39}Ar	^{40}Ar/^{39}Ar	%^{40}Ar	*^{40}Ar/^{39}Ar ATM	f_{39}[b] (%)	Apparent Age Ma[c]
Aliquot: A									
2.4	0.487	4.8066 ± 0.0697	2.287 ± 0.059	0.288 ± 0.025	1517.226 ± 27.480	98.9	16.890 ± 9.523	0.7	90.96 ± 50.02
2.8	3.549	1.3748 ± 0.0191	1.509 ± 0.036	0.092 ± 0.014	423.280 ± 4.418	96.7	14.052 ± 3.897	5.2	75.99 ± 20.64
3.0	4.0636	0.3328 ± 0.0023	0.724 ± 0.010	0.032 ± 0.011	109.462 ± 0.491	90.4	10.527 ± 0.539	6.0	57.23 ± 2.88
3.5	5.2509	0.1546 ± 0.0018	0.540 ± 0.007	0.025 ± 0.011	56.405 ± 0.181	81.3	10.524 ± 0.512	7.7	57.21 ± 2.74
4.6	5.3985	0.0543 ± 0.0007	0.730 ± 0.009	0.040 ± 0.011	26.489 ± 0.099	60.8	10.396 ± 0.194	7.9	56.52 ± 1.04
12.0	7.4718	0.0437 ± 0.0006	2.856 ± 0.028	0.093 ± 0.011	23.271 ± 0.064	55.5	10.353 ± 0.212	11.0	56.30 ± 1.13
Aliquot: B									
2.4	1.5857	3.5569 ± 0.0631	2.488 ± 0.061	0.252 ± 0.024	1082.491 ± 18.922	98.7	13.987 ± 6.266	2.3	75.65 ± 33.19
2.8	6.7374	0.8494 ± 0.0111	1.066 ± 0.028	0.077 ± 0.012	264.285 ± 2.518	95.3	12.361 ± 2.304	9.9	67.02 ± 12.26
3.0	7.3138	0.2300 ± 0.0017	0.637 ± 0.007	0.031 ± 0.011	78.540 ± 0.245	86.8	10.352 ± 0.478	10.8	56.29 ± 2.56
3.5	9.0944	0.0859 ± 0.0010	0.516 ± 0.007	0.023 ± 0.011	35.884 ± 0.091	70.9	10.455 ± 0.278	13.4	56.84 ± 1.49
3.9	6.6562	0.0575 ± 0.0007	0.577 ± 0.008	0.033 ± 0.011	27.416 ± 0.116	62.1	10.401 ± 0.195	9.8	56.55 ± 1.05
4.6	4.0731	0.0536 ± 0.0012	1.198 ± 0.014	0.060 ± 0.011	26.454 ± 0.170	60	10.570 ± 0.355	6.0	57.46 ± 1.90
12.0	6.3291	0.0481 ± 0.0006	3.631 ± 0.033	0.111 ± 0.011	24.563 ± 0.083	58	10.321 ± 0.251	9.3	56.13 ± 1.35

[a]As measured by laser in % of full nominal power (10W) [b]Fraction ^{39}Ar as % of total run [c]Errors are analytical only and do not reflect error in irradiation parameter J [d]Nominal J, referenced to FCT-SAN=28.03 Ma (Renne *et al.*, 1998) All uncertainties quoted at 2σ level

APPENDIX III. WHOLE ROCK GEOCHEMISTRY

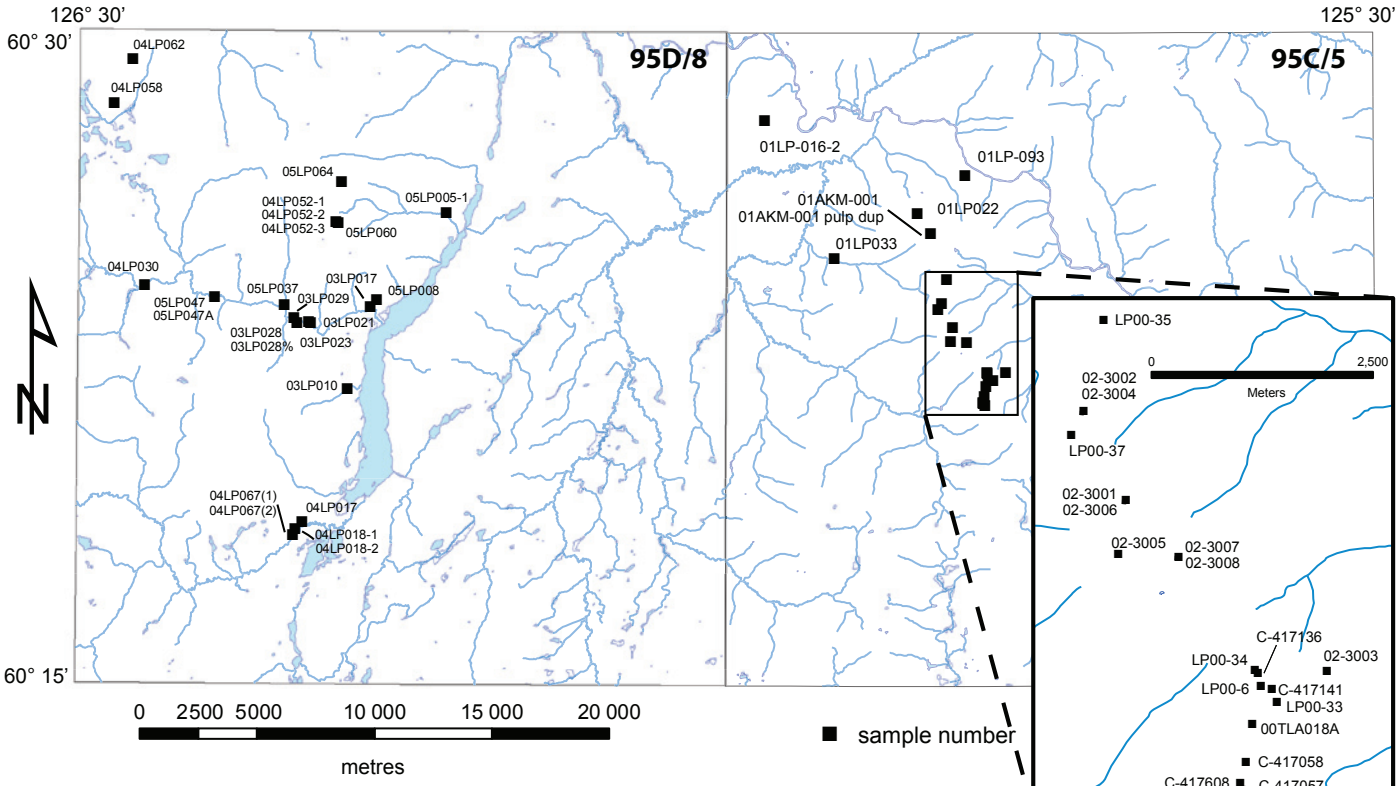


Figure III-1. *Location map for whole rock geochemistry samples, NTS 95C/5 and 95D/8. Inset shows detailed sample locations for part of NTS 95C/5.*

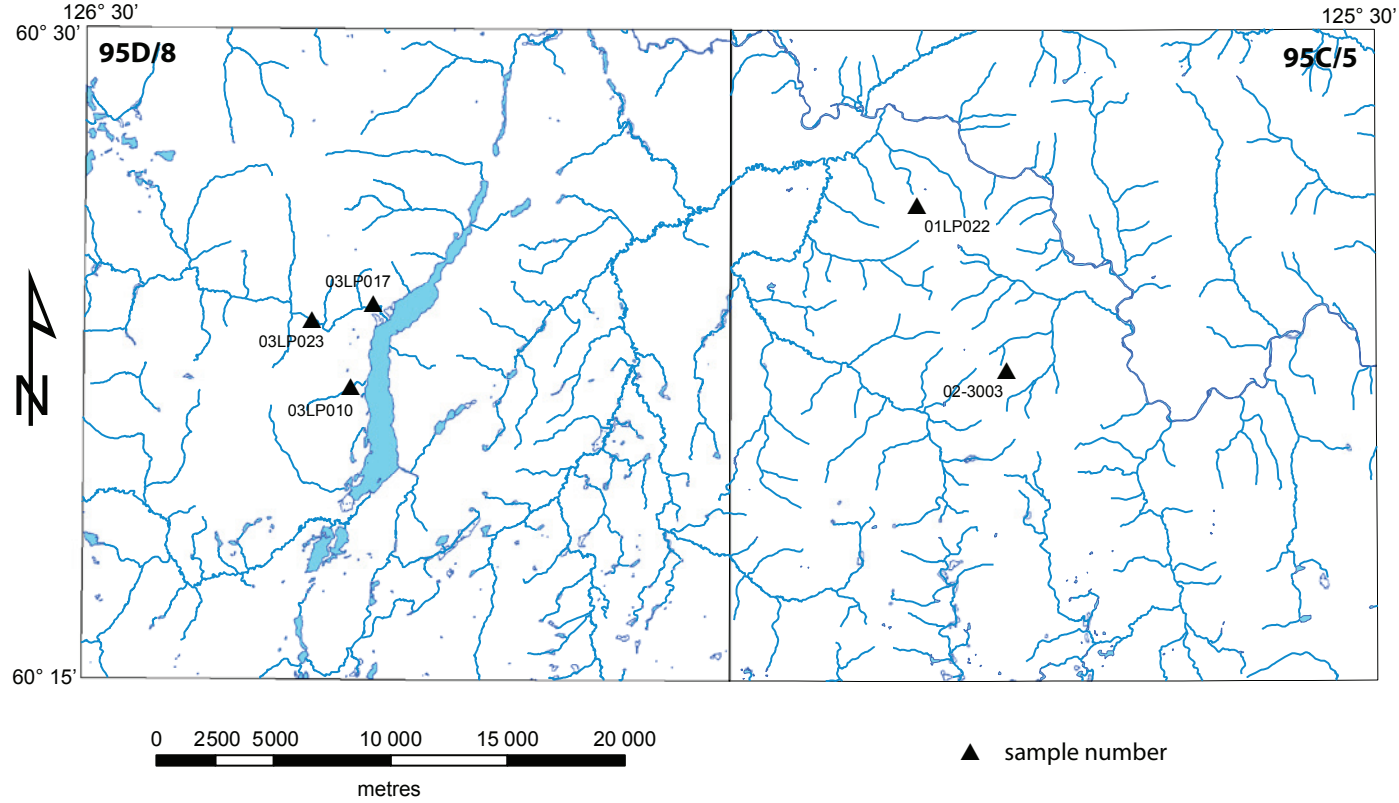


Figure III-2. *Location map for 36 element ICP-MS analysis samples, NTS 95C/5 and 95D/8.*

Table III-1. *Lithogeochemistry of dykes and volcaniclastic rocks within Unit* ***Pa****.*

Sample		LP00-33	LP00-34	00TLA018A	C-417136	C-417141	LP00-9	C-417058	C-417608	C-417057	LP00-6
Station		**00LP033**	**00LP034**	**00TLA018**	**MWB-00-21-10**	**MWB-00-21-43**	**00LP009**	**MWB2001-001007**	**LHA2000-018002**	**MWB2001-001005**	**00LP006**
Rock		**siltstone**	**siltstone**	**volcanic breccia**	**volcanic breccia**	**volcanic breccia**	**basalt clast in cgl**	**basalt clast in cgl**	**basalt clast in cgl**	**basalt clast in cgl**	**dyke**
Unit		**Pa**	**Pa**	**Pa**	**Pa**	**Pa**	**Pa-bc**	**Pa-bc**	**Pa-bc**	**Pa-bc**	**Pa**
UTM E		**345833**	**345601**	**345543**	**345633**	**345782**	**345458**	**345452**	**345381**	**345393**	**345660**
UTM N		**6695449**	**6695823**	**6695210**	**6695783**	**6695591**	**6694401**	**6694792**	**6694546**	**6694471**	**6695638**
UTM Zone		**10**	**10**	**10**	**10**	**10**	**10**	**10**	**10**	**10**	**10**
Datum		**NAD83**	**NAD83**	**NAD83**	**NAD83**	**NAD83**	**NAD83**	**NAD83**	**NAD83**	**NAD83**	**NAD83**
SiO_2 (%)	XRF	54.95	57.03	49.22	50.41	48.69	48.46	58.86	49.57	43.71	43.42
Cr_2O_3 (%)	XRF	NA	NA	0.01	0.01	0.01	NA	0.01	0.01	0.01	NA
Al_2O_3 (%)	XRF	12.85	12.47	12.83	10.28	10.15	11.02	12.07	10.44	13.97	14.82
Fe_2O_3* (%)	XRF	8.58	7.68	13.15	9.63	11.52	13.28	13.39	21.35	14.92	14.42
MnO (%)	XRF	0.097	0.114	0.130	0.227	0.177	0.130	0.060	0.179	0.130	0.314
MgO (%)	XRF	8.06	8.29	7.18	8.11	6.63	5.77	2.15	2.27	5.94	5.65
CaO (%)	XRF	6.30	5.13	9.41	11.56	12.62	6.01	3.36	4.25	6.14	6.49
Na_2O (%)	XRF	1.51	1.31	2.49	3.26	3.64	2.96	4.43	4.77	4.20	2.54
K_2O (%)	XRF	2.01	3.61	0.52	0.78	0.53	1.26	1.79	0.36	1.05	4.60
TiO_2 (%)	XRF	1.427	1.064	2.080	1.600	2.070	2.207	2.480	2.040	1.550	4.169
P_2O_5 (%)	XRF	0.23	0.15	0.28	0.20	0.22	0.30	0.29	0.34	0.15	1.24
L.O.I. (%)		2.81	2.02	2.87	4.02	4.04	7.52	1.23	4.47	8.11	1.30
Total		**98.82**	**98.87**	**100.17**	**100.08**	**100.30**	**98.92**	**100.12**	**100.05**	**99.88**	**98.96**
Sc (ppm)	INNA	NA	NA	23.6	21.1	22.5	NA	25.1	22.7	30.6	NA
V (ppm)	ICP-MS	180	153	299	214	234	292	256	363	359	192
Cr (ppm)	ICP-MS	77	89	38	54	47	36	30	28	31	46
Co (ppm)	ICP-MS	26	41	27	31	24	33	12	12	30	35
Ni (ppm)	ICP-MS	26	43	39	37	45	-20	24	23	36	61
Cu (ppm)	ICP-MS	48	14	13	18	255	13	34	72	-10	26
Zn (ppm)	ICP-MS	70	64	93	62	103	102	57	51	89	167
Ga (ppm)	ICP-MS	19	18	23	14	14	19	13	12	20	27
Ge (ppm)	ICP-MS	1.6	1.8	2.2	2.5	1.8	1.4	1.3	1.0	1.5	1.8
As (ppm)	ICP-MS	-5	-5	-5	7	-5	-5	6	8	-5	7
Rb (ppm)	ICP-MS	86	134	13	15	10	30	49	8	35	204
Sr (ppm)	ICP-MS	104	97	406	138	195	114	120	65	123	1120
Y (ppm)	ICP-MS	43.2	37.4	45.3	28.5	36.4	52.4	38.1	43.8	24.8	49.7
Zr (ppm)	ICP-MS	249	236	210	142	168	202	208	173	117	462
Nb (ppm)	ICP-MS	16.3	14.7	16.4	10.1	11.4	15.9	16.9	14.0	7.5	111
Mo (ppm)	ICP-MS	-2	-2	-2	-2	-2	-2	-2	-2	-2	6
Ag (ppm)	ICP-MS	-0.5	-0.5	-0.5	-0.5	-0.5	-0.5	-0.5	-0.5	-0.5	-0.5
In (ppm)	ICP-MS	-0.1	-0.1	-0.1	-0.1	-0.1	-0.1	-0.1	-0.1	-0.1	0.2
Sn (ppm)	ICP-MS	2	2	2	1	2	2	3	2	2	4
Sb (ppm)	ICP-MS	0.7	2.1	1.7	4.7	1.2	1.3	1.4	1.3	1.0	2.0
Cs (ppm)	ICP-MS	5.9	9.2	0.5	0.4	0.3	2.2	0.7	0.6	1.7	22.6
Ba (ppm)	ICP-MS	208	400	65	56	236	296	567	87	156	1210
La (ppm)	ICP-MS	33.5	34.2	28.5	16.5	18.4	22.3	22.0	27.3	17.9	105
Ce (ppm)	ICP-MS	69.4	69.8	61.1	39.8	43.3	50.8	49.9	60.5	40.7	211
Pr (ppm)	ICP-MS	7.69	7.48	7.20	4.88	5.20	6.18	5.97	7.18	4.88	23.1
Nd (ppm)	ICP-MS	31.4	30.7	30.0	21.1	22.2	28.5	25.2	30.9	20.5	93.1
Sm (ppm)	ICP-MS	6.73	6.36	7.73	5.55	6.00	6.96	6.72	8.53	5.58	16.1
Eu (ppm)	ICP-MS	1.53	1.41	2.16	1.39	1.43	2.01	1.69	2.60	1.42	4.88
Gd (ppm)	ICP-MS	6.26	5.46	7.86	5.41	5.82	7.24	6.50	8.86	5.26	13.0
Tb (ppm)	ICP-MS	1.06	1.01	1.36	0.94	1.08	1.31	1.17	1.56	0.95	1.84
Dy (ppm)	ICP-MS	6.34	5.93	7.67	5.03	5.99	8.07	6.50	8.34	5.02	9.10
Ho (ppm)	ICP-MS	1.24	1.16	1.48	0.94	1.16	1.57	1.25	1.50	0.90	1.54
Er (ppm)	ICP-MS	3.81	3.56	4.51	2.85	3.65	4.78	3.84	4.50	2.51	4.01
Tm (ppm)	ICP-MS	0.569	0.526	0.663	0.428	0.544	0.671	0.580	0.658	0.340	0.510
Yb (ppm)	ICP-MS	3.66	3.51	4.12	2.52	3.43	4.37	3.51	3.85	2.08	2.85
Lu (ppm)	ICP-MS	0.546	0.511	0.587	0.361	0.484	0.637	0.511	0.538	0.276	0.358
Hf (ppm)	ICP-MS	7.2	7.0	5.7	3.9	4.7	6.0	5.9	4.7	3.4	11.8
Ta (ppm)	ICP-MS	1.37	1.32	1.15	0.68	0.76	1.20	1.18	0.90	0.52	9.13
W (ppm)	ICP-MS	1.2	1.5	2.1	3.8	1.4	0.6	1.1	1.0	0.5	1.8
Tl (ppm)	ICP-MS	0.27	0.52	0.08	0.07	0.05	0.13	0.31	0.06	0.19	0.93
Pb (ppm)	ICP-MS	6	9	11	19	13	14	12	20	15	12
Bi (ppm)	ICP-MS	0.4	0.3	1.6	1.6	5.3	0.3	2.3	1.0	1.1	0.4
Th (ppm)	ICP-MS	10.8	11.5	6.25	4.22	4.39	5.85	5.31	4.23	3.26	14.3
U (ppm)	ICP-MS	2.44	2.45	1.71	1.35	1.23	1.42	1.30	1.32	0.81	2.86

*Total iron reported as Fe_2O_3 • Samples were analyzed at Activation Laboratories Ltd., Ancaster, Ontario Canada • Samples were crushed and then pulverized in a ceramic mill. • Major and minor elements were determined by XRF on a fusion sample. • Sc was analyzed using INNA. • Trace elements and REE were analyzed by ICP-MS at research detection limits on a fusion sample containing a lithium metaborate/tetraborate flux. • Analysis below detection limit shown with detection limit as negative number. • NA = not analyzed

Table III-2. *Lithogeochemistry of dykes and clast within Toobally Formation.*

Sample		03LP007v	03LP004	03LP010	03LP017	03LP021
Station		**03LP007**	**03LP004**	**03LP010**	**03LP017**	**03LP021**
Rock		**clast**	**dyke/sill**	**altered dyke/sill**	**altered dyke/sill**	**dyke/sill**
Unit		PT	PT	PT	PT	PT
UTM E		**649694**	**649441**	**649320**	**650123**	**647628**
UTM N		**6696296**	**6698146**	**6694834**	**6698395**	**6697581**
UTM Zone		**9**	**9**	**9**	**9**	**9**
Datum		**NAD83**	**NAD83**	**NAD83**	**NAD83**	**NAD83**
SiO_2 (%)	XRF	39.44	45.35	34.74	52.62	42.08
Al_2O_3 (%)	XRF	11.49	15.26	14.98	14.85	14.68
Cr_2O_3 (%)	XRF	NA	NA	NA	NA	NA
Fe_2O_3* (%)	XRF	8.96	11.24	10.61	10.59	15.01
MnO (%)	XRF	0.123	0.184	0.125	0.045	0.176
MgO (%)	XRF	7.44	7.57	3.72	2.26	4.65
CaO (%)	XRF	11.40	8.72	12.15	1.95	8.23
Na_2O (%)	XRF	0.54	2.41	2.91	0.16	2.88
K_2O (%)	XRF	2.26	2.07	1.45	2.71	0.47
TiO_2 (%)	XRF	2.592	1.672	2.067	2.753	3.369
P_2O_5 (%)	XRF	0.63	0.32	0.20	0.34	0.37
L.O.I. (%)		13.84	4.31	15.64	10.88	6.92
Total		**98.72**	**99.11**	**98.59**	**99.16**	**98.84**
Ba (ppm)	INNA	750	814	268	260	337
Sr (ppm)	INNA	221	257	526	52	698
Y (ppm)	INNA	42	27	21	22	24
Sc (ppm)	INNA	17	34	30	32	20
Zr (ppm)	INNA	253	95	97	201	177
Be (ppm)	INNA	2	1	1	2	2
V (ppm)	INNA	172	258	249	272	270
V (ppm)	ICP-MS	159	247	237	249	257
Cr (ppm)	ICP-MS	31	271	528	254	-20
Co (ppm)	ICP-MS	20	38	52	69	47
Ni (ppm)	ICP-MS	112	80	198	103	52
Cu (ppm)	ICP-MS	390	51	317	635	28
Zn (ppm)	ICP-MS	86	91	80	67	125
Ga (ppm)	ICP-MS	14	16	18	17	20
Ge (ppm)	ICP-MS	2	2	2	3	2
As (ppm)	ICP-MS	23	12	115	60	-5
Rb (ppm)	ICP-MS	63	27	54	69	14
Sr (ppm)	ICP-MS	216	249	503	51	735
Y (ppm)	ICP-MS	40	23	18	23	26

Sample		03LP007v	03LP004	03LP010	03LP017	03LP021
Station		**03LP007**	**03LP004**	**03LP010**	**03LP017**	**03LP021**
Rock		**clast**	**dyke/sill**	**altered dyke/sill**	**altered dyke/sill**	**dyke/sill**
Unit		PT	PT	PT	PT	PT
Zr (ppm)	ICP-MS	275	105	110	210	200
Nb (ppm)	ICP-MS	28	38	23	48	38
Mo (ppm)	ICP-MS	>100	>100	>100	2	2
Ag (ppm)	ICP-MS	-0.5	-0.5	-0.5	-0.5	-0.5
In (ppm)	ICP-MS	-0.2	-0.2	-0.2	-0.2	-0.2
Sn (ppm)	ICP-MS	2	-1	1	2	2
Sb (ppm)	ICP-MS	0.7	-0.5	-0.5	1.5	0.7
Cs (ppm)	ICP-MS	1.7	3.3	3.1	4.1	2.2
Ba (ppm)	ICP-MS	773	828	275	264	362
La (ppm)	ICP-MS	17.0	31.4	15.7	23.6	34.1
Ce (ppm)	ICP-MS	39	62.5	33.8	49.8	73.2
Pr (ppm)	ICP-MS	4.98	6.86	4.12	5.58	8.19
Nd (ppm)	ICP-MS	24.5	28.8	19.5	24.5	35.6
Sm (ppm)	ICP-MS	6.8	5.6	4.4	4.9	6.8
Eu (ppm)	ICP-MS	2.35	2.10	1.29	1.53	2.83
Gd (ppm)	ICP-MS	8.4	5.8	4.6	5.4	6.8
Tb (ppm)	ICP-MS	1.4	0.9	0.7	0.9	1.1
Dy (ppm)	ICP-MS	7.8	4.7	3.8	5.0	5.5
Ho (ppm)	ICP-MS	1.5	0.9	0.7	0.9	1.0
Er (ppm)	ICP-MS	4.4	2.7	2.0	2.7	2.9
Tm (ppm)	ICP-MS	0.66	0.36	0.27	0.39	0.38
Yb (ppm)	ICP-MS	3.9	2.1	1.5	2.2	2.3
Lu (ppm)	ICP-MS	0.62	0.32	0.23	0.33	0.34
Hf (ppm)	ICP-MS	7.4	2.7	3.2	5.5	5.1
Ta (ppm)	ICP-MS	1.5	2.2	1.3	3.2	2.3
W (ppm)	ICP-MS	-1	-1	-1	2	-1
Tl (ppm)	ICP-MS	0.2	0.2	0.2	0.3	-0.1
Pb (ppm)	ICP-MS	25	10	18	-5	7
Bi (ppm)	ICP-MS	-0.4	-0.4	-0.4	-0.4	-0.4
Th (ppm)	ICP-MS	6.2	3.1	1.6	5.2	4.0
U (ppm)	ICP-MS	2.5	0.8	0.4	1.4	0.9

*Total iron reported as Fe_2O_3 • Samples were analyzed at Activation Laboratories Ltd., Ancaster, Ontario Canada • Samples were crushed and then pulverized in a ceramic mill. • Major and minor elements were determined by XRF on a fusion sample. • Ba, Sr, Y, Sc, Zr, Be, V were analyzed using INNA. • Trace elements and REE were analyzed by ICP-MS at research detection limits on a fusion sample containing a lithium metaborate/tetraborate flux. • Analysis below detection limit shown with detection limit as negative number. • NA = not analyzed

Table III-3. *Lithogeochemistry of dykes and volcanic rocks within Crow Formation.*

Sample		05LP005-1	05LP008	03LP023	03LP028	03LP028%	03LP029	04LP017	04LP018-1	04LP018-2	04LP052-1	04LP052-2
Station		**05LP005**	**05LP008**	**03LP023**	**03LP028**	**03LP028**	**03LP029**	**04LP017**	**04LP018**	**04LP018**	**04LP052**	**04LP052**
rock		**flow**	**flow**	**altered breccia**	**lapilli tuff**	**lapilli tuff**	**lapilli tuff**	**volcani-clastic**	**flow**	**flow**	**flow**	**flow**
Unit		**ЄOCv1**	**ЄOCv1**	**ЄOCv2**	**ЄOCv2**	**ЄOCv2**	**ЄOCv2**	**ЄOCv2**	**ЄOCv2**	**ЄOCv2**	**ЄOCv2**	**ЄOCv2**
UTM E		**653170**	**650376**	**647538**	**647053**	**647053**	**646909**	**647676**	**647392**	**647392**	**648485**	**648485**
UTM N		**6702526**	**6698707**	**6697584**	**6697555**	**6697555**	**6697722**	**6689077**	**6688779**	**6688779**	**6701937**	**6701937**
UTM Zone		**9**	**9**	**9**	**9**	**9**	**9**	**9**	**9**	**9**	**9**	**9**
Datum		**NAD83**	**NAD83**	**NAD83**	**NAD83**	**NAD83**	**NAD83**	**NAD83**	**NAD83**	**NAD83**	**NAD83**	**NAD83**
SiO_2 (%)	XRF	47.37	27.87	36.67	47.45	NA	51.12	41.18	47.94	54.73	48.08	43.57
Cr_2O_3 (%)	XRF	18.8	11.97	10.18	14.62	NA	12.90	13.72	11.53	10.51	14.64	17.51
Al_2O_3 (%)	XRF	0.03	0.06	NA	NA	NA	NA	-0.01	-0.01	0.18	0.05	0.06
Fe_2O_3* (%)	XRF	12.13	12.22	15.90	11.39	NA	10.11	10.03	9.91	11.96	11.73	10.30
MnO (%)	XRF	0.156	0.213	0.230	0.162	NA	0.209	0.167	0.168	0.024	0.182	0.233
MgO (%)	XRF	6.65	7.44	4.66	8.55	NA	8.55	4.34	4.90	13.81	7.58	11.91
CaO (%)	XRF	0.91	16.04	7.99	6.21	NA	6.54	8.68	7.52	0.43	4.80	5.23
Na_2O (%)	XRF	4.96	1.91	0.12	3.87	NA	3.10	0.10	2.55	0.03	4.26	2.76
K_2O (%)	XRF	0.34	0.08	1.43	0.63	NA	0.76	3.67	0.91	0.02	1.62	1.39
TiO_2 (%)	XRF	2.56	2.1	2.461	1.596	NA	1.824	3.60	2.23	1.15	1.33	1.50
P_2O_5 (%)	XRF	0.28	0.27	0.43	0.18	NA	0.25	1.12	0.50	0.11	0.44	0.48
L.O.I. (%)		5.75	19.39	18.56	4.35	NA	3.34	13.90	11.93	7.30	5.62	5.37
Total		**99.94**	**99.56**	**98.63**	**99.01**		**98.70**	**100.50**	**100.08**	**100.25**	**100.33**	**100.32**
Ba (ppm)	INNA	NA	NA	92	326	NA	295	NA	NA	NA	NA	NA
Sr (ppm)	INNA	NA	NA	76	380	NA	732	NA	NA	NA	NA	NA
Y (ppm)	INNA	NA	NA	27	16	NA	18	NA	NA	NA	NA	NA
Sc (ppm)	INNA	33.4	34.8	16	31	NA	29	10.9	12.8	18.0	16.7	20.2
Zr (ppm)	INNA	NA	NA	159	105	NA	122	NA	NA	NA	NA	NA
Be (ppm)	INNA	NA	NA	1	1	NA	1	NA	NA	NA	NA	NA
V (ppm)	INNA	NA	NA	178	193	NA	156	NA	NA	NA	NA	NA
V (ppm)	ICP-MS	257	235	162	178	181	143	190	133	138	109	140
Cr (ppm)	ICP-MS	180	310	-20	279	291	250	29	-20	1,140	299	374
Co (ppm)	ICP-MS	14	33	26	45	45	34	23	46	73	33	42
Ni (ppm)	ICP-MS	50	140	25	130	136	69	-20	113	449	162	199
Cu (ppm)	ICP-MS	50	60	13	60	69	-10	12	33	-10	-10	-10
Zn (ppm)	ICP-MS	90	150	42	83	112	122	42	-30	64	61	116
Ga (ppm)	ICP-MS	21	15	14	15	15	15	21	14	12	16	22
Ge (ppm)	ICP-MS	1.5	1.3	2	1	2	2	1.7	1.0	1.4	1.0	2.0
As (ppm)	ICP-MS	-5	-5	21	-5	-5	-5	-5	-5	-5	-5	-5
Rb (ppm)	ICP-MS	8	2	36	10	10	13	116	19	-1	15	21
Sr (ppm)	ICP-MS	254	180	75	378	387	746	422	73	25	175	647
Y (ppm)	ICP-MS	21.3	19	24	17	17	20	38.4	20.4	10.0	23.6	30.1
Zr (ppm)	ICP-MS	135	113	172	110	112	133	413	156	54	179	202
Nb (ppm)	ICP-MS	22.5	17.7	29	27	27	28	137	32.4	11.9	86.7	99.1
Mo (ppm)	ICP-MS	-2	-2	>100	-2	-2	-2	-2	-2	-2	-2	-2
Ag (ppm)	ICP-MS	-0.5	-0.5	-0.5	-0.5	-0.5	-0.5	-0.5	-0.5	-0.5	-0.5	-0.5
In (ppm)	ICP-MS	-0.1	-0.1	-0.2	-0.2	-0.2	-0.2	-0.1	-0.1	-0.1	-0.1	-0.1
Sn (ppm)	ICP-MS	-1	-1	1	1	2	1	1	-1	-1	-1	-1
Sb (ppm)	ICP-MS	0.7	1	1.9	-0.5	0.7	-0.5	-0.2	-0.2	-0.2	-0.2	-0.2
Cs (ppm)	ICP-MS	1.4	0.1	1.4	0.8	0.8	-0.5	3.2	1.5	0.1	0.2	0.5
Ba (ppm)	ICP-MS	151	23	95	336	340	313	673	128	5	415	765
La (ppm)	ICP-MS	20	6.28	21.6	14.9	15.6	25.3	159	12.3	5.66	49.8	64.4
Ce (ppm)	ICP-MS	48.7	16.4	46.3	32.8	34.3	50.4	294	26.9	12.5	98.7	121
Pr (ppm)	ICP-MS	6.21	2.35	5.45	3.92	4.02	5.64	32.0	3.31	1.46	9.97	12.4
Nd (ppm)	ICP-MS	25.9	11.3	24.6	18.0	18.1	25.3	117	16.6	6.26	36.7	44.9
Sm (ppm)	ICP-MS	5.62	3.31	6.0	3.9	3.9	5.0	18.8	5.46	1.46	6.55	8.02
Eu (ppm)	ICP-MS	2.44	1.46	2.15	1.73	1.71	2.17	5.61	2.10	0.484	2.24	3.24
Gd (ppm)	ICP-MS	5.71	4	6.5	4.3	4.2	5.3	14.2	5.86	1.77	5.67	6.67
Tb (ppm)	ICP-MS	0.88	0.69	1.0	0.7	0.7	0.8	1.91	0.88	0.34	0.91	1.05
Dy (ppm)	ICP-MS	4.67	4.09	5.0	3.6	3.6	4.3	9.00	4.51	2.12	5.00	5.84
Ho (ppm)	ICP-MS	0.86	0.72	0.9	0.7	0.7	0.8	1.45	0.77	0.41	0.94	1.09
Er (ppm)	ICP-MS	2.32	1.83	2.7	1.9	1.9	2.1	3.73	2.07	1.08	2.73	3.04
Tm (ppm)	ICP-MS	0.306	0.244	0.36	0.26	0.26	0.28	0.497	0.283	0.142	0.383	0.423
Yb (ppm)	ICP-MS	1.77	1.37	2.2	1.5	1.5	1.7	2.92	1.67	0.81	2.27	2.62
Lu (ppm)	ICP-MS	0.234	0.171	0.33	0.23	0.23	0.25	0.401	0.237	0.110	0.329	0.376
Hf (ppm)	ICP-MS	3.5	2.9	4.4	2.9	2.9	3.5	9.5	3.8	1.5	4.1	4.3
Ta (ppm)	ICP-MS	1.62	1.26	1.8	1.7	1.5	1.6	8.77	1.75	0.59	4.68	4.88
W (ppm)	ICP-MS	-0.5	-0.5	-1	-1	-1	-1	1.7	0.9	-0.5	-0.5	-0.5
Tl (ppm)	ICP-MS	0.1	0.05	0.3	-0.1	-0.1	-0.1	0.82	0.17	-0.05	0.21	0.18
Pb (ppm)	ICP-MS	-5	-5	14	-5	10	9	10	-5	-5	6	9
Bi (ppm)	ICP-MS	-0.1	-0.1	-0.4	-0.4	-0.4	-0.4	2.7	1.4	0.9	1.5	2.1
Th (ppm)	ICP-MS	1.96	1.68	3.6	1.6	1.6	2.4	14.8	2.04	0.88	6.89	7.32
U (ppm)	ICP-MS	0.53	0.39	0.8	0.4	0.4	0.6	4.67	0.63	0.24	1.82	1.84

* Total iron reported as Fe_2O_3 • Samples were analyzed at Activation Laboratories Ltd., Ancaster, Ontario Canada • Samples were crushed and then pulverized in a ceramic mill. • Major and minor elements were determined by XRF on a fusion sample. • Ba, Sr, Y, Sc, Zr, Be, V were analyzed using INNA. • Trace elements and REE were analyzed by ICP-MS at research detection limits on a fusion sample. • Analysis below detection limit shown with detection limit as negative number. • NA = not analyzed % replicate analysis

Table III-3. *(continued) Lithogeochemistry of dykes and volcanic rocks within Crow Formation.*

Sample		04LP052-3	04LP067(1)	04LP067(2)	05LP037	05LP060	05LP064	05LP047	05LP047A	04LP030	04LP058	04LP062
Station		**04LP052**	**04LP067**	**04LP067**	**05LP037**	**05LP060**	**05LP064**	**05LP047**	**05LP047**	**04LP030**	**04LP058**	**04LP062**
rock		**flow**	**flow**	**flow**	**flow**	**flow?**	**flow**	**dyke/sill?**	**dyke/sill?**	**volcani-clastic**	**flow**	**flow**
Unit		**ЄOCv2**	**ЄOCv2**	**ЄOCv2**	**ЄOCv2**	**ЄOCv2**	**ЄOCv2**	**ЄOCv3**	**ЄOCv3**	**ЄOCv4**	**ЄOCv4**	**ЄOCv4**
UTM E		**648485**	**647299**	**647299**	**646474**	**648589**	**648671**	**643488**	**643488**	**640489**	**638839**	**639536**
UTM N		**6701937**	**6688532**	**6688532**	**6698311**	**6701885**	**6703655**	**6698498**	**6698498**	**6698856**	**6706551**	**6708455**
UTM Zone		**9**	**9**	**9**	**9**	**9**	**9**	**9**	**9**	**9**	**9**	**9**
Datum		**NAD83**	**NAD83**	**NAD83**	**NAD83**	**NAD83**	**NAD83**	**NAD83**	**NAD83**	**NAD83**	**NAD83**	**NAD83**
SiO_2 (%)	XRF	47.46	47.38	47.35	45.47	40.32	43.22	46.59	46.20	48.40	49.69	46.67
Cr_2O_3 (%)	XRF	15.89	15.21	15.16	14.66	12.84	13.76	16.70	16.68	14.07	15.89	14.26
Al_2O_3 (%)	XRF	0.10	-0.01	-0.01	0.05	0.10	0.07	0.01	0.05	0.04	0.01	-0.01
Fe_2O_3* (%)	XRF	10.89	12.34	12.38	11.29	13.63	14.21	11.33	11.40	11.54	10.83	14.61
MnO (%)	XRF	0.186	0.193	0.193	0.118	0.132	0.216	0.158	0.163	0.166	0.138	0.136
MgO (%)	XRF	10.03	4.32	4.28	9.38	8.85	11.59	5.15	5.18	7.64	6.14	5.02
CaO (%)	XRF	3.00	4.44	4.43	5.04	8.34	5.74	10.67	10.66	8.78	4.41	6.28
Na_2O (%)	XRF	3.45	4.63	4.66	4.14	0.69	2.89	2.33	2.47	1.87	4.69	4.61
K_2O (%)	XRF	2.86	0.57	0.57	0.39	2.55	0.84	1.40	1.30	2.28	2.14	1.40
TiO_2 (%)	XRF	1.37	2.85	2.84	1.75	1.73	1.78	2.26	2.22	2.42	2.86	3.91
P_2O_5 (%)	XRF	0.44	0.62	0.61	0.42	0.32	0.44	0.33	0.33	0.32	0.44	0.65
L.O.I. (%)		4.17	7.77	7.77	7.21	10.03	4.53	2.14	2.52	2.83	3.15	2.19
Total		**99.85**	**100.31**	**100.23**	**99.92**	**99.53**	**99.29**	**99.07**	**99.17**	**100.36**	**100.39**	**99.73**
Ba (ppm)	INNA	NA	NA		NA	NA	NA	NA	NA	NA	NA	NA
Sr (ppm)	INNA	NA	NA		NA	NA	NA	NA	NA	NA	NA	NA
Y (ppm)	INNA	NA	NA		NA	NA	NA	NA	NA	NA	NA	NA
Sc (ppm)	INNA	17.6	15.4		20.4	28.2	27.9	29.0	29.2	27.9	26.8	29.5
Zr (ppm)	INNA	NA	NA		NA	NA	NA	NA	NA	NA	NA	NA
Be (ppm)	INNA	NA	NA		NA	NA	NA	NA	NA	NA	NA	NA
V (ppm)	INNA	NA	NA		NA	NA	NA	NA	NA	NA	NA	NA
V (ppm)	ICP-MS	122	149		116	164	163	209	222	255	247	314
Cr (ppm)	ICP-MS	338	-20		270	440	380	70	80	238	57	-20
Co (ppm)	ICP-MS	41	41		33	37	47	31	31	42	40	34
Ni (ppm)	ICP-MS	188	-20		140	230	190	30	30	125	35	-20
Cu (ppm)	ICP-MS	12	24		-10	-10	-10	50	50	74	68	13
Zn (ppm)	ICP-MS	101	39		70	70	90	60	70	86	110	83
Ga (ppm)	ICP-MS	19	16		16	15	14	18	18	19	20	20
Ge (ppm)	ICP-MS	1.4	1.1		1.2	1.1	1.2	1.3	1.3	1.5	0.9	1.5
As (ppm)	ICP-MS	-5	-5		-5	-5	-5	6	-5	-5	-5	-5
Rb (ppm)	ICP-MS	37	10		8	64	12	27	25	35	23	15
Sr (ppm)	ICP-MS	259	52		91	81	291	385	395	241	70	245
Y (ppm)	ICP-MS	27.1	21.9		23.9	19.5	22.2	22.7	22.3	26.1	25.9	31.1
Zr (ppm)	ICP-MS	210	167		145	101	120	180	177	176	245	186
Nb (ppm)	ICP-MS	106	34.1		43.5	25.4	34.9	28.0	27.4	31.2	45.1	39.0
Mo (ppm)	ICP-MS	-2	-2		-2	-2	-2	-2	-2	-2	2	-2
Ag (ppm)	ICP-MS	-0.5	-0.5		-0.5	-0.5	-0.5	-0.5	-0.5	-0.5	-0.5	-0.5
In (ppm)	ICP-MS	-0.1	-0.1		-0.1	-0.1	-0.1	-0.1	-0.1	-0.1	-0.1	-0.1
Sn (ppm)	ICP-MS	3	-1		-1	-1	-1	-1	-1	-1	-1	-1
Sb (ppm)	ICP-MS	0.2	-0.2		1.1	0.9	0.9	0.9	0.8	-0.2	-0.2	-0.2
Cs (ppm)	ICP-MS	0.5	0.7		0.2	2.1	0.7	0.3	0.2	0.4	0.3	0.4
Ba (ppm)	ICP-MS	946	50		40	168	371	249	227	288	147	193
La (ppm)	ICP-MS	66.2	23.4		29.7	19.5	28.8	24.4	23.7	25.9	24.1	33.0
Ce (ppm)	ICP-MS	123	51.7		60.4	42.8	60.6	56.7	52.9	56.7	57.4	75.7
Pr (ppm)	ICP-MS	12.3	6.23		7.11	5.50	7.26	7.13	6.63	6.72	7.01	9.09
Nd (ppm)	ICP-MS	42.8	26.8		28.0	22.4	28.7	28.3	26.7	28.0	28.0	38.6
Sm (ppm)	ICP-MS	7.34	7.29		5.74	4.79	5.71	6.05	5.74	6.38	5.88	8.36
Eu (ppm)	ICP-MS	2.61	2.83		2.04	1.69	1.90	2.08	2.01	2.10	1.53	3.00
Gd (ppm)	ICP-MS	6.02	7.53		5.61	4.72	5.50	5.56	5.39	6.15	5.54	8.44
Tb (ppm)	ICP-MS	0.98	1.12		0.85	0.71	0.78	0.86	0.82	1.00	0.92	1.32
Dy (ppm)	ICP-MS	5.44	5.43		4.73	3.91	4.37	4.71	4.68	5.51	5.19	6.88
Ho (ppm)	ICP-MS	0.99	0.89		0.90	0.72	0.84	0.89	0.89	1.02	1.02	1.25
Er (ppm)	ICP-MS	2.79	2.30		2.50	2.07	2.42	2.33	2.45	2.84	2.94	3.34
Tm (ppm)	ICP-MS	0.391	0.294		0.349	0.280	0.333	0.328	0.336	0.383	0.418	0.453
Yb (ppm)	ICP-MS	2.48	1.72		2.11	1.59	1.96	2.00	1.97	2.23	2.56	2.69
Lu (ppm)	ICP-MS	0.360	0.233		0.299	0.223	0.287	0.294	0.270	0.314	0.367	0.358
Hf (ppm)	ICP-MS	4.4	4.4		3.3	2.6	2.8	4.5	4.3	4.7	6.2	5.2
Ta (ppm)	ICP-MS	5.23	2.22		2.47	1.51	2.18	1.96	1.91	1.87	2.57	2.46
W (ppm)	ICP-MS	0.6	4.2		-0.5	-0.5	-0.5	-0.5	1.2	-0.5	1.1	1.1
Tl (ppm)	ICP-MS	0.30	0.09		-0.05	0.20	0.06	0.09	0.09	0.18	0.10	0.10
Pb (ppm)	ICP-MS	9	-5		6	7	-5	-5	-5	-5	-5	6
Bi (ppm)	ICP-MS	1.5	0.6		-0.1	-0.1	-0.1	-0.1	-0.1	0.6	0.5	1.0
Th (ppm)	ICP-MS	7.67	2.56		4.79	2.52	3.47	3.36	2.95	2.52	4.44	2.89
U (ppm)	ICP-MS	2.50	0.74		1.14	0.48	0.67	0.80	0.72	0.62	0.80	0.72

* Total iron reported as Fe_2O_3 • Samples were analyzed at Activation Laboratories Ltd., Ancaster, Ontario Canada • Samples were crushed and then pulverized in a ceramic mill. • Major and minor elements were determined by XRF on a fusion sample. • Ba, Sr, Y, Sc, Zr, Be, V were analyzed using INNA. • Trace elements and REE were analyzed by ICP-MS at research detection limits on a fusion sample. • Analysis below detection limit shown with detection limit as negative number. • NA = not analyzed

Table III-4. *Lithogeochemistry of various samples.*

Sample		01LP-093	01LP-016-2
Station		**01LP093**	**01LP016**
rock		**dyke**	**flow**
Unit		Osu	Pb
UTM E		345050	336631
UTM N		6704252	6706945
UTM Zone		10	10
Datum		NAD83	NAD83
SiO_2 (%)	XRF	49.38	48.95
Al_2O_3 (%)	XRF	16.19	16.77
Fe_2O_3* (%)	XRF	7.86	9.13
MnO (%)	XRF	0.162	0.152
MgO (%)	XRF	2.48	3.81
CaO (%)	XRF	5.13	8.14
Na_2O (%)	XRF	3.97	3.43
K_2O (%)	XRF	4.49	2.36
TiO_2 (%)	XRF	1.524	1.612
P_2O_5 (%)	XRF	0.94	0.92
L.O.I. (%)		7.89	3.45
Total		**100.02**	**98.72**
V (ppm)	ICP-MS	128	214
Cr (ppm)	ICP-MS	-20	43
Co (ppm)	ICP-MS	17	24
Ni (ppm)	ICP-MS	-20	-20
Cu (ppm)	ICP-MS	11	16
Zn (ppm)	ICP-MS	91	101
Ga (ppm)	ICP-MS	22	22
Ge (ppm)	ICP-MS	1.3	1.4
As (ppm)	ICP-MS	-5	-5
Rb (ppm)	ICP-MS	204	66
Sr (ppm)	ICP-MS	447	1210
Y (ppm)	ICP-MS	35.4	34.8
Zr (ppm)	ICP-MS	363	284
Nb (ppm)	ICP-MS	181	69.0
Mo (ppm)	ICP-MS	-2	5
Ag (ppm)	ICP-MS	-0.5	-0.5
In (ppm)	ICP-MS	-0.1	-0.1
Sn (ppm)	ICP-MS	3	2
Sb (ppm)	ICP-MS	-0.2	-0.2
Cs (ppm)	ICP-MS	3.0	1.1
Ba (ppm)	ICP-MS	1240	1560
La (ppm)	ICP-MS	160.0	134.0
Ce (ppm)	ICP-MS	265	229
Pr (ppm)	ICP-MS	24.7	21.8
Nd (ppm)	ICP-MS	91.9	82.2
Sm (pm)	ICP-MS	12.70	12.0
Eu (ppm)	ICP-MS	3.90	3.57
Gd (ppm)	ICP-MS	9.14	9.18
Tb (ppm)	ICP-MS	1.33	1.31
Dy (ppm)	ICP-MS	6.90	6.92
Ho (ppm)	ICP-MS	1.27	1.28
Er (ppm)	ICP-MS	3.65	3.59
Tm (ppm)	ICP-MS	0.510	0.484
Yb (ppm)	ICP-MS	3.57	3.21
Lu (ppm)	ICP-MS	0.514	0.453
Hf (ppm)	ICP-MS	8.5	7.2
Ta (ppm)	ICP-MS	11.4	3.6
W (ppm)	ICP-MS	2.8	1.1
Tl (ppm)	ICP-MS	1.02	0.19
Pb (ppm)	ICP-MS	15	8
Bi (ppm)	ICP-MS	0.3	-0.1
Th (ppm)	ICP-MS	34.9	18.1
U (ppm)	ICP-MS	7.59	2.94

* Total iron reported as Fe_2O_3. • Samples were analyzed at Activation Laboratories Ltd., Ancaster, Ontario Canada. • Samples were crushed and then pulverized in a ceramic mill. • Major and minor elements were determined by XRF on a fusion sample. • Trace elements and REE were analyzed by ICP-MS at research detection limits on a fusion sample. • Analysis below detection limit shown with detection limit as negative number. • NA = not analyzed

Table III-5. *Lithogeochemistry of Pool Creek syenite and dykes, Eocene biotite syenite and Eocene igneous breccia.*

Sample		LP00-35	01AKM001	01AKM001%	02-3001	02-3006%
Station		**00LP035**	**01AKM001**	**01AKM001**	**02LP109**	**02LP109**
Rock		**syenite**	**syenite**	**syenite**	**syenite**	**syenite**
UTM E		**344067**	**343478**	**343478**	**344233**	**344233**
UTM N		**6699844**	**6701813**	**6701813**	**6697803**	**6697803**
UTM Zone		**10**	**10**	**10**	**10**	**10**
Datum		**NAD83**	**NAD83**	**NAD83**	**NAD83**	**NAD83**
SiO_2 (%)	XRF	52.63	54.49	54.65	56.06	56.67
Al_2O_3 (%)	XRF	22.21	20.00	20.08	21.41	20.84
Fe_2O_3* (%)	XRF	4.46	6.56	6.76	4.43	4.51
MnO (%)	XRF	0.179	0.182	0.181	0.082	0.087
MgO (%)	XRF	0.46	0.41	0.41	3.30	3.12
CaO (%)	XRF	2.96	1.34	1.34	0.21	0.20
Na_2O (%)	XRF	2.99	3.73	3.66	3.33	3.48
K_2O (%)	XRF	8.92	8.11	8.29	7.54	7.56
TiO_2 (%)	XRF	0.668	1.057	1.119	0.628	0.714
P_2O_5 (%)	XRF	0.05	0.04	0.05	0.10	0.10
L.O.I. (%)		4.61	2.97	2.93	2.85	2.78
Total		**100.14**	**98.91**	**99.48**	**99.94**	**100.05**
V (ppm)	ICP-MS	26	6	7	6	6
Cr (ppm)	ICP-MS	-20	-20	-20	-20	-20
Co (ppm)	ICP-MS	2	-1	-1	3	3
Ni (ppm)	ICP-MS	-20	-20	-20	38	25
Cu (ppm)	ICP-MS	-10	-10	-10	13	-10
Zn (ppm)	ICP-MS	66	81	87	61	68
Ga (ppm)	ICP-MS	29	30	31	32	31
Ge (ppm)	ICP-MS	1.1	1.1	1.2	1.3	1.4
As (ppm)	ICP-MS	-5	-5	-5	-5	-5
Rb (ppm)	ICP-MS	218	250	259	232	233
Sr (ppm)	ICP-MS	540	315	318	636	685
Y (ppm)	ICP-MS	50.5	46.9	47.3	77.4	67.1
Zr (ppm)	ICP-MS	441	520	534	1210	949
Nb (ppm)	ICP-MS	189	228	244	421	398
Mo (ppm)	ICP-MS	3	2	3	-2	-2
Ag (ppm)	ICP-MS	-0.5	-0.5	-0.5	-0.5	-0.5
In (ppm)	ICP-MS	-0.1	-0.1	-0.1	-0.1	-0.1
Sn (ppm)	ICP-MS	4	6	6	5	6
Sb (ppm)	ICP-MS	0.6	-0.2	-0.2	0.4	0.4
Cs (ppm)	ICP-MS	2.4	1.3	1.4	3.6	3.4
Ba (ppm)	ICP-MS	452	319	320	826	973
La (ppm)	ICP-MS	158	140	146	301	203
Ce (ppm)	ICP-MS	262	243	256	549	421
Pr (ppm)	ICP-MS	22.3	21.6	22.9	41.9	31.4
Nd (ppm)	ICP-MS	68.3	69.8	75.3	121	93.3
Sm (pm)	ICP-MS	9.51	9.80	10.4	17.7	14.2
Eu (ppm)	ICP-MS	2.74	3.18	3.44	4.63	3.75
Gd (ppm)	ICP-MS	8.19	7.76	8.23	12.6	9.97
Tb (ppm)	ICP-MS	1.22	1.41	1.44	2.15	1.77
Dy (ppm)	ICP-MS	6.88	8.25	8.40	12.5	10.5
Ho (ppm)	ICP-MS	1.32	1.63	1.66	2.51	2.13
Er (ppm)	ICP-MS	4.04	4.70	4.78	7.16	6.35
Tm (ppm)	ICP-MS	0.585	0.676	0.658	1.09	1.03
Yb (ppm)	ICP-MS	3.60	4.10	4.14	6.31	6.32
Lu (ppm)	ICP-MS	0.493	0.579	0.585	0.829	0.864
Hf (ppm)	ICP-MS	8.2	11.6	12.1	21.6	15.3
Ta (ppm)	ICP-MS	10.4	15.4	16.0	25.3	24.5
W (ppm)	ICP-MS	3.1	2.7	2.8	3.2	2.7
Tl (ppm)	ICP-MS	0.39	0.38	0.45	0.32	0.36
Pb (ppm)	ICP-MS	15	10	15	8	5
Bi (ppm)	ICP-MS	0.9	0.2	-0.1	0.2	0.2
Th (ppm)	ICP-MS	39.5	27.3	29.7	54.5	47.9
U (ppm)	ICP-MS	3.89	2.05	2.06	9.03	7.56

* Total iron reported as Fe_2O_3 • Samples were analyzed at Activation Laboratories Ltd., Ancaster, Ontario Canada • Samples were crushed and then pulverized in a ceramic mill. • Major and minor elements were determined by XRF on a fusion sample. • Trace elements and REE were analyzed by ICP-MS at research detection limits on a fusion sample. • Analysis below detection limit shown with detection limit as negative number. • NA = not analyzed

% replicate analysis

Table III-5. *(continued) Lithogeochemistry of Pool Creek syenite and dykes, Eocene biotite syenite and Eocene igneous breccia.*

Sample		02-3002	LP00-37	02-3004	02-3008	02-3007	02-3005	01LP033	01LP022	02-3003
Station		**02LP122**	**00LP037**	**02LP122**	**02LP112**	**02LP112**	**02LP116**	**01LP033**	**01LP022**	**02LP124**
Rock		**syenite**	**mafic dyke**	**mafic dyke**	**mafic dyke**	**banded dyke**	**banded dyke**	**biotite syenite**	**igneous breccia**	**igneous breccia**
UTM E		**343801**	**343645**	**343801**	**344795**	**344795**	**344118**	**339341**	**342951**	**346409**
UTM N		**6698828**	**6698568**	**6698828**	**6697141**	**6697141**	**6697201**	**6700936**	**6702740**	**6695777**
UTM Zone		**10**	**10**	**10**	**10**	**10**	**10**	**10**	**10**	**10**
Datum		**NAD83**	**NAD83**	**NAD83**	**NAD83**	**NAD83**	**NAD83**	**NAD83**	**NAD83**	**NAD83**
SiO_2 (%)	XRF	55.74	53.49	56.69	40.08	67.64	60.90	58.38	74.71	77.78
Al_2O_3 (%)	XRF	20.61	18.13	20.47	12.07	16.29	12.25	17.88	12.65	11.73
Fe_2O_3* (%)	XRF	4.51	7.45	4.58	10.96	3.81	13.44	4.56	2.57	2.73
MnO (%)	XRF	0.097	0.205	0.131	0.221	0.036	0.148	0.178	0.008	0.021
MgO (%)	XRF	4.02	2.38	0.88	10.72	1.49	0.36	1.09	0.51	1.05
CaO (%)	XRF	0.14	2.06	2.37	12.37	0.61	0.43	2.51	0.09	0.14
Na_2O (%)	XRF	1.90	1.51	4.45	0.42	7.69	8.94	7.18	0.46	3.28
K_2O (%)	XRF	9.24	9.21	6.59	3.83	1.04	2.75	3.46	7.31	1.72
TiO_2 (%)	XRF	0.630	0.745	0.876	2.637	0.125	0.338	1.040	0.399	0.21
P_2O_5 (%)	XRF	0.05	0.03	0.06	0.63	0.02	0.02	0.34	0.05	0.04
L.O.I. (%)		3.49	5.24	3.19	5.91	1.15	0.48	2.08	1.53	1.47
Total		**100.43**	**100.44**	**100.29**	**99.85**	**99.90**	**100.06**	**98.70**	**100.29**	**100.16**
V (ppm)	ICP-MS	-5	20	13	232	13	8	38	21	9
Cr (ppm)	ICP-MS	-20	-20	-20	603	-20	-20	-20	-20	-20
Co (ppm)	ICP-MS	3	4	2	44	2	2	2	1	2
Ni (ppm)	ICP-MS	-20	91	-20	195	-20	-20	-20	-20	-20
Cu (ppm)	ICP-MS	-10	-10	-10	64	-10	-10	-10	-10	-10
Zn (ppm)	ICP-MS	89	76	46	114	38	56	84	-30	-30
Ga (ppm)	ICP-MS	28	33	29	19	65	39	21	37	28
Ge (ppm)	ICP-MS	1.3	1.2	1.0	1.4	0.9	1.8	1.3	1.7	1.1
As (ppm)	ICP-MS	-5	-5	-5	24	-5	7	-5	-5	-5
Rb (ppm)	ICP-MS	270	207	216	136	68	124	191	167	102
Sr (ppm)	ICP-MS	469	819	886	650	21	79	915	73	92
Y (ppm)	ICP-MS	24.1	51.8	11.0	35.6	9.6	9.5	38.6	76.8	68.7
Zr (ppm)	ICP-MS	426	817	296	260	79	1180	350	691	447
Nb (ppm)	ICP-MS	230	240	145	119	266	844	164	174	148
Mo (ppm)	ICP-MS	-2	-2	-2	10	-2	9	3	-2	-2
Ag (ppm)	ICP-MS	-0.5	-0.5	-0.5	-0.5	-0.5	-0.5	-0.5	-0.5	-0.5
In (ppm)	ICP-MS	-0.1	0.1	-0.1	-0.1	-0.1	0.1	-0.1	-0.1	-0.1
Sn (ppm)	ICP-MS	8	5	2	2	3	39	3	9	12
Sb (ppm)	ICP-MS	-0.2	0.7	-0.2	6.5	2.9	1.2	0.7	0.5	0.2
Cs (ppm)	ICP-MS	2.7	6.4	1.3	4.0	1.7	0.8	28.4	4.3	1.4
Ba (ppm)	ICP-MS	179	360	282	1970	64	211	2190	735	122
La (ppm)	ICP-MS	57.3	120	32.2	115	27.3	54.8	202	153	76.7
Ce (ppm)	ICP-MS	112	201	71.1	250	40.8	91.8	323	302	163.0
Pr (ppm)	ICP-MS	11.3	16.3	7.53	23.6	3.49	5.65	29.2	31.1	15.9
Nd (ppm)	ICP-MS	35.3	48.2	24.1	86.5	10.0	13.7	99.6	122	53.0
Sm (pm)	ICP-MS	5.83	7.27	3.76	14.8	1.50	1.54	13.2	21.8	11.1
Eu (ppm)	ICP-MS	1.68	2.24	1.12	4.66	0.45	0.398	4.48	1.25	0.637
Gd (ppm)	ICP-MS	4.83	7.13	3.01	11.3	1.40	0.94	8.54	16.8	10.6
Tb (ppm)	ICP-MS	0.73	1.19	0.41	1.44	0.22	0.20	1.31	2.59	1.82
Dy (ppm)	ICP-MS	4.31	7.51	2.25	7.32	1.24	1.30	7.18	14.7	11.10
Ho (ppm)	ICP-MS	0.88	1.50	0.42	1.28	0.25	0.29	1.34	2.89	2.34
Er (ppm)	ICP-MS	2.69	4.76	1.12	3.35	0.66	0.95	3.87	8.30	6.82
Tm (ppm)	ICP-MS	0.432	0.707	0.158	0.375	0.092	0.176	0.522	1.24	1.15
Yb (ppm)	ICP-MS	2.77	4.47	1.09	2.45	0.58	1.24	3.50	7.97	6.32
Lu (ppm)	ICP-MS	0.405	0.619	0.173	0.323	0.090	0.208	0.515	1.12	0.847
Hf (ppm)	ICP-MS	9.3	14.9	5.4	5.6	1.8	28.8	7.9	21.5	14.0
Ta (ppm)	ICP-MS	16.3	10.2	9.72	6.79	19.1	38.4	8.55	12.7	12.5
W (ppm)	ICP-MS	1.0	1.7	0.7	1.8	2.1	3.3	7.3	3.2	1.8
Tl (ppm)	ICP-MS	0.33	0.28	0.42	0.50	0.28	0.20	2.01	0.70	0.29
Pb (ppm)	ICP-MS	-5	19	11	8	6	20	15	10	5
Bi (ppm)	ICP-MS	0.2	0.9	0.2	0.2	0.5	1.3	-0.1	0.2	0.6
Th (ppm)	ICP-MS	11.9	28.5	4.30	20.7	3.46	11.3	39.4	37.8	48.4
U (ppm)	ICP-MS	3.15	5.74	0.98	2.75	9.83	23.6	5.86	7.28	7.73

* Total iron reported as Fe_2O_3 • Samples were analyzed at Activation Laboratories Ltd., Ancaster, Ontario Canada • Samples were crushed and then pulverized in a ceramic mill. • Major and minor elements were determined by XRF on a fusion sample. • Trace elements and REE were analyzed by ICP-MS at research detection limits on a fusion sample. • Analysis below detection limit shown with detection limit as negative number. • NA = not analyzed

Table III-6. *ICP analyses – Ting suite, igneous breccia and altered dykes in Toobally Formation.*

Sample		01LP022	02-3003	03LP010	03LP017	03LP023
Station		01LP022	02LP124	03LP010	03LP017	03LP023
Rock		igneous bxa	igneous bxa	altered dyke	altered dyke	altered volcani-clastic
Unit		Eib	Eib	PT	PT	€OCv2
UTM E		342,951	346,409	649320	650,123	647,538
UTM N		6,702,740	6,695,777	6694834	6,698,395	6,697,584
UTM Zone		10	10	9	9	9
Datum		NAD83	NAD83	NAD83	NAD83	NAD83
Mo (ppm)	ICP-MS	0.8	0.6	1.0	1.3	0.6
Cu (ppm)	ICP-MS	377.7	9.7	83.9	2412.0	73.0
Pb (ppm)	ICP-MS	5.8	6.2	1.1	2.9	4.8
Zn (ppm)	ICP-MS	4	33	77	77	35
Ag (ppm)	ICP-MS	0.2	-0.1	-0.1	0.4	-0.1
Ni (ppm)	ICP-MS	2.5	2.2	199.3	130.1	5.6
Co (ppm)	ICP-MS	0.7	1.7	57.8	71.3	19.6
Mn (ppm)	ICP-MS	23	158	940	235	2146
Fe (%)	ICP-MS	2.27	1.6	6.73	6.37	9.92
As (ppm)	ICP-MS	2.3	1.8	23.6	21.3	3.1
U (ppm)	ICP-MS	0.6	1.7	0.1	0.2	0.1
Au (ppb)	ICP-MS	0.7	0.8	-0.5	-0.5	-0.5
Th (ppm)	ICP-MS	8.9	22.2	0.6	1.4	1.0
Sr (ppm)	ICP-MS	9	4	421	37	63
Cd (ppm)	ICP-MS	-0.1	-0.1	-0.1	0.1	-0.1
Sb (ppm)	ICP-MS	0.4	0.1	-0.1	0.1	0.5
Bi (ppm)	ICP-MS	1.1	0.4	-0.1	0.1	-0.1
V (ppm)	ICP-MS	3	2	163	89	54
Ca (%)	ICP-MS	0.02	0.03	7.09	0.84	5.47
P (%)	ICP-MS	0.009	0.009	0.082	0.143	0.101
La (ppm)	ICP-MS	82	70	7	12	6
Cr (ppm)	ICP-MS	7.3	3.9	374.4	90.1	2.2
Mg (%)	ICP-MS	0.03	0.43	1.65	0.64	2.58
Ba (ppm)	ICP-MS	110	17	44	56	14
Ti (%)	ICP-MS	0.011	0.003	0.003	0.002	0.001
B (ppm)	ICP-MS	4	1	4	7	3
Al (%)	ICP-MS	0.37	0.79	2.08	0.75	0.72
Na (%)	ICP-MS	0.004	0.022	0.019	0.008	0.009
K (%)	ICP-MS	0.26	0.10	0.13	0.20	0.11
W (ppm)	ICP-MS	0.4	0.2	-0.1	-0.1	-0.1
Hg (ppm)	ICP-MS	-0.01	-0.01	-0.01	0.02	-0.01
Sc (ppm)	ICP-MS	0.2	0.3	14.8	7.3	10.9
Tl (ppm)	ICP-MS	-0.1	-0.1	-0.1	-0.1	0.1
S (%)	ICP-MS	0.08	-0.05	0.11	0.61	0.42
Ga (ppm)	ICP-MS	2	7	8	3	3
Se (ppm)	ICP-MS	-0.5	-0.5	-0.5	-0.5	4.7

Samples analyzed by Acme Analytical Laboratories Ltd. • 15.0 gm sample leached with 90 ml 2-2-2 HCl-HNO3-H20 at 95 deg. C for one hour, diluted to 300 ml, analysed by ICP-MS. • Some minerals may be partially attacked. Refractory and graphitic samples can limit Au solubility. • Analysis below detection limit shown with detection limit as negative number.

APPENDIX IV. FOSSIL IDENTIFICATION

Table IV-1. *Fossil data for stratigraphic units – Units* ***Ps*** *and* ***Pa****.*

GSC No.	Station	Easting	Northing	UTM Zone	Unit	Material	CAI	Comments	Max Age-Period	Max Age-Details	Min Age-Period	Min Age-Details	Reference
C-417717	01LP009	344331	6697266	10	Ps	conodont			barren - age Indeterminate		barren - age Indeterminate		Nowlan (2004)
C-405705	00TLA021	344943	6695406	10	Ps	palynology		abundant present day contamination					Utting (2000)
C-405706	00TLA023	344607	6695344	10	Ps	palynology		rare black fragments and some modern contamination					Utting (2000)
C-417632	00LP017	345463	6695232	10	Pa	conodont	3,4	contaminated? with Sunblood	Middle Ordovician	late	Late Ordovician		Pyle (2001)
	00LP004	345258	6695468	10	Pa	conodont	2	float - Sunblood	Early Ordovician		Middle Ordovician	early	Pyle (2001)
C-417059	01MWB1-013	345467	6695243	10	Pa	conodont			barren - age Indeterminate		barren - age Indeterminate		McCracken (2003c)
C-417716	01LP002	345967	6695490	10	Pa	conodont			barren - age Indeterminate		barren - age Indeterminate		Nowlan (2004)

References
MacNaughton (2002b), 001-RBM-2002
McCracken (2003a), 6-ADM-2003
McCracken (2003b), 7-ADM-2003
McCracken (2003c), personal communication
Norford (2001), S-3-BSN-2001
Norford (2002), S-1-BSN-2002
Nowlan (2001), 010-GSN-2001
Nowlan (2004), 002-GSN-2004
Orchard (2006), personal communication
Pyle (2001), LJP01-01
Pyle (2004), LJP04-02
Utting (2000), 8-JU-00
Utting (2006), 04-JU-2006

All coordinates NAD83 UTM - zone 10V or 9V

Table IV-2. *Fossil data for stratigraphic units – Toobally Formation.*

GSC No.	Station	Easting	Northing	UTM Zone	Unit	Material	CAI	Comments	Max Age-Period	Max Age-Details	Min Age-Period	Min Age-Details	Reference
C-404752	03LP014	649705	6698302	9	PT	conodont		large dolostone clast	barren - age indeterminate		barren - age indeterminate		Pyle (2004)
C-417153	03LP006	649756	6696339	9	PT	conodont		carbonate clasts	barren - age indeterminate		barren - age indeterminate		Pyle (2004)

References
MacNaughton (2002b), 001-RBM-2002
McCracken (2003a), 6-ADM-2003
McCracken (2003b), 7-ADM-2003
McCracken (2003c), personal communication
Norford (2001), S-3-BSN-2001
Norford (2002), S-1-BSN-2002
Nowlan (2001), 010-GSN-2001
Nowlan (2004), 002-GSN-2004
Orchard (2006), personal communication
Pyle (2001), LJP01-01
Pyle (2004), LJP04-02
Utting (2000), 8-JU-00
Utting (2004), personal communication

All coordinates NAD83 UTM - zone 10V or 9V

Table IV-3. *Fossil data for stratigraphic units – Crow Formation.*

GSC No.	Station	Easting	Northing	UTM Zone	Unit	Material	CAI	Comments	Max Age-Period	Max Age-Details	Min Age-Period	Min Age-Details	Reference
C-417068	01MWB4-003	348796	6689770	10	€Oc	conodont	5		Middle Ordovician	early Whiterockian	Middle Ordovician	early Whiterockian	McCracken (2003b)
C-417718	01LP014	338639	6692236	10	€Oc	conodont	4		Early Ordovician	Ibexian (late Blackhillsian)	Middle Ordovician	early Whiterockian (Rangerian)	Nowlan (2004)
C-417157	04LP037	642782	6698746	9	€Oc	conodont	3		Early Ordovician	early Tremadocian	Early Ordovician	early Tremadocian	Pyle (2004)
C-417705	01TLA016	335684	6689500	10	€Oc	conodont			barren - age indeterminate		barren - age indeterminate		Nowlan (2004)
C-417714	01TLA152	335988	6684012	10	€Oc	conodont			barren - age indeterminate		barren - age indeterminate		Nowlan (2004)
C-417155	04LP007	652482	6690149	9	€Oc	conodont			barren - age indeterminate		barren - age indeterminate		Pyle (2004)
	05LP039	645987	6698397	9	€Oc	conodont			barren - age indeterminate		barren - age indeterminate		Orchard (2006)

References
MacNaughton (2002b),001-RBM-2002
McCracken (2003a),6-ADM-2003
McCracken (2003b),7-ADM-2003
McCracken (2003c),personal communication
Norford (2001),S-3-BSN-2001
Norford (2002),S-1-BSN-2002
Nowlan (2001),010-GSN-2001
Nowlan (2004),002-GSN-2004
Orchard (2006),personal communication
Pyle (2001),LJP01-01
Pyle (2004),LJP04-02
Utting (2000), 8-JU-00
Utting (2006), 04-JU-2006

All coordinates NAD83 UTM - zone 10V or 9V

Table IV-4. *Fossil data for stratigraphic units – Sunblood Formation.*

GSC No.	Station	Easting	Northing	UTM Zone	Unit	Material	CAI	Comments	Max Age-Period	Max Age-Details	Min Age-Period	Min Age-Details	Reference
C-417719	01LP029	336403	6694181	10	OSu	conodont	4?	bottom of unit	Early Ordovician	late	Middle Ordovician	early	Nowlan (2004)
C-417165	04LP063	638946	6708713	9	OSu	conodont	3,4	bottom of unit	Early Ordovician	middle Tremadocian	Early Ordovician	middle Tremadocian	Pyle (2004)
C-417720	01LP055	343123	6706970	10	OSu	conodont	4.5		Middle Ordovician	early Whiterockian	Middle Ordovician	Early Whiterockian	Nowlan (2004)
C-417721	01LP057	343187	6707354	10	OSu	conodont	4.5		Middle Ordovician	middle Whiterockian	Middle Ordovician	Middle Whiterockian	Nowlan (2004)
C-417724	01LP071	344755	6704428	10	OSu	conodont	4.5+		Middle Ordovician	early Whiterockian	Middle Ordovician	Middle Whiterockian	Nowlan (2004)
C-417727	01LP096	345280	6703797	10	OSu	conodont	4.5		Middle Ordovician	early Whiterockian (Rangerian)	Middle Ordovician	early Whiterockian (Kanoshian)	Nowlan (2004)
C-417159	04LP042	639460	6696862	9	OSu	conodont	3		Middle Ordovician	Darriwilian	Middle Ordovician	Darriwilian	Pyle (2004)
C-417164	04LP056	638636	6705814	9	OSu	conodont	3,4	float	Early Ordovician	latest Tremadocian	Early Ordovician	latest Tremadocian	Pyle (2004)
C-417166	04LP064	638374	6702592	9	OSu	conodont	3		Early Ordovician	Arenigian	Middle Ordovician	Darriwilian	Pyle (2004)
C-417167	04LP068	642702	6689561	9	OSu	conodont	3		Early Ordovician	middle Arenigian	Middle Ordovician	middle Arenigian	Pyle (2004)
C-417163	04LP055 west	664180	6710421	9	OSu	conodont	3	top of unit	Late Ordovician	early Caradocian	Late Ordovician	early Caradocian	Pyle (2004)
C-417706	01TLA018	341035	6690031	10	OSu	conodont	5	top of unit	Middle Ordovician	early Whiterockian (Kanoshian)	Middle Ordovician	early Whiterockian (Kanoshian)	Nowlan (2004)
C-417707	01TLA020	341137	6690084	10	OSu	conodont	5	top of unit	Middle Ordovician	early Whiterockian	Middle Ordovician	early Whiterockian	Nowlan (2004)
C-417728	01LP103	350031	6698736	10	OSu	conodont	4.5	top of unit	Middle Ordovician	Rocklandian	Late Ordovician		Nowlan (2004)
C-417638	00LP051	337822	6708581	10	OSu	conodont	3,4	top of unit	Middle Ordovician	late	Late Ordovician		Pyle (2001)
C-307428	05LP015	661711	6709898	9	OSu	conodont			Early Ordovician		early Whiterockian		Nowlan (2008)
C-417715	00LP026	343735	6698076	10	OSu	conodont		float on syenite	barren - age Indeterminate		barren - age Indeterminate		
C-417723	01LP069	344275	6704395	10	OSu	conodont		barren	barren - age Indeterminate		barren - age Indeterminate		Nowlan (2004)
C-417158	04LP039	639866	6698106	9	OSu	conodont		barren	barren - age Indeterminate		barren - age Indeterminate		Pyle (2004)
C-417160	04LP047	640149	6698177	9	OSu	conodont		barren	barren - age Indeterminate		barren - age Indeterminate		Pyle (2004)
C-417161	04LP048	640089	6698913	9	OSu	conodont		barren	barren - age Indeterminate		barren - age Indeterminate		Pyle (2004)
	05LP027	654826	6694755	9	OSu	conodont		barren	barren - age Indeterminate		barren - age Indeterminate		Orchard (2006)

References
MacNaughton (2002b), 001-RBM-2002
McCracken (2003a), 6-ADM-2003
McCracken (2003b), 7-ADM-2003
McCracken (2003c), personal communication
Norford (2001), S-3-BSN-2001
Norford (2002), S-1-BSN-2002
Nowlan (2001), 010-GSN-2001
Nowlan (2004), 002-GSN-2004
Nowlan (2008), 003-GSN-2008
Orchard (2006), personal communication
Pyle (2001), LJP01-01
Pyle (2004), LJP04-02
Utting (2000), 8-JU-00
Utting (2006), 04-JU-2006

All coordinates NAD83 UTM - zone 10V or 9V

Table IV-5. *Fossil data for stratigraphic units – Unit* ***OSs****.*

GSC No.	Station	Easting	Northing	UTM Zone	Unit	Material	CAI	Comments	Max Age-Period	Max Age-Details	Min Age-Period	Min Age-Details	Reference
C-417690	00LP038	337910	6709717	10	OSs	trace fossil			Cambrian		Present		MacNaughton (2002b)
C-405697	00LP038	337910	6709717	10	OSs	palynology		small amount of organic matter, some unidentifiable black fragments					Utting (2000)
C-405700	00LP048	338109	6708993	10	OSs	palynology		rare black fragments					Utting (2000)
C-417163	04LP055 east	664180	6710421	9	OSs	conodont			barren - age indeterminate		barren - age indeterminate		Pyle (2004)

References
MacNaughton (2002b), 001-RBM-2002
McCracken (2003a), 6-ADM-2003
McCracken (2003b), 7-ADM-2003
McCracken (2003c), personal communication
Norford (2001), S-3-BSN-2001
Norford (2002), S-1-BSN-2002
Nowlan (2001), 010-GSN-2001
Nowlan (2004), 002-GSN-2004
Orchard (2006), personal communication
Pyle (2001), LJP01-01
Pyle (2004), LJP04-02
Utting (2000), 8-JU-00
Utting (2006), 04-JU-2006

All coordinates NAD83 UTM - zone 10V or 9V

Table IV-6. *Fossil data for stratigraphic units – Road River Group.*

GSC No.	Station	Easting	Northing	UTM Zone	Unit	Material	CAI	Comments	Max Age-Period	Max Age-Details	Min Age-Period	Min Age-Details	Reference
C-417637	00LP047	338210	6708507	10	SDRR-a	graptolite		bottom of unit	Early Silurian	Wenlock	Early Silurian	Wenlock	Norford (2001)
C-417691	01LP063	345910	6704365	10	SDRR-a	graptolite			Early Silurian	Late Telychian	Early Silurian	Late Telychian	Norford (2002)
C-417701	TOA01-005	335252	6701015	10	SDRR-a	graptolite			Early Silurian		Early Devonian		Norford (2002)
C-417642	00LP063	342746	6706610	10	SDRR-a	conodont	3,4		Late Ordovician		Early Devonian		Pyle (2001)
C-417722	01LP063	345910	6704365	10	SDRR-a	conodont	4.5		Early Silurian	Llandovery	Early Silurian	Llandovery	Nowlan (2004)
C-417736	TOA01-005	335252	6701015	10	SDRR-a	conodont	4.5		Latest Silurian	highest Pridolian	Earliest Devonian	Lochkovian	Nowlan (2004)
C-405699	00LP047	338210	6708507	10	SDRR-a	palynology		black and gray fragments; TAI 5(?)					Utting (2000)
C-405701	00LP055	342437	6706992	10	SDRR-a	palynology		small gray and black fragments; TAI 5?					Utting (2000)
C-405703	00LP065	342318	6706796	10	SDRR-a	palynology							Utting (2000)
C-405704	00LP079	335479	6710094	10	SDRR-a	palynology		abundant small, medium to large gray and black fragments; TAI 5?					Utting (2000)
C-417635	00LP044	339061	6709055	10	SDRR-b	Protospongia			Silurian (probably)		Silurian (probably)		Norford (2001)
C-417636	00LP045	339351	6709362	10	SDRR-b	Hexactractiella			Silurian (probably)		Silurian (probably)		Norford (2001)
C-405698	00LP045	339351	6709362	10	SDRR-b	palynology		unidentifiable black fragments					Utting (2000)

References
MacNaughton (2002b), 001-RBM-2002
McCracken (2003a), 6-ADM-2003
McCracken (2003b), 7-ADM-2003
McCracken (2003c), personal communication
Norford (2001), S-3-BSN-2001
Norford (2002), S-1-BSN-2002
Nowlan (2001), 010-GSN-2001
Nowlan (2004), 002-GSN-2004
Nowland (2008), 003-GSN-2008
Orchard (2006), personal communication
Pyle (2001), LJP01-01
Pyle (2004), LJP04-02
Utting (2000), 8-JU-00
Utting (2006), 04-JU-2006

All coordinates NAD83 UTM - zone 10V or 9V

Table IV-7. *Fossil data for stratigraphic units – Nonda Formation.*

GSC No.	Station	Easting	Northing	UTM Zone	Unit	Material	CAI	Comments	Max Age-Period	Max Age-Details	Min Age-Period	Min Age-Details	Reference
C-417708	01TLA042	350194	6686778	10	SN	conodont	4.5		Middle Ordovician		Middle Devonian		Nowlan (2004)

References
MacNaughton (2002b), 001-RBM-2002
McCracken (2003a), 6-ADM-2003
McCracken (2003b), 7-ADM-2003
McCracken (2003c), personal communication
Norford (2001), S-3-BSN-2001
Norford (2002), S-1-BSN-2002
Nowlan (2001), 010-GSN-2001
Nowlan (2004), 002-GSN-2004
Orchard (2006), personal communication
Pyle (2001), LJP01-01
Pyle (2004), LJP04-02
Utting (2000), 8-JU-00
Utting (2006), 04-JU-2006

All coordinates NAD83 UTM - zone 10V or 9V

Table IV-8. *Fossil data for stratigraphic units – undivided Muncho-McConnell-Stone formations.*

GSC No.	Station	Easting	Northing	UTM Zone	Unit	Material	CAI	Comments	Max Age-Period	Max Age-Details	Min Age-Period	Min Age-Details	Reference
C-417732	01LP124	357426	6694747	10	SDMMS	conodont	5		Age indeterminate		Age indeterminate		McCracken (2003c)
C-417704	01TLA012	344365	6684876	10	SDMMS	conodont	5,6		Middle Ordovician		Middle Devonian		McCracken (2003c)
C-417731	01LP122	356940	6694905	10	SDMMS	conodont	5		Ordovician		Devonian		McCracken (2003c)
C-417712	01TLA121	351061	6700141	10	SDMMS	conodont			barren - age indeterminate		barren - age indeterminate		McCracken (2003c)
C-417729	01LP113	351685	6696083	10	SDMMS	conodont			barren - age indeterminate		barren - age indeterminate		McCracken (2003c)
C-417730	01LP116	353146	6693815	10	SDMMS	conodont			barren - age indeterminate		barren - age indeterminate		McCracken (2003c)
C-432052	02LP135	343981	6682898	10	SDMMS	conodont			barren - age indeterminate		barren - age indeterminate		McCracken (2003a)

References
MacNaughton (2002b), 001-RBM-2002
McCracken (2003a), 6-ADM-2003
McCracken (2003b), 7-ADM-2003
McCracken (2003c), personal communication
Norford (2001), S-3-BSN-2001
Norford (2002), S-1-BSN-2002
Nowlan (2001), 010-GSN-2001
Nowlan (2004), 002-GSN-2004
Orchard (2006), personal communication
Pyle (2001), LJP01-01
Pyle (2004), LJP04-02
Utting (2000), 8-JU-00
Utting (2006), 04-JU-2006

All coordinates NAD83 UTM - zone 10V or 9V

Table IV-9. *Fossil data for stratigraphic units – Dunedin Formation.*

GSC No.	Station	Easting	Northing	UTM Zone	Unit	Material	CAI	Comments	Max Age-Period	Max Age-Details	Min Age-Period	Min Age-Details	Reference
	8-5/C-97618	358244	6696728	10	DD	conodont	2		Early Devonian	Emsian	Middle Devonian	Givetian	Pyle (2001)
C-417702	01TLA008	344687	6684732	10	DD	conodont	4		Early Devonian		Early Devonian		McCracken (2003c)
C-417703	01TLA009	344670	6684636	10	DD	conodont	3		Early Devonian	Emsian	Early Devonian	Emsian	McCracken (2003c)
C-417710	01TLA094	346771	6703327	10	DD-d	conodont	5	bottom of unit	Devonian		Devonian		McCracken (2003c)
C-417725	01LP076	347329	6704064	10	DD-d	conodont	5	bottom of unit	Early Devonian	Lockhovian	Early Devonian		McCracken (2003c)
C-417735	01LP140	354839	6687850	10	DD-d	conodont	3		Middle Devonian	early	Middle Devonian	early	McCracken (2003c)
	00LP060	341317	6707209	10	DD-l	2-hole crinoid			Early Devonian	Emsian (dehiscens)	Middle Devonian	Eifelian (costatus)	
	00LP066	342200	6706892	10	DD-l	2-hole crinoid			Early Devonian	Emsian (dehiscens)	Middle Devonian	Eifelian (costatus)	
	00LP072	341595	6706760	10	DD-l	2-hole crinoid			Early Devonian	Emsian (dehiscens)	Middle Devonian	Eifelian (costatus)	
	00LP077	340892	6707251	10	DD-l	2-hole crinoid			Early Devonian	Emsian (dehiscens)	Middle Devonian	Eifelian (costatus)	
	01LP079	348691	6703429	10	DD-d	2-hole crinoid			Early Devonian	Emsian (dehiscens)	Middle Devonian	Eifelian (costatus)	
	01LP127	357674	6696679	10	DD-d	2-hole crinoid			Early Devonian	Emsian (dehiscens)	Middle Devonian	Eifelian (costatus)	
	01LP128	358244	6696728	10	DD-d	2-hole crinoid			Early Devonian	Emsian (dehiscens)	Middle Devonian	Eifelian (costatus)	
	01LP140	354839	6687850	10	DD-d	2-hole crinoid			Early Devonian	Emsian (dehiscens)	Middle Devonian	Eifelian (costatus)	
	01TLA045	340644	6704776	10	DD-l	2-hole crinoid			Early Devonian	Emsian (dehiscens)	Middle Devonian	Eifelian (costatus)	
	01TLA106	347404	6703925	10	DD-d	2-hole crinoid			Early Devonian	Emsian (dehiscens)	Middle Devonian	Eifelian (costatus)	
	01TLA129	352882	6699902	10	DD-d	2-hole crinoid			Early Devonian	Emsian (dehiscens)	Middle Devonian	Eifelian (costatus)	
	01TLA135	358064	6696633	10	DD-d	2-hole crinoid			Early Devonian	Emsian (dehiscens)	Middle Devonian	Eifelian (costatus)	
C-405702	00LP060	341317	6707209	10	DD-l	palynology		small gray and black fragments; TAI 5?					Utting (2000)
C-417709	01TLA084	346624	6704974	10	DD-d	conodont			barren - age indeterminate		barren - age indeterminate		McCracken (2003c)
C-417711	01TLA110	347155	6702920	10	DD-d	conodont			barren - age indeterminate		barren - age indeterminate		McCracken (2003c)

References
MacNaughton (2002b), 001-RBM-2002
McCracken (2003a), 6-ADM-2003
McCracken (2003b), 7-ADM-2003
McCracken (2003c), personal communication
Norford (2001), S-3-BSN-2001
Norford (2002), S-1-BSN-2002
Nowlan (2001), 010-GSN-2001
Nowlan (2004), 002-GSN-2004
Orchard (2006), personal communication
Pyle (2001), LJP01-01
Pyle (2004), LJP04-02
Utting (2000), 8-JU-00
Utting (2006), 04-JU-2006

All coordinates NAD83 UTM - zone 10V or 9V

Table IV-10. *Fossil data for stratigraphic units – Besa River Formation.*

GSC No.	Station	Easting	Northing	UTM Zone	Unit	Material	CAI	Comments	Max Age-Period	Max Age-Details	Min Age-Period	Min Age-Details	Reference
C-417726	01LP077	348022	6704037	10	DCBR	conodont	5		Devonian		Early Carboniferous		McCracken (2003c)
C-417734	01LP139	358235	6696962	10	DCBR	conodont	5		Devonian		Early Carboniferous		McCracken (2003c)
C-417640	00LP058	341804	6707415	10	DCBR	conodont			barren - age indeterminate		barren - age indeterminate		Nowlan (2001)

References
MacNaughton (2002b), 001-RBM-2002
McCracken (2003a), 6-ADM-2003
McCracken (2003b), 7-ADM-2003
McCracken (2003c), personal communication
Norford (2001), S-3-BSN-2001
Norford (2002), S-1-BSN-2002
Nowlan (2001), 010-GSN-2001
Nowlan (2004), 002-GSN-2004
Orchard (2006), personal communication
Pyle (2001), LJP01-01
Pyle (2004), LJP04-02
Utting (2000), 8-JU-00
Utting (2006), 04-JU-2006

All coordinates NAD83 UTM - zone 10V or 9V

Table IV-11. *Fossil data for stratigraphic units – Mattson Formation.*

GSC No.	Station	Easting	Northing	UTM Zone	Unit	Material	CAI	Comments	Max Age-Period	Max Age-Details	Min Age-Period	Min Age-Details	Reference
C-417713	01TLA150	361343	6696990	10	CM-b	conodont			Carboniferous - Mississippian	Visean	Carboniferous - Mississippian	Serpukhovian	Orchard (2005)
C-417733	01LP134	360704	6697168	10	CM-a	conodont			barren - age indeterminate		barren - age indeterminate		McCracken (2003c)

References
MacNaughton (2002b), 001-RBM-2002
McCracken (2003a), 6-ADM-2003
McCracken (2003b), 7-ADM-2003
McCracken (2003c), personal communication
Norford (2001), S-3-BSN-2001
Norford (2002), S-1-BSN-2002
Nowlan (2001), 010-GSN-2001
Nowlan (2004), 002-GSN-2004
Orchard (2005), MJO-2005-13
Orchard (2006), personal communication
Pyle (2001), LJP01-01
Pyle (2004), LJP04-02
Utting (2000), 8-JU-00
Utting (2006), 04-JU-2006

All coordinates NAD83 UTM - zone 10V or 9V

Table IV-12. *Fossil data for stratigraphic units – Fantasque Formation.*

GSC No.	Station	Easting	Northing	UTM Zone	Unit	Material	CAI	Comments	Max Age-Period	Max Age-Details	Min Age-Period	Min Age-Details	Reference
C-417156	04LP013	651523	6696337	9	PF-s	conodont	2	concretions	Permian		Permian		Pyle (2004)
C-417152	03LP008	651721	6699162	9	PF-s	palynology		poor preservation	age indeterminate		age indeterminate		Utting (2004)
C-417154	03LP009	652630	6699317	9	PF-l	conodont			barren - age indeterminate		barren - age indeterminate		Pyle (2004)
C-404747	03LP013	652758	6699126	9	PF-l	conodont			barren - age indeterminate		barren - age indeterminate		Pyle (2004)

References
MacNaughton (2002b), 001-RBM-2002
McCracken (2003a), 6-ADM-2003
McCracken (2003b), 7-ADM-2003
McCracken (2003c), personal communication
Norford (2001), S-3-BSN-2001
Norford (2002), S-1-BSN-2002
Nowlan (2001), 010-GSN-2001
Nowlan (2004), 002-GSN-2004
Orchard (2006), personal communication
Pyle (2001), LJP01-01
Pyle (2004), LJP04-02
Utting (2000), 8-JU-00
Utting (2006), 04-JU-2006

All coordinates NAD83 UTM - zone 10V or 9V

Table IV-13. *Fossil data for stratigraphic units – Grayling-Toad Formations.*

GSC No.	Station	Easting	Northing	UTM Zone	Unit	Material	CAI	Comments	Max Age-Period	Max Age-Details	Min Age-Period	Min Age-Details	Reference
C-404735	03LP008	651721	6699162	9	TrGT	palynology		contains Devonian reworking	Triassic	Lower	Triassic	Lower	Utting (2006)

References
MacNaughton (2002b), 001-RBM-2002
McCracken (2003a), 6-ADM-2003
McCracken (2003b), 7-ADM-2003
McCracken (2003c), personal communication
Norford (2001), S-3-BSN-2001
Norford (2002), S-1-BSN-2002
Nowlan (2001), 010-GSN-2001
Nowlan (2004), 002-GSN-2004
Orchard (2006), personal communication
Pyle (2001), LJP01-01
Pyle (2004), LJP04-02
Utting (2000), 8-JU-00
Utting (2006), 04-JU-2006

All coordinates NAD83 UTM - zone 10V or 9V

APPENDIX V. ROCK-EVAL ANALYSES

ANALYTICAL CONDITIONS AND INSTRUMENTATION

Programmed Rock-Eval/TOC pyrolysis-oxidation analyses were completed in the Organic Geochemistry Lab at the Geological Survey of Canada – Calgary. All analyses were completed using a Vinci Technologies Rock-Eval VI instrument (Vinci Technologies, 2001). Duplicate analyses of samples were carried out to test reproducibility of data. The start and finish of each sample run consisted of an internal standard (9107, collected from the Upper Cretaceous Colorado Group in Alberta, July 1991) for which the nominal parameters were determined against the base standards (55 000 and 160 000) provided by the instrument manufacturer.

Preparation of rock samples for analysis consists of powdering and homogenizing the sample to a size range of 100 microns to 2 mm using mortar and pestle for an average time of one minute. Powdered samples are then dried at 35°C for two hours to remove moisture.

Crucibles containing the samples are oxidized before use by heating to 850°C for 3 minutes to remove organic contaminants. The crucibles are cleaned with pressurized air to remove any remains of oxidized powder.

Each sample is analyzed in pyrolysis and oxidation modes sequentially. In pyrolysis mode, the sample is heated in an inert atmosphere. This mode provides information on amount and type of hydrocarbons present in the sample. Amounts of hydrocarbons released during heating are measured using a flame ionization detector, and amounts of CO and CO_2 released during heating are measured using an infrared cell. In oxidation mode, the sample is heated in ordinary air. Amounts of CO and CO_2 released during heating are measured with an infrared cell. Oxidation mode provides information on the amount and type of mineral carbon present in the sample.

The sample is placed in a 300°C oven and kept at that temperature for 3 minutes before further heating. The temperature of the oven is then increased to 850°C at the rate of 25°C per minute. A complete analysis requires about 20 minutes. Figure V-1 illustrates sample locations. Table V-1 lists measured parameters monitored during a Rock-Eval run, and Table V-2 lists the various parameters calculated from the measured parameters. Analytical results are presented in Table V-3.

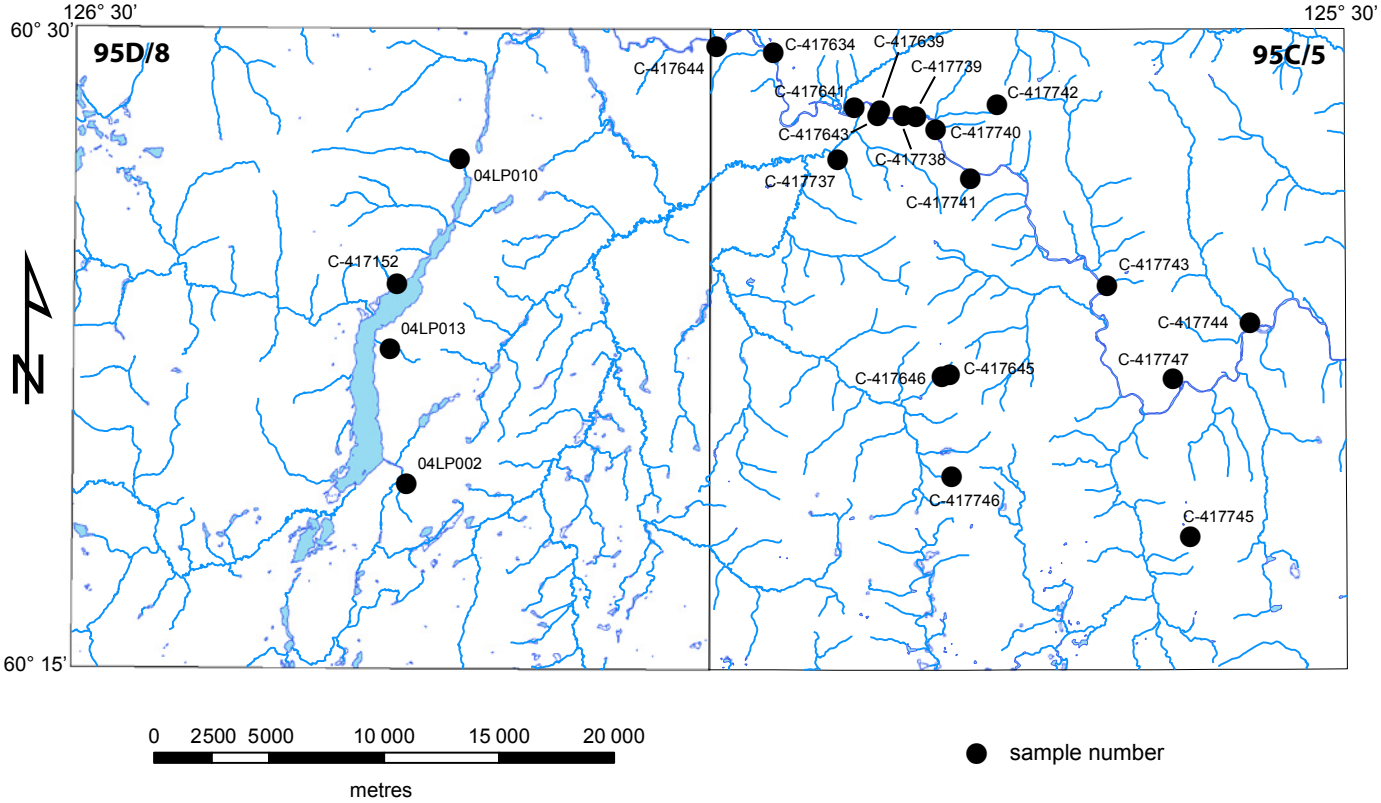


Figure V-1. *Location map for Rock-Eval 6 samples, NTS 95C/5 and 95D/8.*

Table V-1. *Measured parameters for Rock-Eval 6 run*

Parameter	Units	Mode	Description
S1	Mg HC/g rock	Pyrolysis	Free hydrocarbons
S2	Mg HC/g rock	Pyrolysis	Oil generation potential
Tpeak	°C	Pyrolysis	Temperature for S2 maximum release
S3	mgCO_2/g rock	Pyrolysis	CO_2 from organic source
S3′	mgCO_2/g rock	Pyrolysis	CO_2 from mineral source
TpeakS3′	°C	Pyrolysis	Temperature for S3′ maximum release
S3CO	mgCO/g rock	Pyrolysis	CO from organic source
TpS3CO	°C	Pyrolysis	Temperature for S3CO maximum release
S3′CO	mgCO/g rock	Pyrolysis	CO from mineral source
S4CO_2	mgCO_2/g rock	Oxidation	CO_2 from organic source
S4CO	mgCO/g rock	Oxidation	CO from organic source
S5	mgCO_2/g rock	Oxidation	CO_2 from mineral source
S5CO	mgCO/g rock	Oxidation	CO from mineral source
TpS5	°C	Oxidation	Temperature for S5 maximum release

Table V-2. *Calculated parameters from Rock-Eval 6 run.*

Parameter	Unit	Formula	Name
Tmax	°C	Calculated from TpS2-	Tmax
PI		S1/(S1+S2)	Production Index
PC	Wt %	Calculated from S1, S2, S3, S3CO, S3′CO	Pyrolysable organic carbon
RC CO	Wt %	Calculated from S4CO	Residual organic carbon (CO)
RC CO_2	Wt %	Calculated from S4CO_2	Residual organic carbon (CO_2)
RC	Wt %	RC CO + RC CO_2	Residual organic carbon
TOC	Wt %	PC + RC	Total organic carbon
S1/TOC	Mg HC/g TOC	S1*100/TOC	
HI	Mg HC/g TOC	S2*100/TOC	Hydrogen Index
OI	Mg CO_2/g TOC	S3*100/TOC	Oxygen Index
OI CO	Mg CO/g TOC	S3CO*100/TOC	Oxygen Index CO
pyroMinC	Wt %	Calculated from S3′ and S3′CO	Pyrolysis Mineral Carbon
oxiMinC	Wt %	Calculated from S5	Oxidation Mineral Carbon
MinC	Wt %	pyroMinC + oxiMinC	Mineral Carbon

Table V-3. *Rock-Eval 6 analyses for samples from 95C/5 and 95D/8.*

GSC No.	Field No.	UTM E m	UTM N m	UTM Zone	Rock Type	Unit	Qty mg	S1 mg HC/g rock	S2 mg HC/g rock	S'2 mg HC/g rock	PI	S_3CO_2 mg CO_2/g rock	T_{max} °C	T_{peak} °C	S_3CO mg CO/g rock	PC wt %	TOC wt %	RC wt %
9107	standard						99.7	0.95	11.99	0.07	0.07	0.76	442	487	0.09	1.08	5.11	4.03
C-417634	00LP038	337910	6709717	10N	shale	OSs	100.4	0.00	0.02	0.00	0.11	0.15	376	421	0.02	0.00	0.24	0.24
C-417639	00LP055	342437	6706992	10N	shale	SDRR-a	100.8	0.00	0.01	0.00	0.05	0.96	419	464	0.00	0.00	0.27	0.27
C-417641	00LP060*	341317	6707209	10N	limestone	Dd-l	10.4	0.00	0.03	0.00	0.07	0.80	459	504	0.19	0.01	3.29	3.28
C-417643	00LP065	342318	6706796	10N	shale	SDRR-a	10.1	0.00	0.01	0.01	0.00	2.90	579	624	0.00	0.00	2.41	2.41
C-417644	00LP079	335479	6710094	10N	shale	SDRR-a	10.1	0.00	0.00	0.00	0.16	0.83	450	495	0.08	0.00	3.17	3.17
C-417645	00TLA021b	344943	6695406	10N	shale	Ps	101.4	0.00	0.02	0.00	0.16	0.62	419	464	0.10	0.01	0.18	0.17
C-417646	00TLA023	344607	6695344	10N	shale	Ps	100.6	0.00	0.04	0.00	0.09	0.42	376	421	0.16	0.01	0.21	0.20
9107	standard						99.9	0.90	11.81	0.07	0.07	0.75	443	488	0.22	1.07	5.07	4.00
9107	standard						100.1	0.97	13.09	0.08	0.07	0.55	441	488	0.14	1.18	5.05	3.87
C-417737	01TLA043	340493	6704979	10N	bedded chert	DCBR	20.2	0.00	0.07	0.01	0.01	7.03	528	575	0.00	0.01	6.38	6.37
C-417738	01TLA061	343407	6706734	10N	siltstone	SDRR-a	20.7	0.00	0.00	0.00	0.00	0.81	573	620	0.00	0.00	1.61	1.61
C-417739	01TLA062	343990	6706689	10N	siltstone	SDRR-a	20.3	0.00	0.00	0.00	0.00	0.23	546	593	0.00	0.00	0.54	0.54
C-417740	01TLA067	344796	6706115	10N	siltstone	SDRR-a	20.1	0.01	0.13	0.01	0.06	2.00	448	495	0.09	0.02	1.24	1.22
C-417741	01TLA091	346209	6703891	10N	siltstone	SDRR-a	99.9	0.00	0.00	0.00	1.00	0.81	440	487	0.00	0.00	0.23	0.23
C-417742	01TLA098	347516	6707068	10N	shale	CM-a	20.5	0.02	0.10	0.01	0.17	1.39	600	647	0.25	0.02	4.77	4.75
C-417743	01TLA123	351946	6698996	10N	shale	DCBR	20.5	0.00	0.00	0.00	0.00	2.16	533	580	0.13	0.01	4.34	4.33
C-417744	01TLA138	358047	6697114	10N	shale	DCBR	20.5	0.00	0.01	0.00	0.00	2.77	522	569	0.00	0.00	2.39	2.39
C-417745	01TLA154	355073	6687927	10N	mudstone	DCBR	20.4	0.00	0.04	0.01	0.02	3.32	540	587	0.78	0.04	6.74	6.70
C-417746	01LP017	344844	6690966	10N	shale	DCBR	99.5	0.00	0.06	0.00	0.03	2.40	440	487	0.17	0.01	2.23	2.22
C-417747	01LP121	354609	6694794	10N	shale	DCBR	100.6	0.00	0.03	0.00	0.11	1.33	602	649	0.17	0.01	3.31	3.30
9107	standard						100.7	0.69	11.27	0.07	0.06	0.76	443	490	0.23	1.01	5.20	4.19
9107	standard						70.1	0.77	11.59	0.06	0.06	0.70	441	481	0.21	1.04	5.11	4.07
C-417152	03LP008	651721	6699162	9N	siltstone	PF	70.7	0.01	0.26	0.01	0.05	1.28	503	543	0.24	0.03	1.81	1.78
9107	standard						70.7	0.74	11.36	0.06	0.06	0.68	441	481	0.21	1.02	5.11	4.09
	04LP002	652525	6690506	9N	siltstone	DCBR	70.2	0.00	0.01	0.00	0.09	1.12	417	457	0.04	0.00	0.54	0.54
	04LP010	654157	6704722	9N	shale	COC	70.7	0.00	0.00	0.00	1.00	0.14	-40	0	0.05	0.00	0.30	0.30
	04LP013	651523	6696337	9N	siltstone	PF	70.0	0.00	0.00	0.00	0.24	0.31	396	436	0.10	0.00	0.18	0.18

GSC No.	Field No.	Rock Type	Unit	HI mg HC/g TOC	OICO mg CO/g TOC	$OICO_2$ mgCO_2/g TOC	OIRE6	MINC wt %	S_4CO	S_4CO_2	RCCO wt %	S_4CO_2	$S_{5a}CO_2$	$S_{5b}CO_2$	KFID	$RCCO_2$ wt %
9107	standard			236	2	15	12	0.5	18.8	118.3	0.806	118.3	0.0	9.9	1590.356	3.23
C-417634	00LP038	shale	OSs	8	8	63	50	0.0	0.6	7.9	0.026	7.9	0.0	0.7	1590.356	0.22
C-417639	00LP055	shale	SDRR-a	4	0	356	259	0.3	0.8	8.7	0.034	8.7	0.2	3.2	1590.356	0.24
C-417641	00LP060*	limestone	Dd-l	1	6	24	21	0.4	15.5	95.8	0.664	95.8	0.0	14.0	1590.356	2.61
C-417643	00LP065	shale	SDRR-a	1	0	120	87	0.7	7.4	76.7	0.317	76.7	1.8	15.3	1590.356	2.09
C-417644	00LP079	shale	SDRR-a	0	3	26	21	0.6	17.5	88.8	0.750	88.8	0.0	15.3	1590.356	2.42
C-417645	00TLA021b	shale	Ps	11	56	344	282	0.0	0.4	5.7	0.017	5.7	0.0	0.3	1590.356	0.16
C-417646	00TLA023	shale	Ps	19	76	200	189	0.0	0.5	6.5	0.021	6.5	0.0	0.2	1590.356	0.18
9107	standard			234	4	15	13	0.6	19.3	116.5	0.827	116.5	0.0	10.4	1590.356	3.18
9107	standard			261	3	11	10	0.6	21.5	108.0	0.921	108.0	0.0	13.7	1332.839	2.95
C-417737	01TLA043	bedded chert	DCBR	1	0	110	80	0.6	21.7	199.5	0.930	168.3	6.6	3.5	1332.839	5.44
C-417738	01TLA061	siltstone	SDRR-a	0	0	50	36	0.7	5.6	50.3	0.240	48.3	11.3	8.6	1332.839	1.37
C-417739	01TLA062	siltstone	SDRR-a	0	0	43	31	9.2	1.5	17.3	0.064	16.8	42.5	282.4	1332.839	0.47
C-417740	01TLA067	siltstone	SDRR-a	11	7	161	121	6.3	3.3	39.6	0.141	36.0	34.3	180.5	1332.839	1.08
C-417741	01TLA091	siltstone	SDRR-a	0	0	352	256	0.3	0.5	7.7	0.021	7.4	3.9	3.3	1332.839	0.21
C-417742	01TLA098	shale	CM-a	2	5	29	24	0.6	55.1	87.5	2.361	86.8	5.0	10.2	1332.839	2.39
C-417743	01TLA123	shale	DCBR	0	3	50	38	0.4	23.8	121.5	1.020	117.7	6.6	3.1	1332.839	3.31
C-417744	01TLA138	shale	DCBR	0	0	116	84	1.6	7.9	75.1	0.339	60.4	15.0	34.1	1332.839	2.05
C-417745	01TLA154	mudstone	DCBR	1	12	49	42	0.5	34.7	191.3	1.487	176.9	6.8	4.3	1332.839	5.22
C-417746	01LP017	shale	DCBR	3	8	108	83	0.3	8.0	68.7	0.343	46.0	2.9	1.9	1332.839	1.87
C-417747	01LP121	shale	DCBR	1	5	40	32	0.2	23.0	84.8	0.986	83.7	2.4	1.6	1332.839	2.31
9107	standard			218	4	15	13	4.0	21.2	120.4	0.909	112.2	24.6	105.9	1332.839	3.28
9107	standard			228	4	14	12	4.3	17.6	121.5	0.754	112.0	21.6	125.0	1460.65	3.31
C-417152	03LP008	siltstone	PF	15	13	71	59	0.4	5.3	56.8	0.227	47.3	6.7	2.1	1460.65	1.55
9107	standard			223	4	13	12	4.3	18.7	120.6	0.801	110.7	21.9	124.7	1460.65	3.29
	04LP002	siltstone	DCBR	2	7	207	155	6.1	0.5	18.9	0.021	14.3	23.4	190.8	1460.65	0.52
	04LP010	shale	COc	0	17	47	44	0.0	1.9	7.9	0.081	7.9	0.3	0.6	1460.65	0.22
	04LP013	siltstone	PF	0	56	172	157	1.3	1.0	5.1	0.043	4.9	11.1	28.8	1460.65	0.14